# Development of liposome-based sensing strategies for clinical diagnostics

Dissertation zur Erlangung des Doktorgrades der
Naturwissenschaften (Dr. rer. nat.)

an der Fakultät für Chemie und Pharmazie
der Universität Regensburg
Deutschland

vorgelegt von

**Simon Streif**

aus Freiburg i. Br.
im Jahr 2025

Die vorliegende Dissertation entstand in der Zeit von Juni 2021 bis April 2025 am Institut für Analytische Chemie, Chemo- und Biosensorik der Universität Regensburg.

Die Arbeit wurde angeleitet von Prof. Dr. Antje J. Bäumner.

Promotionsgesuch eingereicht am: 30.04.2025

Kolloquiumstermin: 29.07.2025

**Prüfungsausschuss**

Vorsitzender: Prof. Dr. Werner Kunz

Erstgutachterin: Prof. Dr. Antje J. Baeumner

Zweitgutachterin: Prof. Dr. Miriam Breunig

Drittprüfer: Prof. Dr. Axel Dürkop

# Acknowledgement

First of all, I would like to thank **Prof. Dr. Antje J. Bäumner** for the opportunity to work on this interesting project and the excellent supervision throughout. Furthermore, I want to thank **Prof. Dr. Axel Dürkop** and the whole **Liposome Team** for the regular and fruitful discussions, which often provided key insights, shaping the direction of this thesis, especially considering project related troubleshooting.

Next, I want to thank the NanoNeutVir consortium, including the groups of **Prof. Dr. Miriam Breunig**, **Prof. Dr. Ralf Wagner** and **Prof. Dr. Diana Pauly,** and **Dr. Monika Walter** for the great collaboration and the excellent scientific exchange. The meetings in both small and large groups were very insightful and crucial for the many collective achievements within the scope of the project.

Of course, this thesis would not have been possible without the help of my colleagues, especially **Clemens Spitzenberg**, **John Galligan**, **Kilian Höcherl** and **Christina Reiner**, who joined and grew together with me on this sometimes bumpy ride full of personal and research-related highs and lows. And thank you to the whole **AG Bäumner** for the fun times both inside and outside of the lab during the four years.

Thanks to **Vanessa Tomanek** for creating the graphics, conducting ICP-OES measurements and liposome syntheses. And to all **students** that assisted in many different side projects during their bachelor's or master's theses or internships.

I am deeply grateful to my **family**, and my girlfriend **Antonia Bauer** for helping me pursue my dreams and their unwavering support in any way possible. Thank you for being there whenever I need you, and for supporting and encouraging me with all my decisions. And lastly to all the **friends**, who accompanied me on this journey from the start or joined in between.

# Table of Contents

# Declaration of Collaborations

Most of the theoretical and experimental work presented in this thesis was conducted solely by the author. However, parts of the results were gained in collaboration with other researchers. In accordance with §8 Abs. 1 Satz 2 Punkt 7 of the "Ordnung zum Erwerb des akademischen Grades eines Doktors der Naturwissenschaften (Dr. rer. Nat.) an der Universität Regensburg vom 18. Juni 2009", the following paragraphs specify the work that was done by the author and the contributions by third parties.

**Chapter 1: Advances in surrogate neutralization tests for high-throughput screening and the point-of-care**

This chapter has been submitted for publication to the American Chemical Society journal *Analytical Chemistry* (accepted February 2025). The author conducted the literature search and wrote the first draft of the manuscript. Antje J. Baeumner revised the manuscript and is corresponding author. The author conceptualized and Vanessa Tomanek created the abstract graphic.

**Chapter 2.1: Liposome-based high-throughput and point-of-care assays toward the quick, simple and sensitive detection of neutralizing antibodies against SARS-CoV-2 in patient sera**

This chapter has been submitted for publication to the Springer journal *Analytical and Bioanalytical Chemistry* (accepted January 2023). Conceptualization was performed by Antje J. Baeumner, Ralf Wagner and the author. Experimental design and most experimental work was done by the author. Katharina Weiß, Kilian Hoecherl, Clemens Spitzenberg and Kacper Kulikowski helped with liposome related experiments. Sebastian Einhauser conducted the pseudovirus neutralization tests and Christina Noelting the RBD binding antibody tests. Patrick Neckermann, Claudia Asam, David Peterhoff and Sonja Hahner provided the proteins. The author wrote the first draft of the manuscript. Sebastian Einhauser, Patrick Neckermann, Ralf Wagner and Antje J. Baeumner revised the manuscript. Antje J. Baeumner is corresponding author. The author conceptualized and Vanessa Tomanek created the abstract graphic.

**Chapter 2.2: Optimization of the stability of liposomes modified with the receptor binding domain of SARS-CoV-2 Alpha using EDC/sulfo-NHS chemistry**

The conceptualization for this chapter was performed by Antje J. Baeumner and the author. The experimental work was done by the author. Ralf Wagner from the University Hospital

Regensburg and Mikrogen GmbH kindly provided the receptor binding domain and angiotensin-converting enzyme 2 receptor used for this work.

**Chapter 3.1: Development of a serological liposome-based assay for SARS-CoV-2 variants with special emphasis on coupling chemistries required to maintain protein antigenicity**

This chapter has been submitted for publication to the American Chemical Society journal *Analytical Chemistry* (April 2025). Conceptualization was performed by Antje J. Baeumner, Ralf Wagner and the author. Liposome synthesis and liposome-based experiments were performed by the author. Cloning of recombinant protein expression plasmids and expression, purification and quality control of recombinant ACE2 and RBD was conducted by Patrick Neckermann. Biotinylation of RBD was performed by Johannes Konrad, Patrick Neckermann and the author. Sebastian Einhauser conducted the pseudovirus neutralization tests. The author wrote the first draft of the manuscript. Christina Reiner, Kilian Hoecherl, Miriam Breunig, Sebastian Einhauser, Patrick Neckermann, Ralf Wagner and Antje J. Baeumner revised the manuscript. Ralf Wagner and Antje J. Baeumner are corresponding authors. The author conceptualized and Vanessa Tomanek created the abstract graphic.

**Chapter 3.2: Investigating spike protein conjugation as alternative to RBD modified liposomes**

The conceptualization for this chapter was performed by Antje J. Baeumner and the author. The experimental work was done by the author. Ralf Wagner from the University Hospital Regensburg kindly provided the receptor binding domain, stabilized trimeric spike and angiotensin-converting enzyme 2 receptor used for this work.

**Chapter 4: Optimization of the POC neutralization test toward quantitative detection and improved user-friendliness**

The conceptualization for this chapter was performed by Antje J. Baeumner and the author. The experimental work was done by the author. Ralf Wagner from the University Hospital Regensburg kindly provided the receptor binding domain and angiotensin-converting enzyme 2 receptor used for this work. Microcoat Biotechnology GmbH provided the ESEQuant LFR device and expertise regarding the production of lateral flow assays.

# Relevance and Structure of the Thesis

Diagnostic testing has evolved to be an integral part of modern medicine and is indispensable not only for accurate disease diagnosis, but also monitoring, prognosis, and screening[1]. The tests can detect biomarkers, drugs, metabolites, and pathogens and thus help to inform clinical decision-making and guide treatment strategies. For instance, the identification of biomarkers associated with certain tumors has led to targeted cancer therapies, facilitating the tailoring of treatments to the genetic profile of the tumor[2,3]. This process is however commonly linked to biopsies and requires sophisticated equipment, limiting it to clinical settings. Other diagnostic tests can be executed by a lay person, making them a vital part for future healthcare considering developments toward digital and telemedicine-based systems[4]. Well-known examples in this field are the continuous monitoring of blood glucose levels for diabetes patients using electrochemical sensors[5], and testing for the pregnancy hormone human chorionic gonadotropin in urine[6]. Moreover, diagnostic testing plays a crucial role in public health by enabling the early detection and containment of infectious diseases. The COVID-19 pandemic underscored the importance of rapid and reliable diagnostic tests in managing outbreaks and preventing widespread transmission. Besides the widely used rapid antigen tests, which provided the option for at home testing, helping contain the spread of the virus, much development has been achieved in the field of neutralization tests[7,8]. These serological tests enable the assessment of the immune status of large parts of the population and are thought to guide informed decision making regarding the necessity for booster vaccination. While the gold standard, the plaque reduction neutralization test, was quickly adapted to SARS-CoV-2, it is a time-consuming format that requires biosafety level facilities due to the use of live virus[9]. Cell-free, rapid, and easy to use alternatives, so-called surrogate virus neutralization tests (sVNTs), promise to fill the gap to facilitate high-throughput screening and point-of-care (POC) testing. **Chapter 1** provides a critical overview of the development in the field of sVNTs over the past years, which was dominated by SARS-CoV-2 related research. It briefly touches the field of binding antibody tests and discusses commercially available serological tests. The main focus lies on newly developed sVNTs, classified in the categories of HTS and POC tests, each divided into subchapters depending on the detection method. Special subchapters additionally discuss homogeneous HTS assays and POC tests applying a 'signal-on' strategy. Finally, future perspectives for this field of research are analyzed.

**Chapter 2** delves into the implementation of SRB encapsulating liposomes for the detection and quantification of neutralizing antibodies against the receptor binding domain (RBD) of SARS-CoV-2. The chapter highlights the development of both HTS and POC formats using the same signaling conjugate, demonstrating their efficacy and potential for rapid, sensitive

diagnostics. Additionally, it addresses the challenges of long-term stability of RBD-modified liposomes, proposing solutions to enhance their robustness and reliability for diagnostic applications. In **Chapter 3**, the focus shifts to the adaptation of the liposome-based neutralization test for other SARS-CoV-2 variants. It proposes the application of streptavidin- or neutravidin-conjugated liposomes combined with biotinylated proteins as a versatile platform technology, facilitating long-term storage of assay components and simple adaptation for different analytes. A random and two site-directed approaches for biotinylation were investigated using RBD-Alpha as model protein. The best approach, enzymatic biotinylation via the C-terminal Avi-tag, was applied to a total of five different variants of RBD. The highly sensitive detection of neutralizing antibodies in a HTS format was used to investigate the immune escape of Omicron variants. The chapter further explores the drawbacks associated with EDC/sulfo-NHS coupling of RBD and Spike protein to liposomes, ascribed to unfavorable orientation on or interaction with the lipid bilayer.

**Chapter 4** explores strategies to improve the sensitivity and user-friendliness of the liposome-based POC neutralization test for SARS-CoV-2. The chapter identifies key factors such as RBD coverage, serum concentration, and LFA strip width that influence test performance. It also proposes and implements innovative approaches for on-strip incubation and 'signal-on' strategies, aiming to enhance the overall effectiveness and ease of use of POC diagnostic tests.

## References

(1) Bolboacă, S. D. *Computational and Mathematical Methods in Medicine* **2019**, *2019*, 1891569.

(2) Sawyers, C. *Nature* **2004**, *432* (7015), 294–297.

(3) Shariati, M.; Meric-Bernstam, F. *Expert Opin Investig Drugs* **2019**, *28* (11), 977–988.

(4) Rink, S.; Baeumner, A. J. *Anal. Chem.* **2023**.

(5) Saha, T.; Del Caño, R.; Mahato, K.; La Paz, E. de; Chen, C.; Ding, S.; Yin, L.; Wang, J. *Chemical Reviews* **2023**, *123* (12), 7854–7889.

(6) Chard, T. *Hum Reprod* **1992**, *7* (5), 701–710.

(7) Dong, T.; Wang, M.; Liu, J.; Ma, P.; Pang, S.; Liu, W.; Liu, A. *Chem. Sci.* **2023**, *14* (23), 6149–6206.

(8) Rocha, V. P. C.; Quadros, H. C.; Fernandes, A. M. S.; Gonçalves, L. P.; Da Badaró, R. J. S.; Soares, M. B. P.; Machado, B. A. S. *Viruses* **2023**, *15* (7), 1504.

(9) Muruato, A. E.; Fontes-Garfias, C. R.; Ren, P.; Garcia-Blanco, M. A.; Menachery, V. D.; Xie, X.; Shi, P.-Y. *Nat. Commun.* **2020**, *11* (1), 4059.

# Summary

In this thesis, liposomes were used for the development of diagnostic tests due to their unique structural and functional properties. The incorporation of functionalized lipids enables simple modification of liposomes with proteins or other molecules using various established coupling chemistries, making them highly versatile. This is further supported by the potential to encapsulate different signaling molecules, including dyes, fluorophores, redox markers and enzymes, facilitating the use of various detection methods and thus fine-tuning of sensitivity, specificity and overall test performance. This allows for innovative sensing strategies that can be integrated into various existing diagnostic frameworks. Here, the fluorescent dye sulforhodamine B (SRB) was used as encapsulant, facilitating both fluorescence and colorimetric detection.

The first experimental part of this work focuses on the development of a surrogate virus neutralization test for SARS-CoV-2 that can be used for both high-throughput screening (HTS) and point-of-care testing (POCT). This goal was achieved by simple modification of SRB liposomes with the receptor binding domain (RBD) of SARS-CoV-2 using EDC/sulfo-NHS chemistry. The microplate-based HTS assay was able to quantitatively detect neutralizing anti-RBD antibodies and the obtained IC50 values correlated excellently to those from an established pseudovirus neutralization test (pVNT) (r = 0.847). The POC format also showed good correlation to the pVNT (r = 0.614) and allowed for the rapid qualitative detection of neutralizing antibodies. Furthermore, excellent correlation between the HTS and POC format was observed (r = 0.868), highlighting the benefit of using a single signaling conjugate for two independent assays with different detection methods. While original storage stability studies revealed aggregation and loss of angiotensin-converting enzyme 2 receptor (ACE2) binding ability within the first weeks, further optimization improved both the colloidal and protein stability of RBD-modified liposomes, facilitating their use for up to 24 weeks.

The second part focuses on different conjugation strategies for proteins to liposomes. Modification of liposomes with RBD of different SARS-CoV-2 variants using EDC/sulfo-NHS chemistry resulted in unfavorable orientation in the case of Omicron variants due to mutations, preventing interaction with ACE2. Alternatively, the conjugation of different variants of the stabilized trimeric spike protein was investigated, but proved challenging, causing aggregation or inducing leakage of SRB during modification. Various biotinylation strategies were investigated for RBD to enable the use of streptavidin-conjugated liposomes instead, allowing for separate storage of assay components, as well as easy exchange of the conjugated protein. Random biotinylation of amino groups of both the N-terminus and lysine residues using NHS-biotin was shown to be feasible. Better results were achieved by site-directed biotinylation of

a Cys-tag using maleimide-biotin conjugates, allowing for the introduction of spacers, such as polyethylene glycol. Site-directed enzymatic biotinylation of an Avi-tag provided the best results and could be applied to all five investigated RBD variants, excelling with its high consistency. Fine-tuning led to the development of a highly sensitive HTS neutralization test for each variant, cut-off values were determined using five seronegative samples before screening of 10 seropositive samples. This showcased the immune escape of Omicron variants, which showed overall lower IC50 values compared to Alpha and Delta. The obtained IC50 values correlated excellently to the pVNT (r = 0.86). The use of neutravidin instead of streptavidin avoids non-specific interaction with proteins containing the RGD sequence, making the format a versatile platform technology that can easily be adapted to other proteins.

The last part explores strategies to improve the sensitivity and user-friendliness of the POC neutralization test. RBD coverage, serum concentration, and LFA strip width were found to be key factors for the assay performance. Furthermore, strategies for on-strip incubation were investigated, including a polyvinyl alcohol barrier and a wax barrier with gap, aiming to enhance the overall ease of use of POC diagnostic tests. Lastly, the capture of neutralized RBD-liposomes was attempted, using a second test line consisting of anti-human Ig antibodies or Protein A, to provide a 'signal-on' approach. Non-specific interaction of HSA with antibodies and the abundance of other antibodies not directed against RBD were identified as major obstacles, preventing the implementation of this approach.

# Zusammenfassung

In dieser Arbeit wurden Liposomen aufgrund ihrer einzigartigen strukturellen und funktionellen Eigenschaften für die Entwicklung von diagnostischen Tests verwendet. Der Einbau funktionalisierter Lipide ermöglicht die einfache Modifizierung von Liposomen mit Proteinen oder anderen Molekülen unter Verwendung verschiedener etablierter Kopplungschemien, was sie äußerst vielseitig macht. Hinzu kommt die Möglichkeit, verschiedene Signalmoleküle wie Farbstoffe, Fluorophore, Redoxmarker und Enzyme einzukapseln, was den Einsatz verschiedener Nachweismethoden und damit die Feinjustierung von Sensitivität, Spezifität und Gesamttestleistung erleichtert. Dies ermöglicht innovative Detektionsstrategien, die in verschiedene bestehende Diagnosesysteme integriert werden können. Hier wurde der Fluoreszenzfarbstoff Sulforhodamin B (SRB) als Verkapselungsmaterial verwendet, das sowohl den Fluoreszenz- als auch den kolorimetrischen Nachweis ermöglicht.

Der erste experimentelle Teil dieser Arbeit konzentriert sich auf die Entwicklung eines Surrogat-Virusneutralisationstests für SARS-CoV-2, der sowohl für Hochdurchsatz-Screening (HTS) als auch für Point-of-Care-Tests (POCT) verwendet werden kann. Dieses Ziel wurde durch die einfache Modifizierung von SRB-Liposomen mit der Rezeptorbindungsdomäne (RBD) von SARS-CoV-2 unter Verwendung von EDC/Sulfo-NHS-Chemie erreicht. Mit dem mikroplattenbasierten HTS-Assay konnten neutralisierende anti-RBD Antikörper quantitativ nachgewiesen werden, und die erhaltenen IC50-Werte korrelierten hervorragend mit denen eines etablierten Pseudovirus-Neutralisationstests (pVNT) (r = 0.847). Das POC-Format zeigte ebenfalls eine gute Korrelation zum pVNT (r = 0.614) und ermöglichte den schnellen qualitativen Nachweis von neutralisierenden Antikörpern. Darüber hinaus wurde eine ausgezeichnete Korrelation zwischen dem HTS- und dem POC-Format beobachtet (r = 0.868), was den Vorteil der Verwendung eines einzigen Signalkonjugats für zwei unabhängige Assays mit unterschiedlichen Nachweismethoden unterstreicht. Während die ursprünglichen Studien zur Lagerstabilität eine Aggregation und einen Verlust der Bindungsfähigkeit an den Angiotensin-Converting-Enzym-2-Rezeptor (ACE2) innerhalb der ersten Wochen ergaben, konnte eine weitere Optimierung sowohl die kolloidale als auch die Proteinstabilität der RBD-modifizierten Liposomen verbessern, was ihre Verwendung für bis zu 24 Wochen ermöglicht.

Der zweite Teil befasst sich mit verschiedenen Konjugationsstrategien für Proteine an Liposomen. Die Modifizierung von Liposomen mit RBD verschiedener SARS-CoV-2-Varianten mittels EDC/sulfo-NHS Chemie führte im Falle der Omicron-Varianten aufgrund von Mutationen zu einer ungünstigen Ausrichtung, die eine Interaktion mit ACE2 verhindert. Alternativ wurde die Konjugation verschiedener Varianten des stabilisierten trimeren Spike-

Proteins untersucht, was sich jedoch als schwierig erwies, da es bei der Modifikation zu Aggregation oder zum Austritt von SRB kam. Es wurden verschiedene Biotinylierungsstrategien für RBD untersucht, um stattdessen die Verwendung von Streptavidin-konjugierten Liposomen zu ermöglichen, die eine getrennte Lagerung der Testkomponenten sowie einen einfachen Austausch des konjugierten Proteins erlauben. Die zufällige Biotinylierung von Aminogruppen sowohl des N-Terminus als auch von Lysinresten mit NHS-Biotin erwies sich als machbar. Bessere Ergebnisse wurden durch die ortsgerichtete Biotinylierung eines Cys-Tags unter Verwendung von Maleimid-Biotin-Konjugaten erzielt, die die Einführung von Spacern wie Polyethylenglykol ermöglichen. Die ortsgerichtete enzymatische Biotinylierung eines Avi-Tags lieferte die besten Ergebnisse und konnte auf alle fünf untersuchten RBD-Varianten angewandt werden, wobei sie sich durch ihre hohe Konstanz auszeichnete. Die Feinabstimmung führte zur Entwicklung eines hochempfindlichen HTS-Neutralisationstests für jede Variante. Die Cut-off-Werte wurden anhand von fünf seronegativen Proben bestimmt, anschließend wurden 10 seropositive Proben getestet. Letztere verdeutlichten die Immunflucht der Omicron-Varianten, die im Vergleich zu Alpha und Delta insgesamt niedrigere IC50-Werte aufwiesen. Die erhaltenen IC50-Werte korrelierten gut mit dem pVNT (r = 0.86). Durch die Verwendung von Neutravidin anstelle von Streptavidin werden unspezifische Wechselwirkungen mit Proteinen, die die RGD-Sequenz enthalten, vermieden, was das Format zu einer vielseitigen Plattformtechnologie macht, die leicht an andere Proteine angepasst werden kann.

Im letzten Teil werden Strategien zur Verbesserung der Empfindlichkeit und Benutzerfreundlichkeit des POC-Neutralisationstests untersucht. Die RBD-Beladung, die Serumkonzentration und die Breite des LFA-Streifens erwiesen sich als Schlüsselfaktoren. Darüber hinaus wurden Strategien für die Inkubation auf dem Streifen untersucht, darunter eine Polyvinylalkohol-Barriere und eine Wachsbarriere mit Spalt, um die Benutzerfreundlichkeit von POC-Diagnosetests insgesamt zu verbessern. Schließlich wurde versucht, neutralisierte RBD-Liposomen mit Hilfe einer zweiten Testlinie, bestehend aus Anti-Human-Ig Antikörpern oder Protein A, einzufangen, um einen „Signal-on"-Ansatz zu ermöglichen. Die unspezifische Wechselwirkung von HSA mit Antikörpern und die Fülle anderer Antikörper, die nicht gegen RBD gerichtet sind, wurden als Haupthindernisse für die Umsetzung dieses Ansatzes ermittelt.

# 1 Advances in surrogate neutralization tests for high-throughput screening and the point-of-care

---

**Graphical Abstract**
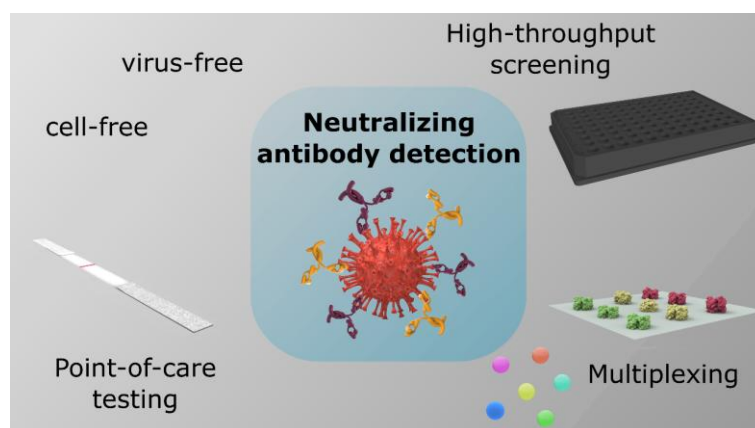


---

**Authors' contributions**

**Antje J. Baeumner** Conceptualization; supervision; writing – review and editing

**Simon Streif** Conceptualization; visualization; literature review; writing – original draft

## 1.1 Introduction

Serological testing has long played a crucial role in disease management and clinical diagnostics. Both infection with viruses and vaccination mediate a humoral immune response, including the generation of specific antibodies. The presence of antibodies can therefore be used qualitatively to detect recent or past infections or quantitatively to determine the immune status of a patient. Antibody profiles generated by different viruses vary and show differences for infection versus vaccination, as the latter often uses only one specific antigen rather than the whole virus. Furthermore, while some vaccinations result in long-term immunity, others require booster shots every few years, or even yearly. Hence, the necessity and benefits of serological testing are typically tailored to the respective viruses or diseases.

Diseases preventable through vaccination include, e.g., hepatitis A, influenza, SARS, chickenpox, measles, mumps, rubella, tetanus, and poliomyelitis. Low mutation rates due to constraints, such as limited host range in the case of measles[1], are key to ensuring long-term immunity by memory B cell and T cell persistence. Vaccination can lead to immunity for up to 30 years and longer for the hepatitis B virus[2]. The influenza viruses, especially influenza A, show rapid antigenic drift, necessitating extensive modeling to predict the most likely strains to be targeted by the annual vaccine[3]. Severe acute respiratory syndrome coronavirus 2 (SARS-CoV-2) also shows high mutation rates, facilitating its immune escape. The COVID-19 pandemic caused by the SARS-CoV-2 virus sparked advancement and innovation in the field of serological testing with regard to both binding and neutralizing antibody detection. The virus consists of four proteins: nucleocapsid (N), envelope (E), membrane (M) and spike (S). Interaction with the host cell is mediated by the S protein as the receptor binding domain (RBD) of the S1 subunit binds to the human angiotensin converting enzyme 2 (ACE2) receptor[4]. Cellular transmembrane protease serine 2 (TMPRSS2) and lysosomal cathepsin proteases cleave the S1 and S2 subunits, followed by membrane fusion initiated by the S2 subunit[5]. While some antibodies target the nucleocapsid protein, the majority are directed against the S protein, more specifically RBD[6,7]. Most SARS-CoV-2 vaccines make use of this observation by introducing mRNA or viral vectors to induce the expression of the S protein as the antigen[8,9] or by directly introducing the S protein[10]. Testing for antinucleocapsid antibodies can thus be used to check for past infections, unless an inactivated vaccine was used, introducing all viral proteins[11]. Antispike and anti-RBD antibodies, which are produced after both infection and vaccination, provide a means to assert the immune status and might serve as a correlate of protection (CoP)[12–14]. For more information on the definition of a CoP for SARS-CoV-2 and other viruses the reviews by Perry et al.[12], Sobhani et al.[15] and Plotkin[16] are recommended.

### *Advances in surrogate neutralization tests for high-throughput screening and the point-of-care*

Two categories of antibodies can be quantified, binding antibodies and neutralizing antibodies (nAbs). The former includes all antibodies directed against a certain antigen, while the latter includes only antibodies that prevent infection, i.e., by blocking the virus host interaction or preventing the host cell fusion. Neutralization tests mimic the interaction of the virus with the host cell and thus quantify the neutralizing antibodies indirectly via their ability to block the interaction. The gold standard is the plaque reduction neutralization test (PRNT), which uses live virus incubated with patient serum dilutions prior to the addition to cells expressing the respective viral receptor. Infection of the cells by the virus results in the formation of plaques, which are quantified by manual or automatic counting. The $PRNT_{50}$ value correlates to the serum dilution required to reduce the plaque formation observed without serum by 50%. The use of live virus makes the PRNT and other conventional neutralization tests (cVNTs), such as the micro neutralization test (microNT), highly accurate but requires a biosafety level (BSL) facility of the virus and results in long turn-around times of up to 3 days[17]. In the case of the viruses mentioned above, BSL-3 would be required for most. To reduce the safety requirements to at least BSL-2 pseudovirus-neutralization tests (pVNTs) have been developed, relying on the use of lentiviruses or vesicular stomatitis virus pseudotyped with the respective viral protein responsible for host cell binding and fusion[18–20]. For more information on live virus neutralization test and pVNT development the recent reviews of Rocha et al.[21], Sun et al.[22] and Vaidya[23] are recommended. In the case of SARS-CoV-2, RBD was identified as the main target for neutralizing antibodies providing the opportunity to further simplify the neutralization tests. Surrogate virus neutralization tests (sVNTs), the focus of this review, rely on the competitive binding of neutralizing antibodies and the cell receptor with the relevant viral protein. In the case of SARS-CoV-2, this is ACE2 and RBD, respectively. These cell-free assays can be divided into two categories, high-throughput screening (HTS) and point-of-care (POC) assays. They do not require any biosafety facilities and have rapid turn-around times, making serological testing widely available. The COVID pandemic showed that such tests can be applied to monitor the development of antibody titers in vaccination studies, providing insights into the immunity against SARS-CoV-2. Still, such sVNTs are not endorsed by regulatory agencies to monitor the immune status, yet[24]. To date, only three sVNTs have been granted emergency use authorization (EUA) by the Food and Drug Administration (FDA)[25]. Lacking standardization and validation during test development as well as difficulties defining a neutralizing antibody titer as CoP due to the rapid mutation of the virus currently hinders progress to take full advantage of sVNTs. However, they are the scientific and technological answer to broad serological testing needed, and not only in pandemic situations. In the following an overview of the development in the field of sVNTs of the last three years is provided. Advantages and disadvantages of the different formats are critically analyzed, and future development potential, especially the applicability toward other viruses, is discussed.

## 1.2 Binding antibody tests

Quantification of patient binding antibodies is used for the assessment of past infections within minutes or hours at the POC. Such tests typically rely on the use of secondary antibodies, which recognize sections of the binding antibody molecules. Thus, such approaches need to account for the different isotypes of patient antibodies and their respective seroconversion. Specifically, immunoglobulin M (IgM) levels rise quickly after infection or vaccination and drop shortly after recovery, while IgA and IgG levels take longer to increase and decrease and are therefore more reliable to serve as indicators for immunity against reinfection[26,27]. Time-resolved screening with combinations of IgM and IgG binding antibody tests can provide detailed information about the seroconversion after infection or vaccination. Such tests only use selected proteins of the virus and can therefore be used without the need for specialized biosafety facilities. It is important to note that the strength of these tests lies in their ability to provide insights about the immune status of large parts of the population. However, because infectiousness precedes seroconversion by multiple days, binding antibody tests are unsuitable as diagnostic tests to stop the spread of the disease. Still, research for improving their sensitivity and specificity, while maintaining the ease-of-use of the standard rapid lateral flow assay (LFA), has intensified over the last 5 years with some remarkable novelties. For example, Hossain et al.[28] used alkaline phosphatase (AP)-conjugated secondary antibodies to enable the use of off-the-shelf glucometer test strips by the incorporation of maltose phosphatase. Streptavidin-magnetic nanoparticles were modified with biotinylated RBD and incubated with serum and the secondary antibodies. Alkaline phosphatase yellow (pNPP) is enzymatically degraded to $PO_4^{3-}$, which maltose phosphorylase stoichiometrically converts to glucose which is then quantified amperometrically in a minipotentiostat. A similar approach was investigated by Peng et al.[29], who used AP-conjugated secondary antibodies to enable electrochemical detection of antibodies using a commercial hand-held potentiostat. Their serological testing platform for the rapid electrochemical detection of SARS-CoV-2 antibodies (SPEEDS) consisted of a streptavidin-coated carbon working electrode modified with biotinylated RBD, a carbon counter electrode and a Ag/AgCl reference electrode. The presence of antibodies was quantitatively determined by the conversion of p-aminophenyl phosphate to p-aminophenol by AP, which was then oxidized to p-quinonimine during chronoamperometry. Other researchers focused on the development of new materials for binding antibody tests. The electrochemical sensor from Nunez et al.[30] was based on zinc oxide nanorods modified with the S protein, facilitating antibody detection in only 5 min. The positive charge of ZnO makes it an interesting option for the adsorption of negatively charged proteins. Further optimization is needed to make the technology market ready, as the system is only stable for 15 days so far. Nanorods were also involved in Shen et al.'s work, who

developed a magnetofluid-integrated multicolor immunochip (MMI-chip)[31]. The eight liquid storage wells of the MMI-chip connected by a mineral oil layer enable multiple reaction and washing steps of magnetic nanoparticles modified with RBD (**Figure 1**). The horseradish peroxidase (HRP)-labeled secondary antibodies are used to oxidize the substrate 3,3′,5,5′-tetramethylbenzidine (TMB), which then etches gold nanorods, decreasing their length and thereby changing the absorption spectra, enabling a semiquantitative visual read-out. Although being a multistep assay, the chip design results in a sealed environment, minimizing external exposure and increasing user-friendliness. Chip fabrication was also the focus of many other publications. Kim et al. developed a microfluidic fluorescent LFA with integrated dry reagents, a mixer, and a vacuum pump[32]. The sample first passes DyLight 550 labeled secondary antibodies in a dry reagent storage chamber, is mixed in a herringbone mixer, and then passes the spike-labeled polystyrene particle storage chamber. These particles are then captured at the detection zone due to pillars, enabling fluorescence measurements using an inverted microscope.
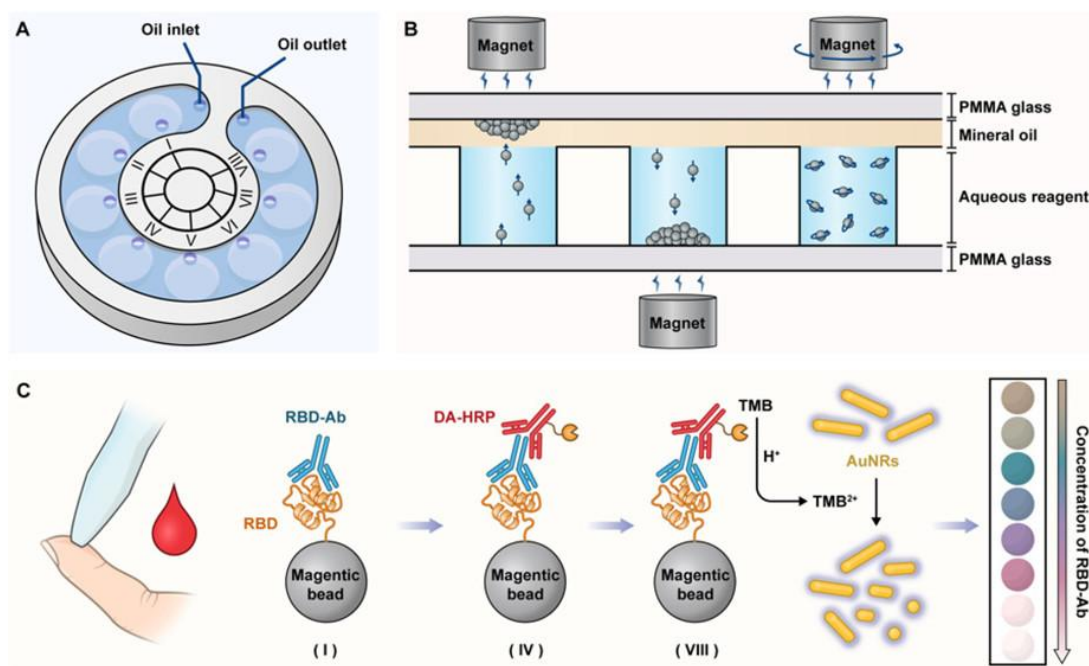


*Figure 1: Schematic illustration of the MMI-Chip. (**A**) Structural diagram of the chip with its eight liquid wells for loading sample (I), washing solution (II and III), detection antibody (IV), washing solution (V-VII), and signal substrate (VII). (**B**) Magnetic bead transportation between wells and mixing using a magnet. (**C**) Workflow of antibody detection in peripheral blood. Reproduced with permission from ref 31. Copyright 2022 American Chemical Society.*

Multiplexing offers another intriguing avenue, allowing for simultaneous IgG and IgM detection of a variety of antigens, opening the possibility to screen several viral variants or several prevalent viruses simultaneously. In the case of SARS-CoV-2, this is of growing interest, as it continuously mutates so that the dominating variant changes quickly. Several multiplexing platforms were developed relying on machine learning, magnetic barcode beads, nanopore

sensing, and more[33–37]. The paper-based multiplexing vertical flow assay (xVFA) by Eryilmaz et al. was able to screen five different SARS-CoV-2 antigens for IgG and IgM antibodies in <20 min[33]. Their device was 3D-printed and used a mobile-phone-based optical reader. The neural network showed 89.5% accuracy for 31 serum samples tested after training. Importantly, they also addressed the limitations caused by the choice of serum panel used during development versus later application. Serum panels consisting of local sera or small numbers of sera may be biased toward less variations in vaccination and infection status. Nan et al.'s naked-eye readable microarray (NRM) based on a thickness sensing nanoplasmonic ruler provided a rapid and POC friendly multiplex sensing platform (**Figure 2**)[35]. Their NRM chips can screen 10 different RBD variants for 16 serum samples (~2 µL each) simultaneously in <30 min. The test is based on a gold nanoparticle (AuNP) monolayer, where the increased thickness caused by captured antibodies results in a decreased reflectance, which, in turn, is measurable using gray value analysis of smartphone images. Their manufacturing requires a tape-based transfer of the AuNP monolayer, which is deemed impractical, however. Exploiting similar effects, Huang et al. have developed a nanoplasmonic immunosensor platform using nanoporous hollow gold nanoparticles modified with RBD to detect anti-RBD antibodies on an anti-IgG coated nanoplasmonic sensor chip[38]. The system can generate a signal within 15 min without the need of signal amplification or washing. Similarly, dual-affinity ratiometric quenching (DARQ) can enable a fast signal generation in a homogeneous format. Kilgour et al. mixed serum with fluorescein-labeled RBD and rhodamine-labeled protein L, obtaining signals in just over 2 min[39]. Liang et al. combined a visual LFA with Raman spectroscopy[40]. They synthesized silver nanoparticles with ultrathin gold shells embedded with 4-mercaptobenzoic acid and conjugated them with secondary antibodies using HS-PEG-COOH and EDC/NHS chemistry. The particles enabled dual-mode qualitative visual and quantitative SERS read-out via a portable Raman spectrometer with a 785 nm laser on a LFA test strip. They later changed to a competitive assay format to allow the detection of neutralizing instead of binding antibodies[41]. This is an excellent example demonstrating that the noncompetitive format of binding antibody tests can often be changed to a competitive format, making the technologies even more universally applicable. In fact, many of the sVNTs discussed in the next chapters have evolved out of binding antibody tests. More information on binding antibody tests can be found in the reviews written by Lee et al.[42], Yari et al.[43] and Dong et al.[44].
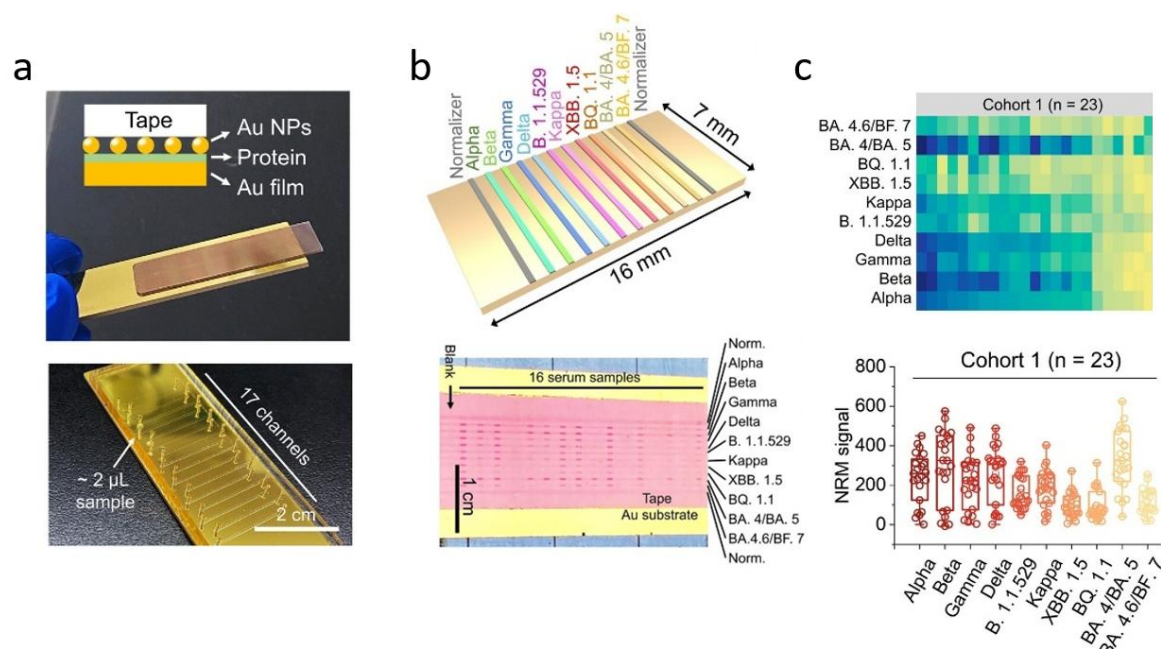
*Figure 2: Visualization of the naked-eye readable barcode and micromosaic (NRM) assays. (**a**) Schematic and photograph illustrating the ready-to-use NRM chip (top) and the microfluidic channels for the serum incubation (bottom). (**b**) Schematic representation of the antigen immobilization layout of the barcode NRM assay (top). Smartphone image of the micromosaic NRM chip, allowing for simultaneous testing of up to 16 samples (bottom). (**c**) Heatmap (top) and box plots (bottom) showing levels of antibodies against multiple SARS-CoV-2 variants in serum samples from random donors after the reopening in China in December 2022 (Cohort 1). Reproduced with permission from ref 35. Copyright 2023 American Chemical Society.*

## 1.3 Commercial binding and neutralizing antibody tests

The cell-free detection of antibodies directed against viral diseases has long been established, starting with enzyme-linked immunosorbent assay (ELISA) concepts against measles, rubella, and hepatitis[45–47] and, more recently, the development of LFAs[48]. In the case of the COVID-19 pandemic, large companies quickly adapted existing technologies to provide diagnostic tools for SARS-CoV-2, including antibody detection. Many of the resulting products gained EUA by the FDA, as indicated above, to enable their distribution, without the need to go through the complete FDA authorization process. Now, over 5 years after the beginning of the outbreak, some of these EUAs have been revoked,[49] and most products are off the market. Once discontinued finding detailed information about the testing principles behind the products can be difficult, as datasheets become unavailable. In these cases, publications using the tests or Web sites listing multiple tests are the best option to obtain more information. At the point of writing, the FDA still lists 75 serological tests granted EUA, the first one issued April 2020 and the most recent one in July 2024[25] and two granted traditional marketing authorization[50]. Of these, most detect IgG, IgM, or total antibody levels. Only three are targeting neutralizing antibodies: the SCoV-2 Detect Neutralizing Ab ELISA (InBios International, Inc.), the Diazyme SARS-CoV-2 Neutralizing Antibody CLIA Kit (Diazyme Laboratories, Inc.), and the cPass

SARS-CoV-2 Neutralization Antibody Detection Kit (GenScript). The list reveals that, besides the classification into binding and neutralizing antibody tests, there are two major groups of tests. ELISAs and chemiluminescence immunoassays (CLIAs) for high-throughput screening, and LFAs for the POCT. The former are mainly microtiter plate assays or microarrays using secondary antibodies labeled with HRP, fluorescence, or chemiluminescence markers. The predominant commercial sVNT in literature is GenScript's cPass SARS-CoV-2 Neutralization Antibody Detection Kit, which uses RBD-conjugated HRP and an ACE2-coated 96-well microplate (**Figure 3a**)[51–54]. Two separate incubation steps at 37 °C are required before signal generation through TMB, with an overall assay time of ~1 h. Many similar assays have been on the market, varying mainly in incubation times, examples are the Leinco COVID-19 ImmunoRank (Leinco Technologies, Inc.)[53] and TECO SARS-CoV-2-AK Surrogate Neutralisation Test (TECOmedical)[52,53]. Fluorescence or chemiluminescence read-outs can shorten the assay time and reduce assay steps and are often fully automated systems. Examples for chemiluminescence assays are the Roche Elecsys Anti-SARS-CoV-2 S[55], which uses biotinylated RBD, ruthenium-RBD conjugates, and streptavidin-conjugated particles for binding antibody detection, and the Diazyme SARS-CoV-2 Neutralizing Antibody CLIA Kit, relying on RBD-modified magnetic microbeads and ACE2-ABEI. They are automated and can generate signals in 18 and 34 min, respectively. Graninger et al. compared seven commercial immunoassays and found that the cPass SARS-CoV-2 Neutralization Antibody Detection Kit showed the most robust quantitative correlation with a live-virus neutralization test, while the ACE2-RBD neutralization assay by DiaPro and the TECO SARS-CoV-2 neutralization antibody assay displayed the highest sensitivity for nAb detection[52]. For the POC detection, LFAs relying on AuNPs or fluorescent markers for signal generation reached the market. The Healgen Scientific SARS-CoV-2 Neutralizing Antibody Rapid Test Cassette[55,56] comprises RBD-conjugated AuNPs which are captured on the ACE2 test line in the absence of neutralizing antibodies. A portable reflectance spectrum analyzer can be used to quantify the response. Similarly, the VERI-Q SARS-CoV-2 Neutralizing Antibody Rapid Test Kit (MiCo BioMed)[57] captures AuNP-RBD bound to ACE2-mouse-Fc on a goat antimouse IgG test line, requiring only 10 µL of serum. More sensitive results can be obtained with fluorescent RBD conjugates used for example in the ichroma COVID-19 nAb test[58]. It is based on capturing an ACE2-biotin conjugate on a streptavidin test line, making it susceptible to interference by biotin. Users are therefore advised to use the test only 24 h after stopping the intake of biotin supplements to ensure assay functionality, where concentrations of 500 ng/mL were shown not to interfere with the assay. When the 1:5 dilution of serum is factored in, this is only slightly below the threshold of 3510 ng/mL (14367 nM) mentioned in the Clinical and Laboratory Standards Institute (CLSI) guideline (EP37), which is 3 times the highest physiological biotin concentration measured in a patient with high biotin dose uptake[59]. Actually, this is a common

problem for diagnostic tests using the streptavidin-biotin interaction, thus testing for biotin interference should be kept in mind during assay development. A different approach is pursued by the PremaLabs Diagnostics SARS-CoV-2 NAb test kit. According to McLean et al., it uses an anti-RBD test line to capture neutralized fluorescently labeled RBD[60]. In the absence of neutralizing antibodies, RBD is bound by ACE2, blocking the binding site of the capture antibody. This approach appears problematic, as neutralizing antibodies binding in a position similar to that of ACE2 could in theory also prevent capture at the test line, causing a false negative result. An advantage of the assay is that it also works with whole blood, while many other tests require serum or plasma. The fluorescence LFIA Finecare 2019-nCoV S-RBD test was advertised with a short assay time of 15 min[61].

To compete with commercially available products newly developed sVNTs should factor in several characteristics. (I) The assay type, i.e., HTS or POC format, including consideration for the involved steps, turn-around time, and need for specialized equipment, which are directly interconnected with the cost of the test. (II) The type of sample that can be used, i.e., serum, plasma, or preferably (finger prick) whole blood for the POC. (III) Desired sensitivity, i.e. qualitative, semiquantitative or quantitative read-out. Besides the choice of signaling agent, the sample volume is important because it directly affects sensitivity. (IV) The choice of conjugation strategy needs to account for the option of adaptation to other variants or viruses. This is intertwined with the protein expression and purification strategy.

## 1.4  New concepts for sVNTs

The following chapters will discuss the advantages and disadvantages of new sVNTs taking into account their applicability as a possible commercial product. For a better overview, they are grouped into HTS and POC formats, with subchapters concerning the method of signal generation and the special cases of homogeneous HTS and signal-on POC sVNTs.

### 1.4.1  High-throughput sVNTs

#### 1.4.1.1  HRP-based detection

Many variations of HRP-based sVNTs have been published, changing target and capture protein as well as signaling conjugates. Correlations to either PRNT or pVNT were provided for some but not all of these, complicating comparison of the formats. **Table 1** lists the capture protein, target protein, signaling conjugate, substrate, incubation time and steps as well as correlations to other neutralization tests for 15 HRP-based sVNTs for easier comparison. Ahn et al. immobilized ACE2 via His$_6$-tag for improved binding of RBD (**Figure 3b**) compared to the commercial cPass sVNT from GenScript (**Figure 3a**)[62]. They biotinylated RBD using sulfo-

NHS-biotin, which is a simple but random strategy because not only the N-terminus but also lysine residues can be biotinylated. Due to a washing step before addition of the streptavidin-HRP conjugate, no interference of biotin is to be expected. The developed sVNT correlated well with both a pVNT ($R^2$ = 0.9006) and the cPass sVNT ($R^2$ = 0.8521), as investigated with a panel consisting of 100 sera, suggesting that biotinylation did not affect antibody or ACE2 binding. Only 2 ng of RBD-biotin are needed per well, while other assays use 100 ng of RBD for coating[63]. This resulted in improved sensitivity, allowing for the use of lower sample volumes compared to its commercial counterpart. Biotinylation of RBD for site-directed immobilization in neutravidin or streptavidin plates should also allow for reduced amounts of RBD in the system[64,65]. Kolesov et al. compared the ACE2 plate plus RBD-HRP system to the RBD plate plus ACE2-HRP system and found the latter to be superior due to better storage performance and easier adaptation to other variants[66]. Mutation of SARS-CoV-2 might affect conjugation, for example by causing different biotinylation patterns for RBD variants as lysines might be exchanged or their direct environment altered. However, this could also affect the immobilization of the protein in the plate. The introduction of Cys-tags or Avi-tags for directed conjugation could be a solution but is time-consuming and might affect protein folding. Liu et al. bypassed such problems by designing recombinant ACE2-Fc-Avi and RBD-Fc-vHRP proteins[67]. The IgG Fc fragment facilitated both purification and dimerization of the ACE2 fusion protein, improving its affinity to RBD. Avi-tag allowed for biotinylation and thus site-directed immobilization in a streptavidin plate. Furthermore, RBD-Fc-vHRP showed ~7 times higher affinity to ACE2 compared to RBD-vHRP. They state that the approach allows for easy adaptation for other RBD variants, because it eliminates the purification and conjugation step for the protein.

Aside from conjugation strategies, the assay layout is of consideration. ELISA's are typically performed in 96-well plates, requiring relatively long incubation times and multiple washing steps. Klüpfel et al. have developed a microarray with chemiluminescence read-out using streptavidin-HRP and $H_2O_2$/luminol to obtain signals in only 7 min[68]. Similarly fast was the approach of Bian et al., who used fiber optic biolayer interferometry in a 96-well plate. The fiber optic probe is coated with streptavidin and biotinylated ACE2 to capture RBD-HRP. They started using 3,3′-diaminobenzidine tetrahydrochloride (DAB), a metal precipitating substrate for signal generation,[69] but later found a more environment- and user-friendly biomaterial 3-Amino-9-ethylcarbazole (AMEC), that increased signal-to-noise ratios and enabled fiber regeneration up to 6 times[70]. The later version was also used for multiplexing. Wang et al. developed another device using fiber optics[71]. Their track-etched microporous membrane filtration microplate allows for washing via capillary syphoning, solely requiring absorbent

paper. Read-out via smartphone is possible due to the use of individual optical fibers connected to the 64 wells, making the device usable at the POC.
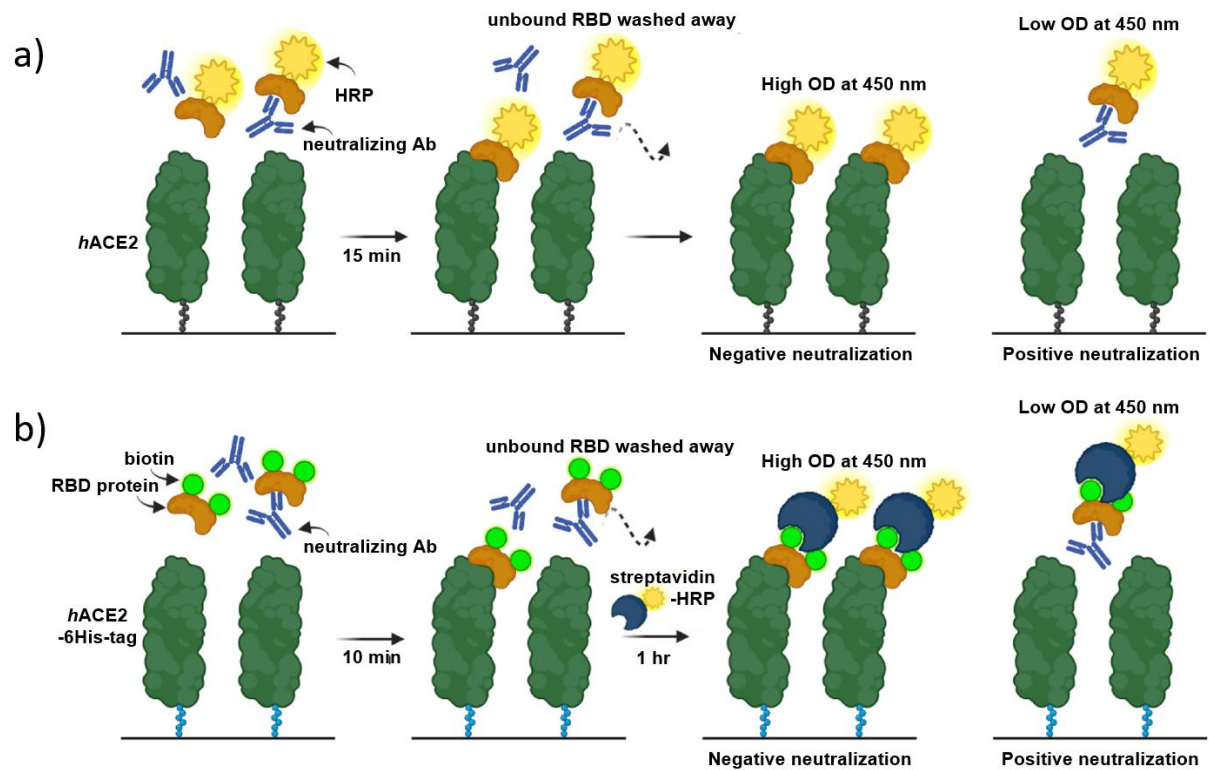


***Figure 3:*** *Illustration of the assay principle of (**a**) GenScript's cPass sVNT kit and (**b**) Ahn et al.'s biotin-based sVNT. Reprinted with permission from ref 62. Copyright 2023 Elsevier.*

**Table 1:** *List of HRP-based surrogate virus neutralization tests.*

| Capture protein (immobilized) | Target protein | Signaling conjugate | Substrate | Correlation to other neutralization tests | Incubation steps and time (excl. substrate reaction) | Ref. |
|---|---|---|---|---|---|---|
| **Enzyme-linked immunosorbent assays (ELISA's) (common microplate-based assays)** | | | | | | |
| His$_6$-ACE2 | RBD-biotin | Streptavidin-HRP | TMB | pVNT, R² = 0.9006, n = 100 / cPass, R² = 0.8521, n = 100 | 10 min + 1 h RT | 62 |
| ACE2 | His-tag-RBD | Anti-His-Ab-HRP | TMB | pVNT, r² = 0.7135, n = 62 | 2x 1 h 37 °C | 72 |
| ACE2 | StrepTag-Spike | Anti-Strep-Ab + anti-Fc-HRP | TMB | cPass, R² = 0.9129, n = 32 | 1 h 37 °C + 1 h RT | 73 |
| ACE2-Fc-Avi-biotin (streptavidin plate) | RBD-Fc-vHRP | RBD-Fc-vHRP | TMB | pVNT, R²= 0.91, n = 19 (WT) / pVNT, R² = 0.90, n = 15 (Delta) | 2x 1 h 37 °C | 67 |
| ACE2/RBD | RBD/ACE2-HRP | RBD/ACE2-HRP | TMB | PRNT, r = 0.855, n = 73 | 2x 30 min 37 °C | 66 |
| RBD | ACE2-biotin | Poly-HRP-streptavidin | TMB | PRNT, R² = 0.6, n = 57 / pVNT, R² = 0.76, n = 20 | 2x 1 h RT | 63 |
| RBD | ACE2-3xFLAG | Anti-FLAG-Ab-HRP | TMB | cVNT, r² = 0.97, n = 26 (non-linear fit) / pVNT, r² = 0.90, n = 29 (non-linear fit) | 3x 30 min 37 °C | 74 |
| RBD | ACE2-biotin | Streptavidin-HRP | SigmaFast OPD | only 5 samples compared to pVNT | 2x 1 h + 20 min RT | 75 |
| mFc-RBD | ACE2-biotin | Streptavidin-HRP | TMB | PRNT, r$_S$ = 0.83, n = 32 | 30 min + 2x 1 h RT | 76 |
| RBD-biotin (neutravidin plate) | ACE2-Fc | Protein-L-HRP | TMB | pVNT, r = 0.74, n = 144 | 1 h + 30 min RT | 64 |
| RBD-biotin (ELISA plate) | His-tag-ACE2 | Anti-His-Ab-HRP | TMB | not correlated | 2 h + 1 h RT | 65 |
| ACE2 | Spike-biotin | Streptavidin-HRP | CL substrate | only used for antibody screening | 1 h + 20 min + 4.5 min | 77 |
| **Alternative formats using HRP-conjugates for signal generation (Microarray, Fiber optic biolayer interferometry, Track-etched microporous membrane)** | | | | | | |
| ACE2 | RBD-biotin | Streptavidin-HRP | H$_2$O$_2$/luminol | YHLO NT, R = -0.87, n = 33 | 7 min | 68 |
| ACE2-biotin (streptavidin probe) | RBD-HRP | RBD-HRP | DAB | ELISA, r = 0.859, n = 15 | 5 min RT (+2 min substrate) | 69 |
| | RBD-HRP | RBD-HRP | AMEC | pVNT, r = 0.983 / 3 sera tested for 3 variants | | 70 |
| ACE2-PS-microbeads (in solution) | RBD-HRP | RBD-HRP | TMB | pVNT, R² = 0.7856, n = 81 | 30 min RT | 71 |

## 1.4.1.2 Fluorescence detection

Fluorescence detection for sVNTs to improve sensitivity compared to the HRP-based assays or to enable multiplexing was investigated by multiple groups. **Table 2** lists the capture protein, target protein, signaling conjugate, substrate, incubation time, and steps as well as correlations to other neutralization tests and comments for 10 fluorescence-based sVNTs for easier comparison. Most dominant is the use of phycoerythrin-conjugated streptavidin as the signaling conjugate[78–83]. Combined with beads that are labeled with a set of spectrally distinct dyes, the main advantage of this approach is its potential for multiplexing. When scanned individually with a red 635 nm laser in a flow cell, up to 80 different beads can be classified and analyzed by the excitation of phycoerythrin with a green 532 nm laser using a Luminex instrument[80]. MagPlex or other magnetic beads were labeled with ACE2, Spike, or RBD as the capture probe, incubated with the target (Spike-biotin or ACE2-Fc/biotin) and serum, followed by the signaling conjugate before analysis in the respective device. The studies revealed good correlation of the developed sVNTs to microneutralization tests, PRNT or cVNT, highlighting their sensitivity. The automation of the system allowed for screening of larger serum panels, with several hundred being used for validation in some cases. Hoffman et al.[81] and Lynch et al.[82] made use of the multiplexing capability and tested several variants. Their assay also had the lowest turnaround times with 60 and 52 min, respectively. Unfortunately, the correlation to different established neutralization tests by each group makes a direct comparison between these sVNTs impossible. This highlights a major obstacle with neutralization tests in general and a call for widely available standards. The WHO generated the international standard for anti-SARS-CoV-2 (NIBSC code: 20/136) and an international reference panel for anti-SARS-CoV-2 (NIBSC code: 20/268) consisting of a seronegative and four seropositive samples with low-to-high antibody levels. Demand obviously was greater than availability, and hence these were only obtained by some of the interested industrial and academic parties. Aside from Hoffman et al.,[81] the reference panel was also used by Ho et al.,[84] who developed a microarray with Spike variant dots and Cy5-ACE2 and Cy3-antihuman antibodies for signal generation. Their test, referred to as CoVariant, showed an excellent correlation to GenScript's cPass sVNT for the WHO reference panel (R² = 0.9728) and was used for the Alpha, Beta, Gamma, Delta and Omicron (B.1.1.529) variants in clinical follow-up studies[85,86]. Results for a similar assay referred to as CoVariant-SCAN were previously published by Heggestad et al. who used RBD instead of Spike and AlexaFluor647 labeled ACE2 instead of Cy5[87]. Another Spike microarray was developed by Su et al. for antibody profiling and ACE2 inhibitor screening using ACE2-biotin and Cy5-streptavidin and Cy3-anti IgG/A/M (**Figure 4**)[88]. Yang et al. devised an automatic testing-on-a-probe biosensor[89]. The RBD-modified probe was subsequently incubated with biotinylated ACE2 and Cy5-streptavidin-polysaccharide before read-out with interim wash steps. This generated qualitative results within 18 min for a single sample or

40 min for 20 samples and correlated well to both PRNT and pVNT. A different advantage can be gained by using liposomes encapsulating sulforhodamine B (SRB), as they facilitate both fluorescence and colorimetric read-out and can thus be used for both an ELISA-type HTS and an LFA-based POC assay[90], respectively.
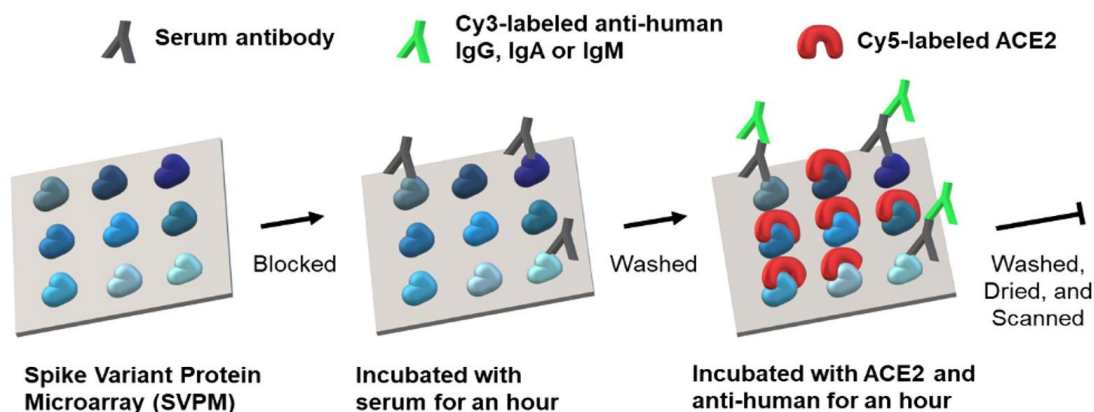


*Figure 4: Schematic of the assay procedure for the spike variant protein microarray (SVPM). Reproduced with permission from ref 88. Copyright 2022 American Chemical Society.*

### 1.4.1.3  Other detection methods

In addition to the two major detection categories of HRP or fluorescence-based detection strategy, SPR, thin-film interferometry, bioluminescence, and chromogenic read-outs have been described, which may provide additional information through their different signaling mechanisms[91–95]. Dong et al. tested online functionalization of a four-channel SPR-chip with S1, Protein G and ACE2 for the simultaneous quantification of antibodies and fully and partially neutralized viral particles[91]. The value of this approach is provided through its detailed information for antibody screening with a reasonable sample throughput considering key performance characteristics of a turn-around time of <12 min, and autosampler-enabled continuous measurements with a single chip for up to 6 days. Modification of a plasmonic chip with a lipid bilayer as the artificial cell membrane provided a biomimetic nanoplasmonic sensor[96]. While the test uses the same underlying principle as the other discussed tests and could be used for nAb detection, the authors went instead for the investigation of monoclonal nAbs as an antiviral therapy, highlighting an alternative application of the sVNT platforms. Thin-film interferometry enabled the development of an automated label-free sVNT based on measuring the binding ability of RBD to ACE2 after neutralization[93]. In a first cycle, the RBD-coated sensing probe is incubated with serum dilutions followed by ACE2 addition after a washing step. In a second cycle, the probe is only incubated with ACE2. The neutralization rate can be calculated as the ratio of the first to the second cycle. Similar to the fluorescence- or HRP-based microarrays discussed above, Springer et al. used a commercial SARS-CoV-2 VoC ViraChip IgG microarray adapted to nAb detection for multiple RBD variants with an ACE2-alkaline phosphatase conjugate for colorimetric signal generation[95]. A colorimetric read-

out was also generated by Kwak et al.'s Janus nanozymes (Ir-Au nanodisks) in combination with TMB/$H_2O_2$[92]. Recently, the use of nano luciferase (NanoLuc) has come into focus for signal generation. Schoefbanker et al. used it for a sensitive ELISA-type assay, incubating RBD-NanoLuc first with serum followed by incubation in an ACE2-coated plate[94]. The main advantage, however, lies in the use of split NanoLuc to facilitate homogeneous assay formats that will be discussed in detail in the next chapter.

## 1.4.1.4 Homogeneous assays

Heterogeneous sVNTs discussed so far almost all required multiple incubation, addition, or washing steps, naturally, making their manual execution laborious and often time-consuming. This could be overcome in several cases by automation, which usually requires special equipment and is therefore costly. Instead, the concept of split reporter molecules avoids the need for washing steps and in some cases even reduces the number of incubation steps. These include split-NanoLuc[97–101], split-oligonucleotides[102] and NIR-II FRET systems[103]. The NanoLuc Binary Technology (BiT) uses two subunits of NanoLuc, the large subunit (LgBiT) consisting of domains β1-9 and the small subunit (SmBiT) consisting of domain β10. The subunits can be either conjugated to proteins or expressed as recombinant fusion proteins, omitting the need for conjugation. The subunits fuse when brought into close proximity, resulting in an active NanoLuc. Alves et al. used commercially available Lumit antibodies (antirabbit Ab-SmBiT and antimouse Ab-LgBiT) and prepared rabbit-Fc-RBD and mouse-Fc-ACE2 for quick adaptation to SARS-CoV-2[97]. Another group prepared LgBiT-ACE2 and SmBiT-S1, circumventing the additional interaction of secondary antibody and Fc fragment[98]. Kim et al. went one step further and used the trimeric full-length Spike to detect neutralizing antibodies against the whole protein and not just those directed against RBD or S1[99]. This remains a topic of debate because many sVNTs rely on the use of only RBD and still correlate well with PRNTs and pVNTs using the whole virus or the S protein. They used a trisplit NanoLuc and produced multiple SmBiT-S variants, including Omicron (B.1.1.529), proving the potential for quick adaptation to emerging variants (**Figure 5**). All assays required 2-3 incubation steps with assay times between 2 h down to slightly over 30 min[98]. The NanoLuc system has been also otherwise identified as a powerful tool in HTS formats, such as for the detection of binding antibodies against the glycoprotein of the nipah virus, producing comparable results to an ELISA[104]. The split-oligonucleotide neighboring inhibition assay (SONIA) used real-time qPCR to measure the ability of neutralizing antibodies blocking the binding between DNA-barcoded S1 and ACE2[102]. Upon interaction of S1 and ACE2, ligation-mediated PCR-amplification of the DNA barcodes is enabled. Due to the amplification reaction, high sensitivity and specificity is achieved in comparison to traditional pVNTs but requires 140 min until read-out. The low volume requirements (4 µL) and broad allowance for the

*Table 2: List of fluorescence-based surrogate virus neutralization tests.*

| Capture protein | Target protein | Signalling conjugate | Comments and correlation to other neutralization tests | Incubation steps and time | Ref. |
|---|---|---|---|---|---|
| **Luminex platform** | | | | | |
| Spike-MagPlex beads | ACE2-Fc | Anti-mouse-IgG-Phycoerythrin | BioPlex 200 reader (BioRad) PRNT, $R^2 = 0.825$, n = 206 | 2x 1 h + 45 min | [80] |
| RBD/Spike-MagPlex beads | ACE2-biotin | Streptavidin-Phycoerythrin | MagPix (Luminex) Wuhan, Delta, and Omicron (B.1.1.529) cVNT (100% qualitative agreement, n = 72 + ECDC and WHO standard) | 45 min + 15 min | [81] |
| Spike variant magnetic beads | ACE2-biotin | Streptavidin-Phycoerythrin | BioPlex 2200 (BioRad) $PRNT_{50}$, $r_s = 0.80$ (76 seropositive and 102 seronegative samples) WT, $\alpha$, $\beta$, $\gamma$, $\delta$, $\kappa$, $\epsilon$ (451 seropositive samples) | 52 min | [82] |
| ACE2-MagPlex beads | Spike-biotin | Streptavidin-R-Phycoerythrin | FlexMap 3D (Luminex) microNT (several hundred sera, no statistical analysis) | 2x 1 h RT | [78] |
| **Microarrays** | | | | | |
| Spike variants | Cy5-ACE2 | Cy3-anti-human-Ab | WHO reference panel in cPass and CoVariant ($R^2 = 0.9728$, n = 5) simultaneous detection of Ig possible | 2x 1 h | [84] [85] [86] |
| RBD variants | ACE2-AlexaFluor647 | ACE2-AlexaFluor647 | CoVariant SCAN (WT, B.1.1.7, B.1.351 and P.1) microNT, r = 0.74, n = 16 | 1 h | [87] |
| Spike variants | ACE2-biotin | Cy5-streptavidin Cy3-anti IgG/A/M | Focus on antibody profiling ACE2 inhibitors Ramipril and Perindopril | 2x 1 h | [88] |
| **Others** | | | | | |
| RBD-coated probe tip | ACE2-biotin | Streptavidin-Cy5-polysaccharide | Automated system PRNT, r = -0.82, n = 46 pVNT, r = -0.80, n = 46 | 40 min (20 tests) 18 min (1 test) | [89] |
| ACE2 | RBD-liposomes encapsulating SRB | RBD-liposomes encapsulating SRB | Dual use for colorimetric LFA and fluorescence microplate HTS assay pVNT, $r_s = 0.847$, n = 20 | 1 h 30 °C + 2 h RT | [90] |
| ACE2-biotin-SA-beads S1-biotin-SA-beads RBD-biotin-SA-beads | RBD/S1-Fc ACE2-Fc/His ACE2-Fc/His | AF488-conjugated polyclonal secondary Ab or PE-anti His tag monoclonal Ab | Flow cytometry, investigation of different models iACE2/RBD-Fc, iACE2/S1-Fc and iS1/ACE2-His worked best PRNT, R = 0.896, n = 20 (iACE2/RBD-Fc) | 30 min 37 °C 30 min + 20 min RT | [105] |

sample type including serum and dried blood spot eluent, renders it an interesting lab-based technology. Zhao et al. could use whole blood as a sample for their assay relying on a pair of lanthanide downshifting nanoparticles to enable a near-infrared II Förster resonance energy transfer (NIR-II FRET)[103]. The $Nd^{3+}$-doped particles served as an energy donor and were modified with RBD, while the $Yb^{3+}$-doped ones served as an energy acceptor modified with ACE2. While an interesting concept, the system currently only measures in a cuvette, making it impractical for HTS. Impedance measurements are another possibility to facilitate homogeneous assays as shown by Manshadi et al. with their ACE2-modified interdigitated electrode, but have only been tested in spiked mouse serum so far[106].
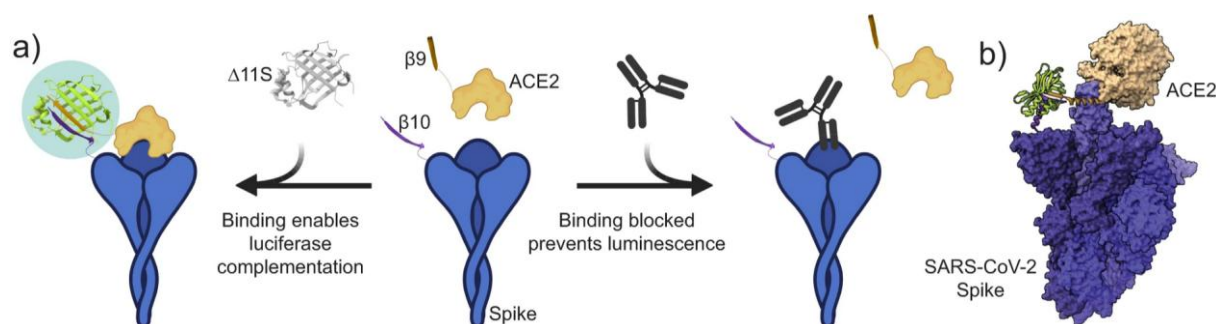


*Figure 5: Illustration of (a) the homogeneous sVNT using Tripart NanoLuc peptide fragments and (b) the molecular model of the predicted refolding of NanoLuc (PDB: 5IBO) (green) after complementation of fragments β10 and β9 driven by the interaction between SARS-CoV-2 spike trimer (purple) and ACE2 (fawn) (PDB: 7A97). Reprinted with permission from ref 99. Copyright 2022 Macmillan Publishers Ltd.. The article is licensed under a Creative Commons Attribution 4.0 International License http://creativecommons.org/licenses/by/4.0/.*

### 1.4.2 POC neutralization tests

#### 1.4.2.1 Colorimetric and fluorescence detection

AuNPs, the predominant signaling agent for LFAs, were used in many commercial POC neutralization tests, meanwhile, academia investigated ways to improve these assays and find potential alternatives. A comparison of 11 colorimetric and 4 fluorescence lateral flow neutralization tests (LFNTs) is given in **Table 3**. Novelties included the overlaying of test strips for multiplexing[107], laser cut test strips for improved sensitivity,[108] and the use of additional test lines[109]. Specifically, Deenin et al. used a paper puncher to prepare mirrored concave holes on the ACE2 test line of two test strips[107]. Delta and Omicron RBD-AuNPs were immobilized on the conjugate pads, enabling multiplexed read-out of the stacked test strips. The smaller test line additionally resulted in improved sensitivity due to concentration of the nanoparticles on the test line. This was also the reasoning behind Mahmud et al.'s laser engraving of both blood filter and nitrocellulose membrane (**Figure 6**)[108]. The blood sample is incubated with the RBD-biotin-streptavidin-AuNPs on the filter pad for 2 min before the addition of running buffer. The laser engraved narrow partition slows the flow and concentrates the sample which passes five individual ACE2 spots. The additional spots improve sensitivity and facilitate a semiquantitative read-out by counting of the visible spots. The usability of whole blood makes

the assay highly useful for the POC and was therefore investigated by several other groups as well[109,110]. The addition of an RBD test line by Fulford et al. enabled simultaneous detection of total anti-RBD antibodies[109]. These correlated less well to a microNT than the neutralizing antibody titers as anticipated, making the added value of such a test line questionable. Variation of the geometric design of the LFA test strips on a large scale for industrial fabrication poses a challenge but could be worthwhile in light of the added benefits. A different solution was presented by a paper-based cellulose-pulldown assay using HRP and TMB for signal generation[111]. While nitrocellulose is better suited for general immobilization of proteins cellulose is cheaper and more readily available. The use of the cellulose binding domain (CBD) facilitates immobilization of the RBD-CBD fusion protein. Wax printing provides a simple means to generate the desired geometries without the need for laser cutting or similar approaches but has waned in research use recently due to the disappearance of commercially available desktop printers. Other colorimetric LFNTs included the use of nanoshells[112], cellulose nanobeads[113], red latex microbeads[114], and liposomes[90]. All assays required 10-20 µL of sample, run times varied between 9 and 25 min and the obtained results allowed qualitative or at best semiquantitative statements. A preincubation step of RBD and serum, as performed for the assay using RBD-liposomes, can potentially enhance sensitivity but is by itself insufficient. The strength of these colorimetric assays is the potential for analysis via smartphone. To provide meaningful data with qualitative statements the assays would need to be tuned to a CoP. Tong et al. managed to develop a quantitative colorimetric LFNT based on the use of RBD-modified polydopamine nanoparticles[115]. These needed to be coated by three polyelectrolytes, a $SiO_2$, and a poly(ethylene glycol) (PEG) layer to prevent nonspecific binding, making particle formation rather complex. Their deep-learning algorithm enabled reliable detection with different smartphones and they could show good correlation to a commercial ELISA ($r_S = 0.951$) and better performance than a AuNP-based LFNT.

To overcome the issue of sensitivity, some groups turned to a fluorescence read-out, as seen more frequently in the LFA field recently. The use of EuNPs conjugated to RBD enabled a quantitative read-out within 20 min with a fluorescence ICS card reader[116]. The Alexa Fluor 594-labeled monoFc-ACE2 based assay of Lim et al. gave semiquantitative results within 10 min, is adaptable to multiple variants, and works with both venous and finger prick blood[117]. Most fluorophores show quenching when in an aggregated state, which is promoted when captured on the test line, resulting in lower sensitivity. Aggregation-induced emission (AIE) luminogens, on the other hand, can benefit from the close proximity of the molecules. Bian et al. encapsulated AIE490 in polystyrene nanoparticles and observed a 10-fold increase of fluorescence compared to free AIE490; the AIE490-NP's were even brighter than quantum dots[118]. Modified with ACE2, the particles facilitated semiquantitative detection of nAbs. The

limit of detection (LOD) was 4 times lower compared to a colorimetric LFA using AuNPs. Slight modification of the assay to obtain a fluorescence-quenching read-out could further improve the LOD 9-fold and will be discussed in more detail in the chapter dealing with signal-on strategies.
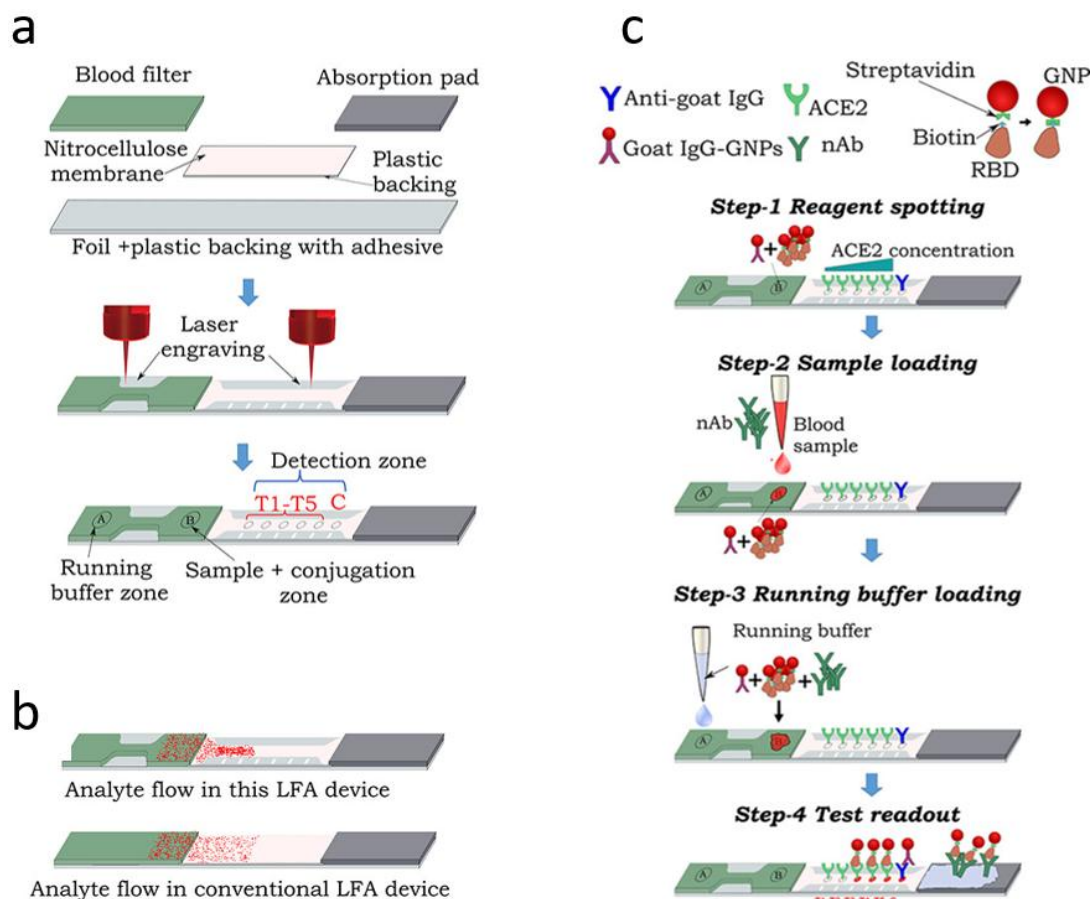


*Figure 6: Schematics of the laser-engraved LFNT. (a) Schematic illustrating the fabrication of the LFA test strip. (b) Visualization of the analyte concentration with custom geometry versus traditional LFA geometry. (c) Schematic of the LFNT procedure. Reproduced with permission from ref 108. Copyright 2024 American Chemical Society.*

**Table 3:** *List of colorimetric and fluorescence LFNT's.*

| Capture protein (immobilized) | Target protein | Signaling conjugate | Comments and correlation to other neutralization tests | Incubation steps and time | Ref. |
|---|---|---|---|---|---|
| **AuNP-based colorimetric LFNT's** | | | | | |
| ACE2 | RBD-AuNP's | RBD-AuNP's | multiplexing (Delta and Omicron) ELISA, $R^2$ = 0.8777, n = 21 | 15 min | 107 |
| ACE2 | RBD-AuNP's | RBD-AuNP's | pVNT, r = 0.918, n = 165 | not mentioned | 119 |
| ACE2 | RBD-biotin | anti-biotin-AuNP's | additional RBD test line for anti-RBD-Ig microNT, $R^2$ = 0.72, n = 135 | 20 min | 109 |
| ACE2 (5 spots) | RBD-biotin | streptavidin-AuNP's | laser-cut narrow membrane no correlation | 2 min + 15 min | 108 |
| ACE2 | Spike-biotin | streptavidin-AuNP's | WHO standard and 10 sera tested, only compared to commercial binding antibody test | 15 min | 110 |
| **Other colorimetric LFNT's** | | | | | |
| RBD-CBD | biotinylated monoFc-ACE2 | streptavidin-HRP (+ TMB) | paper-based cellulose pull-down assay, smartphone read-out pVNT, r = 0.7, n = 48 | 5 min + 3 min | 111 |
| ACE2 | RBD-nanoshells | RBD-nanoshells | microNT, n = 38, grouped by IC50 values | 10 min | 112 |
| ACE2 | RBD | anti-RBD-cellulose nanobeads | also works as antigen test when used without free RBD 10 seropositive and 5 seronegative samples tested, not correlated | 20 min | 113 |
| ACE2 | RBD-red latex microbeads | RBD-red latex microbeads | not correlated | 9 min | 114 |
| ACE2 | RBD-liposomes encapsulating SRB | RBD-liposomes encapsulating SRB | Dual use for colorimetric LFA and fluorescence microplate HTS assay pVNT, $r_S$ = 0.614, n = 20 | 15 min + 25 min | 90 |
| ACE2 | RBD-PVP@SiO$_2$ @PEG@Ab NP's | RBD-PVP@SiO$_2$ @PEG@Ab NP's | ELISA, $r_S$ = 0.951, n = 30 | 20 min | 115 |
| **Fluorescence LFNT's** | | | | | |
| ACE2 | RBD-EuNP's | RBD-EuNP's | cVNT, 88.76% coincidence rate, 216 seronegative and 140 seropositive samples tested | 20 min | 116 |
| RBD-CBD | Alexa Fluor 594-labeled monoFc-ACE2 | Alexa Fluor 594-labeled monoFc-ACE2 | paper-based; venous and finger prick blood; adapted for variants pVNT, r = 0.91, n = 20; cPass, r = 0.839, n = 44 | 3 min + 8 min | 117 |
| RBD | ACE2-ultrabright AIE490NP | ACE2-ultrabright AIE490NP | correlation of fluorescence-quenching LFNT in follow-up publication pVNT, $R^2$ = 0.9796, n = 103 | 20 min | 118 120 |
| ACE2 | RBD-biotin | QD-streptavidin | ELISA, $R^2$ = 0.85, n = 40 pVNT, $R^2$ = 0.53, n = 40 | 10 min | 121 |

33

## 1.4.2.2 Other detection methods

Other read-outs included NIR[122], magnetoresistive[123] and thermal and Raman detection[41] as well as particle counting[124]. NIR is interesting as it benefits from low background signals in biological matrices. Song et al. even developed a hand-held NIR detection device that was 8 times more sensitive than its commercial counterpart[122]. They used $Nd^{3+}$- and $Yb^{3+}$-codoped down-conversion nanoparticles, coated with poly(acrylic acid) to enable EDC/sulfo-NHS coupling of RBD and an ACE2 test line to facilitate read-out within 15 min. Their assay was in qualitative agreement with a commercial ELISA for Alpha and Omicron variants as investigated using 50 sera, but no correlation to an established neutralization test was provided. The giant magnetoresistive (GMR) neutralization test developed by Ng et al. provides an alternative read-out strategy but currently relies on subsequent 1 h incubation steps of serum with RBD-biotin and on the ACE2-chip including washing, necessitating simplification before the assay is ready for the POC[123]. Generally, GMR is an attractive alternative for conventional POC detection as biological samples are nonmagnetic, making the assays virtually background-free, and hand-held and automated POC readers have been established[125,126]. Zhao at el. used AgNPs with Au shell, a PEG-COOH layer allowing for conjugation of the S protein, and an LFA test strip with an ACE2 test line. They compared visual, photothermal, and SERS read-outs[41]. The thermal camera captured images during irradiation with an 808 nm laser (2 W/cm²) and provided 10 times more sensitive results compared to the visual detection. A portable Raman spectrometer with 785 nm laser produced quantitative results identical with those of photothermal detection. This combination of technologies should be investigated more for its applicability for the POC because it could provide a means for qualitative visual read-out by laypersons with the option for quantitative read-out, e.g., by mobile health clinics in areas with limited resources.

## 1.4.2.3 Signal-on strategies

All of the tests described above are "signal-off" strategies because they are based on signal generation in the absence of neutralizing antibodies. Low titers are thus difficult to quantify, as the resulting decrease of bound conjugates might be too small to be measured. Consequently, the tests have poor resolution in the lower and good resolution in the upper nAb titer range. Thus, "signal-on" strategies have been investigated addressing this issue. Besides improved sensitivity, this can make the tests more user-friendly, with increasing signal intensities correlating to increasing and not decreasing antibody titers and thus immunity.

The straightforward approach is to try to capture the neutralized RBD or S protein conjugates. This was done by either an antihuman IgG[127], antihuman IgG + IgM + IgA[128], or protein A[129] in addition to an ACE2 test line (**Figure 7a**). However, these capture all antibodies of the targeted isotype and not only anti-RBD/Spike antibodies. This can be seen by the smaller signal

increase for neutralized compared to the signal decrease for a non-neutralized conjugate (**Figure 7b**). Rather than relying solely on the signal of the neutralized test line, the tests use the ratio of neutralized to non-neutralized test line signals for quantification of nAbs. With total IgG and IgM levels around 10 and 1 g/L, respectively[130], it becomes clear that these test lines need to be highly concentrated to capture sufficient antibodies, while sample volumes have to be kept low to avoid overloading them. Connelly et al. went for a rather high 1:800 dilution of plasma or whole blood, starting out with 1 μL[129]. Only 150 μL of this dilution was then added to an RBD-conjugated 5 mm circular-punched colloidal gold pad. Finally, 75 μL of this solution was used for the LFA, corresponding to only 0.14 nL of the original sample. At such low concentrations it would be expected that only the most potent seropositive samples, if any, could be detected. Nonetheless, they showed the successful capture of neutralized conjugates.

Duan et al. used 10 μL of serum or 20 μL of whole blood, as did most of the previously discussed LFNTs, for their EuNP-based test and obtained an area under the ROC curve of 0.955 for 266 samples when compared with the cPass sVNT[128]. Their results were also in good agreement with the WHO reference panel. Using an antihuman Ig test line, his-RBD and anti-his-antibody-modified quantum dots, Li et al. also required 10 μL of patient sample[127]. The assay showed excellent correlation to an ELISA and good correlation to a pVNT. Two other groups presented "signal-on" strategies with RBD test lines. Zhang et al. developed a double-antigen sandwich LFA using RBD-conjugated latex beads (LB) or fluorescence beads (FB)[131]. They screened nine types of RBD as antigen pairs for the LB and four types for the FB, immobilizing one as test line and conjugating the other to the beads, and chose the combinations that resulted in the lowest signal for a seronegative and the highest signal for a seropositive sample. The optimized systems showed excellent sensitivity and specificity compared to a live-virus neutralization test, as investigated with serum panels consisting of 389 (FB) and 554 (LB) samples. It unfortunately remains unclear what the difference between the nine investigated RBDs is and whether adaptation to other variants is feasible or would require expression and screening of multiple RBD types once again. Bian et al. used the previously discussed AIE490NPs conjugated to RBD or BSA as test lines[120]. Upon binding of ACE2-AuNPs to the RBD-AIE490NPs the fluorescence of the latter is quenched. In the absence of neutralizing antibodies, the assay shows the maximum colorimetric signal for their AuNPs and the minimum fluorescence signal for the RBD-AIE490NP test line. The BSA-AIE490NPs serve as reference, providing the maximum obtainable fluorescence signal. The fluorescence-quenching LFNT showed excellent correlation to a pVNT ($R^2$ = 0.9796, n = 50) and intra- and inter-assay precisions below 15%.
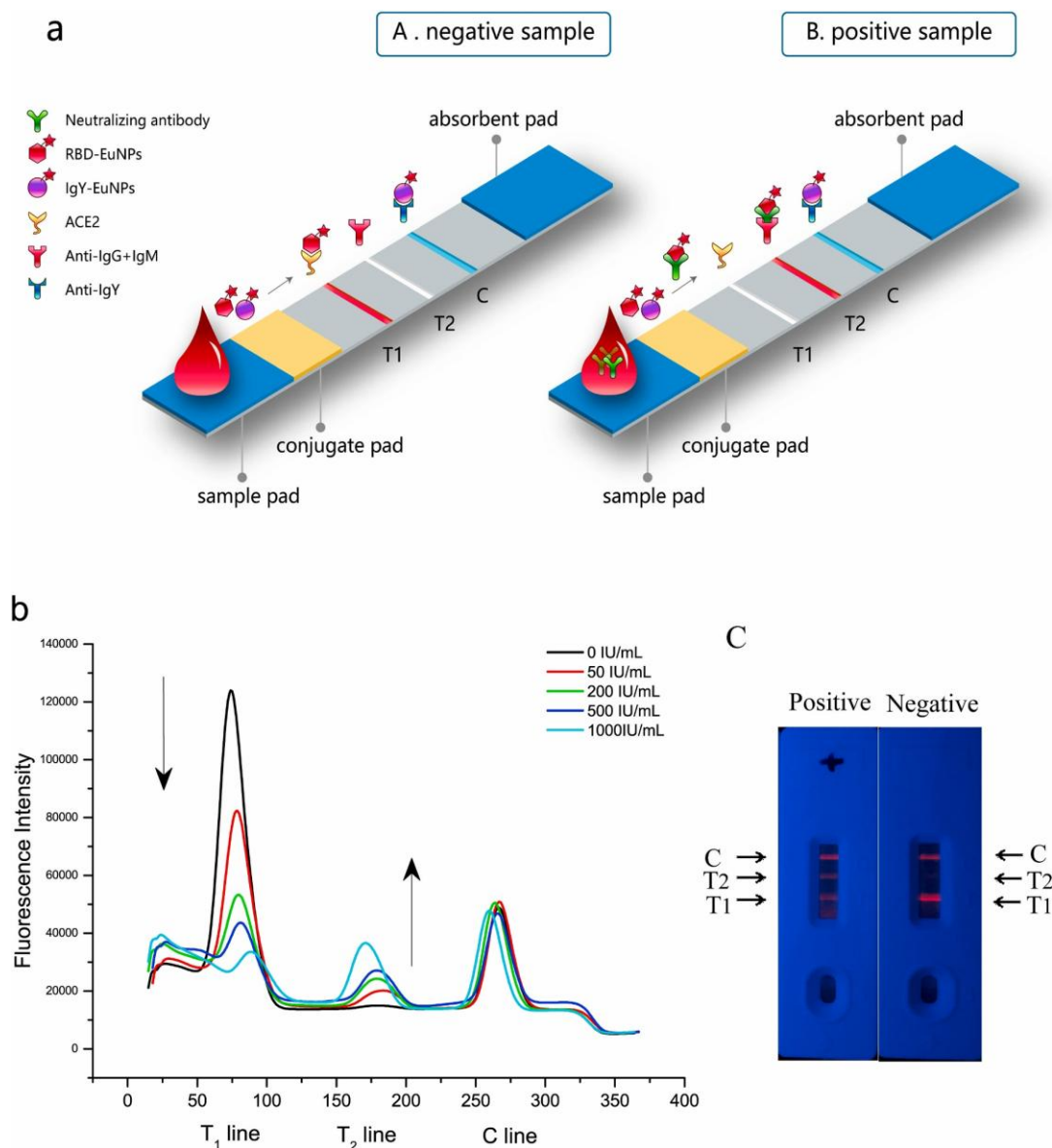
*Figure 7: (a) Schematic of the EuNP-based signal-on LFNT. (b) Inverse relationship of the fluorescence signals toward different concentrations of neutralizing antibody. (c) Positive and negative samples tested using the LFNT cassette. Reprinted with permission from ref 128. Copyright 2022 Elsevier.*

## 1.5  Conclusions and Perspectives

Serological testing continues to be an important tool for the understanding of the immune response and fight against diseases. While binding antibody tests and cell-based neutralization tests have been established for different viruses the recent SARS-CoV-2 pandemic has brought the development of surrogate virus neutralization tests into focus. These promise to fill the gap for rapid, cost-efficient, and large-scale assessment of the immune status of large parts of the population. Much development has occurred within the last 5 years, focusing on

high-throughput screening and POC testing, and many products have reached the market. However, federal agencies such as the U.S. FDA, CDC, NIH, and ECDC have not endorsed their use to assess the need for booster vaccinations due to lack of validation and standardization. Furthermore, the rapid genetic drift of the virus highlights the need for test adaptability while complicating studies to define specific neutralizing antibody titers that work as CoP, which, in turn, requires screening of large serum panels. The sVNT's discussed in this review include many valuable variations of commercialized assay formats as well as novel ones that can improve sensitivity and throughput, reduce assay time, and cost and enable multiplexing. Important advancements for HTS assays include the automated use of microarrays and Luminex technology for multiplexing, and assay simplification achieved by homogeneous platforms enabled, e.g., by the use of split-NanoLuc strategies. For POC detection, several multimodal systems have been developed that could make sensitive serological testing more widely available with the option for qualitative visual or quantitative read-out using portable detectors. It is important to note that at this point there is still no single assay that fulfills all criteria claiming superiority to all the others; rather, each assay has their own strengths and weaknesses. Many choices have to be made prior to and during assay development, including decisions on especially assay and sample type, the desired sensitivity, and the option of adaptation to other variants or viruses.

Due to the pandemic, most advancements in sVNT technology were made based on SARS-CoV-2 as model analyte; however, because the tests need to be adapted to virus variants, they can just as easily be adapted to other viruses altogether. The WHO Pathogens prioritization framework from July 2024 lists bacteria and 29 families of viruses, of which 14 are assigned with a low risk, 2 with a low to medium risk, 2 with a medium risk, and 12 with a high risk for causing Public Health Emergencies of International Concern (PHEICs)[132]. The last category includes Poxviridae as only family of DNA viruses and 10 families of RNA viruses, which include many well-known viruses such as ebola, dengue, influenza, monkeypox, nipah, zika and chikungunya. The list is subject to change because climate change, deforestation, urbanization, international travel, and other major global changes can have a direct or indirect influence on the spread of viruses[133]. Serological testing with PRNTs and pVNTs has been conducted for many of these viruses and, in some cases, identified neutralizing antibodies as CoP, as is the case for SARS-CoV-2, nipah, and ebola according to Escudero-Pérez et al.[134]. Neutralizing antibodies detected using a PRNT or a flow-cytometry based neutralization test were also found to work as potential CoP for chikungunya[135] and dengue viruses[136], respectively. Because such a correlation has been identified, further simplification of the assay could be useful if large-scale screening outside of BSL facilities is desired, e.g. to assist with the licensing of vaccines[137]. This purpose could be served by sVNTs, given that they are

properly validated with the use of standard reference serum panels and the results are found to be in agreement to those of the PRNT.

It is important to consider the potential targets of neutralizing antibodies for each virus to evaluate the possibility for sVNT development. The major target is often the receptor binding protein of the virus[138–140], which is responsible for the interaction between the virus and host cell, but others such as the envelope protein might also be of importance[141,142]. For viruses in the Paramyxoviridae and Orthomyxoviridae families, which includes influenza, neutralizing antibodies target the hemagglutinin glycoproteins, which bind to sialic acid residues on the host cell[143]. Thus, conjugation strategies for both small molecules and proteins would be required. If the targeted protein is subject to frequent mutation, this has to be accounted for regarding the choice of conjugation strategy, which is often directly intertwined with protein expression. Multiplexing for several variants could be of interest in this case and of higher importance than the need for POC application. In general, there are many variables that need to be taken into account when developing sVNTs, which are best addressed by the collaboration of experts from different fields including virology, bioanalytical chemistry, and clinicians. In the end, the technology advancement in HTS and POC for neutralizing antibody detection will, furthermore, affect our ability to detect many other biomarkers that are based on protein-protein interactions. This can be exploited in drug development, in biomarker-based companion diagnostic and precision medicine, and also in the fields relating to prevention such as the secondary health market, lifestyle, nutrition, and food safety applications.

## 1.6  References

(1) Schrag, S. J.; Rota, P. A.; Bellini, W. J. *J. Virol.* **1999**, *73* (1), 51–54.
(2) Bruce, M. G.; Bruden, D.; Hurlburt, D.; Zanis, C.; Thompson, G.; Rea, L.; Toomey, M.; Townshend-Bulson, L.; Rudolph, K.; Bulkow, L.; Spradling, P. R.; Baum, R.; Hennessy, T.; McMahon, B. J. *J. Infect. Dis.* **2016**, *214* (1), 16–22.
(3) Cdc. *Selecting Viruses for the Seasonal Influenza Vaccine.* https://www.cdc.gov/flu/vaccine-process/vaccine-selection.html (accessed 2025-01-09).
(4) Klein, S.; Cortese, M.; Winter, S. L.; Wachsmuth-Melm, M.; Neufeldt, C. J.; Cerikan, B.; Stanifer, M. L.; Boulant, S.; Bartenschlager, R.; Chlanda, P. *Nat. Commun.* **2020**, *11* (1), 5885.
(5) Walls, A. C.; Park, Y.-J.; Tortorici, M. A.; Wall, A.; McGuire, A. T.; Veesler, D. *Cell* **2020**, *181* (2), 281-292.e6.
(6) Shi, R.; Shan, C.; Duan, X.; Chen, Z.; Liu, P.; Song, J.; Song, T.; Bi, X.; Han, C.; Wu, L.; Gao, G.; Hu, X.; Zhang, Y.; Tong, Z.; Huang, W.; Liu, W. J.; Wu, G.; Zhang, B.; Wang, L.; Qi,

J.; Feng, H.; Wang, F.-S.; Wang, Q.; Gao, G. F.; Yuan, Z.; Yan, J. *Nature* **2020**, *584* (7819), 120–124.

(7) Lau, E. H. Y.; Hui, D. S. C.; Tsang, O. T. Y.; Chan, W.; Kwan, M. Y. W.; Chiu, S. S.; Cheng, S. M. S.; Ko, R. L. W.; Li, J. K. C.; Chaothai, S.; Tsang, C. H.; Poon, L. L. M.; Peiris, M. *eClinicalMedicine* **2021**, *41*, 101174.

(8) Barros-Martins, J.; Hammerschmidt, S. I.; Cossmann, A.; Odak, I.; Stankov, M. V.; Morillas Ramos, G.; Dopfer-Jablonka, A.; Heidemann, A.; Ritter, C.; Friedrichsen, M.; Schultze-Florey, C.; Ravens, I.; Willenzon, S.; Bubke, A.; Ristenpart, J.; Janssen, A.; Ssebyatika, G.; Bernhardt, G.; Münch, J.; Hoffmann, M.; Pöhlmann, S.; Krey, T.; Bošnjak, B.; Förster, R.; Behrens, G. M. N. *Nat. Med.* **2021**, *27* (9), 1525–1529.

(9) Polack, F. P.; Thomas, S. J.; Kitchin, N.; Absalon, J.; Gurtman, A.; Lockhart, S.; Perez, J. L.; Pérez Marc, G.; Moreira, E. D.; Zerbini, C.; Bailey, R.; Swanson, K. A.; Roychoudhury, S.; Koury, K.; Li, P.; Kalina, W. V.; Cooper, D.; Frenck, R. W.; Hammitt, L. L.; Türeci, Ö.; Nell, H.; Schaefer, A.; Ünal, S.; Tresnan, D. B.; Mather, S.; Dormitzer, P. R.; Şahin, U.; Jansen, K. U.; Gruber, W. C. *N. Engl. J. Med.* **2020**, *383* (27), 2603–2615.

(10) Keech, C.; Albert, G.; Cho, I.; Robertson, A.; Reed, P.; Neal, S.; Plested, J. S.; Zhu, M.; Cloney-Clark, S.; Zhou, H.; Smith, G.; Patel, N.; Frieman, M. B.; Haupt, R. E.; Logue, J.; McGrath, M.; Weston, S.; Piedra, P. A.; Desai, C.; Callahan, K.; Lewis, M.; Price-Abbott, P.; Formica, N.; Shinde, V.; Fries, L.; Lickliter, J. D.; Griffin, P.; Wilkinson, B.; Glenn, G. M. *N. Engl. J. Med.* **2020**, *383* (24), 2320–2332.

(11) Zhang, Y.; Zeng, G.; Pan, H.; Li, C.; Hu, Y.; Chu, K.; Han, W.; Chen, Z.; Tang, R.; Yin, W.; Chen, X.; Hu, Y.; Liu, X.; Jiang, C.; Li, J.; Yang, M.; Song, Y.; Wang, X.; Gao, Q.; Zhu, F. *Lancet Infect. Dis.* **2021**, *21* (2), 181–192.

(12) Perry, J.; Osman, S.; Wright, J.; Richard-Greenblatt, M.; Buchan, S. A.; Sadarangani, M.; Bolotin, S. *PLOS ONE* **2022**, *17* (4), e0266852.

(13) Khoury, D. S.; Cromer, D.; Reynaldi, A.; Schlub, T. E.; Wheatley, A. K.; Juno, J. A.; Subbarao, K.; Kent, S. J.; Triccas, J. A.; Davenport, M. P. *Nat. Med.* **2021**, *27* (7), 1205–1211.

(14) Earle, K. A.; Ambrosino, D. M.; Fiore-Gartland, A.; Goldblatt, D.; Gilbert, P. B.; Siber, G. R.; Dull, P.; Plotkin, S. A. *Vaccine* **2021**, *39* (32), 4423–4428.

(15) Sobhani, K.; Cheng, S.; Binder, R. A.; Mantis, N. J.; Crawford, J. M.; Okoye, N.; Braun, J. G.; Joung, S.; Wang, M.; Lozanski, G.; King, C. L.; Roback, J. D.; Granger, D. A.; Boppana, S. B.; Karger, A. B. *Vaccines (Basel)* **2023**, *11* (11), 1644.

(16) Plotkin, S. A. *Clin. Vaccine Immunol.* **2010**, *17* (7), 1055–1065.

(17) Muruato, A. E.; Fontes-Garfias, C. R.; Ren, P.; Garcia-Blanco, M. A.; Menachery, V. D.; Xie, X.; Shi, P.-Y. *Nat. Commun.* **2020**, *11* (1), 4059.

(18) Einhauser, S.; Peterhoff, D.; Niller, H. H.; Beileke, S.; Günther, F.; Steininger, P.; Burkhardt, R.; Heid, I. M.; Pfahlberg, A. B.; Überla, K.; Gefeller, O.; Wagner, R. *Diagnostics* **2021**, *11* (10), 1843.

(19) Nie, J.; Li, Q.; Wu, J.; Zhao, C.; Hao, H.; Liu, H.; Zhang, L.; Nie, L.; Qin, H.; Wang, M.; Lu, Q.; Li, X.; Sun, Q.; Liu, J.; Fan, C.; Huang, W.; Xu, M.; Wang, Y. *Emerg. Microbes Infect.* **2020**, *9* (1), 680–686.

(20) Riepler, L.; Rössler, A.; Falch, A.; Volland, A.; Borena, W.; Laer, D. von; Kimpel, J. *Vaccines (Basel)* **2020**, *9* (1).

(21) Rocha, V. P. C.; Quadros, H. C.; Fernandes, A. M. S.; Gonçalves, L. P.; Da Badaró, R. J. S.; Soares, M. B. P.; Machado, B. A. S. *Viruses* **2023**, *15* (7), 1504.

(22) Sun, Y.; Huang, W.; Xiang, H.; Nie, J. *Vaccines (Basel)* **2024**, *12* (5), 554.

(23) Vaidya, S. R. *Viruses* **2023**, *15* (4), 939.

(24) Antibody (Serology) Testing for COVID-19: Information for Patients and Consumers. *FDA,* Thu, Nov 14, 2024. https://www.fda.gov/medical-devices/coronavirus-covid-19-and-medical-devices/antibody-serology-testing-covid-19-information-patients-and-consumers (accessed 2025-01-10).

(25) In Vitro Diagnostics Emergency Use Authorizations (EUAs) - Serology and Other Adaptive Immune Response Tests for SARS-CoV-2. *FDA,* Mon, Dec 30, 2024. https://www.fda.gov/medical-devices/covid-19-emergency-use-authorizations-medical-devices/in-vitro-diagnostics-emergency-use-authorizations-euas-serology-and-other-adaptive-immune-response (accessed 2025-01-09).

(26) Sun, B.; Feng, Y.; Mo, X.; Zheng, P.; Wang, Q.; Li, P.; Peng, P.; Liu, X.; Chen, Z.; Huang, H.; Zhang, F.; Luo, W.; Niu, X.; Hu, P.; Wang, L.; Peng, H.; Huang, Z.; Feng, L.; Li, F.; Zhang, F.; Li, F.; Zhong, N.; Chen, L. *Emerg. Microbes Infect.* **2020**, *9* (1), 940–948.

(27) Kontou, P. I.; Braliou, G. G.; Dimou, N. L.; Nikolopoulos, G.; Bagos, P. G. *Diagnostics* **2020**, *10* (5), 319.

(28) Hossain, F.; Shen, Q.; Balasuriya, N.; Law, J. L. M.; Logan, M.; Houghton, M.; Tyrrell, D. L.; Joyce, M. A.; Serpe, M. J. *Anal. Chem.* **2023**, *95* (19), 7620–7629.

(29) Peng, R.; Pan, Y.; Li, Z.; Qin, Z.; Rini, J. M.; Liu, X. *Biosens. Bioelectron.* **2022**, *197*, 113762.

(30) Nunez, F. A.; Castro, A. C. H.; Oliveira, V. L. de; Lima, A. C.; Oliveira, J. R.; Medeiros, G. X. de; Sasahara, G. L.; Santos, K. S.; Lanfredi, A. J. C.; Alves, W. A. *ACS Biomater. Sci. Eng.* **2023**, *9* (1), 458–473.

(31) Shen, H.; Chen, X.; Zeng, L.; Xu, X.; Tao, Y.; Kang, S.; Lu, Y.; Lian, M.; Yang, C.; Zhu, Z. *Anal. Chem.* **2022**, *94* (23), 8458–8465.

(32) Kim, J.; Lee, S.; Kim, H. *Sens. Actuators B Chem.* **2023**, *394*, 134381.

(33) Eryilmaz, M.; Goncharov, A.; Han, G.-R.; Joung, H.-A.; Ballard, Z. S.; Ghosh, R.; Zhang, Y.; Di Carlo, D.; Ozcan, A. *ACS Nano* **2024**, *18* (26), 16819–16831.

(34) Mou, L.; Zhang, Y.; Feng, Y.; Hong, H.; Xia, Y.; Jiang, X. *Anal. Chem.* **2022**, *94* (5), 2510–2516.

(35) Nan, J.; Chen, Y.; Sun, W.; Yue, Y.; Che, Y.; Shan, H.; Xu, W.; Liu, B.; Zhu, S.; Zhang, J.; Yang, B. *Nano Lett.* **2023**, *23* (23), 10892–10900.

(36) Su, W.-Y.; Ho, T.-S.; Tsai, T.-C.; Du, P.-X.; Tsai, P.-S.; Keskin, B. B.; Shizen, M. A.; Lin, P.-C.; Lin, W.-H.; Shih, H.-C.; Syu, G.-D. *Biosens. Bioelectron.* **2023**, *241*, 115709.

(37) Zhang, Z.; Wang, X.; Wei, X.; Zheng, S. W.; Lenhart, B. J.; Xu, P.; Li, J.; Pan, J.; Albrecht, H.; Liu, C. *Biosens. Bioelectron.* **2021**, *181*, 113134.

(38) Huang, L.; Li, Y.; Luo, C.; Chen, Y.; Touil, N.; Annaz, H.-E.; Zeng, S.; Dang, T.; Liang, J.; Hu, W.; Xu, H.; Tu, J.; Wang, L.; Shen, Y.; Liu, G. L. *Biosens. Bioelectron.* **2022**, *199*, 113868.

(39) Kilgour, K. M.; Turner, B. L.; Daniele, M.; Menegatti, S. *Anal. Chem.* **2023**, *95* (27), 10368–10375.

(40) Liang, P.; Guo, Q.; Zhao, T.; Wen, C.-Y.; Tian, Z.; Shang, Y.; Xing, J.; Jiang, Y.; Zeng, J. *Anal. Chem.* **2022**, *94* (23), 8466–8473.

(41) Zhao, T.; Liang, P.; Ren, J.; Zhu, J.; Yang, X.; Bian, H.; Li, J.; Cui, X.; Fu, C.; Xing, J.; Wen, C.; Zeng, J. *Anal. Chim. Acta* **2023**, *1255*, 341102.

(42) Lee, S.; Bi, L.; Chen, H.; Lin, D.; Mei, R.; Wu, Y.; Chen, L.; Joo, S.-W.; Choo, J. *Chem. Soc. Rev.* **2023**, *52* (24), 8500–8530.

(43) Yari, P.; Liang, S.; Chugh, V. K.; Rezaei, B.; Mostufa, S.; Krishna, V. D.; Saha, R.; Cheeran, M. C.-J.; Wang, J.-P.; Gómez-Pastora, J.; Wu, K. *Anal. Chem.* **2023**, *95* (42), 15419–15449.

(44) Dong, T.; Wang, M.; Liu, J.; Ma, P.; Pang, S.; Liu, W.; Liu, A. *Chem. Sci.* **2023**, *14* (23), 6149–6206.

(45) Kahane, S.; Goldstein, V.; Sarov, I. *Intervirology* **1979**, *12* (1), 39–46.

(46) Duermeyer, W.; Wielaard, F.; van der Veen, J. *J. Med. Virol.* **1979**, *4* (1), 25–32.

(47) Vejtorp, M.; Fanøe, E.; Leerhoy, J. *Acta path. microbiol. immunol. scand. Sect B* **1979**, *87B* (3), 155–160.

(48) Lee, H.; Ryu, J. H.; Yun, S.; Jang, J. H.; Choi, A. R.; Cho, S. Y.; Park, C.; Lee, D. G.; Oh, E. J. *Infect. Chemother.* **2020**, *52* (4), 611–615.

(49) Historical Information about Device Emergency Use Authorizations. *FDA,* Mon, Jan 13, 2025. https://www.fda.gov/medical-devices/emergency-use-authorizations-medical-devices/historical-information-about-device-emergency-use-authorizations (accessed 2025-01-15).

(50) COVID-19 Tests Granted Traditional Marketing Authorization by the FDA. *FDA,* Tue, Jan 14, 2025. https://www.fda.gov/medical-devices/coronavirus-covid-19-and-medical-devices/covid-19-tests-granted-traditional-marketing-authorization-fda (accessed 2025-01-15).

(51) Indrati, A. R.; Horian, E.; Dewi, N. S.; Suraya, N.; Tiara, M. R.; Djauhari, H.; Alisjahbana, B. *Diagnostics* **2024**, *14* (16), 1776.

(52) Graninger, M.; Jani, C. M.; Reuberger, E.; Prüger, K.; Gaspar, P.; Springer, D. N.; Borsodi, C.; Weidner, L.; Rabady, S.; Puchhammer-Stöckl, E.; Jungbauer, C.; Höltl, E.; Aberle, J. H.; Stiasny, K.; Weseslindtner, L. *Microbiol. Spectr.* **2023**, *11* (1), e0231422.

(53) Kohmer, N.; Rühl, C.; Ciesek, S.; Rabenau, H. F. *J. Clin. Med.* **2021**, *10* (10).

(54) Perera, Ranawaka A. P. M.; Ko, R.; Tsang, O. T. Y.; Hui, D. S. C.; Kwan, M. Y. M.; Brackman, C. J.; To, E. M. W.; Yen, H.; Leung, K.; Cheng, S. M. S.; Chan, K. H.; Chan, K. C. K.; Li, K.-C.; Saif, L.; Barrs, V. R.; Wu, J. T.; Sit, T. H. C.; Poon, L. L. M.; Peiris, M. *J. Clin. Microbiol.* **2021**, *59* (2).

(55) McGrath, J.; O'Doherty, L.; Conlon, N.; Dunne, J.; Brady, G.; Ibrahim, A.; McCormack, W.; Walsh, C.; Domegan, L.; Walsh, S.; Kenny, C.; Allen, N.; Fleming, C.; Bergin, C. *Front. Public Health* **2023**, *11*, 1245464.

(56) Huang, R.-L.; Fu, Y.-C.; Wang, Y.-C.; Hong, C.; Yang, W.-C.; Wang, I.-J.; Sun, J.-R.; Chen, Y.; Shen, C.-F.; Cheng, C.-M. *Vaccines (Basel)* **2022**, *10* (2).

(57) Kweon, O. J.; Bae, J.-Y.; Lim, Y. K.; Choi, Y.; Lee, S.; Park, M.-S.; Suh, I. B.; Kim, H.; Jee, Y. S.; Lee, M.-K. *Sci. Rep.* **2023**, *13* (1), 4961.

(58) Hirabidian, M.; Bocket, L.; Demaret, J.; Vuotto, F.; Rabat, A.; Faure, K.; Labalette, M.; Hober, D.; Lefevre, G.; Alidjinou, E. K. *J. Clin. Virol.* **2022**, *155*, 105268.

(59) Luong, J. H. T.; Vashist, S. K. *ACS Omega* **2020**, *5* (1), 10–18.

(60) McLean, G. R.; Zhang, Y.; Ndoyi, R.; Martin, A.; Winer, J. *Vaccines (Basel)* **2022**, *10* (12), 2149.

(61) Shurrab, F. M.; Younes, N.; Al-Sadeq, D. W.; Liu, N.; Qotba, H.; Abu-Raddad, L. J.; Nasrallah, G. K. *Int. J. Infect. Dis.* **2022**, *118*, 132–137.

(62) Ahn, M.-J.; Kang, J.-A.; Hong, S. M.; Lee, K.-S.; Kim, D. H.; Song, D.; Jeong, D. G. *Biochem. Biophys. Res. Commun.* **2023**, *646*, 8–18.

(63) Abe, K. T.; Li, Z.; Samson, R.; Samavarchi-Tehrani, P.; Valcourt, E. J.; Wood, H.; Budylowski, P.; Dupuis, A. P.; Girardin, R. C.; Rathod, B.; Wang, J. H.; Barrios-Rodiles, M.; Colwill, K.; McGeer, A. J.; Mubareka, S.; Gommerman, J. L.; Durocher, Y.; Ostrowski, M.; McDonough, K. A.; Drebot, M. A.; Drews, S. J.; Rini, J. M.; Gingras, A.-C. *JCI Insight* **2020**, *5* (19).

(64) Byrnes, J. R.; Zhou, X. X.; Lui, I.; Elledge, S. K.; Glasgow, J. E.; Lim, S. A.; Loudermilk, R. P.; Chiu, C. Y.; Wang, T. T.; Wilson, M. R.; Leung, K. K.; Wells, J. A. *mSphere* **2020**, *5* (5).

(65) Cao, Y.; Su, B.; Guo, X.; Sun, W.; Deng, Y.; Bao, L.; Zhu, Q.; Zhang, X.; Zheng, Y.; Geng, C.; Chai, X.; He, R.; Li, X.; Lv, Q.; Zhu, H.; Deng, W.; Xu, Y.; Wang, Y.; Qiao, L.; Tan, Y.; Song, L.; Wang, G.; Du, X.; Gao, N.; Liu, J.; Xiao, J.; Su, X.; Du, Z.; Feng, Y.; Qin, C.; Qin, C.; Jin, R.; Xie, X. S. *Cell* **2020**, *182* (1), 73-84.e16.

(66) Kolesov, D. E.; Sinegubova, M. V.; Dayanova, L. K.; Dolzhikova, I. V.; Vorobiev, I. I.; Orlova, N. A. *Diagnostics* **2022**, *12* (2).

(67) Liu, H.; Liu, T.; Wang, A.; Liang, C.; Zhu, X.; Zhou, J.; Chen, Y.; Liu, Y.; Qi, Y.; Chen, W.; Zhang, G. *Anal. Chem.* **2024**, *96* (46), 18437–18444.

(68) Klüpfel, J.; Paßreiter, S.; Rumpf, M.; Christa, C.; Holthoff, H.-P.; Ungerer, M.; Lohse, M.; Knolle, P.; Protzer, U.; Elsner, M.; Seidel, M. *Anal. Bioanal. Chem.* **2022**, 1–14.

(69) Bian, S.; Shang, M.; Sawan, M. *Biosens. Bioelectron.* **2022**, *204*, 114054.

(70) Bian, S.; Shang, M.; Tao, Y.; Wang, P.; Xu, Y.; Wang, Y.; Shen, Z.; Sawan, M. *Vaccines (Basel)* **2024**, *12* (4), 352.

(71) Wang, C.; Wu, Z.; Liu, B.; Zhang, P.; Lu, J.; Li, J.; Zou, P.; Li, T.; Fu, Y.; Chen, R.; Zhang, L.; Fu, Q.; Li, C. *Biosens. Bioelectron.* **2021**, *192*, 113550.

(72) Bošnjak, B.; Stein, S. C.; Willenzon, S.; Cordes, A. K.; Puppe, W.; Bernhardt, G.; Ravens, I.; Ritter, C.; Schultze-Florey, C. R.; Gödecke, N.; Martens, J.; Kleine-Weber, H.; Hoffmann, M.; Cossmann, A.; Yilmaz, M.; Pink, I.; Hoeper, M. M.; Behrens, G. M. N.; Pöhlmann, S.; Blasczyk, R.; Schulz, T. F.; Förster, R. *Cell. Mol. Immunol.* **2021**, *18* (4), 936–944.

(73) Eliadis, P.; Mais, A.; Papazisis, A.; Loxa, E. K.; Dimitriadis, A.; Sarrigeorgiou, I.; Backovic, M.; Agallou, M.; Zouridakis, M.; Karagouni, E.; Lazaridis, K.; Mamalaki, A.; Lymberi, P. *Vaccines (Basel)* **2024**, *12* (8), 914.

(74) Kostin, N. N.; Bobik, T. V.; Skryabin, G. A.; Simonova, M. A.; Knorre, V. D.; Abrikosova, V. A.; Mokrushina, Y. A.; Smirnov, I. V.; Aleshenko, N. L.; Kruglova, N. A.; Mazurov, D. V.; Nikitin, A. E.; Gabibov, A. G. *Acta Naturae* **2022**, *14* (3), 109–119.

(75) Phelan, T.; Dunne, J.; Conlon, N.; Cheallaigh, C. N.; Abbott, W. M.; Faba-Rodriguez, R.; Amanat, F.; Krammer, F.; Little, M. A.; Hughes, G.; Bergin, C.; Kerr, C.; Sundaresan, S.; Long, A.; McCormack, W.; Brady, G. *Viruses* **2021**, *13* (7).

(76) Wisnewski, A. V.; Liu, J.; Lucas, C.; Klein, J.; Iwasaki, A.; Cantley, L.; Fazen, L.; Campillo Luna, J.; Slade, M.; Redlich, C. A. *PLOS ONE* **2022**, *17* (1), e0262657.

(77) Wu, W.; Tan, X.; Zupancic, J.; Schardt, J. S.; Desai, A. A.; Smith, M. D.; Zhang, J.; Xie, L.; Oo, M. K.; Tessier, P. M.; Fan, X. *Anal. Chem.* **2022**, *94* (10), 4504–4512.

(78) Mravinacova, S.; Jönsson, M.; Christ, W.; Klingström, J.; Yousef, J.; Hellström, C.; Hedhammar, M.; Havervall, S.; Thålin, C.; Pin, E.; Tegel, H.; Nilsson, P.; Månberg, A.; Hober, S. *New Biotechnol.* **2022**, *66*, 46–52.

(79) Gniffke, E. P.; Harrington, W. E.; Dambrauskas, N.; Jiang, Y.; Trakhimets, O.; Vigdorovich, V.; Frenkel, L.; Sather, D. N.; Smith, S. E. P. *J. Infect. Dis.* **2020**, *222* (12), 1965–1973.

(80) Fenwick, C.; Turelli, P.; Pellaton, C.; Farina, A.; Campos, J.; Raclot, C.; Pojer, F.; Cagno, V.; Nusslé, S. G.; D'Acremont, V.; Fehr, J.; Puhan, M.; Pantaleo, G.; Trono, D. *Sci. Transl. Med.* **2021**, *13* (605).

(81) Hoffman, T.; Kolstad, L.; Akaberi, D.; Järhult, J. D.; Rönnberg, B.; Lundkvist, Å. *Viruses* **2023**, *15* (6), 1280.

(82) Lynch, K. L.; Zhou, S.; Kaul, R.; Walker, R.; Wu, A. H. *Clin. Chem.* **2022**, *68* (5), 702–712.

(83) Roth, S.; Danielli, A. *Sensors* **2021**, *21* (14), 4814.

(84) Ho, T.-S.; Du, P.-X.; Su, W.-Y.; Santos, H. M.; Lin, Y.-L.; Chou, Y.-Y.; Keskin, B. B.; Pau, C. H.; Syu, G.-D. *Biosens. Bioelectron.* **2022**, *204*, 114067.

(85) Du, P.-X.; Chang, S.-S.; Ho, T.-S.; Shih, H.-C.; Tsai, P.-S.; Syu, G.-D. *Virulence* **2024**, *15* (1), 2351266.

(86) Kuo, H.-C.; Kuo, K.-C.; Du, P.-X.; Keskin, B. B.; Su, W.-Y.; Ho, T.-S.; Tsai, P.-S.; Pau, C. H.; Shih, H.-C.; Huang, Y.-H.; Weng, K.-P.; Syu, G.-D. *Mol. Cell. Proteomics* **2023**, *22* (4), 100507.

(87) Heggestad, J. T.; Britton, R. J.; Kinnamon, D. S.; Wall, S. A.; Joh, D. Y.; Hucknall, A. M.; Olson, L. B.; Anderson, J. G.; Mazur, A.; Wolfe, C. R.; Oguin, T. H.; Sullenger, B. A.; Burke, T. W.; Kraft, B. D.; Sempowski, G. D.; Woods, C. W.; Chilkoti, A. *Sci. Adv.* **2021**, *7* (49), eabl7682.

(88) Su, W.-Y.; Du, P.-X.; Santos, H. M.; Ho, T.-S.; Keskin, B. B.; Pau, C. H.; Yang, A.-M.; Chou, Y.-Y.; Shih, H.-C.; Syu, G.-D. *Anal. Chem.* **2022**, *94* (17), 6529–6539.

(89) Yang, H. S.; Racine-Brzostek, S. E.; Karbaschi, M.; Yee, J.; Dillard, A.; Steel, P. A. D.; Lee, W. T.; McDonough, K. A.; Qiu, Y.; Ketas, T. J.; Francomano, E.; Klasse, P. J.; Hatem, L.; Westblade, L.; Wu, H.; Chen, H.; Zuk, R.; Tan, H.; Girardin, R. C.; Dupuis, A. P.; Payne, A. F.; Moore, J. P.; Cushing, M. M.; Chadburn, A.; Zhao, Z. *Biosens. Bioelectron.* **2021**, *178*, 113008.

(90) Streif, S.; Neckermann, P.; Spitzenberg, C.; Weiss, K.; Hoecherl, K.; Kulikowski, K.; Hahner, S.; Noelting, C.; Einhauser, S.; Peterhoff, D.; Asam, C.; Wagner, R.; Baeumner, A. J. *Anal. Bioanal. Chem.* **2023**, *415* (8), 1421–1435.

(91) Dong, T.; Han, C.; Jiang, M.; Zhang, T.; Kang, Q.; Wang, P.; Zhou, F. *ACS Sens* **2022**, *7* (11), 3560–3570.

(92) Kwak, S.-H.; Jeong, D. G.; Shon, H. K.; Kim, D.-H.; Lee, T. G.; Wi, J.-S.; Na, H.-K. *ACS Appl. Mater. Interfaces* **2023**, *15* (48), 55975–55983.

(93) Luo, Y. R.; Yun, C.; Chakraborty, I.; Wu, A. H. B.; Lynch, K. L. *J. Clin. Microbiol.* **2021**, *59* (7).

(94) Schoefbaenker, M.; Neddermeyer, R.; Guenther, T.; Mueller, M. M.; Romberg, M.-L.; Classen, N.; Hennies, M. T.; Hrincius, E. R.; Ludwig, S.; Kuehn, J. E.; Lorentzen, E. U. *Vaccines (Basel)* **2023**, *11* (12), 1832.

(95) Springer, D. N.; Höltl, E.; Prüger, K.; Puchhammer-Stöckl, E.; Aberle, J. H.; Stiasny, K.; Weseslindtner, L. *Vaccines (Basel)* **2024**, *12* (1), 94.

(96) Batool, R.; Soler, M.; Colavita, F.; Fabeni, L.; Matusali, G.; Lechuga, L. M. *Biosens. Bioelectron.* **2023**, *226*, 115137.

(97) Alves, J.; Engel, L.; Vasconcelos Cabral, R. de; Rodrigues, E. L.; Jesus Ribeiro, L. de; Higa, L. M.; Da Costa Ferreira Júnior, O.; Castiñeiras, Terezinha Marta P. P.; Carvalho Leitão, I. de; Tanuri, A.; Goueli, S. A.; Zegzouti, H. *Sci. Rep.* **2021**, *11* (1), 18428.

(98) Huang, D.; Tran, J. T.; Peng, L.; Yang, L.; Suhandynata, R. T.; Hoffman, M. A.; Zhao, F.; Song, G.; He, W.; Limbo, O.; Callaghan, S.; Landais, E.; Andrabi, R.; Sok, D.; Jardine, J. G.; Burton, D. R.; Voss, J. E.; Fitzgerald, R. L.; Nemazee, D. *J. Immunol.* **2021**, *207* (1), 344–351.

(99) Kim, S. J.; Yao, Z.; Marsh, M. C.; Eckert, D. M.; Kay, M. S.; Lyakisheva, A.; Pasic, M.; Bansal, A.; Birnboim, C.; Jha, P.; Galipeau, Y.; Langlois, M.-A.; Delgado, J. C.; Elgort, M. G.; Campbell, R. A.; Middleton, E. A.; Stagljar, I.; Owen, S. C. *Nat. Commun.* **2022**, *13* (1), 3716.

(100) Li, J.; Wang, J.-L.; Zhang, W.-L.; Tu, Z.; Cai, X.-F.; Wang, Y.-W.; Gan, C.-Y.; Deng, H.-J.; Cui, J.; Shu, Z.-C.; Long, Q.-X.; Chen, J.; Tang, N.; Hu, X.; Huang, A.-L.; Hu, J.-L. *Biosens. Bioelectron.* **2022**, *209*, 114226.

(101) Lin, C.-H.; Yang, X.-R.; Lin, M.-W.; Chang, H.-J.; Lee, C.-H.; Lin, C.-S. *Biosens. Bioelectron.* **2024**, *263*, 116630.

(102) Danh, K.; Karp, D. G.; Singhal, M.; Tankasala, A.; Gebhart, D.; Jesus Cortez, F. de; Tandel, D.; Robinson, P. V.; Seftel, D.; Stone, M.; Simmons, G.; Bagri, A.; Schreiber, M. A.; Buser, A.; Holbro, A.; Battegay, M.; Morris, M. K.; Hanson, C.; Mills, J. R.; Granger, D.; Theel, E. S.; Stubbs, J. R.; Corash, L. M.; Tsai, C. *Nat. Commun.* **2022**, *13* (1), 4212.

(103) Zhao, L.; Song, Q.; Mai, W.; Deng, M.; Lei, Y.; Chen, L.; Kong, W.; Zhang, L.; Zhang, L.; Li, Y.; Ye, H.; Qin, Y.; Zhang, T.; Hu, Y.; Ji, T.; Wei, W. *Chem. Eng. J.* **2023**, *468*, 143616.

(104) Bergeron, É.; Chiang, C.-F.; Lo, M. K.; Karaaslan, E.; Satter, S. M.; Rahman, M. Z.; Hossain, M. E.; Aquib, W. R.; Rahman, D. I.; Sarwar, S. B.; Montgomery, J. M.; Klena, J. D.; Spiropoulou, C. F. *Emerg. Microbes Infect.* **2024**, *13* (1), 2398640.

(105) Yao, X.; Zhang, Z.; Mei, Q.; Li, S.; Xing, L.; Long, Y.; Zhang, D.; Wang, J.; Wang, X.; Xie, B.; Yang, B.; Gao, Y.; Wu, C.; Meng, Q. *Front. Immunol.* **2022**, *13*, 1041860.

(106) Manshadi, M. K. D.; Mansoorifar, A.; Chiao, J.-C.; Beskok, A. *Anal. Chem.* **2023**, *95* (2), 836–845.

(107) Deenin, W.; Khongchareonporn, N.; Ruxrungtham, K.; Ketloy, C.; Hirankarn, N.; Wangkanont, K.; Rengpipat, S.; Yakoh, A.; Chaiyo, S. *Anal. Chem.* **2024**, *96* (14), 5407–5415.

(108) Mahmud, M. A.; Xu, L. H.; Usatinsky, A.; dos Santos, C. C.; Little, D. J.; Tsai, S. S. H.; Rackus, D. G. *Anal. Chem.* **2024**.

(109) Fulford, T. S.; Van, H.; Gherardin, N. A.; Zheng, S.; Ciula, M.; Drummer, H. E.; Redmond, S.; Tan, H.-X.; Boo, I.; Center, R. J.; Li, F.; Grimley, S. L.; Wines, B. D.; Nguyen, T. H. O.; Mordant, F. L.; Ellenberg, P.; Rowntree, L. C.; Kedzierski, L.; Cheng, A. C.; Doolan, D. L.; Matthews, G.; Bond, K.; Hogarth, P. M.; McQuilten, Z.; Subbarao, K.; Kedzierska, K.; Juno, J. A.; Wheatley, A. K.; Kent, S. J.; Williamson, D. A.; Purcell, D. F. J.; Anderson, D. A.; Godfrey, D. I. *eBioMedicine* **2021**, *74*, 103729.
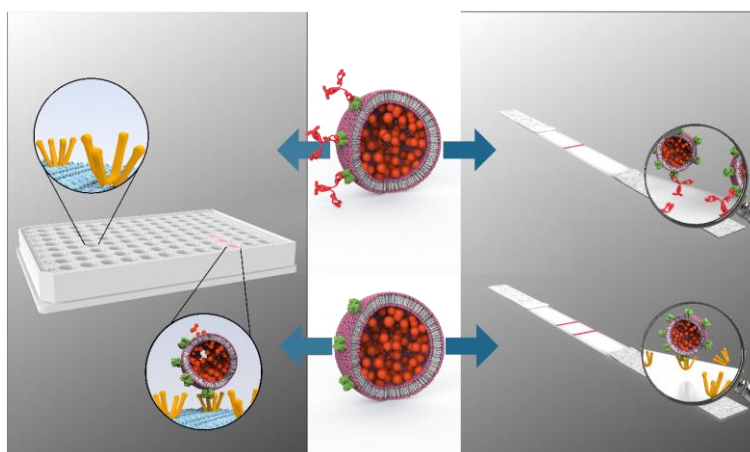
(110) Schobesberger, S.; Thumfart, H.; Selinger, F.; Spitz, S.; Gonzalez, C.; Pei, L.; Poglitsch, M.; Ertl, P. *Anal. Chem.* **2024**, *96* (7), 2900–2907.

(111) Kongsuphol, P.; Jia, H.; Cheng, H. L.; Gu, Y.; Shunmuganathan, B. D.; Chen, M. W.; Lim, S. M.; Ng, S. Y.; Tambyah, P. A.; Nasir, H.; Gao, X.; Tay, D.; Kim, S.; Gupta, R.; Qian, X.; Kozma, M. M.; Purushotorman, K.; McBee, M. E.; MacAry, P. A.; Sikes, H. D.; Preiser, P. R. *Commun. Med.* **2021**, *1* (1), 46.

(112) Lake, D. F.; Roeder, A. J.; Kaleta, E.; Jasbi, P.; Pfeffer, K.; Koelbela, C.; Periasamy, S.; Kuzmina, N.; Bukreyev, A.; Grys, T. E.; Wu, L.; Mills, J. R.; McAulay, K.; Gonzalez-Moa, M.; Seit-Nebi, A.; Svarovsky, S. *J. Clin. Virol.* **2021**, *145*, 105024.

(113) Lee, J.-H.; Lee, Y.; Lee, S. K.; Kim, J.; Lee, C.-S.; Kim, N. H.; Kim, H. G. *Biosens. Bioelectron.* **2022**, *203*, 114034.

(114) Liang, Z.; Peng, T.; Jiao, X.; Zhao, Y.; Xie, J.; Jiang, Y.; Meng, B.; Fang, X.; Yu, X.; Dai, X. *Biosensors* **2022**, *12* (2), 103.

(115) Tong, H.; Cao, C.; You, M.; Han, S.; Liu, Z.; Xiao, Y.; He, W.; Liu, C.; Peng, P.; Xue, Z.; Gong, Y.; Yao, C.; Xu, F. *Biosens. Bioelectron.* **2022**, *213*, 114449.

(116) Li, Y.; He, J.; Zhang, Y.; Liang, D.; Zhang, J.; Ji, R.; Wu, Y.; Su, Z.; Ke, C.; Xu, N.; Tang, Y.; Xu, J. *Front. Cell. Infect. Microbiol.* **2023**, *13*, 1203625.

(117) Lim, S. M.; Cheng, H. L.; Jia, H.; Kongsuphol, P.; D/O Shunmuganathan, B.; Chen, M. W.; Ng, S. Y.; Gao, X.; Turaga, S. P.; Heussler, S. P.; Somani, J.; Sengupta, S.; Tay, D. M. Y.; McBee, M. E.; Young, B. E.; MacAry, P. A.; Sikes, H. D.; Preiser, P. R. *Bioeng. Trans. Med.* **2022**, *7* (2), e10293.

(118) Bian, L.; Li, Z.; an He; Wu, B.; Yang, H.; Wu, Y.; Hu, F.; Lin, G.; Zhang, D. *Biomaterials* **2022**, *288*, 121694.

(119) Yu, H.; Liu, H.; Yang, Y.; Guan, X. *ACS Omega* **2022**, *7* (41), 36254–36262.

(120) Bian, L.; Fu, Q.; Gan, Z.; Wu, Z.; Song, Y.; Xiong, Y.; Hu, F.; Zheng, L. *Adv. Sci.* **2023**, e2305774.

(121) Wang, X.; Shao, S.; Ye, H.; Li, S.; Gu, B.; Tang, B. *Sci. Rep.* **2023**, *13* (1), 22253.

(122) Song, Q.; Zhao, L.; Mai, W.; Xia, D.; Ding, W.; Zhou, X.; Deng, M.; Lei, Y.; Chen, L.; Li, Y.; Mai, X.; Zhang, L.; Chen, Z.; Qin, Y.; Ren, R.; Wei, W.; Ji, T. *Biosens. Bioelectron.* **2023**, *234*, 115353.

(123) Ng, E.; Choi, C.; Wang, S. X. *Sens. Actuators B Chem.* **2023**, *387*, 133773.

(124) Liang, Y.; Buchanan, B. C.; Khanthaphixay, B.; Zhou, A.; Quirk, G.; Worobey, M.; Yoon, J.-Y. *Biosens. Bioelectron.* **2023**, *229*, 115221.

(125) Wu, K.; Klein, T.; Krishna, V. D.; Su, D.; Perez, A. M.; Wang, J.-P. *ACS Sens* **2017**, *2* (11), 1594–1601.

(126) Cortade, D. L.; Wang, S. X. *Anal. Bioanal. Chem.* **2022**, *414* (24), 7211–7221.

(127) Li, J.; Liu, B.; Tang, X.; Wu, Z.; Lu, J.; Liang, C.; Hou, S.; Zhang, L.; Li, T.; Zhao, W.; Fu, Y.; Ke, Y.; Li, C. *Int. J. Infect. Dis.* **2022**, *121*, 58–65.

(128) Duan, X.; Shi, Y.; Zhang, X.; Ge, X.; Fan, R.; Guo, J.; Li, Y.; Li, G.; Ding, Y.; Osman, R. A.; Jiang, W.; Sun, J.; Luan, X.; Zhang, G. *Biosens. Bioelectron.* **2022**, *199*, 113883.

(129) Connelly, G. G.; Kirkland, O. O.; Bohannon, S.; Lim, D. C.; Wilson, R. M.; Richards, E. J.; Tay, D. M.; Jee, H.; Hellinger, R. D.; Hoang, N. K.; Hao, L.; Chhabra, A.; Martin-Alonso, C.; Tan, E. K. W.; Koehler, A. N.; Yaffe, M. B.; London, W. B.; Lee, P. Y.; Krammer, F.; Bohannon, R. C.; Bhatia, S. N.; Sikes, H. D.; Li, H. *Cell Rep. Methods* **2022**, 100273.

(130) Jazayeri, M. H.; Pourfathollah, A. A.; Rasaee, M. J.; Porpak, Z.; Jafari, M. E. *Biomedicine & Aging Pathology* **2013**, *3* (4), 241–245.

(131) Zhang, Y.; Chen, Y.; He, Y.; Li, Y.; Zhang, X.; Liang, J.; He, J.; Lu, S.; Gao, Z.; Xu, J.; Tang, Y. *Talanta* **2023**, *255*, 124200.

(132) *Pathogens prioritization: a scientific framework for epidemic and pandemic research preparedness.* https://www.who.int/publications/m/item/pathogens-prioritization-a-scientific-framework-for-epidemic-and-pandemic-research-preparedness (accessed 2025-01-23).

(133) Mallapaty, S. *Nature* **2024**, *632* (8025), 488.

(134) Escudero-Pérez, B.; Lawrence, P.; Castillo-Olivares, J. *Front. Immunol.* **2023**, *14*, 1156758.

(135) Yoon, I.-K.; Srikiatkhachorn, A.; Alera, M. T.; Fernandez, S.; Cummings, D. A. T.; Salje, H. *Int. J. Infect. Dis.* **2020**, *95*, 167–173.

(136) Katzelnick, L. C.; Montoya, M.; Gresh, L.; Balmaseda, A.; Harris, E. *PNAS* **2016**, *113* (3), 728–733.

(137) Milligan, G. N.; Schnierle, B. S.; McAuley, A. J.; Beasley, D. W. C. *Vaccine* **2019**, *37* (50), 7427–7436.

(138) Brady, A. M.; El-Badry, E.; Padron-Regalado, E.; Escudero González, N. A.; Joo, D. L.; Rota, P. A.; Crooke, S. N. *Vaccines (Basel)* **2024**, *12* (7), 816.

(139) Tahara, M.; Bürckert, J.-P.; Kanou, K.; Maenaka, K.; Muller, C. P.; Takeda, M. *Viruses* **2016**, *8* (8), 216.

(140) Kim, H.; Webster, R. G.; Webby, R. J. *Viral Immunol.* **2018**, *31* (2), 174–183.

(141) Dejnirattisai, W.; Wongwiwat, W.; Supasa, S.; Zhang, X.; Dai, X.; Rouvinski, A.; Jumnainsong, A.; Edwards, C.; Quyen, N. T. H.; Duangchinda, T.; Grimes, J. M.; Tsai, W.-Y.; Lai, C.-Y.; Wang, W.-K.; Malasit, P.; Farrar, J.; Simmons, C. P.; Zhou, Z. H.; Rey, F. A.; Mongkolsapaya, J.; Screaton, G. R. *Nat. Immunol.* **2015**, *16* (2), 170–177.

(142) Davis, E. H.; Barrett, A. D. T. *Viral Immunol.* **2020**, *33* (1), 12–21.

(143) Nobusawa, E. *Nihon Rinsho* **1997**, *55* (10), 2562–2569.

# 2 Development of a surrogate virus neutralization test using liposomes modified with the receptor binding domain of SARS-CoV-2 Alpha

## 2.1 Liposome-based high-throughput and point-of-care assays toward the quick, simple and sensitive detection of neutralizing antibodies against SARS-CoV-2 in patient sera

**Graphical Abstract**

# Liposome-based high-throughput and point-of-care assays toward the quick, simple and sensitive detection of neutralizing antibodies against SARS-CoV-2 in patient sera

**Authors' contributions**

**Claudia Asam** Cloning of recombinant protein expression plasmids; expression, purification, and quality control of recombinant ACE2 and RBD

**Antje J. Baeumner** Conceptualization; writing – review and editing

**Sebastian Einhauser** Pseudovirus neutralization assays; writing – review and editing

**Sonja Hahner** Expression, purification, and quality control of recombinant ACE2 and RBD

**Kilian Hoecherl** Liposome synthesis and optimization

**Kacper Kulikowski** Liposome synthesis and optimization

**Patrick Neckermann** Cloning of recombinant protein expression plasmids; expression, purification, and quality control of recombinant ACE2 and RBD; writing – review and editing

**Christina Noelting** RBD binding antibody test

**David Peterhoff** Expression, purification, and quality control of recombinant ACE2 and RBD

**Clemens Spitzenberg** Liposome synthesis and optimization

**Simon Streif** Conceptualization; HTS experiments; POC experiments; liposome synthesis and optimization; writing – original draft

**Ralf Wagner** Conceptualization; writing — review and editing

**Katharina Weiss** POC experiments

***Liposome-based high-throughput and point-of-care assays toward the quick, simple and sensitive detection of neutralizing antibodies against SARS-CoV-2 in patient sera***

## Abstract

The emergence of severe acute respiratory syndrome-related coronavirus 2 (SARS-CoV-2) in 2019 caused an increased interest in neutralizing antibody tests to determine the immune status of the population. Standard live-virus based neutralization assays such as e.g. plaque-reduction assays or pseudovirus neutralization tests cannot be adapted to the point-of-care (POC). Accordingly, tests quantifying competitive binding inhibition of the angiotensin-converting enzyme 2 (ACE2) receptor to the receptor binding domain (RBD) of SARS-CoV-2 by neutralizing antibodies have been developed. Here, we present a new platform using sulforhodamine B encapsulating liposomes decorated with RBD as foundation for the development of both a fluorescent, highly feasible high-throughput (HTS) and a POC-ready neutralizing antibody assay. RBD-conjugated liposomes are incubated with serum and subsequently immobilized in an ACE2-coated plate or mixed with biotinylated ACE2 and used in test strip with streptavidin test line, respectively. Polyclonal neutralizing human antibodies were shown to cause complete binding inhibition, while S309 and CR3022 human monoclonal antibodies only caused partial inhibition, proving the functionality of the assay. Both formats, the HTS and POC assay, were then tested using 20 sera containing varying titers of neutralizing antibodies, and a control panel of sera including prepandemic sera and reconvalescent sera from respiratory infections other than SARS-CoV-2. Both assays correlated well with a standard pseudovirus neutralization test ($r = 0.847$ for HTS and $r = 0.614$ for POC format). Furthermore, excellent correlation ($r = 0.868$) between HTS and POC formats was observed. The flexibility afforded by liposomes as signaling agents using different dyes and sizes can hence be utilized in the future for a broad range of multianalyte neutralizing antibody diagnostics.
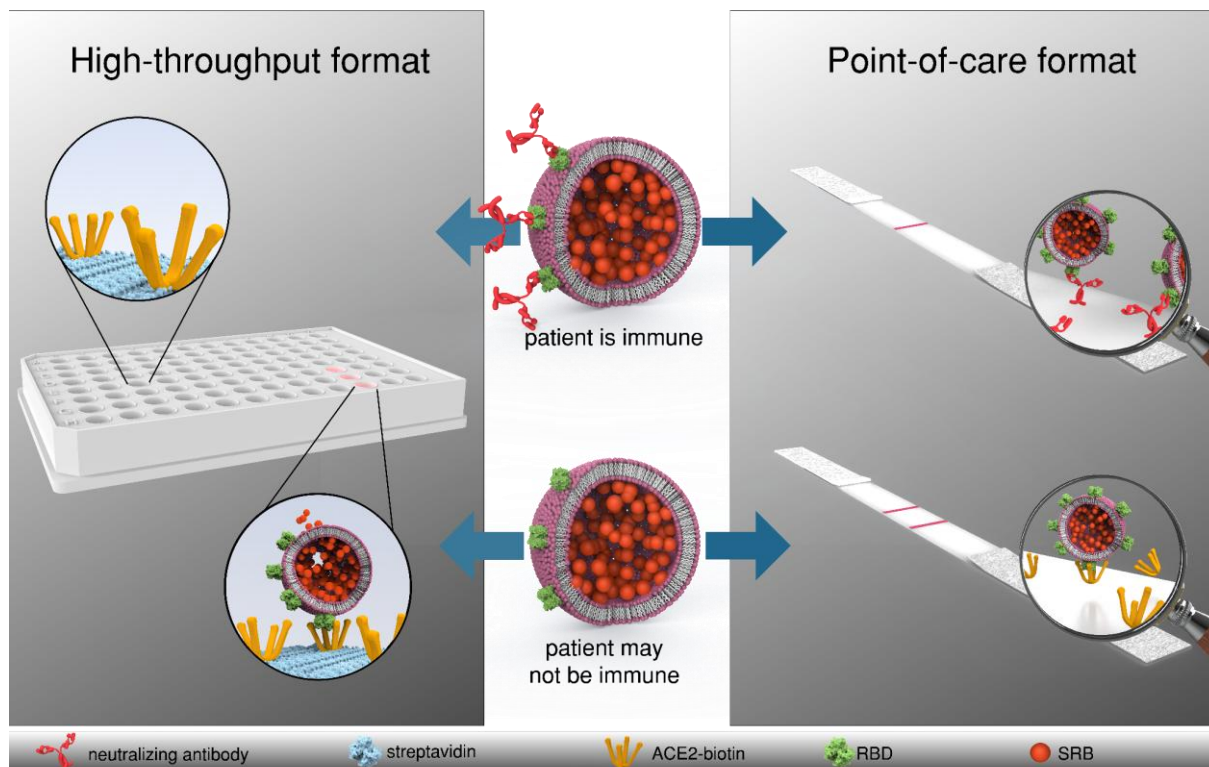
**Figure 1:** *Schematic of the developed high-throughput (i) and point-of care (ii) formats for the detection of neutralizing antibodies directed against the receptor binding domain of SARS-CoV-2. RBD-conjugated liposomes are incubated with patient serum and subsequently i) immobilized in an ACE2-coated microplate or ii) mixed with ACE2-biotin and added to a nitrocellulose membrane with streptavidin test line. In presence of neutralizing antibodies, no liposome-binding takes place, and no signals are observed in either format. In the absence of neutralizing antibodies liposomes are i) bound in the microplate, enabling detection of the released sulforhodamine B via fluorescence after washing and lysis or ii) bound by the test line, enabling a colorimetric detection via camera or naked eye.*

### 2.1.1  Introduction

COVID-19, a disease caused by the infection with severe acute respiratory syndrome-related coronavirus 2 (SARS-CoV-2), had affected more than 600 million and killed >6 million people worldwide in just 2.5 years. Recovery from an infection coincides with the production of neutralizing antibodies (nAb) as part of the humoral immune response helping to contain an active infection, reducing the risk for reinfection and contributing towards prevention of severe disease[1,2]. Similar responses can be induced by the various approved vaccines, in particular spike (S) protein encoding mRNA vaccines (BNT162b2 - BioNTech/ Pfizer, mRNA-1273 - Moderna), adenovirus vectored vaccines (ChAdOx1 nCoV-19 - AstraZeneca, Ad26.COV2.S - Johnson&Johnson), protein vaccines (NVX-CoV2373 - NovaVax) and inactivated vaccines (CoronaVac – Sinovac Life Sciences)[3–6]. Compared to commonly used antibody binding assays, neutralizing antibodies represent a superior correlate for protection from infection or severe disease[7]. The gold standard for nAb titer determination is the 50% plaque-reduction neutralization test (PRNT$_{50}$), requiring up to 3 days and a biosafety level 3 (BSL-3) laboratory due to the use of live virus[8]. Alternative cell based assay formats include pseudovirus

neutralization tests (pVNT), only requiring BSL-2 facilities due to the use of lentivirus or vesicular stomatitis virus pseudotyped with SARS-CoV-2 spike protein[9,10]. These assays quantify the total nAb titer, including all nAb's directed against various domains of the spike (S) protein of SARS-CoV-2, which is responsible for docking of the virus to the host cells and cell-entry via membrane-fusion.

The S protein consists of two subunits, S1 and S2. The former surface-exposed subunit contains the receptor-binding domain (RBD), which binds specifically to the human angiotensin converting enzyme 2 (ACE2) receptor[11]. Subsequent cleavage of S1 and S2 by host cell proteases (especially TMPRSS2) activates the S2 subunit, facilitating fusion of viral and host membranes, causing the release of the viral genome into the host cell cytoplasm[12]. The predominant subunit eliciting virus neutralization was found to be the receptor-binding domain[13,14], thus making the RBD a natural choice for assay development, reinforced even further by higher yields in production compared to recombinant trimeric Spike protein. This knowledge enabled the development of surrogate virus neutralization tests (sVNT) based on the competitive binding of nAb's and ACE2 to RBD. These competitive binding assays include both ELISA's for high-throughput analysis in a laboratory setting as well as paper-based lateral flow assays for point of care testing. Different competitive ELISA's relying on horseradish peroxidase- (HRP) conjugated RBD or ACE2 for detection are commercially available, such as the cPass™ SARS-CoV-2 Neutralization Antibody Detection Kit from GenScript®, the SARS-CoV-2 sVNT Kit from ProteoGenix and the iFlash-2019-nCoV Neutralization Antibody Test from YHLO. Other sensing strategies have been investigated in pursuit of shorter assay times, increased throughput and improved sensitivity. A flow-based chemiluminescence microarray immunoassay could detect nAb's in blood samples in just 7 min[15], while a four-channel SPR sensor enabled simultaneous detection of anti-S1 antibodies as well as free and neutralized virus particles[16]. The use of a Tri-part split-NanoLuc® facilitated a homogeneous neutralization test[17] and the use of Luminex beads holds the potential for multiplexing[18]. For detection of neutralizing antibody titers at the point-of-care multiple versions of sVNT lateral flow assays have been proposed, using ACE2 or RBD test lines and different markers conjugated to RBD or ACE2. A photometric read-out is commonly used, enabled with RBD-conjugated gold nanoparticles[19,20] or green-gold nanoshells[21], ACE2-biotin with streptavidin-conjugated HRP using 3,3′,5,5′-tetramethylbenzidine (TMB) as substrate[22] or cellulose nanobeads conjugated to monoclonal non-neutralizing anti-RBD antibodies[23]. Conjugation of RBD to EuNP's even enabled a fluorescent read-out[24]. For improved sensitivity a second test line can be added to capture neutralized particles, the signal being directly proportional to the nAb titer, while the intensity of the normal test line is proportional to the inverse of the nAb titer[19,24].

Here, we investigated the use of sulforhodamine B (SRB) encapsulating liposomes conjugated to RBD as a signaling alternative. In previous work SRB liposomes were shown to surpass gold nanoparticles in sensitivity in a lateral flow assay[25]. Additionally, the encapsulated SRB enables the use of the liposomes in fluorescence-based microplate assays. This feature allows for the use of one marker in two different assay formats such as ELISA and lateral flow assay, facilitating better comparison of the two while reducing fabrication steps. The presence of carboxylic acid groups on the liposomal surface facilitates protein modification via simple coupling strategies, such as EDC/NHS chemistry, and the large inner cavities allow for encapsulation of different markers, e.g. *m*-carboxyluminol[26] or redox markers such as ferri/ferro hexacyanide[27] and hence easily support chemiluminescent, electrochemical or optical multianalyte approaches.

### 2.1.2  Experimental section

#### 2.1.2.1  Chemicals and consumables

All chemicals were of analytical reagent grade. Cholesterol from sheep wool (C8667, ≥ 99%), *N*-Hydroxysulfosuccinimide sodium salt (sulfo-NHS), purity ≥ 98%, Fluorescein 5(6)-isothiocyanate (FITC) (≥ 90%, 46950) and Sephadex-G50 were purchased from Sigma Aldrich/Merck (Darmstadt, Germany); 1,2-dipalmitoyl-sn-glycero-3-phosphoethanolamine-*N*-(glutaryl) (sodium salt) (*N*-glutaryl-DPPE) from NOF America Corporation (NY, USA); the remaining phospholipids 1,2-Dimyristoyl-sn-glycero-3-phosphoethanolamine (DMPE), 1,2-dipalmitoyl-sn-glycero-3-phosphocholine (DPPC), 1,2-dipalmitoyl-sn-glycero-3-phospho-(1'-rac-glycerol) (sodium salt) (DPPG) and the extruder set from Avanti Polar Lipids (Alabaster, AL, USA). Sulforhodamine B (SRB) (S1307), (1-Ethyl-3-(3-dimethylaminopropyl) carbodiimide-hydrochloride) (EDC) (PG82079) and neutralizing SARS-CoV-2 Spike Protein (RBD) Polyclonal Antibodies (PA5-114451) were purchased from Thermo Fisher Scientific (Waltham, MA, USA); *n*-Octyl-β-D-glucopyranoside (OG) (≥ 98%, CN23), 2-(N-Morpholino)-ethane sulphonic acid (MES) (≥ 99%, 4259) and *N*-2-Hydroxyethylpiperazine-*N*'-2-ethane sulphonic acid (HEPES) (≥ 99.5%, HN78) from Carl Roth (Karlsruhe, Germany). Custom lateral flow test strips (streptavidin test line, <anti-FITC> control line, CN150 membrane) (LFP-915) and standard capacity streptavidin microplates (604500) were purchased from Microcoat Biotechnologie GmbH (Bernried, Germany). For additional information on common reagents and buffer compositions see SI.

**Recombinant Proteins**

Monoclonal human anti-RBD IgG1 antibodies (S309) (BYT-ORB746635) were purchased from Biozol (Eching, Germany). All recombinant proteins were expressed in different scales using

the commercial Expi-Fectamine™ system (Thermofisher Inc) according to manufacturer's instructions. Monoclonal human anti-RBD IgG1 antibody (CR3022) was purified from cell culture supernatants using HiTrap Protein A HP column (Cytiva) as described[28]. RBD B1.1.7 with C-terminal Avi-His6 tag was purified using a HisTrap excel column (Cytiva) with a linear gradient of 10 column volumes from phosphate-buffered saline to phosphate buffered saline with 500 mM Imidazole essentially as described earlier[28]. The external domain of ACE2 (amino acids 18-740) with C-terminal Avi-His6 tag was purified using a HisTrap excel column (Cytiva) with a linear gradient of 10 column volumes from phosphate-buffered saline to phosphate buffered saline with 500 mM Imidazole. Afterwards, the buffer was exchanged to 20 mM Bistris with 10 mM NaCl, pH 6.8 and the protein was further polished using HiTrap DEAE FF column, with a linear gradient from 10 to 1000 mM NaCl in 20 mM BisTris, pH 6.8. All proteins were buffer exchanged to phosphate-buffered saline and stored at 4 °C.

ACE2 was site-specifically biotinylated at the Avi-tag using BirA biotin-protein ligase standard reaction kit (Avidity) according to the manufacturer protocol.

Proteins were quality controlled with SDS-PAGE. Binding was confirmed by a slightly modified ELISA protocol[28] using biotinylated ACE2 and Streptavidin-HRP (1:5000, Roche) instead of antibodies.

**Antisera**

Sera were obtained from the seroprevalence cohort TiKoCo-19, provided by Mikrogen GmbH or purchased. In brief, TiKoCo19 samples comprised sera after SARS-CoV-2 acquisition, vaccination or both. Multiple serological tests were applied to determine seropositivity[29,30]. The TiKoCo-19 study was approved by the Ethics Committee of the University of Regensburg, Germany (vote 20-1867-101). The study complies with the 1964 Helsinki declaration and its later amendments. All participants provided written informed consent. Additional sera from COVID-19 reconvalescent as well as vaccinated individuals were collected in the Munich area ('Munich Cohort') after a call for voluntary donation of serum samples for serological analysis related to SARS-CoV-2. The samples were drawn by the family doctors, according to the legal specifications communicated to us by the Ethics commission of the Bavarian Medical Board [Ethik-Kommission der Bayerischen Landesärztekammer](R008-067 mat/ch), based on §24 MPG (Medizinproduktegesetz) and European norm http://eur-lex.europa.eu/legal-content/DE/TXT/?uri=OJ:L:2017:117:TOC. Volunteers gave their written consent for testing. The logistic support of Mikrogen GmbH collected the anonymized sera and all necessary information. The use of sera given by human research participants has been performed in accordance with the Declaration of Helsinki. Pre-pandemic pooled human complement serum (ICSER, seronegative PHS) was purchased from Innovative Research (Novi, Michigan, USA).

Seronegative pre-pandemic anonymized plasma samples from healthy adult blood donors (blood donations) were purchased from the Bavarian Red Cross. RSV, Influenza A, Adenovirus and Mycoplasm seropositive samples were purchased from commercial vendors.

## 2.1.2.2  Liposome synthesis

Liposomes were synthesized using the reverse-phase evaporation method as described previously[31]. The encapsulant (4.5 mL) was prepared by dissolution of SRB and NaCl in 20 mM HEPES, pH 7.5, at 60 °C using sonication. Lipids (**Table S1**) were dissolved in 3 mL chloroform and 0.5 mL methanol and sonicated for 1 min. 2 mL encapsulant were added to the lipid mixture and the solution was sonicated for 4 min at 60 °C. Organic solvents were evaporated at a rotary evaporator (LABOROTA 4001, Heidolph, Germany) at 60 °C by stepwise reduction of pressure (900 mbar for 10 min, 850 mbar for 5 min, 800 mbar for 5 min, 780 mbar for 20 min). The solution was vortexed for 1 min, another 2 mL of encapsulant were added and the solution was vortexed again for 1 min. The residual organic solvents were evaporated at 60 °C (750 mbar for 20 min, 600 mbar for 5 min, 500 mbar for 5 min, 400 mbar for 20 min). The solution was then extruded using polycarbonate membranes with pore sizes of 1 µm, 0.4 µm and 0.2 µm. Extrusion was conducted at 65 °C with repeated pushing of the syringes, amounting to 21 repetitions for the 1 µm pore size and 11 repetitions for each of the smaller pore sizes. Excess encapsulant was then removed by size exclusion chromatography using a Sephadex G-50 column, followed by dialysis overnight against HSS buffer with 2 buffer exchanges in a dialysis membrane Spectra/Por© 4 (MWCO: 12-14 kDa).

## 2.1.2.3  Characterization of liposomes

The phospholipid concentration was determined using an inductively coupled plasma optical emission spectrometer (ICP-OES) (SpectroBlue TI/EOP) from SPECTRO Analytical Instruments GmbH (Kleve, Germany). Phosphorous standard dilutions between 0 µM and 100 µM in 0.5 M $HNO_3$ were used for calibration of the device. Phosphorous was detected at 177.495 nm. Before each measurement, 0 µM and 100 µM phosphorus dilutions were used to re-calibrate the device. Liposome stock solutions were diluted 1:100 in 0.5 M $HNO_3$ and their phosphorous content determined. Total lipid concentrations were calculated using the phospholipid concentration and the lipid composition used during synthesis.

Size and ζ-potential were measured via dynamic light scattering (DLS) using a Malvern Zetasizer Nano-ZS. Liposome stock solutions were diluted 1:100 in HSS buffer in a polymethyl methacrylate (PMMA) semi-micro cuvette (Brand, Germany) for size and a disposable folded capillary cell (Malvern Panalytical, Germany) for ζ-potential measurements. The measurement temperature was set to 25 °C, the refractive index was 1.34, the material absorbance was zero

and the dispersant viscosity 1.1185 mPa s. For ζ-potential a dielectric constant of 78.5 was used and an equilibration time of 60 s applied before each measurement.

### 2.1.2.4 Modification of liposomes

RBD was conjugated to carboxylated liposomes via EDC/NHS chemistry. First, liposomes were incubated for 1 h at room temperature (RT) and 300 rpm with EDC and sulfo-NHS (1:100:180 ratio of carboxy-groups:EDC:sulfo-NHS). The desired amount of protein was added, and the solution incubated for another 1.5 h at RT and 300 rpm. The reaction was quenched by addition of 10 mM L-lysine-hydrochloride. Finally, the solution was dialyzed against HSS buffer overnight with one buffer exchange in a Spectra-Por® Float-A-Lyzer® G2 (1 mL, MWCO: 1000 kDa).

For FITC-conjugation liposomes were dialyzed against a carbonate buffer (100 mM NaHCO$_3$, 250 mM NaCl, pH 9) overnight. FITC dissolved in DMSO (1 mg/mL) was added to the liposomes (1:50 ratio of amine groups to FITC) and incubated overnight at RT and 300 rpm. The solution was dialyzed against HSS buffer overnight with three buffer exchanges in a dialysis membrane Spectra/Por© 4 (MWCO: 12-14 kDa). Total lipid concentrations were determined using ICP-OES and the conjugated liposomes were stored at 4 °C.

### 2.1.2.5 HTS neutralization test

If not stated otherwise all microtiter-plate based assays were run according to the following protocol. A standard capacity streptavidin microplate was coated with ACE2-biotin (1 µg/mL in PBS, 100 µL) for 1 h at RT and 300 rpm. Meanwhile, liposomes (0.5 µM total lipids) were incubated with serum dilutions (4 v%, followed by 2-fold series dilution) in HSS buffer for 1 h at 30 °C and 300 rpm in a ThermoMixer C (Eppendorf SE, Germany). The plate was washed two times with PBS-T (150 µL) and three times with HSS (150 µL) before addition of the liposome-serum mixture (100 µL). After 2 h incubation at RT and 300 rpm the plate was washed three times with HSS buffer (150 µL). Captured liposomes were lysed by 10 min incubation with 30 mM OG (100 µL). The fluorescence intensities were measured three consecutive times with a BioTek SYNERGY neo2 fluorescence reader ($\lambda_{Ex}$ = 560 $nm$ and $\lambda_{Em}$ = 585 $nm$, bandwidth 10, gain 150). Binding inhibition values were calculated as: $binding\ inhibition\ (\%) = \left(1 - \frac{fluor.\ int.}{fluor.\ int.\ neg.\ control}\right) \cdot 100$. Errors were calculated using Gaussian error propagation. IC50 values were determined with GraphPad Prism 9 (GraphPad Software, San Diego, CA, USA) using the 'log(inhibitor) vs. normalized response with variable slope' algorithm.

### 2.1.2.6  POC neutralization test

If not stated otherwise all lateral flow assays were run according to the following protocol. Liposomes were pre-incubated with serum (5 µL) in HSS buffer (47 µL) for 15 min at RT and 300 rpm. ACE2-biotin (3 equivalents per RBD) were added to the mixture (resulting in 50 µL total volume, 10 µM RBD-conjugated liposomes, 12.9 µM FITC-conjugated liposomes and 10 v% serum). The solution was pipetted into a clear microplate and test strips were dipped into the solutions. After 5 min the strips were washed using 25 µL HSS buffer. Pictures were taken 20 min after washing buffer addition using a Canon EOS 550D camera with a Canon EFS 18-55mm lens from 15 cm distance with consistent lighting and the following settings: ISO 100, aperture 3.5, exposure time 1/30 s, focal length 18 mm, white balance daylight (5200K). The raw files were analyzed using ImageJ. The color channels were split, the background of the green channel was subtracted for background smoothing (50 pixels) before black/white inversion. The brightness was adjusted to make the lines visible for the naked eye. The intensities of the background, test and control line were measured threefold using a rectangle of 80x45 pixels. The average intensities were calculated and the background signal subtracted. Binding inhibition values were calculated as:

$$binding\ inhibition\ (\%) = \left(1 - \frac{test\ line\ intensity}{control\ line\ intensity}\right) \cdot 100.$$

### 2.1.2.7  *recom*Line SARS-CoV-2 IgG assay

The commercial *recom*Line SARS-CoV-2 IgG assay (Mikrogen GmbH, Neuried, Germany) was conducted as given in the instructions. Briefly, a nitrocellulose membrane test strip loaded with RBD was incubated with diluted serum or plasma for 1 h and washed. Horseradish peroxidase-conjugated anti-human IgG antibodies were added and incubated for 45 min. The coloring solution containing TMB was added after washing and incubated for 8 min before the signals were analyzed.

### 2.1.2.8  Pseudovirus neutralization test

The pseudovirus based neutralization assay (pVNT) using the Vesicular Stomatitis Virus (VSV-Δ G*FLuc) pseudotyped with wt-SARS-CoV-2-Spike-ΔER was performed as described earlier[32]. In brief, a fixed inoculum of 25,000 ffu was neutralized with a 2-fold serum dilution series starting from 1 in 20 for 1 h. Luciferase activity was determined 20 h post infection of HEK293T-ACE2-cells using BrightGlo (Promega Corp, Madison, WI, USA).

## 2.1.3  Results and discussion

Liposomes were developed to bear the unique property of offering a highly sensitive fluorescent and a rapid, simple colorimetric read-out. This was accomplished using the encapsulation of SRB as previously demonstrated[25,31,33]. Key assay development points described here were the investigation of RBD, ACE2 and liposome concentration, ACE2 immobilization and the optimization of SRB liposomes with respect to signaling strength. For the proof-of-principle assay, binding and neutralizing antibodies as well as seronegative and neutralizing sera were used. Finally, the screening of a serum panel consisting of 20 neutralizing sera previously analyzed by a standard pseudovirus neutralization test was performed.

Recombinant RBD B1.1.7 and biotinylated ACE2 was produced as described above and quality was controlled by SDS-PAGE and ELISA (**Figure S1**). SDS-PAGE revealed purity of the proteins (**Figure S1 A** and **B**) and ELISA confirmed rigid binding of biotinylated ACE2 to RBD B1.1.7 with a dissociation constant of 5.4 ± 3 nM (**Figure S1 C**).

### 2.1.3.1  High-throughput format (HTS)

Universal liposomes were synthesized and adapted toward the specific detection of neutralizing SARS-CoV-2 antibodies (nAb) in a competitive assay format. Initially, the optimum RBD coverage of the liposome surface regarding immobilization efficiency was investigated. Between 0.1 mol% and 0.5 mol% RBD were coupled to the liposomes via EDC/NHS chemistry and the modified liposomes were immobilized in an ACE2-coated plate. Best results were achieved with 0.2 mol% RBD, while 0.5 mol% RBD resulted in decreased signal intensities (**Figure S2**). This could be either due to crosslinking of excess RBD to RBD coupled to the liposomal surface, as the excess EDC and NHS is not removed before addition of RBD, or the RBD is packed too densely. Both would result in steric hindrance, diminishing the liposomes binding potential to ACE2. In case of the ACE2 concentration used for coating of the microplate, it was found that higher concentrations lead to more liposome binding (**Figure S3**). Finally, for the encapsulant concentration it was found that 50 mM SRB encapsulant led to significant signal improvements over liposomes with 10 mM SRB and allowed the detection at various liposome concentrations (**Figure S4**). In later studies, this concentration was further increased to 150 mM SRB (the maximum possible concentration still leading to colloidally, long-term and serum stable liposomes) to obtain an even more sensitive test. In initial studies for the detection of nAbs, titration curves of nAbs, binding antibodies and non-neutralizing sera were measured. Expected results were obtained for the antibodies studied (**Figure S5**). Signals obtained for the serum samples on the other hand showed a clear interference of the sera with the assay as lower serum concentrations (<0.1%) increased the overall fluorescent signals, whereas higher concentrations lead to a decrease. It is assumed that serum proteins

adsorb to the microplate's surface, despite the use of BSA and other blocking agents, and interact with the released SRB after liposome lysis, decreasing the hydration-mediated quenching[34]. This leads, in general, to an increase of the overall fluorescence signal. Yet, at higher serum concentrations the abundance of serum constituents may inhibit the interaction of RBD-conjugated liposomes and immobilized ACE2, resulting in a decrease of signal intensities even in the absence of neutralizing antibodies. Therefore, the ACE2 immobilization strategy was changed from mere adsorption to site-directed binding through a biotin tag on the ACE2 protein and commercially available streptavidin-coated microtiter plates. This led to three improvements of the assay: (i) less ACE2 was needed for the immobilization, hence saving on reagents (1 µg/mL vs. 5 µg/mL), (ii) serum proteins would not adsorb to the surface and hence would not enhance the SRB fluorescence signal in an uncontrolled fashion, and (iii) binding between RBD-conjugated liposomes and ACE2-coated surfaces was improved due to the site-directed immobilization, i.e 4x higher signals were obtained (**Figure S6-8**).

With these optimized conditions, the antibody titration curves showed complete prevention of liposome binding by the RBD specific neutralizing antibodies (PA5-114451), while monoclonal antibodies directed against the CR3022 cryptic site and the S309 proteoglycan site caused only partial inhibition (**Figure 2**). This suggests that the polyclonal PA5-114451 antibodies fully block binding of the RBD decorated liposomes to the immobilized ACE2 receptor, presumably due to antibodies that are binding within the receptor-binding motif and therefore outcompete ACE2 (class1 and 2 antibodies)[35]. The S309 (class 3) and CR3022 (class 4) antibodies are not binding within the receptor-binding motif of RBD[35,36]. S309 is a neutralizing antibody that binds distal from the receptor-binding motif and has neutralizing capabilities *in vitro*[37]. CR3022 is described as a binding but non-neutralizing antibody, since its epitope is not accessible in trimeric spike protein due to masking by the neighboring protomer[38,39]. Moreover, both epitopes are not affected by N501Y mutation of B1.1.7[40]. However, in this assay, monomeric RBD B1.1.7 is employed where the CR3022 epitope is fully accessible for binding antibodies. Thus, CR3022 might exhibit apparent inhibitory activity against the now artificially exposed epitope. Our results may suggest that both antibodies seem to cause steric hindrance for the interaction of the liposomes with the immobilized ACE2 but are not preventing it, resulting in partial inhibition, since both antibodies only bind allosteric to the receptor-binding motif.
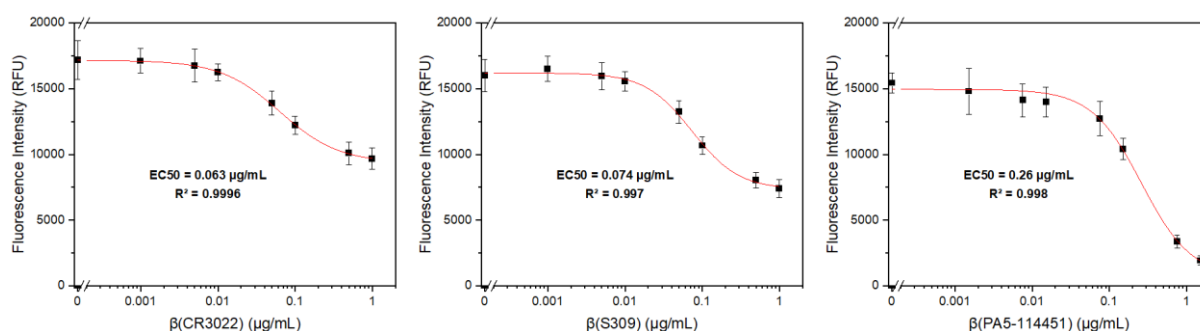
*Figure 2: Fluorescence intensities of RBD-conjugated liposomes (50 mM SRB, 1 µM total lipid concentration) tested with binding (CR3022 and S309) and neutralizing (PA5-114451) anti-RBD antibodies (0 µg/mL to 1 µg/mL). n = 3. Curves were fitted using Origin 2022's Logistic function.*

For proof of principle few carefully selected antisera - a seronegative pooled human serum (PHS), and three sera with known weak, intermediate and strong neutralizing activity – were used to gather initial data regarding liposome binding inhibition (**Figure 3**). In all cases, IC50 values for the neutralization could be determined, which overall correlated with the neutralization activity determined previously via a pseudovirus neutralization test[32] (**Figure 3 c**). However, the IC50 values for the weak and intermediate neutralizing sera were lower in the HTS format compared to the pVNT and the $R^2$ value decreased below 0.8 for the weakly neutralizing serum, which suggests that higher serum concentrations would be required for a reliable determination of the IC50 value of sera with low nAb titers. Interestingly, a slight enhancement of the fluorescent signals could still be observed with the seronegative sample (a pooled, commercially available serum) with increasing serum concentration, which was also seen with other samples, mainly seronegative ones from donors with other respiratory diseases (**Figure S9**). This suggests that some sera may indeed cause non-specific binding to the microtiter plate surface albeit its blocked surface, and hence lead to a small increase in fluorescence. However, this effect has no impact on the determination of the IC50 values as the resulting negative binding inhibition values are counted as 0% binding inhibition for the analysis.
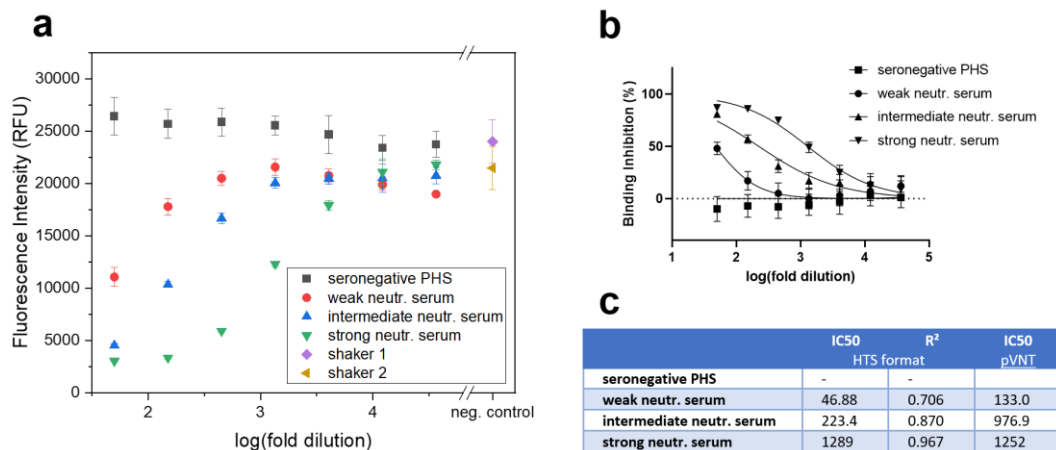
*Figure 3: Fluorescence intensities (**a**), binding inhibition curves (**b**) and IC50 values determined via GraphPad Prism 9 using the 'log(inhibitor) vs. normalized response with variable slope' algorithm (**c**) of RBD-conjugated liposomes (50 mM SRB, 1 µM total lipid concentration) tested with seronegative pooled human serum (PHS), a weakly, intermediate and a strongly neutralizing serum (2 v% followed by 3-fold series dilution). n = 3. Seronegative PHS and strong neutr. serum samples were incubated at 30 °C and 300 rpm in shaker 1, intermediate and weak neutr. serum in shaker 2. IC50 values determined for the weak, intermediate and strong neutralizing sera in the pVNT are listed in c for comparison.*

Finally, the liposome-based assay was challenged with a serum panel of 20 neutralizing sera, ranging from weak to very strong neutralization as determined by an established pseudovirus neutralization test[32]. It could be seen that the liposome assay had a good correlation with the established test (Spearman's r = 0.75, **Figure 4 a**), however, the $R^2$ values were in some instances too low (**Table S2**). Thus, higher serum concentrations and liposomes encapsulating 150 mM SRB were investigated. The higher fluorescence intensities obtainable with these liposomes enabled the reduction of liposome concentration from 1 µM to 0.5 µM and hence an improvement in sensitivity. IC50 values could be determined for all sera (**Table S2**, **Figure S10**). Reliable IC50 values could be obtained for 15 out of the 20 sera. The other 5 showed values outside of the investigated range of serum dilutions (1:25 to 1:1600) so that low IC50 values correlated to low R² values. Strong correlation was observed between the IC50 values determined with the HTS and pseudovirus neutralization assay (Spearman's r = 0.847, **Figure 4b**). Additionally, 10 pre-pandemic sera were analyzed using the optimized assay conditions. No neutralization was observed for any of the samples despite the increased serum concentrations (**Figure S11**), hinting at high specificity of the assay. In the future, further improvement of the sensitivity can be achieved using even higher serum concentrations or by optimization of the RBD coverage regarding proper orientation. Extensive screening including hundreds of seronegative and neutralizing samples could then enable validation of the developed neutralization test toward product development.
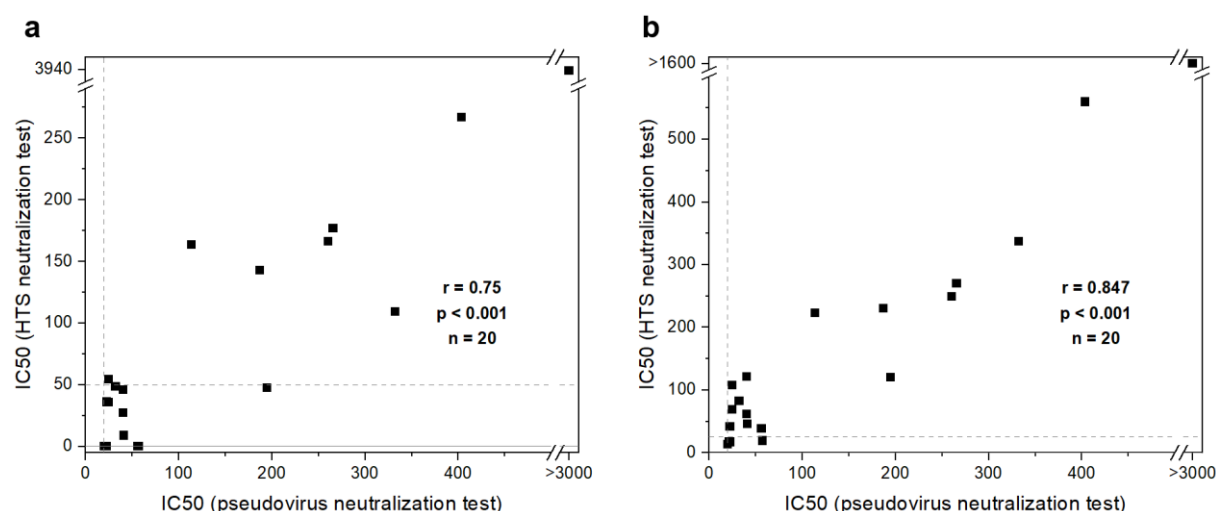
***Figure 4:*** *Correlation of IC50 values for 20 neutralizing sera (TiKoCo-19) obtained with a standard pseudovirus neutralization test[32] with IC50 values obtained with the new liposome HTS neutralization test.* **a)** *50 mM SRB liposomes, 1 µM total lipid concentration, 2% serum followed by 3-fold series dilution and* **b)** *150 mM SRB liposomes, 0.5 µM total lipid concentration, 4% serum followed by 2-fold series dilution. n = 3. The lowest dilution factors used in the neutralization tests are displayed as dashed grey lines. A Spearman correlation was conducted for the 20 samples in a (r = 0.75, p < 0.001) and b (r = 0.847, p < 0.001) using SPSS.*

## 2.1.3.2 Point-of-care format (POC)

In addition to the development of the high-throughput format a POC test based on a lateral flow assay was investigated. 150 mM SRB encapsulating liposomes were used to establish a robust POC test. The POC assay format is vastly simplified in contrast to the HTS format resulting in a 1 or 2-step assay. Here, RBD-conjugated liposomes are incubated with serum. Subsequently, biotinylated ACE2 is added to the solution and the mixture is applied to an LFA membrane containing streptavidin in the test line. Hence, RBD-conjugated liposomes bound to ACE2 will collect at the test line, so that the presence of neutralizing antibodies results in lower to no signal (**Figure 1**). In initial experiments liposome concentration (**Figure S12**), ACE2-biotin concentration (**Figure S13**) and incubation times (**Figure S14**) were optimized. The final protocol included 10 µM liposomes, 3x ACE2-biotin concentration in relation to RBD concentration per sample, and no required incubation of ACE2-biotin with the liposome-serum mixture. Furthermore, a control line was developed using immobilized anti-FITC antibody and FITC-conjugated SRB liposomes. It was found that a concentration of 12.9 µM FITC-conjugated liposomes produced the same signal intensity as 10 µM RBD-conjugated liposomes in presence of seronegative pooled human serum (**Figure S15**). Under these conditions, mean binding inhibition of -2 ± 3% for the seronegative serum was observed, proving the reproducibility of the format (**Figure S16**).

In a proof-of-principle test, 4 sera were analyzed and demonstrated that with the current format weakly and strongly neutralizing sera could easily be distinguished (**Figure 5**). Complete binding inhibition was observed for the intermediate and strongly neutralizing human sera, while no signal decrease was observed for the weakly neutralizing serum. In an attempt for

further simplification of the assay protocol, ACE2-biotin addition before or after pre-incubation of liposomes with serum using the same sera proved better performance of the latter (**Figure S17**). While this results in an additional pipetting step after the pre-incubation, the added sensitivity may in the end be beneficial.
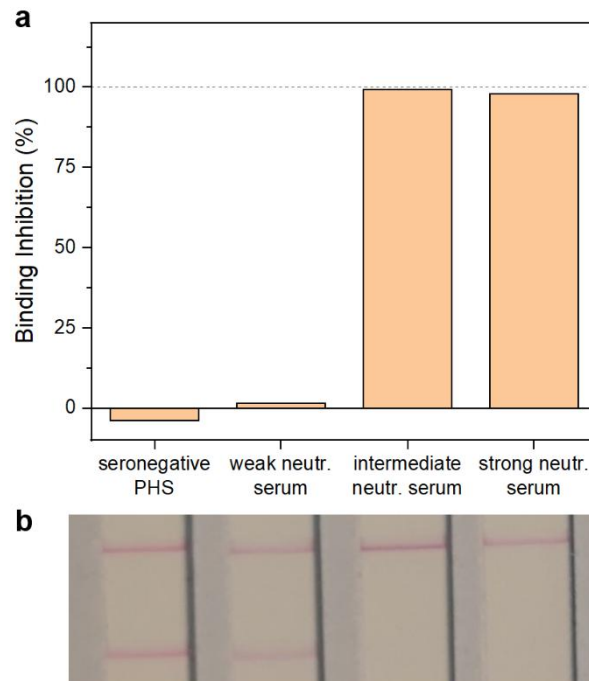


*Figure 5: Proof-of-principle assay for the POC format using RBD-conjugated liposomes (150 mM SRB) and ACE2-biotin applied to LFAs with a streptavidin test line and an anti-FITC control line. Test strips (**a**) and binding inhibition values (**b**) of seronegative pooled human serum (PHS), a weakly, intermediate and a strongly neutralizing serum are shown. n = 1.*

Furthermore, to reduce the overall assay time, the pre-incubation of liposomes with serum was investigated between 0 min, 5 min and 15 min (**Figure S18**). Not surprisingly, the longer the incubation, the more binding inhibition can be observed. However, the effect was not too pronounced, making 5 min pre-incubation feasible. Nonetheless, an incubation time of 15 min was chosen for all studies in this work to gain optimum sensitivity and ease simultaneous handling of large quantities of test strips. A washing step was also added to reach optimum sensitivity, causing a slight signal increase, but is not crucial, background intensities remaining identical with and without it (data not shown).

Further assay optimizations included avoidance of non-specific binding of liposomes to the LFA membrane strip as this would directly affect signal read-out in the test line. This might i.e. result in fewer liposomes binding to the test or control line and therefore be interpreted as false-positive or false-negative signal. This was already observed for the control liposomes with the weakly neutralizing serum (**Figure S17**) and confirmed for 5 out of 24 sera, which were well characterized and carefully selected from the Munich Cohort serum panel (Suppl. **Table S3**; comprising (i) prepandemic sera, (ii) SARS-CoV-2 reconvalescent sera, (iii) sera

obtained from vaccinated individuals, (iv) reconvalescent sera following infection with respiratory disease viruses other than SARS-CoV-2 and (v) sera from previously mycoplasma infected individuals known to be cross-reactive). Noteworthy, this effect was most pronounced for 2 sera with known previous mycoplasma infection (**Figure S19**). Using a membrane with larger pore sizes significantly reduced this non-specific binding (**Figure S20**). This suggests that these sera caused an agglomeration of liposomes too large to pass through the nitrocellulose pores. Additionally, the investigated sera highlighted the different behavior of seronegative samples and those from convalescent and vaccinated donors in the assay. They had previously been analyzed for RBD-binding antibodies in the *recom*Line SARS-CoV-2 IgG assay. Screening of the sera showed that high binding antibody titers (>500 BAU/mL) corresponded to strong binding inhibition in the POC test. Complete binding inhibition was observed for all 5 sera with high titers (**Figure S19**). For intermediate titers between 100 and 200 BAU/mL no correlation between signal decrease and antibody titer was observed. Seronegative samples expectedly showed no binding inhibition, while in some cases a reduced control line intensity even resulted in negative binding inhibition values.

To determine the background threshold, six seronegative samples were tested in triplicates, resulting in binding inhibition values around 0% in most cases, with exception of blood donations 4498 and 4500 with values of 10 ± 7% and -10 ± 3%, respectively (**Figure S21**). The average of all 18 measurements (0%) + 3x the standard deviation (11%) was used as preliminary cut-off (33%) for further experiments. Additional 10 seronegative samples were tested to verify the accuracy of the cut-off. All sera produced binding inhibition values <0% (**Figure S22**), hinting at good specificity of the assay. However, two sera showed exceptionally low values of -24% and -53% (blood donations 4505 and 4507) due to reduced control line intensities. No non-specific binding was observed, suggesting that serum constituents affected the interaction of FITC-modified liposomes with the immobilized anti-FITC antibodies.

Following the above assay optimization and determination of background threshold, the identical serum panel (n = 20), which was already used to validate the HTS assay format (**Figure 3**), was analyzed with the optimized POC assay (**Figure S23**, **Table S2**). Complete binding inhibition of >95% was observed in the POC format for 3 out of the 20 sera. Another 4 sera showed high values above 80%, while the remaining 13 sera showed values <60%. A total of 10 sera gave values below the established threshold of 33%. Correlation of these binding inhibition values to the IC50 values determined with the pVNT showed a Spearman's r of 0.614 (**Figure 6 a**). Despite the mediocre quantitative correlation, those results still prove sufficient qualitative detection of neutralizing antibodies by the POC assay. Specifically, all but one serum with IC50 values >100 show >80% binding inhibition, while sera with IC50 values between 20 and 70 showed anywhere between 0 and 50% binding inhibition. Furthermore,

very good correlation was observed for the two liposome-based formats with a Spearman's r of 0.868 (**Figure 6 b**). IC50 values >200 correlated close to complete binding inhibition, values <50 corresponded to 0-30% binding inhibition. As the POC format is significantly faster and simpler to perform it leads to a qualitative nature-only at this point, which will be improved upon in the future. Here, better sensitivity and hence actually quantification can be achieved by increasing the liposome diameter[25], entrapping other dyes or investigation of directed protein immobilization on the liposome surface.
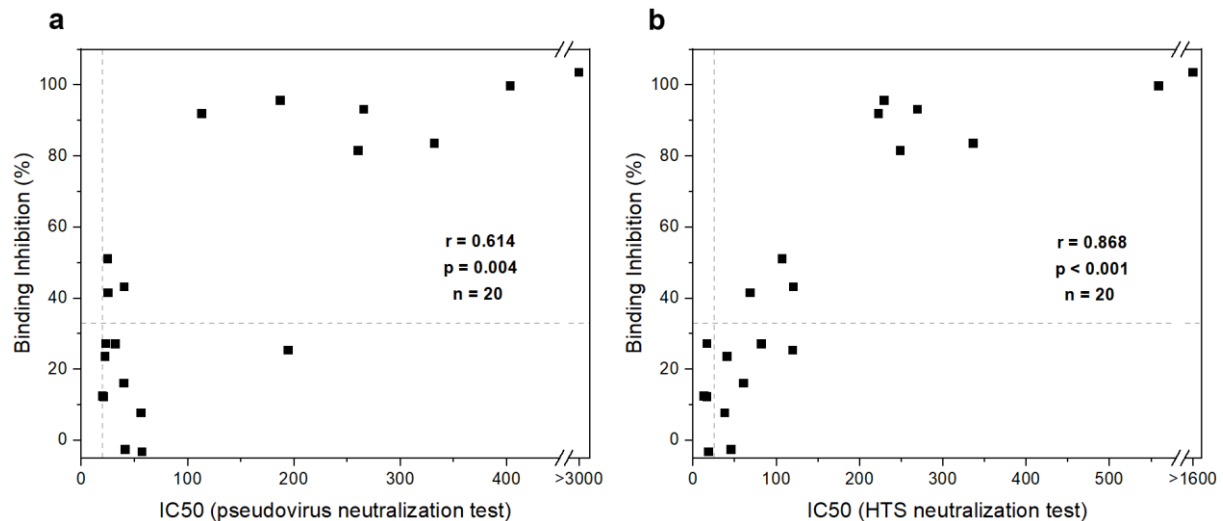


*Figure 6: Correlation of binding inhibition values determined in the POC neutralization test and IC50 values determined in the pseudovirus (a) and the HTS neutralization test (b) of 20 neutralizing sera (TiKoCo-19). Spearman correlation coefficients of r = 0.614 (a) and r = 0.868 (b) were calculated using SPSS. The lowest dilution factors used in the neutralization tests and the preliminary cut-off calculated for the POC test are displayed as dashed grey lines.*

### 2.1.3.3 Liposome stability

Liposomes without any proteins coupled to their surface or those coupled to streptavidin have previously been shown to be highly stable when stored at 4 °C for years[25]. In contrast, RBD-conjugated liposomes were found to be stable for only 1 month at 4 °C (**Figure S24**). Longer storage times led to agglomeration and precipitation of the liposomes. Thus, in the future, a formulation of the RBD-liposome buffer will be studied by adding stabilizing agents to avoid the protein-mediated aggregation. Alternatively, streptavidin-coupled liposomes can be used in combination with biotinylated RBD. From a commercial viewpoint this approach has the advantage that the competitive assays could be quickly adapted for other analytes using different biotinylated proteins, which could be stored separately.

## 2.1.4 Conclusion

The developed SRB liposomes enable both the sensitive detection and quantification of neutralizing antibodies against RBD in a microplate-based high-throughput assay as well as the qualitative detection in a lateral flow-based POC format. Very good correlation was observed between the two formats, while only the HTS format showed strong correlation to an established pseudovirus neutralization test (pVNT), confirming the ability of the assay to detect neutralizing antibodies in the desired range. The HTS format could determine IC50 values within the investigated range for 15 out of the 20 sera tested with the pseudovirus neutralization test. Further improvement of the sensitivity could be achieved with the use of higher serum concentrations or the use of different liposome species, e.g. chemiluminescent or HRP liposomes, enabling reliable IC50 determination even for weakly neutralizing sera. Another option may be the optimization of RBD coverage regarding neutralization, lower coverage could improve the sensitivity at the expense of signal intensity. The advantage over currently used ELISA-type HTS formats is the quick and not-time-dependent signal read-out afforded by the liposomes. In contrast to the enzyme reaction-based readout strategies, more reproducible and simpler HTS strategies can therefore be achieved. The POC format enables fast detection of neutralizing antibodies, albeit only in a qualitative manner at this point. Nevertheless, extrapolation with population based data[41], would support a quantitative readout, as the majority of the population's titers (vaccinated or recently infected) should be in the assay's dynamic range. The use of a membrane with larger pore size might improve the correlation to the pVNT and enable a semi-quantitative determination of nAb's. Implementation of a signal on strategy by addition of a secondary test line consisting of anti-human IgG antibodies to capture neutralized liposomes might also improve the sensitivity of the assay, as shown in literature[19,24]. Additionally, this setup might make the test more intuitive for users, stronger test line intensities correlating to higher neutralizing antibody titers. Optimization of the assay, i.e. shortening of pre-incubation time and omitting of the washing step, would allow for assessment of the immune status of a patient within <30 min after blood-draw.

Both test formats demonstrate that even though liposomes are significantly larger than gold nanoparticles (20 – 80 nm) and enzymes (<10 nm) their multivalency overcomes possible steric hindrance in the competitive assay format and hence enable the development of highly effective and reliable HTS and POC diagnostic tests. Furthermore, since the signaling molecules are hidden from the assay itself by being inside the liposomes, several unique characteristics are afforded by liposomes. Specifically, entrapping different dyes can easily prepare liposomes for multi-analyte strategies, and control lines can be made with e.g. blue or green rather than magenta liposomes. Also, the concentration range of an analyte that is covered within the dynamic range of the assay can easily be adapted by using different dye

concentrations encapsulated within the liposomes. The same can be achieved by simply changing the liposomes diameter[25]. The entrapment of other marker molecules inside the liposomes even broadens read-out capabilities far beyond fluorescence and colorimetric approaches and have been demonstrated with chemiluminescent, bioluminescent, electrochemical and electrochemiluminescent detection strategies before. Finally, in contrast to most other signaling agents, the chemical surface of liposomes can easily be adapted to a specific coupling chemistry or matrix without the need for complex reactions. The addition of lipids with varying head groups instead easily establishes alternative chemistries, such as biotinylation, amine groups, click chemistry or ganglioside receptors. These properties make liposomes a versatile tool for a multitude of assays, including competitive binding assays, such as neutralization tests, as demonstrated in this work.

### 2.1.5 References

(1) Long, Q.-X.; Tang, X.-J.; Shi, Q.-L.; Li, Q.; Deng, H.-J.; Yuan, J.; Hu, J.-L.; Xu, W.; Zhang, Y.; Lv, F.-J.; Su, K.; Zhang, F.; Gong, J.; Wu, B.; Liu, X.-M.; Li, J.-J.; Qiu, J.-F.; Chen, J.; Huang, A.-L. *Nat. Med.* **2020**, *26* (8), 1200–1204.

(2) Garcia-Beltran, W. F.; Lam, E. C.; Astudillo, M. G.; Yang, D.; Miller, T. E.; Feldman, J.; Hauser, B. M.; Caradonna, T. M.; Clayton, K. L.; Nitido, A. D.; Murali, M. R.; Alter, G.; Charles, R. C.; Dighe, A.; Branda, J. A.; Lennerz, J. K.; Lingwood, D.; Schmidt, A. G.; Iafrate, A. J.; Balazs, A. B. *Cell* **2021**, *184* (2), 476-488.e11.

(3) Barros-Martins, J.; Hammerschmidt, S. I.; Cossmann, A.; Odak, I.; Stankov, M. V.; Morillas Ramos, G.; Dopfer-Jablonka, A.; Heidemann, A.; Ritter, C.; Friedrichsen, M.; Schultze-Florey, C.; Ravens, I.; Willenzon, S.; Bubke, A.; Ristenpart, J.; Janssen, A.; Ssebyatika, G.; Bernhardt, G.; Münch, J.; Hoffmann, M.; Pöhlmann, S.; Krey, T.; Bošnjak, B.; Förster, R.; Behrens, G. M. N. *Nat. Med.* **2021**, *27* (9), 1525–1529.

(4) Polack, F. P.; Thomas, S. J.; Kitchin, N.; Absalon, J.; Gurtman, A.; Lockhart, S.; Perez, J. L.; Pérez Marc, G.; Moreira, E. D.; Zerbini, C.; Bailey, R.; Swanson, K. A.; Roychoudhury, S.; Koury, K.; Li, P.; Kalina, W. V.; Cooper, D.; Frenck, R. W.; Hammitt, L. L.; Türeci, Ö.; Nell, H.; Schaefer, A.; Ünal, S.; Tresnan, D. B.; Mather, S.; Dormitzer, P. R.; Şahin, U.; Jansen, K. U.; Gruber, W. C. *N. Engl. J. Med.* **2020**, *383* (27), 2603–2615.

(5) Keech, C.; Albert, G.; Cho, I.; Robertson, A.; Reed, P.; Neal, S.; Plested, J. S.; Zhu, M.; Cloney-Clark, S.; Zhou, H.; Smith, G.; Patel, N.; Frieman, M. B.; Haupt, R. E.; Logue, J.; McGrath, M.; Weston, S.; Piedra, P. A.; Desai, C.; Callahan, K.; Lewis, M.; Price-Abbott, P.; Formica, N.; Shinde, V.; Fries, L.; Lickliter, J. D.; Griffin, P.; Wilkinson, B.; Glenn, G. M. *N. Engl. J. Med.* **2020**, *383* (24), 2320–2332.

(6) Zhang, Y.; Zeng, G.; Pan, H.; Li, C.; Hu, Y.; Chu, K.; Han, W.; Chen, Z.; Tang, R.; Yin, W.; Chen, X.; Hu, Y.; Liu, X.; Jiang, C.; Li, J.; Yang, M.; Song, Y.; Wang, X.; Gao, Q.; Zhu, F. *Lancet Infect. Dis.* **2021**, *21* (2), 181–192.

(7) Favresse, J.; Gillot, C.; Bayart, J.-L.; David, C.; Simon, G.; Wauthier, L.; Closset, M.; Dogné, J.-M.; Douxfils, J. *J. Med. Virol.* **2022**.

(8) Muruato, A. E.; Fontes-Garfias, C. R.; Ren, P.; Garcia-Blanco, M. A.; Menachery, V. D.; Xie, X.; Shi, P.-Y. *Nat. Commun.* **2020**, *11* (1), 4059.

(9) Nie, J.; Li, Q.; Wu, J.; Zhao, C.; Hao, H.; Liu, H.; Zhang, L.; Nie, L.; Qin, H.; Wang, M.; Lu, Q.; Li, X.; Sun, Q.; Liu, J.; Fan, C.; Huang, W.; Xu, M.; Wang, Y. *Emerg. Microbes Infect.* **2020**, *9* (1), 680–686.

(10) Riepler, L.; Rössler, A.; Falch, A.; Volland, A.; Borena, W.; Laer, D. von; Kimpel, J. *Vaccines (Basel)* **2020**, *9* (1).

(11) Klein, S.; Cortese, M.; Winter, S. L.; Wachsmuth-Melm, M.; Neufeldt, C. J.; Cerikan, B.; Stanifer, M. L.; Boulant, S.; Bartenschlager, R.; Chlanda, P. *Nat. Commun.* **2020**, *11* (1), 5885.

(12) Walls, A. C.; Park, Y.-J.; Tortorici, M. A.; Wall, A.; McGuire, A. T.; Veesler, D. *Cell* **2020**, *183* (6), 1735.

(13) Shi, R.; Shan, C.; Duan, X.; Chen, Z.; Liu, P.; Song, J.; Song, T.; Bi, X.; Han, C.; Wu, L.; Gao, G.; Hu, X.; Zhang, Y.; Tong, Z.; Huang, W.; Liu, W. J.; Wu, G.; Zhang, B.; Wang, L.; Qi, J.; Feng, H.; Wang, F.-S.; Wang, Q.; Gao, G. F.; Yuan, Z.; Yan, J. *Nature* **2020**, *584* (7819), 120–124.

(14) Lau, E. H. Y.; Tsang, O. T. Y.; Hui, D. S. C.; Kwan, M. Y. W.; Chan, W.; Chiu, S. S.; Ko, R. L. W.; Chan, K. H.; Cheng, S. M. S.; Perera, Ranawaka A. P. M.; Cowling, B. J.; Poon, L. L. M.; Peiris, M. *Nat. Commun.* **2021**, *12* (1), 63.

(15) Klüpfel, J.; Paßreiter, S.; Rumpf, M.; Christa, C.; Holthoff, H.-P.; Ungerer, M.; Lohse, M.; Knolle, P.; Protzer, U.; Elsner, M.; Seidel, M. *Anal. Bioanal. Chem.* **2022**, 1–14.

(16) Dong, T.; Han, C.; Jiang, M.; Zhang, T.; Kang, Q.; Wang, P.; Zhou, F. *ACS Sens* **2022**, *7* (11), 3560–3570.

(17) Kim, S. J.; Yao, Z.; Marsh, M. C.; Eckert, D. M.; Kay, M. S.; Lyakisheva, A.; Pasic, M.; Bansal, A.; Birnboim, C.; Jha, P.; Galipeau, Y.; Langlois, M.-A.; Delgado, J. C.; Elgort, M. G.; Campbell, R. A.; Middleton, E. A.; Stagljar, I.; Owen, S. C. *Nat. Commun.* **2022**, *13* (1), 3716.

(18) Fenwick, C.; Turelli, P.; Pellaton, C.; Farina, A.; Campos, J.; Raclot, C.; Pojer, F.; Cagno, V.; Nusslé, S. G.; D'Acremont, V.; Fehr, J.; Puhan, M.; Pantaleo, G.; Trono, D. *Sci. Transl. Med.* **2021**, *13* (605).

(19) Connelly, G. G.; Kirkland, O. O.; Bohannon, S.; Lim, D. C.; Wilson, R. M.; Richards, E. J.; Tay, D. M.; Jee, H.; Hellinger, R. D.; Hoang, N. K.; Hao, L.; Chhabra, A.; Martin-Alonso, C.; Tan, E. K. W.; Koehler, A. N.; Yaffe, M. B.; London, W. B.; Lee, P. Y.; Krammer, F.; Bohannon, R. C.; Bhatia, S. N.; Sikes, H. D.; Li, H. *Cell Rep. Methods* **2022**, 100273.

(20) Huang, R.-L.; Fu, Y.-C.; Wang, Y.-C.; Hong, C.; Yang, W.-C.; Wang, I.-J.; Sun, J.-R.; Chen, Y.; Shen, C.-F.; Cheng, C.-M. *Vaccines (Basel)* **2022**, *10* (2).

(21) Lake, D. F.; Roeder, A. J.; Kaleta, E.; Jasbi, P.; Pfeffer, K.; Koelbela, C.; Periasamy, S.; Kuzmina, N.; Bukreyev, A.; Grys, T. E.; Wu, L.; Mills, J. R.; McAulay, K.; Gonzalez-Moa, M.; Seit-Nebi, A.; Svarovsky, S. *J. Clin. Virol.* **2021**, *145*, 105024.

(22) Kongsuphol, P.; Jia, H.; Cheng, H. L.; Gu, Y.; Shunmuganathan, B. D.; Chen, M. W.; Lim, S. M.; Ng, S. Y.; Tambyah, P. A.; Nasir, H.; Gao, X.; Tay, D.; Kim, S.; Gupta, R.; Qian, X.; Kozma, M. M.; Purushotorman, K.; McBee, M. E.; MacAry, P. A.; Sikes, H. D.; Preiser, P. R. *Commun. Med.* **2021**, *1* (1), 46.

(23) Lee, J.-H.; Lee, Y.; Lee, S. K.; Kim, J.; Lee, C.-S.; Kim, N. H.; Kim, H. G. *Biosens. Bioelectron.* **2022**, *203*, 114034.

(24) Duan, X.; Shi, Y.; Zhang, X.; Ge, X.; Fan, R.; Guo, J.; Li, Y.; Li, G.; Ding, Y.; Osman, R. A.; Jiang, W.; Sun, J.; Luan, X.; Zhang, G. *Biosens. Bioelectron.* **2022**, *199*, 113883.

(25) Rink, S.; Kaiser, B.; Steiner, M.-S.; Duerkop, A.; Baeumner, A. J. *Anal. Bioanal. Chem.* **2022**, *414* (10), 3231–3241.

(26) Mayer, M.; Takegami, S.; Neumeier, M.; Rink, S.; Jacobi von Wangelin, A.; Schulte, S.; Vollmer, M.; Griesbeck, A. G.; Duerkop, A.; Baeumner, A. J. *Angew Chem Int Ed Engl* **2018**, *57* (2), 408–411.

(27) Wongkaew, N.; He, P.; Kurth, V.; Surareungchai, W.; Baeumner, A. J. *Anal. Bioanal. Chem.* **2013**, *405* (18), 5965–5974.

(28) Peterhoff, D.; Glück, V.; Vogel, M.; Schuster, P.; Schütz, A.; Neubert, P.; Albert, V.; Frisch, S.; Kiessling, M.; Pervan, P.; Werner, M.; Ritter, N.; Babl, L.; Deichner, M.; Hanses, F.; Lubnow, M.; Müller, T.; Lunz, D.; Hitzenbichler, F.; Audebert, F.; Hähnel, V.; Offner, R.; Müller, M.; Schmid, S.; Burkhardt, R.; Glück, T.; Koller, M.; Niller, H. H.; Graf, B.; Salzberger, B.; Wenzel, J. J.; Jantsch, J.; Gessner, A.; Schmidt, B.; Wagner, R. *Infection* **2021**, *49* (1), 75–82.

(29) Einhauser, S.; Peterhoff, D.; Beileke, S.; Günther, F.; Niller, H.-H.; Steininger, P.; Knöll, A.; Korn, K.; Berr, M.; Schütz, A.; Wiegrebe, S.; Stark, K. J.; Gessner, A.; Burkhardt, R.; Kabesch, M.; Schedl, H.; Küchenhoff, H.; Pfahlberg, A. B.; Heid, I. M.; Gefeller, O.; Überla, K.; Wagner, R. *Viruses* **2022**, *14* (6).

(30) Wagner, R.; Peterhoff, D.; Beileke, S.; Günther, F.; Berr, M.; Einhauser, S.; Schütz, A.; Niller, H. H.; Steininger, P.; Knöll, A.; Tenbusch, M.; Maier, C.; Korn, K.; Stark, K. J.; Gessner, A.; Burkhardt, R.; Kabesch, M.; Schedl, H.; Küchenhoff, H.; Pfahlberg, A. B.; Heid, I. M.; Gefeller, O.; Überla, K. *Viruses* **2021**, *13* (6).

(31) Edwards, K. A.; Curtis, K. L.; Sailor, J. L.; Baeumner, A. J. *Anal. Bioanal. Chem.* **2008**, *391* (5), 1689–1702.

(32) Einhauser, S.; Peterhoff, D.; Niller, H. H.; Beileke, S.; Günther, F.; Steininger, P.; Burkhardt, R.; Heid, I. M.; Pfahlberg, A. B.; Überla, K.; Gefeller, O.; Wagner, R. *Diagnostics* **2021**, *11* (10), 1843.

(33) Edwards, K. A.; Meyers, K. J.; Leonard, B.; Baeumner, A. J. *Anal. Bioanal. Chem.* **2013**, *405* (12), 4017–4026.

(34) Kitamura, M.; Murakami, K.; Yamada, K.; Kawai, K.; Kunishima, M. *Dyes and Pigments* **2013**, *99* (3), 588–593.

(35) Barnes, C. O.; Jette, C. A.; Abernathy, M. E.; Dam, K.-M. A.; Esswein, S. R.; Gristick, H. B.; Malyutin, A. G.; Sharaf, N. G.; Huey-Tubman, K. E.; Lee, Y. E.; Robbiani, D. F.; Nussenzweig, M. C.; West, A. P.; Bjorkman, P. J. *Nature* **2020**, *588* (7839), 682–687.

(36) Yuan, M.; Liu, H.; Wu, N. C.; Wilson, I. A. *Biochem. Biophys. Res. Commun.* **2021**, *538*, 192–203.

(37) Pinto, D.; Park, Y.-J.; Beltramello, M.; Walls, A. C.; Tortorici, M. A.; Bianchi, S.; Jaconi, S.; Culap, K.; Zatta, F.; Marco, A. de; Peter, A.; Guarino, B.; Spreafico, R.; Cameroni, E.; Case, J. B.; Chen, R. E.; Havenar-Daughton, C.; Snell, G.; Telenti, A.; Virgin, H. W.; Lanzavecchia, A.; Diamond, M. S.; Fink, K.; Veesler, D.; Corti, D. *Nature* **2020**, *583* (7815), 290–295.

(38) Yuan, M.; Wu, N. C.; Zhu, X.; Lee, C.-C. D.; So, R. T. Y.; Lv, H.; Mok, C. K. P.; Wilson, I. A. *Science (New York, N.y.)* **2020**, *368* (6491), 630–633.

(39) Wu, N. C.; Yuan, M.; Bangaru, S.; Huang, D.; Zhu, X.; Lee, C.-C. D.; Turner, H. L.; Peng, L.; Yang, L.; Burton, D. R.; Nemazee, D.; Ward, A. B.; Wilson, I. A. *PLoS Pathog* **2020**, *16* (12), e1009089.

(40) Yuan, M.; Huang, D.; Lee, C.-C. D.; Wu, N. C.; Jackson, A. M.; Zhu, X.; Liu, H.; Peng, L.; van Gils, M. J.; Sanders, R. W.; Burton, D. R.; Reincke, S. M.; Prüss, H.; Kreye, J.; Nemazee, D.; Ward, A. B.; Wilson, I. A. *Science (New York, N.y.)* **2021**, *373* (6556), 818–823.

(41) Peterhoff, D.; Einhauser, S.; Beileke, S.; Niller, H.-H.; Günther, F.; Schachtner, M.; Asbach, B.; Steininger, P.; Tenbusch, M.; Peter, A. S.; Gessner, A.; Burkhardt, R.; Heid, I. M.; Wagner, R.; Überla, K. *Vaccines (Basel)* **2022**, *10* (2), 324.

## 2.1.6 Supplementary information

### 2.1.6.1 Experimental section

#### 2.1.6.1.1 Chemicals and consumables

Sucrose, sodium azide, sodium chloride and dialysis membrane Spectra/Por© 4 (MWCO: 12-14 kDa) (2718.1) were purchased from Carl Roth. Phosphorous standard was obtained from Bernd Kraft GmbH (Den Haag, Netherlands). Chloroform, methanol and Spectra-Por® Float-A-Lyzer® G2 (1 mL, MWCO: 1000 kDa) were purchased from Fisher Scientific (Hampton, NH, USA). Whatman Nucleopore™ Track-Etched membranes (1.0 µm, 0.4 µm and 0.2 µm diameter) and Tween® 20 were obtained from Sigma Aldrich/Merck (Darmstadt, Germany).

#### 2.1.6.1.2 Buffer compositions

High sucrose saline (HSS) buffer contained 200 mM sucrose, 200 mM NaCl, 10 mM HEPES and 0.01 w% $NaN_3$, pH 7.5. PMB contained 10 mM HEPES, 150 mM NaCl, 135 nM $CaCl_2$ and 1 mM $MgCl_2$, pH 7.4. PBS contained 137 mM NaCl, 2.7 mM KCl, 10 mM $Na_2HPO_4$ and 1.8 mM $KH_2PO_4$, pH 7.4. PBS-T contained 0.1 w% Tween® 20 in PBS.

#### 2.1.6.1.3 Liposome composition

*Table S1: Lipid and encapsulant compositions of all used liposomes.*

| | | | | lipids | | encapsulant | |
|---|---|---|---|---|---|---|---|
| | cholesterol /mg | DPPC /mg | DPPG /mg | DMPE /mg | *N*-glut.-DPPE /mg | SRB /mg | NaCl /mg |
| 10 mM SRB COOH-liposomes | 2.4 | 66.4 | 17.9 | - | 4.2 | 26.7 | 55.0 |
| 50 mM SRB COOH-liposomes | 9.8 | 14.4 | 8.5 | - | 4.0 | 126.3 | 52.9 |
| 150 mM SRB COOH-liposomes | 9.6 | 14.2 | 8.2 | - | 3.9 | 376.8 | 36.9 |
| 100 mM SRB NH$_2$-liposomes | 10.0 | 14.9 | 8.8 | 2.0 | - | 252.2 | 53.6 |

## 2.1.6.2 Results

### 2.1.6.2.1 Quality control of recombinant proteins

Purity of recombinant proteins was proven using reducing SDS-PAGE. Only the protein of interest could be observed (**Figure S1 A** and **B**). To analyze correct folding and biotinylation of RBD and ACE2, an ELISA experiment was performed using coated RBD on the solid phase and titration of biotinylated ACE2 compared to non-biotinylated ACE2. The ELISA revealed rigid binding of biotinylated ACE2 with a dissociation constant of 5.4 nM ± 3 (**Figure S1 C**).
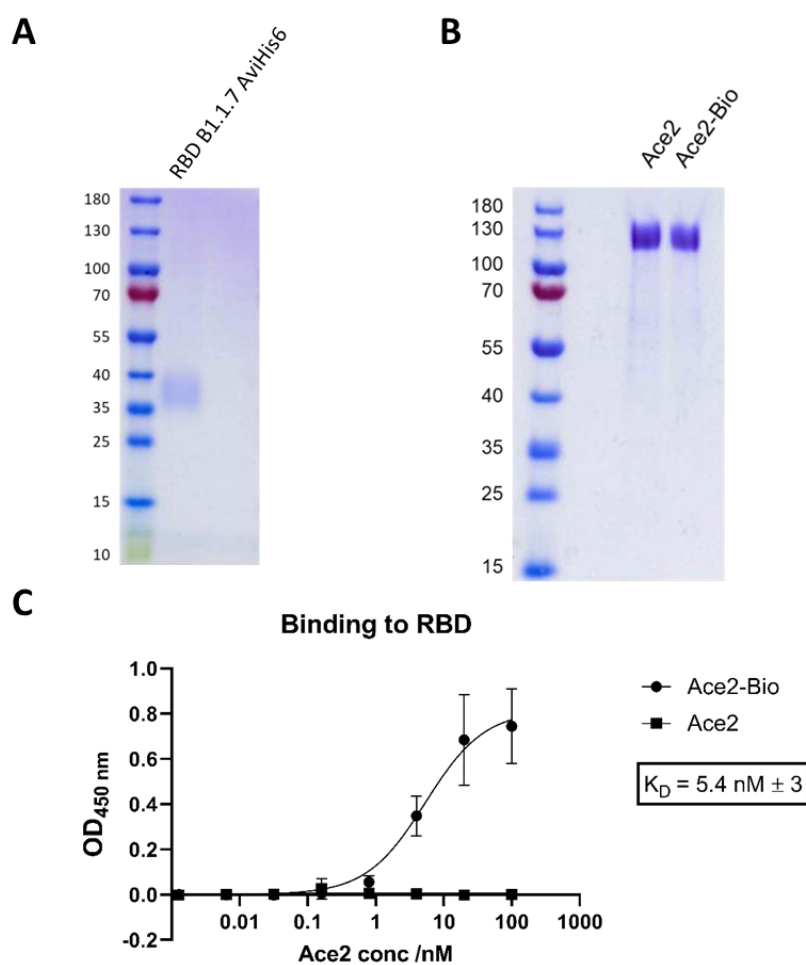


***Figure S1:*** *Quality control of recombinant proteins. Reducing SDS-PAGE of RBD B1.1.7 (**A**) and biotinylated and non-biotinylated ACE2 (**B**). 2 µg protein were loaded per lane. (**C**): Binding of biotinylated and non-biotinylated ACE2 against RBD B1.1.7 measured by ELISA. Values were fitted using non-linear curve regression (one-side hyperbola fit). n = 3.*

2.1.6.2.2  High-throughput format (HTS)

*2.1.6.2.2.1  Assay development*

Different RBD concentrations were conjugated to 10 mM SRB liposomes bearing 4 mol% lipids with carboxylated headgroups via EDC/NHS chemistry. Immobilization in an ACE2-coated microplate showed that 0.2 mol% RBD performed best. A concentration of 0.5 mol% resulted in decreased liposome immobilization, either due to dense packing or cross-linking of RBD, causing steric hindrance for the RBD-ACE2 interaction. Investigation of 0.3 mol% and 0.4 mol% showed no improvement compared to the 0.2 mol% RBD (data not shown).
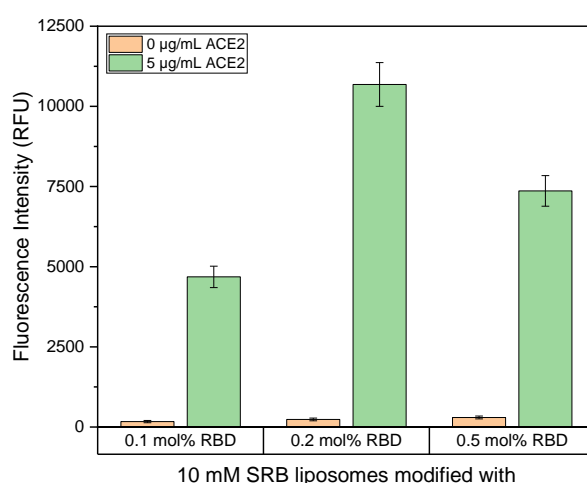


**Figure S2:** *Fluorescence intensities of 10 mM SRB encapsulating liposomes conjugated to 0.1 mol%, 0.2 mol% and 0.5 mol% RBD (10 μM total lipid concentration) immobilized in a Nunc MaxiSorp high binding microplate coated with 0 or 5 μg/mL ACE2 in PBS (100 μL). The plate was previously blocked with 1 w/v% BSA in PBS-T (150 μL) and washed with PBS-T (2x, 150 μL) and PMB (3x, 150 μL). Samples were incubated for 3h at RT and 300 rpm, washed with PMB (3x, 150 μL) and lysed by addition of 30 mM OG in bidest. $H_2O$ (100 μL, 10 min inc., RT, 300 rpm). The fluorescence was measured using a BioTek SYNERGY neo2 fluorescence reader ($\lambda_{Ex}$ = 560 nm and $\lambda_{Em}$ = 585 nm, bandwidth 10, gain 150). n = 3.*

Investigation of ACE2-coating showed that higher concentrations produced better signal intensities. A concentration of 5 μg/mL ACE2 was chosen for coating. No higher concentrations were investigated to safe on reagents.
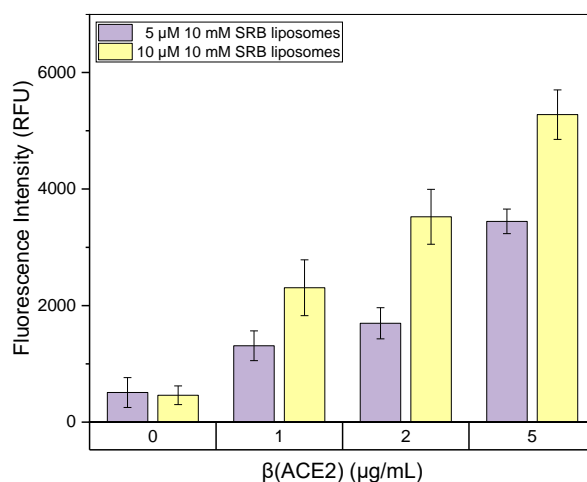
***Figure S3:*** *Fluorescence intensities of 10 mM SRB encapsulating liposomes conjugated to 0.2 mol% RBD (5 µM and 10 µM total lipid concentration) immobilized in a Nunc MaxiSorp high binding microplate coated with 0, 1, 2 or 5 µg/mL ACE2 in PBS (100 µL). The plate was previously blocked with 1 w/v% BSA in PBS-T (150 µL) and washed with PBS-T (2x, 150 µL) and PMB (3x, 150 µL). Samples were incubated for 3h at RT and 300 rpm, washed with PMB (3x, 150 µL) and lysed by addition of 30 mM OG in bidest. $H_2O$ (100 µL, 10 min inc., RT, 300 rpm). The fluorescence was measured using a BioTek SYNERGY neo2 fluorescence reader ($\lambda_{Ex}$ = 560 nm and $\lambda_{Em}$ = 585 nm, bandwidth 10, gain 150). n = 3.*

A titration curve of 50 mM SRB liposomes conjugated to 0.2 mol% RBD showed a linear correlation of fluorescence intensity and liposome concentration between the investigated 0.1 µM and 10 µM. Concentrations of 0.5 µM and 1 µM were chosen for further experiments.
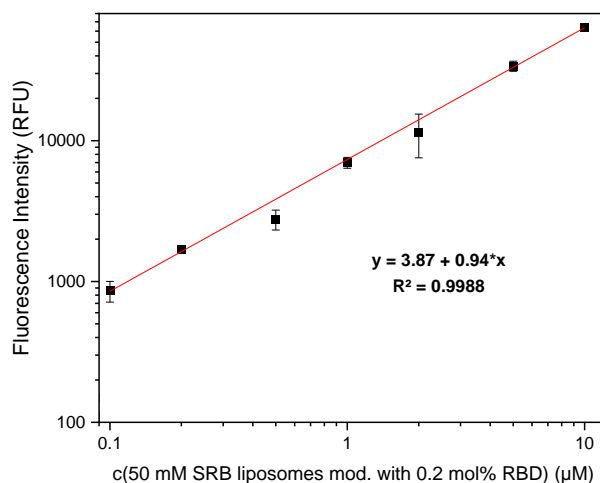


***Figure S4:*** *Fluorescence intensities of RBD-conjugated liposomes in PMB (50 mM SRB, 0, 0.1, 0.2, 0.5, 1, 2, 5 and 10 µM total lipid concentration) immobilized in a Nunc MaxiSorp high binding microplate coated with 5 µg/mL ACE2 in PBS (100 µL). The plate was previously blocked with 1 w/v% BSA in PBS-T (150 µL) and washed with PBS-T (2x, 150 µL) and PMB (3x, 150 µL). Samples were incubated for 3h at RT and 300 rpm, washed with PMB (3x, 150 µL) and lysed by addition of 30 mM OG in bidest. $H_2O$ (100 µL, 10 min inc., RT, 300 rpm). The fluorescence was measured using a BioTek SYNERGY neo2 fluorescence reader ($\lambda_{Ex}$ = 560 nm and $\lambda_{Em}$ = 585 nm, bandwidth 10, gain 150). n = 3.*

Titration curves of antibodies directed against the receptor binding site (PA5-114451) and the CR3022 and S309 binding sites of RBD showed complete inhibition of RBD-ACE2 interaction by the former. CR3022 caused partial inhibition, signals not allowing for a sigmoidal fit. S309 caused a signal decrease of >50%, but did not result in complete inhibition. The lower EC50 value compared to PA5-114451 suggests that the S309 antibody has a higher affinity.
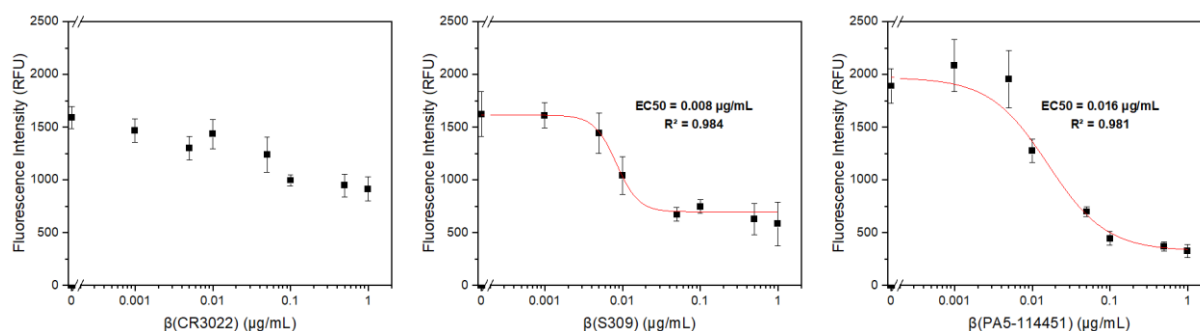


***Figure S5:*** *Fluorescence intensities of RBD-conjugated liposomes (50 mM SRB, 0.5 µM total lipid concentration) tested with non-neutralizing (CR3022 and S309) and neutralizing anti-RBD antibodies (PA5-114451) (0 µg/mL to 1 µg/mL) immobilized (after 1 h pre-incubation at RT, 300 rpm and 32-fold concentration) for 3 h at RT in a Nunc MaxiSorp high binding microplate coated with 5 µg/mL ACE2. After washing with HSS (3x, 150 µL) liposomes were lysed by addition of 30 mM OG in bidest. $H_2O$ (100 µL, 10 min inc., RT, 300 rpm). The fluorescence was measured using a BioTek SYNERGY neo2 fluorescence reader ($\lambda_{Ex}$ = 560 nm and $\lambda_{Em}$ = 585 nm, bandwidth 10, gain 150). n = 3. Curves were fitted using Origin's logistic function.*

To improve signal intensities and reduce the effect of serum concentration on the fluorescence intensity directed immobilization of biotinylated ACE2 in a streptavidin-coated microtiter plate was investigated. A 4-fold increase of signal intensities was observed compared to mere adsorption of ACE2 in a Nunc MaxiSorp high binding microtiter plate (**Figure S6**). Further investigations showed that 1 µg/mL ACE2-biotin already produced satisfactory signal intensities, compared to the previously used 5 µg/mL ACE2 (**Figure S7**). Also, no additional blocking step was needed. Comparison of 1-3 h incubation time showed that 2 h resulted in significantly better signals compared to 1 h, while 3 h only caused a minor improvement. An incubation time of 2 h was chosen as compromise for high signal intensities and shorter assay turn-around times. In the end, it was shown that ACE2-biotin immobilization could be accomplished within 1 h at RT and 300 rpm or overnight at 4 °C. The presence of 0.1 v% non-neutralizing serum did not affect signal intensities, unlike previously observed for non-directed ACE2 immobilization (**Figure S8**).
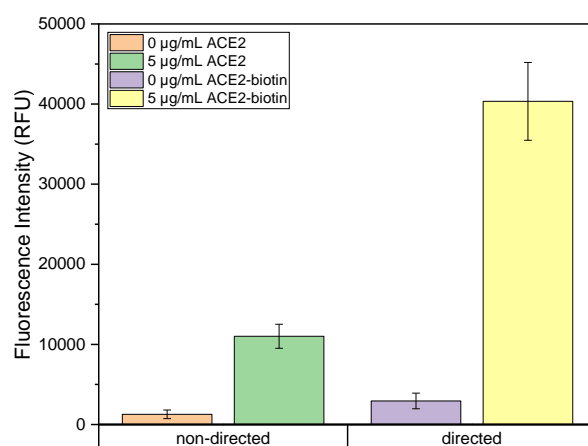
***Figure S6:*** *Fluorescence intensities of RBD-conjugated liposomes (50 mM SRB, 1 µM total lipid concentration) immobilized for 3 h at RT in a Nunc MaxiSorp high binding microplate coated with 5 µg/mL ACE2 in PBS (100 µL) and blocked with 1 w/v% BSA in PBS-T (non-directed) or in a streptavidin microplate coated with 5 µg/mL ACE2-biotin in PBS (100 µL) (site-directed). After washing with HSS (3x, 150 µL) liposomes were lysed by addition of 30 mM OG in bidest. H$_2$O (100 µL, 10 min inc., RT, 300 rpm). The fluorescence was measured using a BioTek SYNERGY neo2 fluorescence reader ($\lambda_{Ex}$ = 560 nm and $\lambda_{Em}$ = 585 nm, bandwidth 10, gain 150). n = 4.*
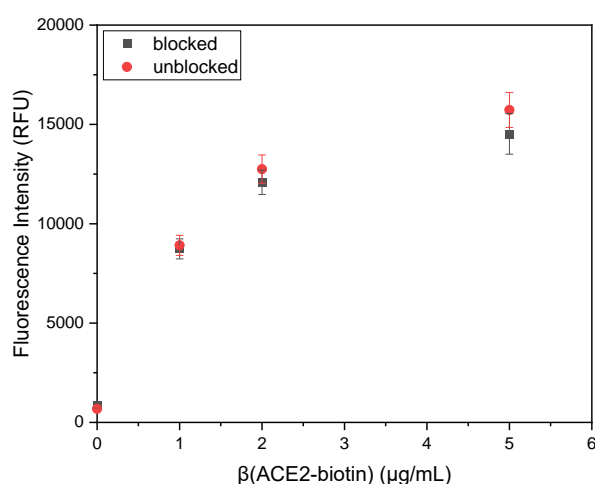


***Figure S7:*** *Fluorescence intensities of RBD-conjugated liposomes (50 mM SRB, 1 µM total lipid concentration) immobilized for 3 h at RT in a streptavidin microplate coated with 0, 1, 2 and 5 µg/mL ACE2-biotin in PBS (100 µL) unblocked or blocked with 1 w/v% BSA in PBS-T. After washing with HSS (3x, 150 µL) liposomes were lysed by addition of 30 mM OG in bidest. H$_2$O (100 µL, 10 min inc., RT, 300 rpm). The fluorescence was measured using a BioTek SYNERGY neo2 fluorescence reader ($\lambda_{Ex}$ = 560 nm and $\lambda_{Em}$ = 585 nm, bandwidth 10, gain 150). n = 4.*
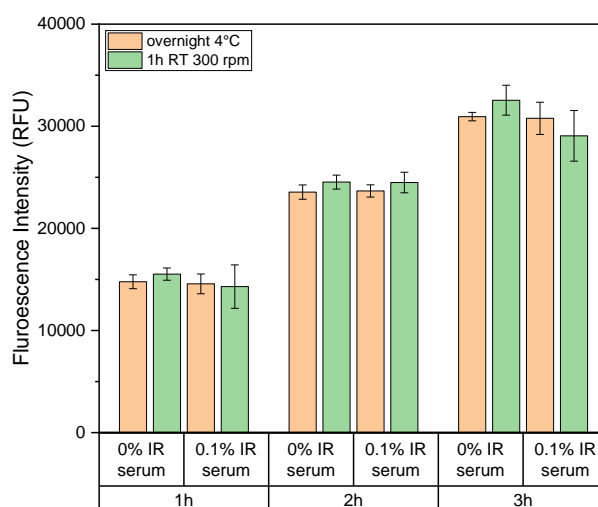
**Figure S8:** *Fluorescence intensities of RBD-conjugated liposomes (50 mM SRB, 1 μM total lipid concentration) with and without 0.1 v% seronegative pooled human serum (IR serum) immobilized for 1 h, 2 h or 3 h at RT in a streptavidin microplate coated with 1 μg/mL ACE2-biotin in PBS (100 μL) overnight at 4 °C or for 1 h at RT and 300 rpm. After washing with HSS (3x, 150 μL) liposomes were lysed by addition of 30 mM OG in bidest. $H_2O$ (100 μL, 10 min inc., RT, 300 rpm). The fluorescence was measured using a BioTek SYNERGY neo2 fluorescence reader ($\lambda_{Ex}$ = 560 nm and $\lambda_{Em}$ = 585 nm, bandwidth 10, gain 150). n = 4.*

### 2.1.6.2.2.2  Serum panel screening

8 seronegative samples (as determined with the *recom*Line SARS-CoV-2 IgG assay, **Table S3**) were analyzed with the HTS neutralization test. As expected, no binding inhibition was observed, hence no IC50 values could be obtained (**Figure S9**). Interestingly, a fluorescence enhancing effect was observed for seronegative samples from donors with other respiratory diseases (RSV, Influenza A, Adenovirus, Mycoplasm).
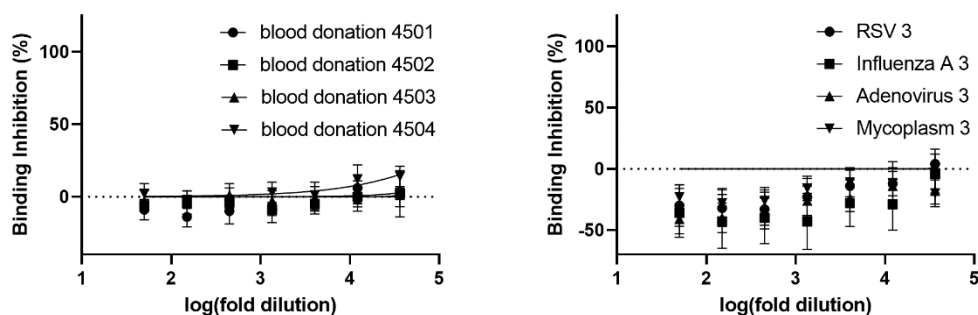


**Figure S9:** *Best-fit graphs for seronegative sera, as determined with the recomLine SARS-CoV-2 IgG assay, tested in the HTS neutralization test as calculated using GraphPad Prism 9's 'log(inhibitor) vs. normalized response with variable slope' algorithm. Binding inhibition, given as percentage, was calculated as (1 − fluor. int./fluor. int. neg. control)\*100. 2 v% serum, 3-fold series dil. 50 mM SRB lipos. (1 μM).*

*Table S2:* *Summary of IC50 values of neutralizing sera (nS) tested in the pseudovirus neutralization test and the liposome-based HTS neutralization test. Best-fit IC50 values including R² values were calculated using GraphPad Prism 9 ('log(inhibitor) vs. normalized response – Variable slope' algorithm). IC50 values obtained with the liposome-based HTS neutralization test with R² values <0.9, <0.8 and <0.5 are marked respectively. Additionally, the binding inhibition values obtained in the POC neutralization test are listed.*

| | pseudovirus neutr. test | HTS neutr. test 2 v% serum, 3-fold series dil. 50 mM SRB lipos. (1 µM) | | HTS neutr. test 4 v% serum, 2-fold series dil. 150 mM SRB lipos. (0.5 µM) | | POC neutr. test |
|---|---|---|---|---|---|---|
| No. | IC50 | IC50 | R² | IC50 | R² | Binding inhibition |
| nS1 | 21.32 | - | - | 17.09 | 0.6621 | 12% |
| nS2 | 187.4 | 142.9 | 0.9675 | 229.8 | 0.9809 | 96% |
| nS3 | >3000 | 3939 | 0.9909 | 26870 | 0.9052 | 103% |
| nS4 | 57.47 | - | - | 19.00 | 0.7929 | -3% |
| nS5 | 332.3 | 109.2 | 0.9226 | 336.6 | 0.9726 | 83% |
| nS6 | 194.7 | 47.66 | 0.8813 | 119.8 | 0.9310 | 25% |
| nS7 | 40.43 | 27.23 | 0.6254 | 60.89 | 0.8521 | 16% |
| nS8 | 113.7 | 163.4 | 0.9554 | 222.9 | 0.9876 | 92% |
| nS9 | 20 | - | - | 13.21 | 0.7381 | 12% |
| nS10 | 25.21 | 54.30 | 0.8222 | 107.4 | 0.9693 | 51% |
| nS11 | 41.45 | 8.855 | 0.4568 | 45.72 | 0.8881 | -3% |
| nS12 | 260.6 | 166.1 | 0.9490 | 249.1 | 0.9849 | 81% |
| nS13 | 32.41 | 48.64 | 0.7657 | 82.39 | 0.9734 | 27% |
| nS14 | 56.37 | - | - | 38.28 | 0.8988 | 8% |
| nS15 | 403.8 | 266.9 | 0.9719 | 559.5 | 0.9817 | 100% |
| nS16 | 265.9 | 176.8 | 0.9646 | 269.8 | 0.9676 | 93% |
| nS17 | 22.5 | - | - | 41.06 | 0.9044 | 23% |
| nS18 | 25.23 | 35.55 | 0.6064 | 68.74 | 0.9264 | 41% |
| nS19 | 40.5 | 45.83 | 0.8473 | 120.7 | 0.9418 | 43% |
| nS20 | 23.2 | 36.01 | 0.4296 | 16.83 | 0.8637 | 27% |

**Table S2** lists IC50 values for 20 neutralizing sera tested in the pseudovirus neutralization test[1] and the HTS neutralization test (initial format using 50 mM SRB liposomes and optimized format using 150 mM SRB liposomes) as well as binding inhibition values obtained in the POC neutralization test. Binding inhibition curves obtained in the HTS neutralization test are shown in **Figure S10**. Additional 10 seronegative samples were investigated with the optimized conditions (**Figure S11**). No binding inhibition was observed for any of the investigated samples.
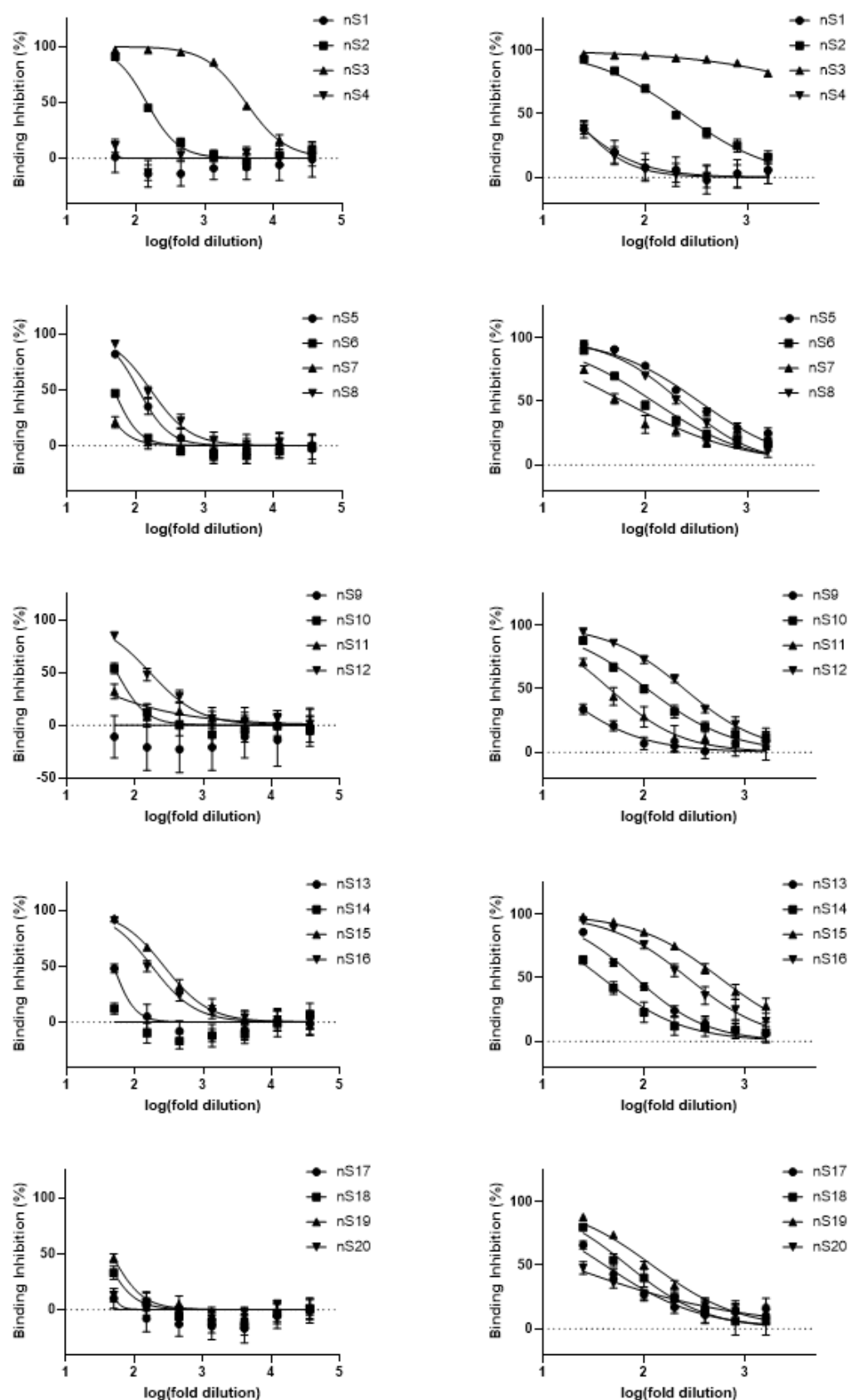
***Figure S10:*** *Best-fit graphs for 20 neutralizing sera (nS) tested in the HTS neutralization test as calculated using GraphPad Prism 9's 'log(inhibitor) vs. normalized response with variable slope' algorithm. Binding inhibition, given as percentage, was calculated as (1 – fluor. int./fluor. int. neg. control)\*100. Left graphs - 2 v% serum, 3-fold series dil. 50 mM SRB lipos. (1 µM). Right graphs - 4 v% serum, 2-fold series dil. 150 mM SRB lipos. (0.5 µM).*
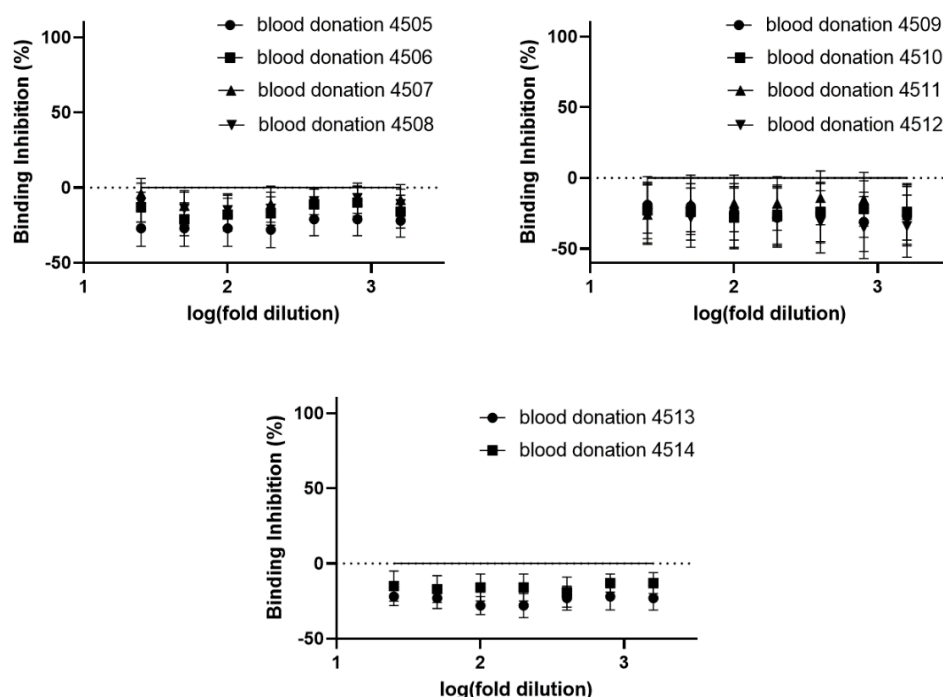
*Figure S11:* *Best-fit graphs for seronegative sera, as determined with the recomLine SARS-CoV-2 IgG assay, tested in the HTS neutralization test as calculated using GraphPad Prism 9's 'log(inhibitor) vs. normalized response with variable slope' algorithm. Binding inhibition, given as percentage, was calculated as (1 − fluor. int./fluor. int. neg. control)\*100. 4 v% serum, 2-fold series dil. 150 mM SRB lipos. (0.5 µM).*

## 2.1.6.3 Point-of-care format (POC)

The use of 150 mM SRB liposomes conjugated to 0.2 mol% RBD with 1 equivalent ACE2-biotin and 10 v% non-neutralizing serum on test strips with streptavidin test line was investigated. A linear correlation of signal intensity and liposome concentration was observed between the investigated 5 µM and 20 µM (**Figure S12**). For further studies a concentration of 10 µM was chosen as a compromise between low liposome concentration for a highly sensitive assay and a well visible signal.

***Figure S12:*** *Test strips (**a**) and their signal intensities (**b**) of RBD-conjugated liposomes (150 mM SRB, 5-20 µM total lipid concentration) tested with seronegative pooled human serum (10 v%). Samples were pre-incubated for 15 min at RT and 300 rpm in HSS. ACE2-biotin (1 equivalent per RBD) was added to samples before addition to the test strip. Samples were washed after 5 min (25 µL HSS) and pictures were taken after another 20 min using a Canon EOS 550D camera with a Canon EFS 18-55mm lens. Images were analyzed using ImageJ. n = 3.*

Investigation of ACE2-biotin concentration showed no improvement for 2 or more equivalents of ACE2-biotin per RBD molecule (**Figure S13**). Repetition of the study showed optimum signal intensity using 3 equivalents (data not shown). This concentration was hence chosen for all further studies. No additional incubation step was needed after addition of ACE2-biotin to the pre-incubated liposome-serum mixture (**Figure S14**).
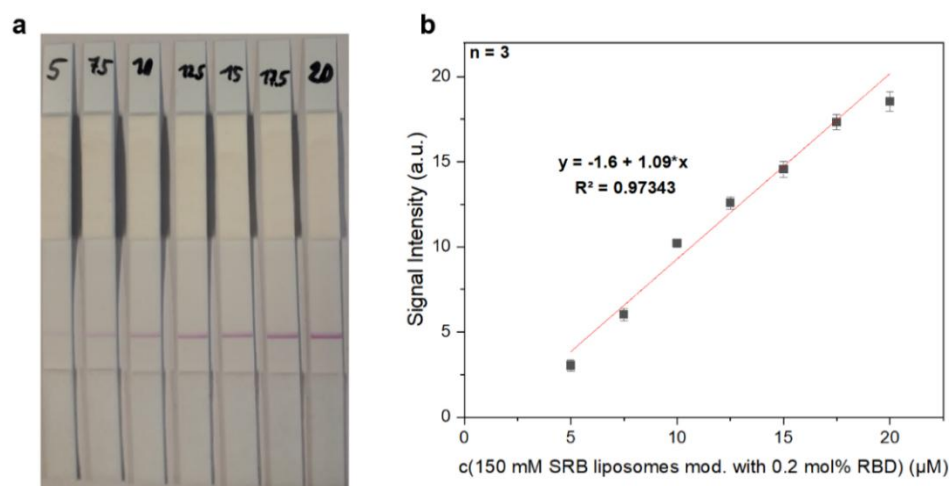


***Figure S13:*** *Test strips (**a**) and their signal intensities (**b**) of RBD-conjugated liposomes (150 mM SRB, 10 µM total lipid concentration) tested with seronegative pooled human serum (10 v%). Samples were pre-incubated for 15 min at RT and 300 rpm in HSS. ACE2-biotin (1, 2, 3, 4 or 5 equivalents per RBD) was added to samples before addition to the test strip. Samples were washed after 5 min (25 µL HSS) and pictures were taken after another 20 min using a Canon EOS 550D camera with a Canon EFS 18-55mm lens. Images were analyzed using ImageJ. n = 1.*
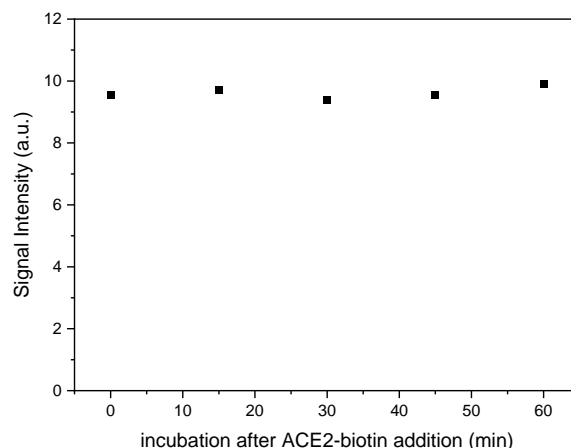
***Figure S14:*** *Signal intensities of RBD-conjugated liposomes (150 mM SRB, 10 µM total lipid concentration) tested with seronegative pooled human serum (10 v%). Samples were pre-incubated for 15 min at RT and 300 rpm in HSS. ACE2-biotin (3 equivalents per RBD) was added to samples and a second incubation step (0-60 min) added before addition to the test strip. Samples were washed after 5 min (25 µL HSS) and pictures were taken after another 20 min using a Canon EOS 550D camera with a Canon EFS 18-55mm lens. Images were analyzed using ImageJ. n = 1.*

Liposomes conjugated with fluorescein 5(6)-isothiocyanate (FITC) were developed to serve as a control that could be captured on an <anti-FITC> line on the nitrocellulose membrane. FITC was coupled to amine groups on the liposomal surface in carbonate buffer (100 mM NaHCO$_3$, 250 mM NaCl, pH 9) overnight followed by dialysis. A linear range of signal intensity to liposome concentration was observed between 3 µM and 16.5 µM and a concentration of 12.9 µM FITC-conjugated liposomes was shown to produce an identical signal intensity as 10 µM RBD-conjugated liposomes (**Figure S15**).
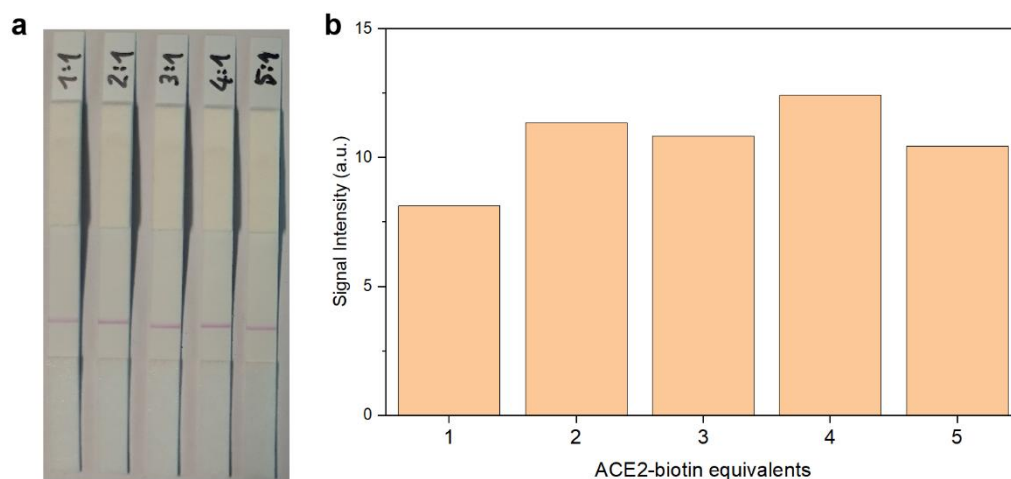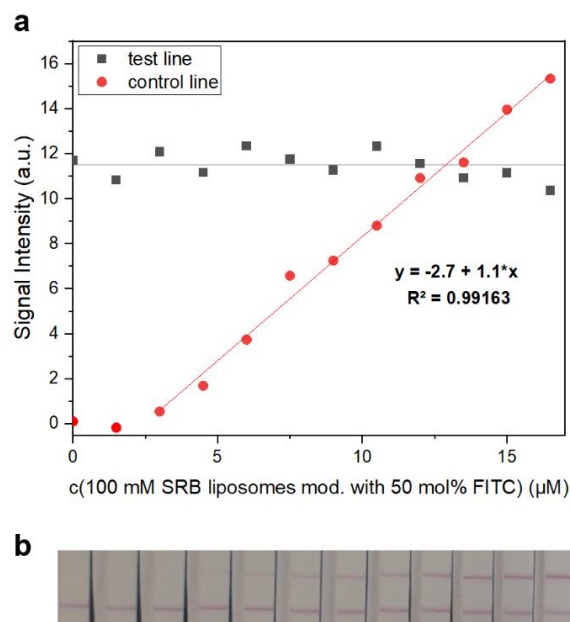


***Figure S15:*** *Test strips (**b**) and their signal intensities (**a**) of RBD-conjugated liposomes (150 mM SRB, 10 µM total lipid concentration) and control liposomes (100 mM SRB, 50% FITC, 0-16.5 µM total lipid concentration) tested with seronegative pooled human serum (10 v%). Samples were pre-incubated for 15 min at RT and 300 rpm in HSS. ACE2-biotin (3 equivalents per RBD) was added to samples before addition to the test strip. Samples were washed after 5 min (25 µL HSS) and pictures were taken after another 20 min using a Canon EOS 550D camera with a Canon EFS 18-55mm lens. Images were analyzed using ImageJ. n = 1.*

Reproducibility of the assay was investigated with seronegative pooled human serum. Six test strips were run under identical conditions, resulting in binding inhibition values between -4% and 4%, with a mean of -2 ± 3% (**Figure S16**).
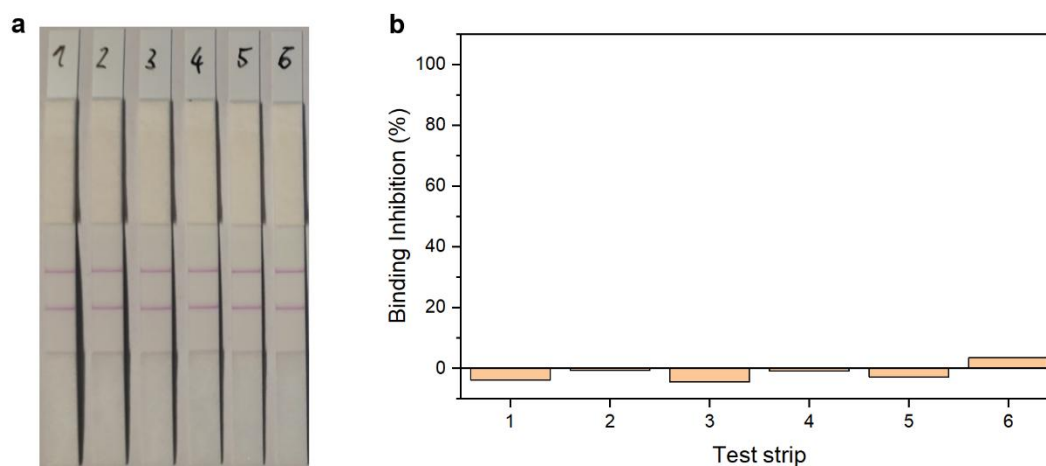


*Figure S16: Test strips (a) and binding inhibition values (b) of seronegative pooled human serum samples. n = 1.*

Addition of ACE2-biotin before and after pre-incubation of liposomes with serum was investigated for a weakly, intermediate and strongly neutralizing sera. Complete binding inhibition was observed for the strongly neutralizing serum in both cases due to its high neutralization potential (**Figure S17**). The intermediate neutralizing serum showed higher binding inhibition in case of ACE2-biotin addition after pre-incubation, as anticipated. This mimics the realistic interaction of SARS-CoV-2 with the immune system, antibodies present in serum or respiratory fluids being able to neutralize the virus before it reaches potential host cells. If ACE2-biotin is added before pre-incubation instead, it can bind to RBD, and neutralization is dependent on its dissociation. For the weakly neutr. serum a weaker test line was also observed for addition after pre-incubation. However, due to non-specific binding reduced control line intensities were obtained, resulting in false-negatives. Later studies revealed that the non-specific binding is likely caused by formation of agglomerates too large to pass through the pores of the membrane. The use of a membrane with larger pore size (CN95, Sartorius) resulted in reduced non-specific binding compared to the CN150 membrane (**Figure S20**).
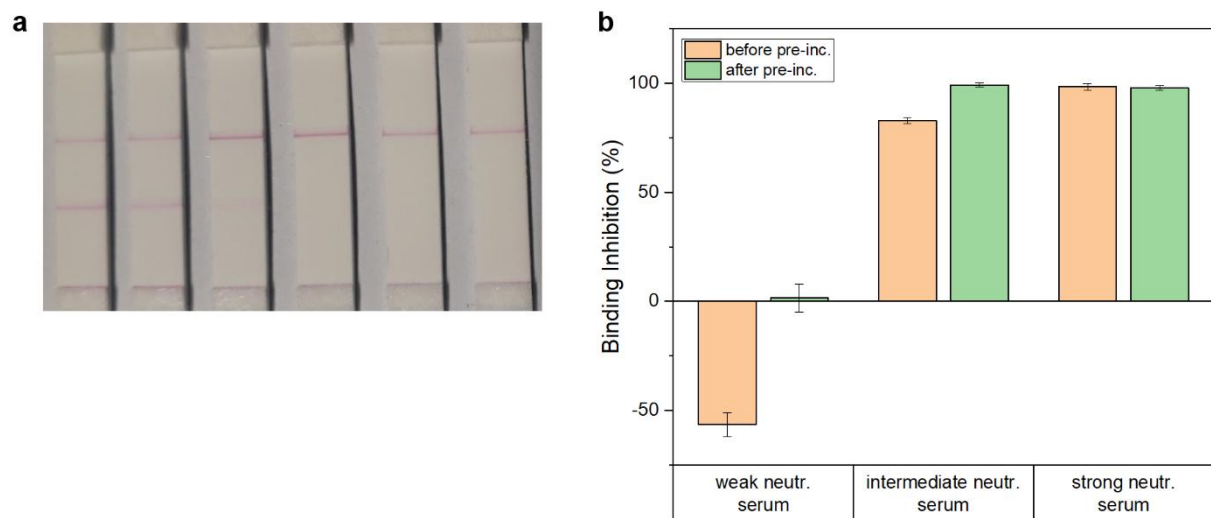
***Figure S17:*** *Test strips (**a**) and binding inhibition values (**b**) of a weak, intermediate and a strongly neutralizing serum tested with ACE2-biotin addition before or after the pre-incubation of liposomes with serum. n = 1.*

Investigation of the influence of the pre-incubation time revealed slightly increased binding inhibition for 15 min over 5 min and 0 min (**Figure S18**). However, 5 min would make for a good compromise in a final product, shortening turn-around time of the assay.



***Figure S18:*** *Test strips (**a**) and binding inhibition values (**b**) of sera no. 46, 93 and 94 from the serum panel previously tested for binding antibodies against SARS-CoV-2 RBD using the recomLine SARS-CoV-2 IgG assay tested in the lateral flow neutralization test with 0 min, 5 min and 15 min pre-incubation of liposomes with serum. n = 1.*

24 sera from a serum panel previously tested for binding anti-RBD antibodies with the *recom*Line SARS-CoV-2 assay were analyzed with the established POC neutralization test. Samples included timelines from vaccinated and convalescent donors as well as seronegat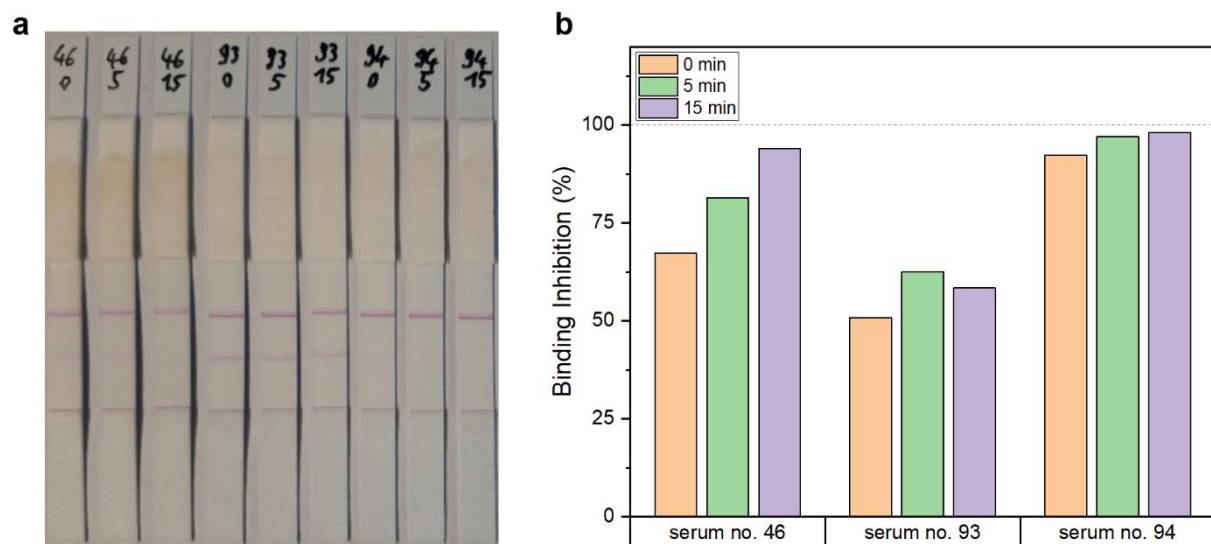ive samples from patients with other respiratory diseases. The resulting binding inhibition values are displayed in **Figure S19**, details regarding days passed since infection or vaccination can be found in **Table S3**.



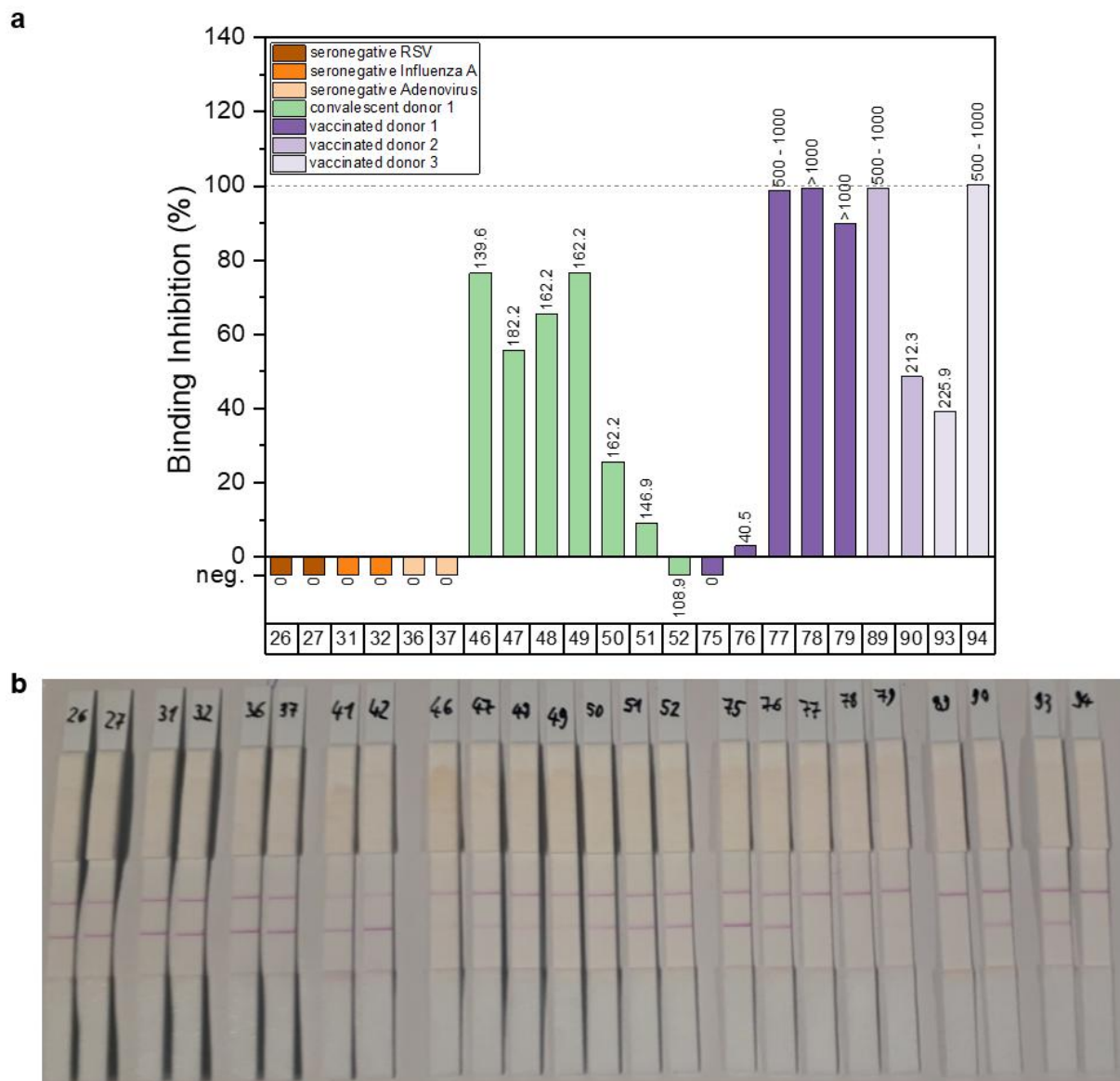***Figure S19:*** *Test strips (**b**) and binding inhibition values (**a**) of 24 samples from the Munich Cohort serum panel previously tested for binding antibodies against SARS-CoV-2 RBD using the recomLine SARS-CoV-2 IgG assay. n = 1. No binding inhibition values could be determined for sera no. 41 and 42 due to extensive non-specific binding of FITC-conjugated liposomes, resulting in a decreased control line intensity.*

***Figure S20:*** *Test strips (1-4 from left to right) run with sera no. 41 (strips 1 and 2) and 76 (strips 3 and 4) from the serum panel previously tested for binding antibodies against SARS-CoV-2 RBD using the recomLine SARS-CoV-2 IgG assay. Strips 1 and 3 contained a streptavidin test line and <anti-FITC> control line on CN150 membrane. Strips 2 and 4 contained a streptavidin test line and FITC control line on CN95 membrane.*

Six seronegative samples were analyzed to determine the threshold of the assay. The experiment was conducted three times on different days with room temperature varying between 22 and 26 °C. Samples showed binding inhibition values around 0% in most cases, with exception of blood donations 4498 and 4500 with values of 10 ± 7% and -10 ± 3% (**Figure S21**). The average of all 18 measurements (0%) + 3x the standard deviation (11%) was used as preliminary cut-off (33%) for further experiments.
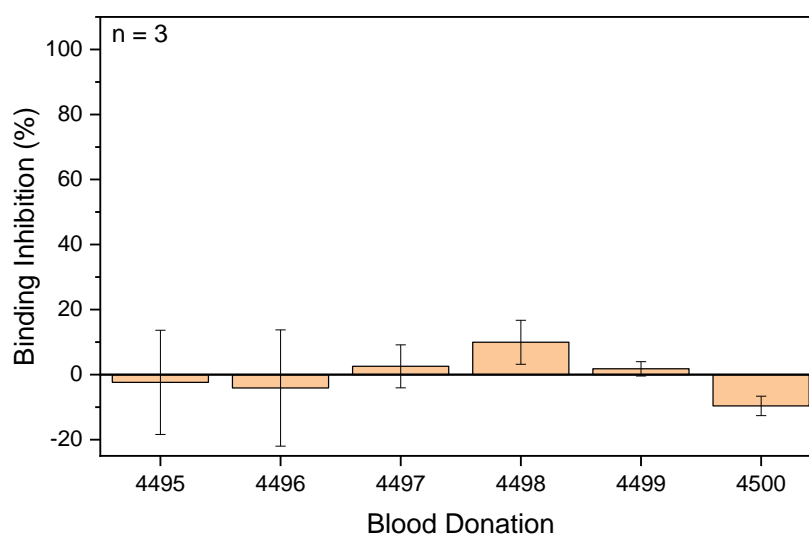


***Figure S21:*** *Binding inhibition values of seronegative samples (blood donation 4495-4500) from the serum panel previously tested for binding antibodies against SARS-CoV-2 RBD using the recomLine SARS-CoV-2 IgG assay. n = 3.*

Investigation of additional 10 seronegative samples suggests good sensitivity of the assay. No binding inhibition was observed for any sample. However, reduced control line intensities for blood donations 4505 and 4507 resulted in exceptionally low values of -24% and -53%.
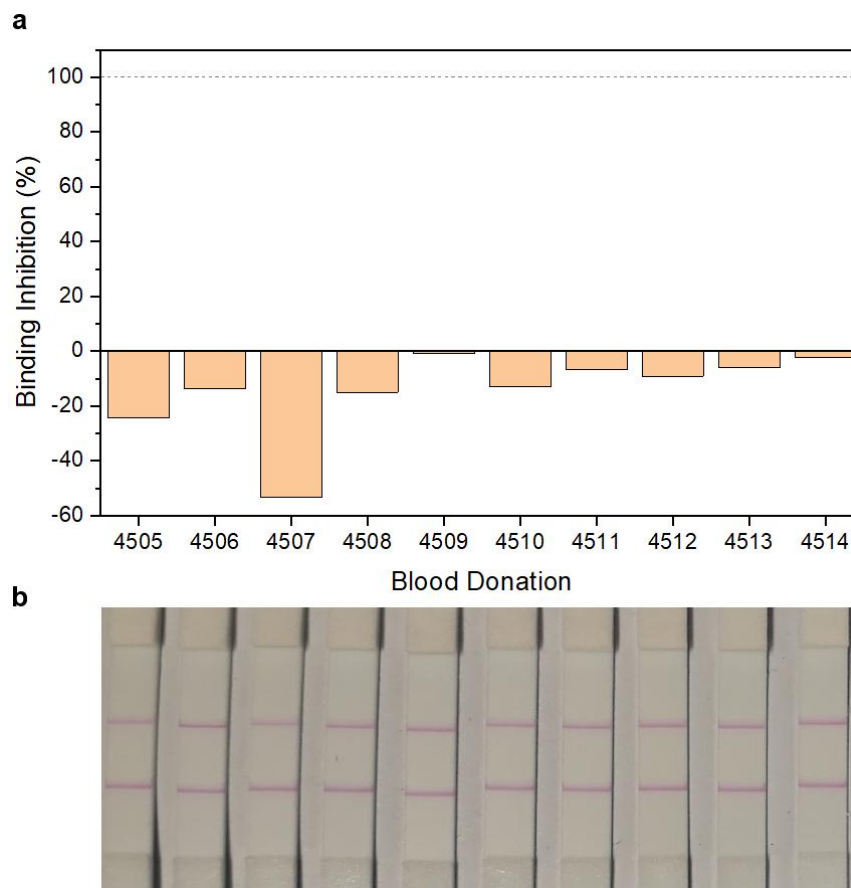


**Figure S22:** *Test strips (b) and binding inhibition values (a) of seronegative samples (blood donation 4505-4514) from the serum panel previously tested for binding antibodies against SARS-CoV-2 RBD using the recomLine SARS-CoV-2 IgG assay. n = 1.*

**Table S3:** *List of used serum samples tested for binding antibodies against SARS-CoV-2 RBD using the recomLine SARS-CoV-2 IgG assay. Antibody titers are given as binding antibody units per mL. Vaccinated donor 1 was vaccinated with Spikevax® vaccine from Moderna, vaccinated donors 2 and 3 with Comirnaty® vaccine from BioNTech/Pfizer.*

| No. | Sample ID | classification | comment | RBD [BAU/mL] |
|-----|-----------|----------------|---------|--------------|
| 1 | **blood donation 4495** | seronegative | | 0 |
| 2 | **blood donation 4496** | seronegative | | 0 |
| 3 | **blood donation 4497** | seronegative | | 0 |
| 4 | **blood donation 4498** | seronegative | | 0 |
| 5 | **blood donation 4499** | seronegative | | 0 |
| 6 | **blood donation 4500** | seronegative | | 0 |

| 7 | **blood donation 4501** | seronegative | | 0 |
|---|---|---|---|---|
| 8 | **blood donation 4502** | seronegative | | 0 |
| 9 | **blood donation 4503** | seronegative | | 0 |
| 10 | **blood donation 4504** | seronegative | | 0 |
| 11 | **blood donation 4505** | seronegative | | 0 |
| 12 | **blood donation 4506** | seronegative | | 0 |
| 13 | **blood donation 4507** | seronegative | | 0 |
| 14 | **blood donation 4508** | seronegative | | 0 |
| 15 | **blood donation 4509** | seronegative | | 0 |
| 16 | **blood donation 4510** | seronegative | | 0 |
| 17 | **blood donation 4511** | seronegative | | 0 |
| 18 | **blood donation 4512** | seronegative | | 0 |
| 19 | **blood donation 4513** | seronegative | | 0 |
| 20 | **blood donation 4514** | seronegative | | 0 |
| 26 | **RSV 1** | seronegative | RSV infection | 0 |
| 27 | **RSV 2** | seronegative | RSV infection | 0 |
| 28 | **RSV 3** | seronegative | RSV infection | 0 |
| 31 | **Influenza A 1** | seronegative | Influenza A infection | 0 |
| 32 | **Influenza A 2** | seronegative | Influenza A infection | 0 |
| 33 | **Influenza A 3** | seronegative | Influenza A infection | 0 |
| 36 | **Adenovirus 1** | seronegative | Adenovirus infection | 0 |
| 37 | **Adenovirus 2** | seronegative | Adenovirus infection | 0 |
| 38 | **Adenovirus 3** | seronegative | Adenovirus infection | 0 |
| 41 | **Mycoplasm 1** | seronegative | Mycoplasm infection | 0 |
| 42 | **Mycoplasm 2** | seronegative | Mycoplasm infection | 0 |
| 43 | **Mycoplasm 3** | seronegative | Mycoplasm infection | 0 |
| 46 | **convalescent donor 1.1** | convalescent | 27 days after symptom onset | 139.6 |
| 47 | **convalescent donor 1.2** | convalescent | 34 days after symptom onset | 182.2 |
| 48 | **convalescent donor 1.3** | convalescent | 41 days after symptom onset | 162.2 |
| 49 | **convalescent donor 1.4** | convalescent | 50 days after symptom onset | 162.2 |
| 50 | **convalescent donor 1.5** | convalescent | 62 days after symptom onset | 162.2 |
| 51 | **convalescent donor 1.6** | convalescent | 90 days after symptom onset | 146.9 |
| 52 | **convalescent donor 1.7** | convalescent | 132 days after symptom onset | 108.9 |
| 75 | **vaccinated donor 1.1** | vaccinated | before vaccination | 0 |
| 76 | **vaccinated donor 1.2** | vaccinated | 1st vaccination | 40.5 |
| 77 | **vaccinated donor 1.3** | vaccinated | 23 days after 2nd vaccination | 500 - 1000 |
| 78 | **vaccinated donor 1.4** | vaccinated | 86 days after 2nd vaccination | >1000 |
| 79 | **vaccinated donor 1.5** | vaccinated | 174 days after 2nd vaccination | >1000 |
| 89 | **vaccinated donor 2.1** | vaccinated | 60 days after 2nd vaccination | 500 - 1000 |
| 90 | **vaccinated donor 2.2** | vaccinated | 188 days after 2nd vaccination | 212.3 |
| 93 | **vaccinated donor 3.1** | vaccinated | 162 days after 2nd vaccination | 225.9 |
| 94 | **vaccinated donor 3.2** | vaccinated | 3rd vaccination | 500 - 1000 |

The 20 neutralizing sera previously tested in both a pseudovirus neutralization test and the developed HTS neutralization test were subsequently tested in the POC format (**Figure S23**). Obtained binding inhibition values can be found in **Table S2**.
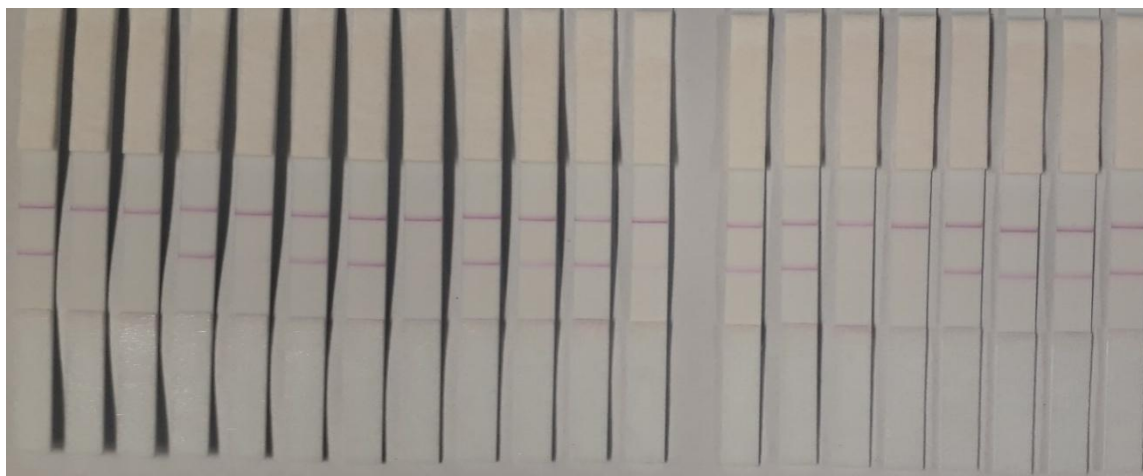


*Figure S23: Test strips of 20 neutralizing sera (left to right: nS1-20) tested in the POC neutralization test. n = 1.*

## 2.1.6.4 Liposome stability

The stability of 150 mM SRB liposomes conjugated to 0.2 mol% RBD was monitored over the course of 10 weeks. Both Z-average and polydispersity index (PDI) showed an increase after 6 weeks coinciding with the observation of precipitation in the storage container (**Figure S24 a**). The liposomes appear to aggregate after >1 month of storage at 4 °C. Leakage was studied by fluorescence measurements of unlysed liposomes in HSS buffer and lysed liposomes in bidest. $H_2O$ with 30 mM OG. The latter results in the max. fluorescence intensity, which allows for calculation of unlysed fluorescence given as percentage by normalization of the unlysed to the lysed fluorescence. An increase of unlysed fluorescence from 15% to 20% was observed within the first week (**Figure S24 b**), potentially due to partial diffusion of SRB outside of the liposomes, but it may also be within the margin of error. No further increase was observed in the weeks after, suggesting that the liposomes remain stable and do not leak any SRB.
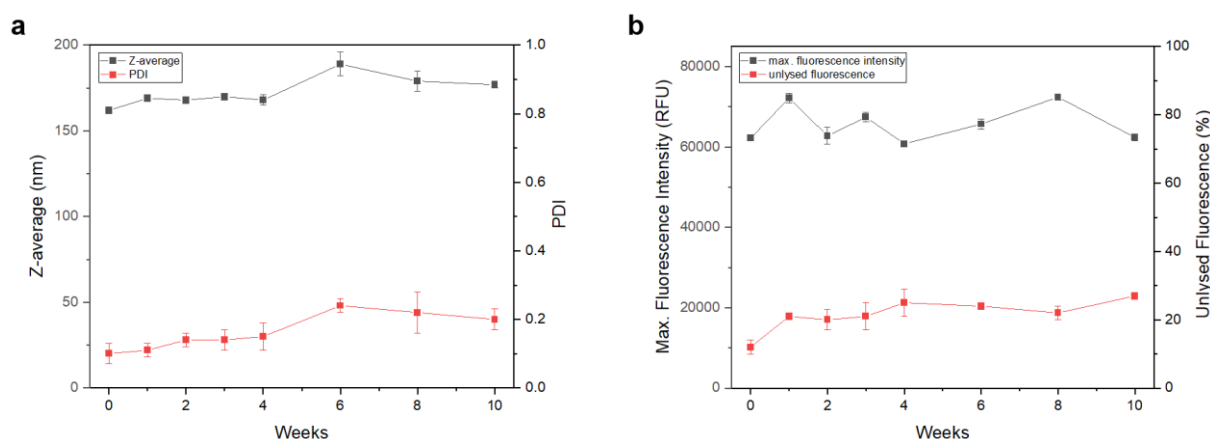


***Figure S24:*** *Z-average and PDI (**a**) and max. fluorescence intensity and unlysed fluorescence (**b**) of RBD-conjugated liposomes (150 mM SRB) over the course of 10 weeks. Liposomes (900 µM total lipids in HSS) were stored at 4 °C in the dark in between measurements and were vortexed for 20 s before being used. Unlysed fluorescence was calculated by normalization of the fluorescence intensity of liposomes in HSS (5 µM total lipids) to the fluorescence intensity of lysed liposomes (5 µM total lipids, lysed by 10 min incubation with 30 mM OG in bidest. $H_2O$).*

## 2.1.6.5 References

(1) Einhauser, S.; Peterhoff, D.; Niller, H. H.; Beileke, S.; Günther, F.; Steininger, P.; Burkhardt, R.; Heid, I. M.; Pfahlberg, A. B.; Überla, K.; Gefeller, O.; Wagner, R. *Diagnostics* **2021**, *11* (10), 1843.

## 2.2 Optimization of the stability of liposomes modified with the receptor binding domain of SARS-CoV-2 Alpha using EDC/sulfo-NHS chemistry

**Abstract**

Long-term stability of assay components is crucial for commercialization of tests. Here, the long-term stability of liposomes modified with RBD, required for the newly established liposome-based surrogate virus neutralization test, discussed in chapter 2.1, was optimized. Out of the 10 investigated stabilizing excipients, including amino acids, carbohydrates, detergents, proteins and polymers, only BSA or HSA improved colloidal stability of RBD liposomes. Storage in HSS buffer was found to be detrimental to the functionality of RBD, the ACE2 binding ability decreasing rapidly within one month already. Follow-up studies showed that the use of PBS buffer with increased osmolality, e.g. by the addition of sucrose, could maintain the functionality of RBD. However, interaction of RBD with the lipid bilayer appeared to increase membrane permeability, allowing for the slow diffusion of SRB out of the liposomes, correlating to a loss of signal intensity in the ACE2 binding assay. Addition of sucrose or NaCl to increase osmolality did not slow the diffusion of SRB. The liposome concentration during storage was found to influence both diffusion of SRB and ACE2 binding ability, higher concentrations improving stability. Storage of RBD liposomes at 100 µM total lipids in PBS buffer with 200 mM sucrose and 0.04 w/v% HSA as stabilizer were determined as optimum storage conditions, facilitating RBD liposome stability for 24 weeks. For longer storage times, separate storage of liposomes and RBD would be required to prevent leakage of SRB and ensure protein functionality.

**This chapter has not been published.**

## 2.2.1 Introduction

Development of new diagnostic tests includes the optimization of storage conditions for each assay component to allow for their long-term storage. The In Vitro Diagnostic Regulation (IVDR) requires manufacturers to provide detailed information regarding shelf-life, component stability, transport stability, as well as in-use stability[1]. These can be acquired through either real-time or accelerated stability studies. The latter are performed at elevated temperatures, the stability at the desired storage temperature is extrapolated using an Arrhenius plot[2]. Their advantage lies in the short time needed to obtain results, speeding up the process of optimization. However, the data are only accepted for initial shelf-life claims and must be followed up with real-time studies. Hence, if sufficient time is available, real-time studies should be preferred to accelerated studies.

The stability of proteins is affected by multiple factors, including their concentration, the ionic strength and pH of the buffer, as well as temperature[3]. Conjugation to signaling agents, such as nanoparticles, adds further interactions that can have a destabilizing effect, which depend on both the orientation of the protein as well as the nanoparticle surface characteristics[4,5]. The change of surface charge upon protein conjugation for example can result in electrostatically induced aggregation of previously colloidally stable nanoparticles. Different storage conditions might be required for protein, nanoparticle and protein-nanoparticle conjugate. Addition of stabilizing excipients can prevent agglomeration or unfolding of the protein, or protein conjugate, via different strategies. Detergents, for instance, can interact with hydrophobic sections of a protein, minimizing protein-protein interaction, or accumulate at the liquid-air interface, or liquid-solid interface with the storage container, preventing surface-induced aggregation[6]. Carbohydrates, such as glycerol, trehalose or sucrose, can form hydrogen bonds with the protein, replacing water, and thus serve as both stabilizers and cryoprotectants[7]. Freezing or lyophilization of the protein or conjugate solution can enhance storage stability, but requires extensive studies, because the process can also have a negative impact, for example due to the stress induced during ice crystal formation[8]. Amino acids are often added as co-stabilizers besides sucrose or trehalose. Histidine, glycine and arginine are commonly used, increasing ionic strength and minimizing electrostatic interactions between proteins[6,9]. The use of polymers, such as dextran, poly(ethylene glycol) and poly(vinyl pyrrolidone), can also improve protein stability, effectively acting as barriers, reducing protein-protein interactions[8].

Liposomes are typically colloidally stable due to their positive or negative surface charges, mediated by incorporation of lipids with functionalized headgroups. Upon modification with a protein the surface charge can be reduced, or the proteins might exhibit subunits with different charge. This can promote interaction of the modified liposomes, leading to agglomeration, and

requires the performance of stability studies. In the case of streptavidin modified liposomes, long-term stability at 4 °C for more than one year was determined with an accelerated stability study at 37 °C[10]. Storage of RBD modified liposomes without the addition of stabilizers showed aggregation after 4 weeks[11]. Here, we optimized the long-term storage stability of RBD modified liposomes, investigating the influence of different buffers and stabilizers.

## 2.2.2 Experimental section

### 2.2.2.1 Chemicals and consumables

All chemicals were of analytical reagent grade. Bovine serum albumin fraction V (BSA), cholesterol from sheep wool (C8667, ≥ 99%), D-(+)-Trehalose dihydrate, glycine, human serum albumin (HSA), L-arginine monohydrochloride, L-lysine monohydrochloride, medium binding BRAND 96-well black flat bottom microplates, *N*-Hydroxysulfosuccinimide sodium salt (sulfo-NHS, purity ≥ 98%), poly-L-lysine (0.1 w/v% in $H_2O$), Sephadex-G50, Whatman Nucleopore™ Track-Etched membranes (1.0 µm, 0.4 µm and 0.2 µm diameter) and Tween 20 were purchased from Sigma Aldrich/Merck (Darmstadt, Germany); 1,2-dipalmitoyl-sn-glycero-3-phosphoethanolamine-*N*-(glutaryl) (sodium salt) (*N*-glutaryl-DPPE) from NOF America Corporation (NY, USA); the remaining phospholipids 1,2-dipalmitoyl-sn-glycero-3-phosphocholine (DPPC), 1,2-dipalmitoyl-sn-glycero-3-phospho-(1'-rac-glycerol) (sodium salt) (DPPG) and the extruder set from Avanti Polar Lipids (Alabaster, AL, USA). Dextran (amino, 10000 Mw and 70000 Mw), sulforhodamine B (SRB) (S1307) and (1-Ethyl-3-(3-dimethylaminopropyl) carbodiimide-hydrochloride) (EDC) (PG82079), were purchased from Thermo Fisher Scientific (Waltham, MA, USA); n-Octyl-β-D-glucopyranoside (OG) (≥ 98%, CN23), 2-(*N*-Morpholino)-ethane sulphonic acid (MES) (≥ 99%, 4259), *N*-2-Hydroxyethylpiperazine-*N'*-2-ethane sulphonic acid (HEPES) (≥ 99.5%, HN78), sucrose, sodium azide, sodium chloride and dialysis membrane Spectra/Por© 4 (MWCO: 12-14 kDa) (2718.1) from Carl Roth (Karlsruhe, Germany). Clear streptavidin coated 96-well microplates (KaiSA96) were purchased from Uniogen (Turku, Finland). Phosphorous standard was obtained from Bernd Kraft GmbH (Den Haag, Netherlands). Chloroform, methanol and Spectra-Por® Float-A-Lyzer® G2 (1 mL, MWCO: 1000 kDa) were purchased from Fisher Scientific (Hampton, NH, USA). RBD and ACE2-biotin were provided by our collaborators from the University Hopsital Regensburg and Microcoat Biotechnologie GmbH.

### 2.2.2.2 Buffer compositions

Hepes sucrose saline (HSS) buffer contained 200 mM sucrose, 200 mM NaCl, 10 mM HEPES and 0.01 w/v% NaN$_3$, pH 7.5. PBS buffer contained 137 mM NaCl, 2.7 mM KCl, 10 mM

$Na_2HPO_4$ and 1.8 mM $KH_2PO_4$, pH 7.4. PBS-T contained 0.1 w/v% Tween 20 in PBS. MES buffer contained 50 mM MES, 200 mM sucrose and 200 mM NaCl, pH 5.5.

### 2.2.2.3 Liposome synthesis

Reverse-phase evaporation was chosen as synthesis method for liposomes as described previously[12]. SRB and NaCl (150 mM SRB and 140 mM NaCl for high cholesterol liposomes, 10 mM SRB and 210 mM NaCl for low cholesterol liposomes) were dissolved in 20 mM HEPES, pH 7.5 (4.5 mL) by sonication at 60 °C to prepare the encapsulant. Lipid mixtures (high cholesterol: 41.4 mol% cholesterol, 32.2 mol% DPPC, 18.4 mol% DPPG, 8.0 mol% *N*-glutaryl-DPPE; low cholesterol: 5.0 mol% cholesterol, 72.8 mol% DPPC, 18.2 mol% DPPG, 4.0 mol% *N*-glutaryl-DPPE) were prepared by addition of 3 mL chloroform and 0.5 mL methanol and sonication for 1 min, followed by addition of encapsulant (2 mL) and sonication for 4 min at 60 °C. A rotary evaporator (LABOROTA 4001, Heidolph, Germany) was used to evaporate the organic solvents at 60 °C by stepwise reduction of pressure (900 mbar for 10 min, 850 mbar for 5 min, 800 mbar for 5 min, 780 mbar for 20 min). The solution was vortexed another two times for 1 min with intermittent encapsulant addition (2 mL). The residual organic solvents were evaporated at 60 °C (750 mbar for 20 min, 600 mbar for 5 min, 500 mbar for 5 min, 400 mbar for 20 min). The size was controlled by extrusion at 65 °C using polycarbonate membranes with pore sizes of 1 μm, 0.4 μm and 0.2 μm. Solutions were repeatedly pushed through the membranes with decreasing pore sizes, amounting to 21 repetitions for the 1 μm pore size and 11 repetitions for each of the smaller pore sizes. Size exclusion chromatography using a Sephadex G-50 column, followed by dialysis overnight against HSS buffer with 2 buffer exchanges in a dialysis membrane Spectra/Por© 4 (MWCO: 12-14 kDa) were used to remove excess encapsulant.

### 2.2.2.4 Liposome characterization

An inductively coupled plasma optical emission spectrometer (ICP-OES) (SpectroBlue TI/EOP) from SPECTRO Analytical Instruments GmbH (Kleve, Germany) was used to determine phospholipid concentrations, which in turn were used to calculate total lipid concentrations based on the mixture of lipids used for the synthesis. Phosphorous standard dilutions between 0 μM and 100 μM in 0.5 M $HNO_3$ were used for calibration of the device. Phosphorous was detected at 177.495 nm. Re-calibration was performed before each measurement using the 0 μM and 100 μM phosphorus dilutions. Liposome stock solutions were diluted 1:100 or 1:60 in 0.5 M $HNO_3$ and their phosphorous content determined.

Size and ζ-potential were measured via dynamic light scattering (DLS) using a Malvern Zetasizer Nano-ZS. Liposome stock solutions were diluted to 25 μM total lipids in HSS buffer in a polymethyl methacrylate (PMMA) semi-micro cuvette (Brand, Germany) for size and a

disposable folded capillary cell (Malvern Panalytical, Germany) for ζ-potential measurements.
The measurement temperature was set to 25 °C, the refractive index was 1.34, the material
absorbance was zero and the dispersant viscosity 1.1185 mPa s. For ζ-potential
measurements a dielectric constant of 78.5 was used and an equilibration time of 60 s applied
before each measurement.

### 2.2.2.5  Liposome modification

Proteins were conjugated to carboxylated liposomes via EDC/sulfo-NHS chemistry. Liposomes
were incubated with EDC and sulfo-NHS (1:100:180 ratio of carboxy-groups:EDC:sulfo-NHS)
for 1 h at room temperature (RT) and 300 rpm followed by addition of protein and another 1.5 h
incubation at RT and 300 rpm. Excess reagents were removed via dialysis against HSS buffer
overnight with one buffer exchange in a Spectra-Por® Float-A-Lyzer® G2 (1 mL, MWCO:
1000 kDa) for large volumes or via size exclusion chromatography with Sephadex G-50 or
G-100 for small volumes (<50 µL). Total lipid concentrations were determined using ICP-OES
and the conjugated liposomes were stored at 4 °C in Protein LoBind tubes.

### 2.2.2.6  Determination of maximum and unlysed fluorescence

Liposomes were diluted in HSS (5 µM total lipids) and added to a black 96-well microplate
(100 µL per well, n = 4). The fluorescence was measured three consecutive times with a
BioTek SYNERGY neo2 fluorescence reader ($\lambda_{Ex} = 560\ nm$ and $\lambda_{Em} = 585\ nm$, bandwidth 10,
gain 100). Liposomes were lysed by addition of 300 mM OG (10 µL per well) and incubation
for 10 min at RT and 300 rpm before the fluorescence was measured again. Fluorescence
intensities of the lysed liposomes are referred to as maximum fluorescence intensities. Unlysed
fluorescence was calculated by normalization of the fluorescence intensity of the liposomes
before addition of OG (unlysed) to that after incubation with OG (lysed). Errors were calculated
using Gaussian error propagation.

### 2.2.2.7  Heterogeneous ACE2 binding assay

ACE2-biotin (1 µg/mL ACE2 in PBS, 100 µL per well) was incubated in a streptavidin plate for
1 h at RT and 300 rpm. The plate was washed two times with PBS-T (150 µL per well) and
three times with HSS (150 µL per well) before being used. Liposomes (1 µM total lipids) were
added to the MTP (100 µL per well, n = 3) and incubated for 2 h at RT and 300 rpm. The plate
was washed three times with HSS buffer (150 µL per well) before 30 mM OG in bidest. water
(100 µL per well) was added. After 10 min incubation the fluorescence was measured three
consecutive times with a BioTek SYNERGY neo2 fluorescence reader ($\lambda_{Ex} = 560\ nm$ and
$\lambda_{Em} = 585\ nm$, bandwidth 10, gain 150). In case of normalization to initial fluorescence
intensities errors were calculated using Gaussian error propagation.

### 2.2.3  Results and discussion

2.2.3.1  Investigation of various stabilizing agents

The stability of both high cholesterol and low cholesterol liposomes modified with 0.2 mol% RBD was investigated. The former can encapsulate up to 150 mM SRB and are used in the previously discussed heterogeneous SARS-CoV-2 neutralization test, while the latter can encapsulate a maximum of 10 mM SRB and are used in the homogeneous SARS-CoV-2 neutralization test developed by Christina Reiner. Several stabilizing excipients, including amino acids, carbohydrates, detergents, proteins and polymers, were tested, checking different concentrations of each. An overview of which samples showed agglomeration can be found in **Table 1**. Poly-L-lysine already showed visible precipitation after the weekend (3 days), potentially even sooner. The negatively charged liposomes interacted with the positively charged poly-L-lysine, accelerating the agglomeration process. A similar effect was visible with 70 kDa amino dextran after 1 day for high cholesterol and after 2 weeks for low cholesterol RBD liposomes. The low cholesterol liposomes also showed precipitation in presence of arginine, lysine and glycine after 1 month. The small molecules appear to be insufficient to prevent interaction of the RBD liposomes with one another and instead accelerate the process of agglomeration. DLS measurements of high cholesterol RBD liposome samples after 2 months showed no agglomeration in any of the unprecipitated samples (data not shown). DLS measurements of the remaining low cholesterol RBD liposomes after 2 months, on the other hand, revealed agglomeration for most of them, including both the stock solution and the control without stabilizers (sample 1) (**Table S1**). The effect was more pronounced for the latter, which had a ~10x lower concentration during storage (250 μM total lipids vs. 2.2 mM). Only Tween20 (0.05 w/v% and 0.005 w/v%) and 0.1 w/v% BSA appeared to have a stabilizing effect, the Z-average remaining around 125 nm and the PdI around 0.25 (0 days: 122 ± 4 nm, PdI 0.19 ± 0.01). Higher BSA concentrations (1 w/v%) led to a large PdI and decreasing Z-average, due to the formation of BSA aggregates seen as 10 nm peak. No such peak was observed for the high cholesterol liposomes. However, the PdI did also increase from ~0.1 to 0.3, suggesting that BSA leads to agglomeration when high concentrations are being used.

The fluorescence of the most promising samples, containing either Tween20 or BSA, was measured to check if the liposomes remained stable. As expected, Tween20 caused leakage of SRB during storage (**Table S2**), rendering it useless as stabilizing agent. This is likely due to increased membrane fluidity in presence of the detergent even at low concentrations. The liposomes did not appear to lyse, as the DLS measurement still showed the expected size and polydispersity. BSA, on the other hand, appears to be a promising candidate, unlysed fluorescence remaining constant for 0.1 w/v% BSA. Fine-tuning of the BSA concentration might yield stable high cholesterol and low cholesterol RBD liposomes and was further

***Optimization of the stability of liposomes modified with the receptor binding domain
of SARS-CoV-2 Alpha using EDC/sulfo-NHS chemistry***

investigated by the author (high cholesterol liposomes) and Christina Reiner (low cholesterol
liposomes) in follow-up studies.

*__Table 1:__ List of stabilizers and their concentrations tested with 250 µM high cholesterol and low cholesterol
liposomes modified with 0.2 mol% RBD in HSS (100 µL total volume). The number of days until precipitation was
first noticed by naked eye or agglomeration observed in the DLS measurement is shown for all samples (marked
light orange). Promising stabilizing agents are marked in light green.*

| No. | stabilizer | concentration | high cholesterol RBD liposomes | low cholesterol RBD liposomes |
|---|---|---|---|---|
| | | | agglomeration noticed after | |
| 1 | - | | | 2 months (DLS) |
| 2 | arginine-HCl | 20 mM | | 4 weeks |
| 3 | lysine-HCl | 20 mM | | 4 weeks |
| 4 | glycine | 20 mM | | 4 weeks |
| 5 | glycine | 100 mM | | 4 weeks |
| 6 | Tween20 | 0.05 w/v% | | |
| 7 | Tween20 | 0.005 w/v% | | |
| 8 | poly-L-lysine | 0.01 w/v% | 3 days | 3 days |
| 9 | poly-L-lysine | 0.001 w/v% | 3 days | 3 days |
| 10 | glycerol | 1 v% | | 2 months (DLS) |
| 11 | glycerol | 0.1 v% | | 2 months (DLS) |
| 12 | Trehalose | 200 mM | | 2 months (DLS) |
| 13 | Trehalose | 1 mM | | 2 months (DLS) |
| 14 | Dextran, amino, 10kDa | 0.1 w/v% | | 4 weeks |
| 15 | Dextran, amino, 10kDa | 1 w/v% | | 2 months (DLS) |
| 16 | Dextran, amino, 70kDa | 0.1 w/v% | 1 day | 13 days |
| 17 | Dextran, amino, 70kDa | 1 w/v% | 1 day | 13 days |
| 18 | BSA | 0.1 w/v% | | |
| 19 | BSA | 1 w/v% | 2 months (DLS) | 2 months (DLS) |

The max. fluorescence intensity of the high cholesterol RBD liposomes (measured for 5 µM
total lipids) after 2 months of storage was almost 2 times higher for the stock solution (1.09 mM
total lipids) compared to that of the diluted samples (250 µM total lipids) from the stability study.
Investigation of the binding of the stock solution compared to the control and 0.1 w/v% BSA
(sample 19) samples of the storage stability study to ACE2 showed ~50% lower signal
intensities for the latter two (**Figure S1**). Both findings suggest that the used concentrations
were differing by a factor of 2, which could only be explained by adsorption of the protein-
modified liposomes to the storage vials or severe photobleaching. Samples were stored at
250 µM total lipids (100 µL) in normal reaction vials and were in contact with another reaction
vial and a cuvette after dilution for the DLS measurement. These same diluted solutions were
then used for the fluorescence measurement. Concentration and volume of these solutions
was insufficient to confirm the theory with ICP measurements. The sample stabilized with

0.1 w/v% BSA showed slightly improved binding compared to the control, suggesting that it may have helped to maintain RBD folding and functionality and reduce adsorption to storage vials. Addition of BSA to dilute protein solutions as filler protein is common practice to protect against degradation and loss of protein. Studies were henceforth conducted using Protein LoBind Eppendorf cups to minimize adsorption of RBD liposomes during storage.

DLS measurements of the control and 0.1 w/v% BSA samples after 4 months revealed no change of Z-average and PdI for high cholesterol RBD liposomes **Figure 1 A**). The low cholesterol RBD liposomes, on the other hand, showed another increase of the Z-average to >400 nm and of the PdI to ~ 0.8 for the control, but not for the sample containing BSA (**Figure 1 B**). A new stability study testing different concentrations of BSA was therefore started.
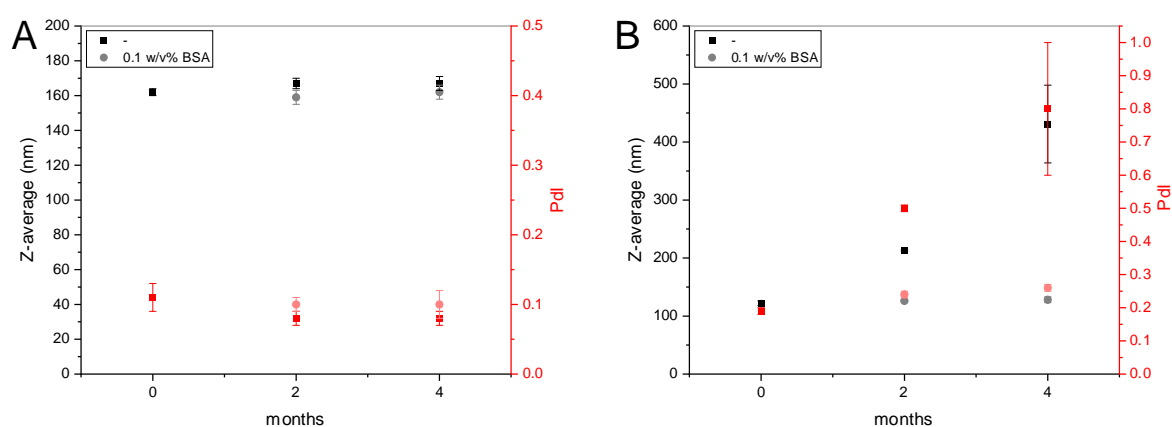


*Figure 1: Z-average and PdI of high cholesterol (**A**) and low cholesterol liposomes (**B**) modified with 0.2 mol% RBD, stored in HSS with BSA (0 or 0.1 w/v%) for 4 months. n = 3.*

2.2.3.2  Investigation of different BSA concentrations as stabilizing agent

High cholesterol liposomes (25 µM total lipids) modified with 0.1 mol% RBD were stored in HSS with different BSA concentrations (0, 0.01, 0.05 and 0.1 w/v%). The lower RBD content compared to the previous study was chosen because it resembles the optimum concentration for the LFA (see chapter 4). Surprisingly, the two samples with the higher BSA concentrations showed a drastic increase of unlysed fluorescence from ~10% to >40% after 2 weeks (**Table 2**). This suggested that the liposomes either agglomerated strongly, or that SRB diffused out of the liposomes. The former theory was not supported by DLS measurements, which showed identical size by intensity peaks for the liposomes (179 ± 5 nm). However, BSA aggregates were detected as second peak of ~10 nm, which led to smaller Z-average (146 ± 4 nm and 132 ± 3 nm), which is the intensity weighted mean hydrodynamic diameter, and increased PdI (0.21 ± 0.01 and 0.32 ± 0.01) compared to the BSA free sample (167 ± 3 nm, 0.07 ± 0.02). Perhaps BSA aggregates are able to interact with the RBD liposomes, increasing membrane fluidity and thus causing leakage of SRB. Free SRB molecules can then intercalate into BSA or RBD molecules, resulting in a fluorescence increase due to reduction of the hydration-

mediated quenching effect[13]. The data suggests that leakage only takes place after initial addition of BSA, unlysed fluorescence intensities remaining unchanged between 2 and 8 weeks of storage.

***Table 2***: *Unlysed fluorescence of high cholesterol liposomes modified with 0.1 mol% RBD and purified via SEC, stored with BSA (0, 0.01, 0.05 and 0.1 w/v%, 25 µM total lipids) in HSS for 16 weeks.*

| stabilizer | Unlysed fluorescence | | | | |
|---|---|---|---|---|---|
| | **0 weeks** | **2 weeks** | **4 weeks** | **8 weeks** | **16 weeks** |
| - | 13 ± 1% | 10 ± 1% | 11 ± 1% | 15 ± 5% | 26 ± 2% |
| **0.01 w/v% BSA** | | 9 ± 1% | 9 ± 1% | 11 ± 1% | 22 ± 1% |
| **0.05 w/v% BSA** | | 43 ± 8% | 43 ± 5% | 40 ± 2% | |
| **0.1 w/v% BSA** | | 53 ± 6% | 57 ± 13% | 53 ± 11% | |

Interestingly, an increase of the unlysed fluorescence was also observed for the control and the lowest BSA concentration after 16 weeks (**Figure 2 A**). Maximum fluorescence intensities decreased slightly over time, either due to adsorption of RBD liposomes to the reaction vial, despite the use of Protein LoBind Eppendorf Tubes, or photobleaching. The low concentration of the solutions makes them prone to both effects, corresponding to a high surface area to liposome ratio and lower fluorophore concentration. DLS measurements revealed an increase of the Z-average after 16 weeks for the control, but not the 0.01 w/v% BSA sample (**Figure 2 B**). The studies showed that colloidal stability of both high cholesterol and low cholesterol RBD liposomes could be improved with BSA, if the right ratio of liposomes to BSA is used. The 25 µM total lipids and 0.01 w/v% BSA resemble the same ratio as the 250 µM total lipids and 0.1 w/v% BSA tested in the previous study, which also prevented agglomeration.
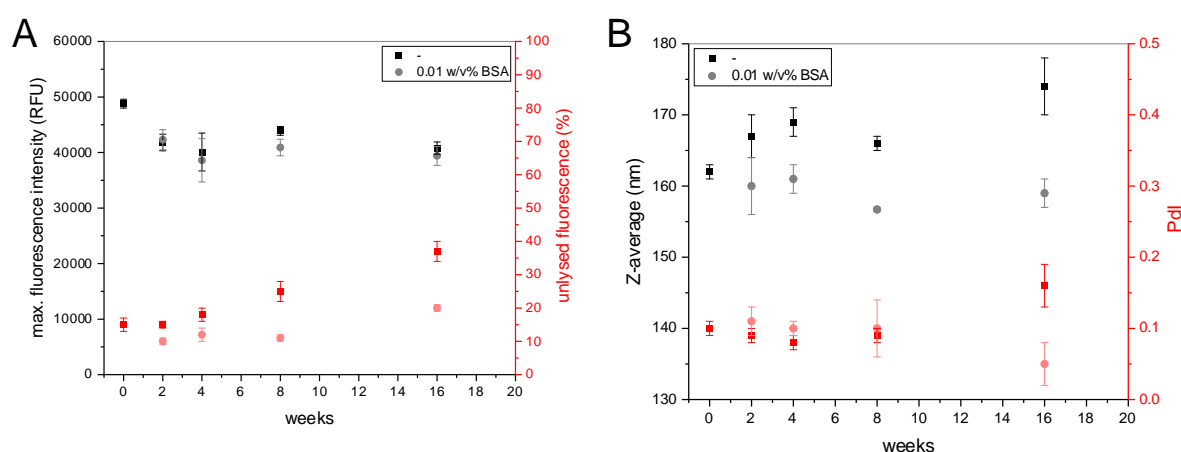


***Figure 2***: *Maximum and unlysed fluorescence (**A**, n = 4) and Z-average and PdI (**B**, n = 3) of high cholesterol liposomes modified with 0.1 mol% RBD and purified via SEC, stored in HSS with BSA (0 or 0.01 w/v%) for 16 weeks.*

However, a binding assay showed that the ACE2 binding ability of the high cholesterol RBD liposomes had drastically decreased during the 16 weeks of storage (data not shown). In the previous study, the lower fluorescence intensities observed in the ACE2-biotin coated

streptavidin plate had been attributed to adsorption of liposomes to the storage vial. This time, the use of low binding storage vials should have prevented adsorption. A follow-up study showed that the ACE2 binding decreased significantly after 1 month already (**Figure 3**). The HSS buffer might be unfavorable for storage of RBD, which could have denatured or formed aggregates, worsening interaction with ACE2. Different storage buffers were therefore investigated in a new storage stability study.
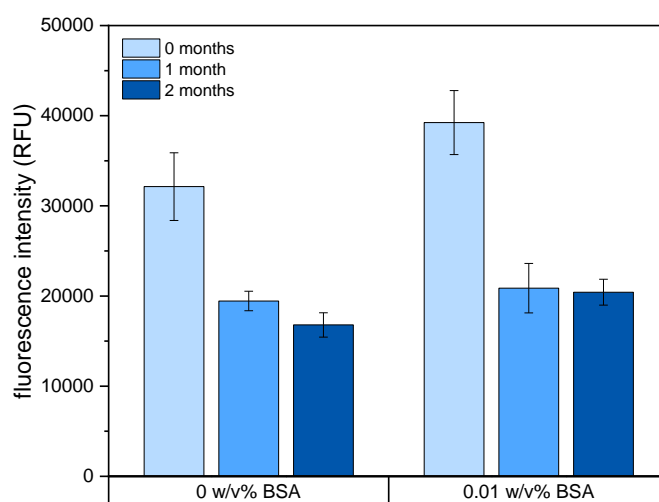


***Figure 3:*** *ACE2 binding assay of high cholesterol liposomes modified with 0.1 mol% RBD and purified using SEC, stored in HSS with BSA (0 or 0.01 w/v%) for 2 months. n = 3.*

### 2.2.3.3 Investigation of different buffers

To ensure liposome integrity, it is important that the osmolality of the storage buffer is at least 50 to 100 mOsmol/kg higher than that of the encapsulant (430 mOsmol/kg)[14]. The commonly used storage buffer HSS has a calculated osmolality of 610 mOsmol/kg. For RBD, refrigeration at 4 °C in PBS buffer resembles the optimum storage conditions, as determined by Patrick Neckermann. With a calculated osmolality of 313 mOsmol/kg PBS is unsuitable for storage of RBD-modified liposomes, because the lower osmolality would likely cause leakage of SRB over time. To increase the osmolality to acceptable levels, the use of double-concentrated PBS (2xPBS) and PBS with additional 200 mM sucrose (PBSS) was investigated. These have calculated osmolalities of 626 mOsmol/kg and 513 mOsmol/kg, respectively. Storage of high cholesterol liposomes modified with 0.1 mol% RBD in 2xPBS and PBSS for 12 weeks revealed 30-40% lower signal intensities in an ACE2-biotin coated streptavidin plate compared to the initial data-point (0 weeks) (**Figure 4**). Addition of 0.01 w/v% BSA reduced the signal loss to ~15% in both buffers. Storage in HSS, on the other hand, resulted in 80% lower signals without BSA and 60% lower signals with BSA. Storage at higher concentration (250 µM instead of 25 µM total lipids) improved matters, but still resulted in 40% signal loss for the BSA-containing sample. The data show that the change to PBS buffer with increased osmolality and BSA as

stabilizing agent allows for long-term storage of RBD-liposomes, without causing leakage of SRB or degradation of RBD. Storage at higher concentrations might further improve stability.
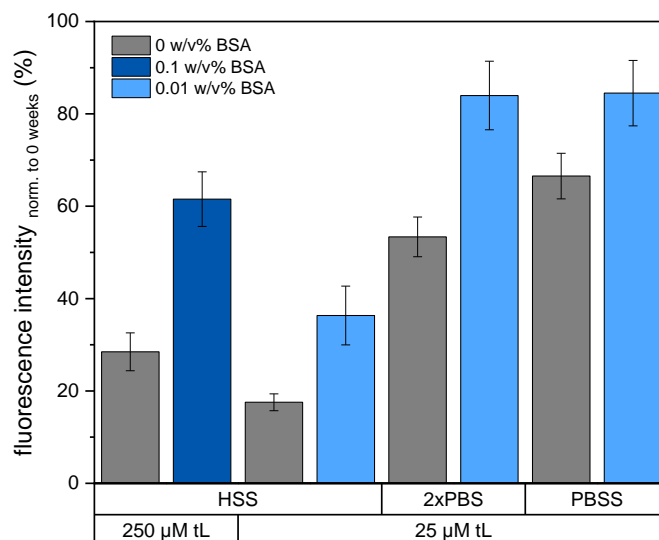


*Figure 4: ACE2 binding assay of high cholesterol liposomes modified with 0.1 mol% RBD and purified using dialysis, stored in HSS, 2xPBS or PBSS with BSA (0, 0.01 or 0.1 w/v%) for 12 weeks. Fluorescence intensities were normalized to those obtained at the start of the storage stability study (0 weeks). n = 3.*

The use of HSA instead of BSA was investigated, as it would make commercialization easier according to our collaborators at Microcoat Biotechnologie GmbH. The RBD content was increased to 0.2 mol% again, the optimum for the HTS format and the value our collaborators were interested in. PBSS buffer was chosen for storage rather than 2xPBS, as the added sucrose makes it more alike to HSS, the preferred liposome storage buffer. Liposomes were stored at 25 µM, 100 µM, or 400 µM total lipids in PBSS with varying HSA concentration (0.001 w/v% to 0.16 w/v%). For easier comparison, concentrations will be referred to in relation to RBD, assuming all RBD molecules were effectively coupled to the liposomes. HSA to RBD ratios ranged from 0:1 to 1500:1, a ratio of 300:1 was chosen for comparison of the different total lipid concentrations. DLS measurements showed a decreasing Z-average with increasing HSA concentration (**Figure S2**). The formation of a protein corona around the liposome could result in a reduction of the hydrodynamic diameter of the particles. Furthermore, small protein clusters can be detected as 2$^{nd}$ peak at ~10 nm for high HSA or BSA concentration, resulting in a decreased Z-average. Surprisingly, DLS measurements after 24 weeks revealed an increased Z-average for liposomes stored without HSA and a decreasing one for those stored with HSA. No change of Z-average was observed after 16 weeks. The change could be traced back to insufficient remaining sample volumes, resulting in DLS measurements close to the meniscus instead of the bulk solution. The measurements after 24 and 36 weeks are therefore unreliable. It can only be concluded that all samples showed colloidal stability for at least 16 weeks.

### Optimization of the stability of liposomes modified with the receptor binding domain of SARS-CoV-2 Alpha using EDC/sulfo-NHS chemistry

The ACE2 binding ability of all samples with 25 µM total lipid concentration started to decrease rapidly after 12 weeks, addition of HSA only slightly decreasing the rate of signal loss (**Figure 5 A**). Fluorescence intensities decreased to <70% after 12 weeks and were down to 10-30% after 36 weeks. This coincided with a linear increase of unlysed fluorescence for all samples (**Figure 5 B**). Initial values ranged from 10% to 30%, increasing HSA concentration correlating to higher unlysed fluorescence intensity. This is likely due to intercalation of free SRB into HSA, resulting in reduced hydration-mediated quenching. After 36 weeks unlysed fluorescence values had increased to 62-82%, suggesting that a large fraction of SRB had diffused through the lipid bilayer. No such behavior had been observed for high cholesterol liposomes modified with other proteins, such as streptavidin or BSA, or for low cholesterol RBD liposomes. The data suggest that RBD continuously interacts with the lipid bilayer, increasing membrane permeability to an extent that SRB can slowly diffuse through it.
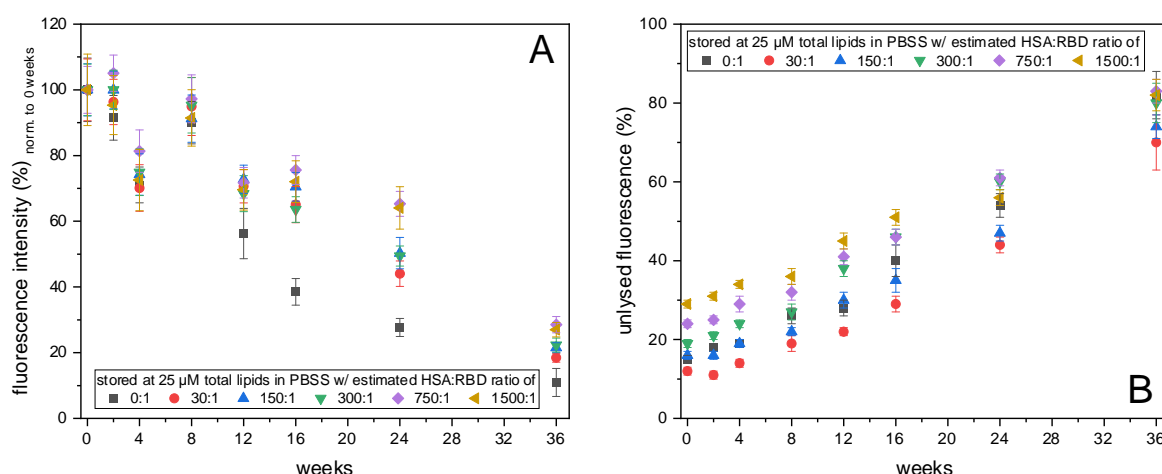


**Figure 5**: Comparison of ACE2 binding (**A**, n = 3) and unlysed fluorescence (**B**, n = 4) of high cholesterol liposomes modified with 0.2 mol% RBD and purified via dialysis, stored at 25 µM total lipids in PBSS with various ratios of HSA:RBD, after up to 36 weeks of storage. The 4 weeks ACE2 binding data point was an outlier caused by degraded ACE2-biotin.

Storage of RBD liposomes in PBSS with HSA at higher total lipid concentration was found to reduce the rate of leakage but was unable to fully prevent it (**Figure 6 B**). Best results were achieved with 100 µM total lipids and 0.04 w/v% HSA (300:1 ratio of HSA to RBD), the ACE2 binding ability of the sample remained constant for 24 weeks (**Figure 6 A**). Interestingly, the unlysed fluorescence had increased from ~20% to almost 40% after 24 weeks. The fact that this increase did not coincide with a decreasing signal in the ACE2 binding assay supports the theory that the leaked SRB largely intercalates into RBD. Further leakage after 36 weeks coincided with a 50% lower signal in the ACE2 binding assay. This could either be due to loss of leaked, non-intercalated SRB during washing, or RBD may have started to degrade, losing its ability to bind to ACE2. To further improve long-term stability, a storage stability study of 100 µM RBD liposomes in PBSS with additional NaCl or sucrose was started. However, the

higher osmolality was unable to prevent leakage of SRB, unlysed fluorescence increasing from ~15% to ~30% after 24 weeks (**Figure S3**), identical to the observations in PBSS (**Figure 6 B**).
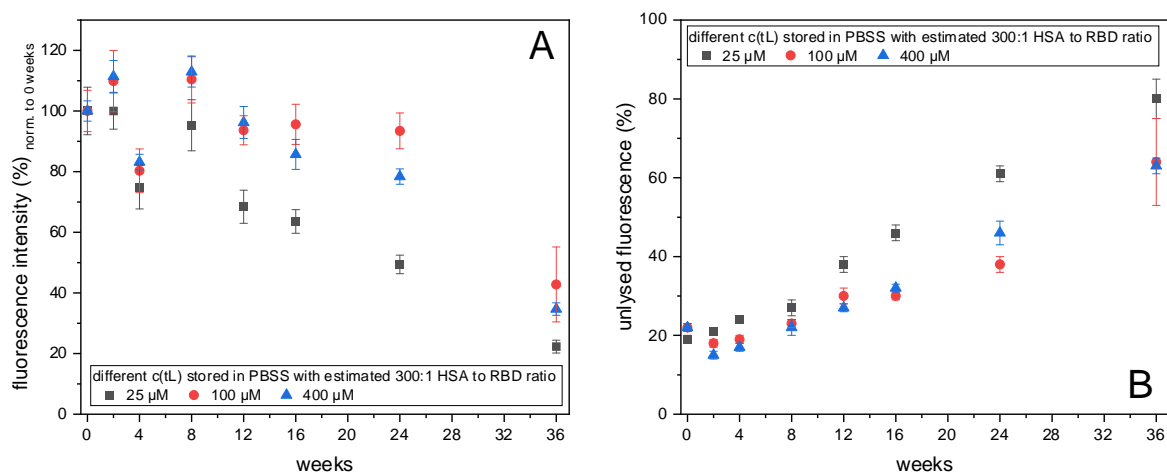


***Figure 6:*** *Comparison of ACE2 binding (**A**, n = 3) and unlysed fluorescence (**B**, n = 4) of high cholesterol liposomes modified with 0.2 mol% RBD and purified via dialysis, stored at 25, 100 or 400 μM total lipids in PBSS with an estimated ratio of 300 HSA per RBD, after up to 36 weeks of storage. The 4 weeks ACE2 binding data point was an outlier caused by degraded ACE2-biotin.*

### 2.2.4  Conclusion

The long-term stability of liposomes modified with RBD was successfully optimized. Out of the investigated stabilizing excipients, including amino acids, carbohydrates, detergents, proteins and polymers, only BSA improved colloidal stability of low cholesterol liposomes. Subsequent storage stability studies for high cholesterol RBD liposomes determined the ratio of BSA to RBD as an important factor, with SRB leakage occurring for high BSA concentrations. While 0.01 w/v% BSA enabled colloidal stability of 25 μM RBD liposomes for at least 4 months, the ACE2 binding ability was found to quickly deteriorate, highlighting the need to find conditions that prevent agglomeration and leakage of SRB, as well as maintain the ACE2 binding ability of RBD. This was achieved with a PBS buffer containing additional sucrose and HSA. Liposome concentration during storage was found to be crucial, 100 μM total lipids stored in PBSS with HSA maintaining the RBD functionality for 24 weeks. However, none of the investigated conditions could fully prevent leakage of SRB over time, a problem which was found to be specific to RBD and high cholesterol liposomes. Cholesterol is typically added to liposome formulations because of its stabilizing effect, preventing agglomeration and leakage of small molecules[15–17]. More precisely, cholesterol inserts between phospholipid molecules, which results in an increased fluidity for tightly packed saturated phospholipids, and reduced fluidity for unsaturated phospholipids. Furthermore, it has a temperature-buffering role, disrupting the formation of a rigid membrane at low temperature and reducing fluidity at higher temperature, promoting an intermediate gel state instead of the crystalline or liquid crystalline

state[18,19]. Drug or fluorophore release studies are often performed at 37 °C to mimic physiological conditions[20], which is close to the phase transition temperature of 41 °C of the frequently used phospholipids DPPC and DPPG[21], cholesterol therefore likely reducing the membrane fluidity. In the case of the investigated storage of high cholesterol and low cholesterol RBD liposomes at 4 °C, the membrane might instead be more fluid with higher cholesterol content. Modification with RBD increases the fluidity of the former to such an extent that SRB can permeate through the membrane, while the low cholesterol liposomes remain impermeable. This interaction is likely promoted by the predominantly positive charge of RBD at physiological pH[22], as well as its structure. No such interaction was observed for other proteins, such as BSA or streptavidin, which are negatively charged or neutral at physiological pH, respectively[23,24]. Reduction of the cholesterol content would be an option to achieve stable RBD liposomes. However, the cholesterol content was shown to be a crucial factor for SRB encapsulation. While 42 mol% cholesterol facilitate the encapsulation of up to 150 mM SRB, a maximum of 10 mM SRB can be encapsulated with 5 mol% cholesterol, higher concentrations leading to the formation of multilamellar liposomes[25], encapsulation yields dropping toward zero. Reduction of the SRB content would result in lower sensitivities and is thus undesirable. Instead of pursuing further attempts to optimize the stability of high cholesterol RBD liposomes, or to synthesize liposomes with lower cholesterol and SRB content, an altogether different approach was selected, which will be discussed in the next chapter. Briefly, long-term stable streptavidin-liposomes were used in combination with biotinylated RBD to enable separate storage, preventing leakage of SRB, as well as degradation of RBD.

### 2.2.5  References

(1) *Annex I (IVDR): General safety and performance requirements - Medical Device Regulation WebApp english language*. https://de-mdr-ivdr.tuvsud.com/Annex-I-General-safety-and-performance-requirements-IVDR.html (accessed 2025-03-07).

(2) Sean. How to Use the Arrhenius Equation in Stability Studies. *FTLOScience,* Dec 8, 2022. https://ftloscience.com/how-to-use-arrhenius-equation/ (accessed 2025-03-07).

(3) Arakawa, T.; Prestrelski, S. J.; Kenney, W. C.; Carpenter, J. F. *Adv Drug Deliv Rev* **2001**, *46* (1-3), 307–326.

(4) Aubin-Tam, M.-E.; Hwang, W.; Hamad-Schifferli, K. *PNAS* **2009**, *106* (11), 4095–4100.

(5) Bigman, L. S.; Levy, Y. *Chemical Physics* **2018**, *514*, 95–105.

(6) *Use of Stabilizers and Surfactants to Prevent Protein Aggregation*. https://www.sigmaaldrich.com/DE/de/technical-documents/technical-article/pharmaceutical-and-biopharmaceutical-manufacturing/downstream-processing/stabilizers-and-surfactants-to-prevent-protein-aggregation (accessed 2025-03-07).

(7) Jamrichová, D.; Tišáková, L.; Jarábková, V.; Godány, A. *Nova Biotechnologica et Chimica* **2017**, *16* (1), 1–11.

(8) Thakral, S.; Sonje, J.; Munjal, B.; Suryanarayanan, R. *Adv Drug Deliv Rev* **2021**, *173*, 1–19.

(9) Challener, C. *Excipient Selection for Protein Stabilization*, 2015 Supplement; MJH Life Sciences, 2015.

(10) Rink, S.; Kaiser, B.; Steiner, M.-S.; Duerkop, A.; Baeumner, A. J. *Anal. Bioanal. Chem.* **2022**, *414* (10), 3231–3241.

(11) Streif, S.; Neckermann, P.; Spitzenberg, C.; Weiss, K.; Hoecherl, K.; Kulikowski, K.; Hahner, S.; Noelting, C.; Einhauser, S.; Peterhoff, D.; Asam, C.; Wagner, R.; Baeumner, A. J. *Anal. Bioanal. Chem.* **2023**, *415* (8), 1421–1435.

(12) Edwards, K. A.; Curtis, K. L.; Sailor, J. L.; Baeumner, A. J. *Anal. Bioanal. Chem.* **2008**, *391* (5), 1689–1702.

(13) Kitamura, M.; Murakami, K.; Yamada, K.; Kawai, K.; Kunishima, M. *Dyes and Pigments* **2013**, *99* (3), 588–593.

(14) Esch, M. B.; Baeumner, A. J.; Durst, R. A. *Anal. Chem.* **2001**, *73* (13), 3162–3167.

(15) Papahadjopoulos, D.; Jacobson, K.; Nir, S.; Isac, T. *Biochimica et biophysica acta* **1973**, *311* (3), 330–348.

(16) Virden, J. W.; Berg, J. C. *Langmuir* **1992**, *8* (6), 1532–1537.

(17) Laouini, A.; Jaafar-Maalej, C.; Sfar, S.; Charcosset, C.; Fessi, H. *International Journal of Pharmaceutics* **2011**, *415* (1-2), 53–61.

(18) Demel, R. A.; Kruyff, B. de. *Biochimica et biophysica acta* **1976**, *457* (2), 109–132.

(19) Muhammad Ahmed. *Journal of Membrane Science & Technology* **2024**, *14* (4), 1–2.

(20) Kaddah, S.; Khreich, N.; Kaddah, F.; Charcosset, C.; Greige-Gerges, H. *Food Chem Toxicol* **2018**, *113*, 40–48.

(21) Silvius, J. R.; Mak, N.; McElhaney, R. N. *Biochimica et biophysica acta* **1980**, *597* (2), 199–215.

(22) Božič, A.; Podgornik, R. *Bioinformatics Advances* **2024**, *4* (1), vbae053.

(23) Almonte, L.; Lopez-Elvira, E.; Baró, A. M. *ChemPhysChem* **2014**, *15* (13), 2768–2773.

(24) Fologea, D.; Ledden, B.; McNabb, D. S.; Li, J. *Applied physics letters* **2007**, *91* (5), 539011–539013.

(25) Hoecherl, K.; Streif, S.; Rink, S.; Behrent, A.; Holzhausen, F.; Griesche, C.; Rogoll, C.; Foedlmeier, M.; Gebhard, A.; Kulikowski, K.; Schaefer, N.; Pauly, D.; Baeumner, A. J. *Anal. Bioanal. Chem.* **2025**.

## 2.2.6 Supplementary information

***Table S1:*** *DLS measurement of unprecipitated low cholesterol liposomes modified with 0.2 mol% RBD after 2 months of storage in HSS with different additives. Agglomerated samples are marked in light orange, promising stabilizing agents are marked in light green. n = 3.*

| No. | stabilizer | concentration | Z-average / nm | PdI |
|---|---|---|---|---|
| day 0 | - | - | 122 ± 4 | 0.19 ± 0.01 |
| stock | - | - | 169 ± 4 | 0.41 ± 0.01 |
| 1 | - | | 213 ± 1 | 0.50 ± 0.01 |
| 6 | TWEEN20 | 0.05 w/v% | 125 ± 2 | 0.24 ± 0.01 |
| 7 | TWEEN20 | 0.005 w/v% | 116 ± 3 | 0.26 ± 0.01 |
| 10 | glycerol | 1 v% | 245 ± 3 | 0.55 ± 0.04 |
| 11 | glycerol | 0.1 v% | 253 ± 3 | 0.54 ± 0.03 |
| 12 | Trehalose | 200 mM | 295 ± 11 | 0.53 ± 0.01 |
| 13 | Trehalose | 1 mM | 334 ± 5 | 0.60 ± 0.01 |
| 15 | Dextran, amino, 10kDa | 1 w/v% | 234 ± 9 | 0.56 ± 0.02 |
| 18 | BSA | 0.1 w/v% | 126 ± 2 | 0.24 ± 0.01 |
| 19 | BSA | 1 w/v% | 76 ± 3 | 0.68 ± 0.05 |

***Table S2:*** *Unlysed fluorescence intensities of samples 1, 6, 7 and 19 as well as the stock solutions of high cholesterol and low cholesterol RBD liposomes after 2 months of storage. Lysed samples are marked in light orange, promising stabilizing agents are marked in light green. n = 4.*

| No. | stabilizer | concentration | max. fluor. int. /RFU | unlysed fluorescence |
|---|---|---|---|---|
| **high cholesterol RBD liposomes** | | | | |
| stock | - | - | 71300 ± 1400 | 11 ± 2% |
| 1 | - | | 36700 ± 500 | 12 ± 3% |
| 6 | Tween20 | 0.05 w/v% | 47200 ± 260 | 62 ± 1% |
| 7 | Tween20 | 0.005 w/v% | 42400 ± 800 | 55 ± 3% |
| 19 | BSA | 0.1 w/v% | 41100 ± 500 | 6.5 ± 0.3 % |
| | | | | |
| **low cholesterol RBD liposomes** | | | | |
| stock | - | - | 5440 ± 400 | 21 ± 3% |
| 1 | - | | 2990 ± 40 | 18 ± 2% |
| 6 | Tween20 | 0.05 w/v% | 5400 ± 100 | 91 ± 4% |
| 7 | Tween20 | 0.005 w/v% | 4590 ± 160 | 107 ± 5% |
| 19 | BSA | 0.1 w/v% | 3920 ± 180 | 16 ± 1% |
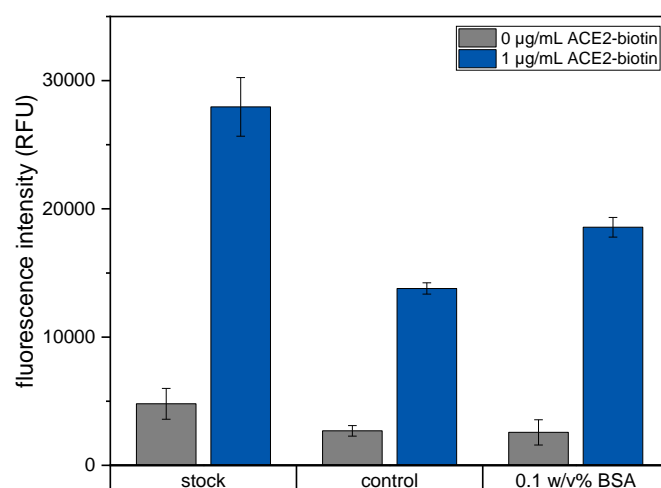
**Figure S1:** *ACE2 binding assay of high cholesterol RBD liposome stock, control and 0.1 w/v% BSA samples, after 2 months of storage. n = 3.*
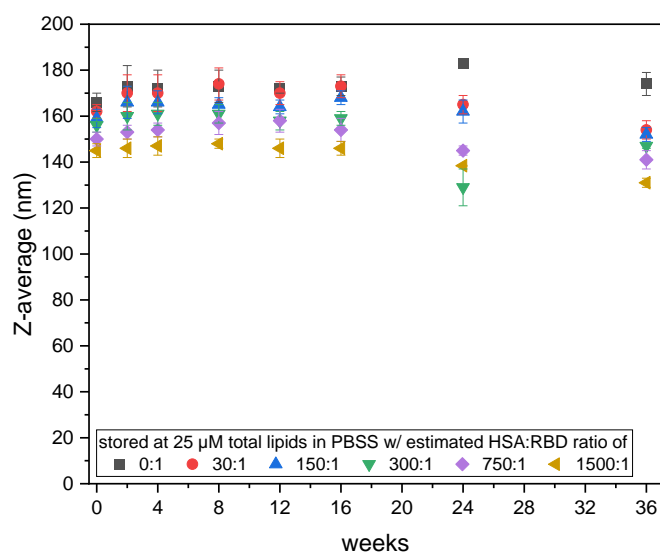


**Figure S2:** *Comparison of Z-average values of high cholesterol liposomes modified with 0.2 mol% RBD and purified via dialysis, stored at 25 µM total lipids in PBSS with various ratios of HSA:RBD, after up to 36 weeks of storage. n = 3.*
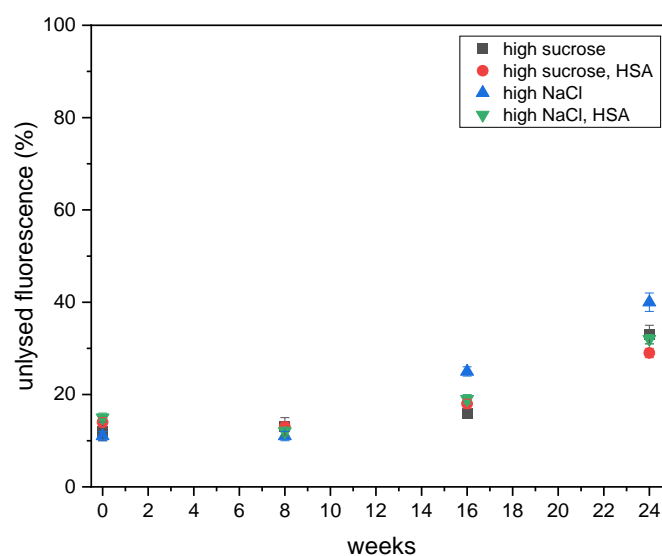
***Figure S3:*** *Comparison of unlysed fluorescence of high cholesterol liposomes modified with 0.2 mol% RBD purified via dialysis, stored at 100 µM total lipids in PBSS with additional sucrose (100 mM) or NaCl (63 mM) with and without 0.04 w/v% HSA (300:1 ratio of HSA to RBD), after up to 24 weeks of storage. n = 4.*

# 3 Studying conjugation strategies for the receptor binding domain and spike protein of SARS-CoV-2 variants for a versatile neutralization test

## 3.1 Development of a serological liposome-based assay for SARS-CoV-2 variants with special emphasis on coupling chemistries required to maintain protein antigenicity

**Graphical Abstract**
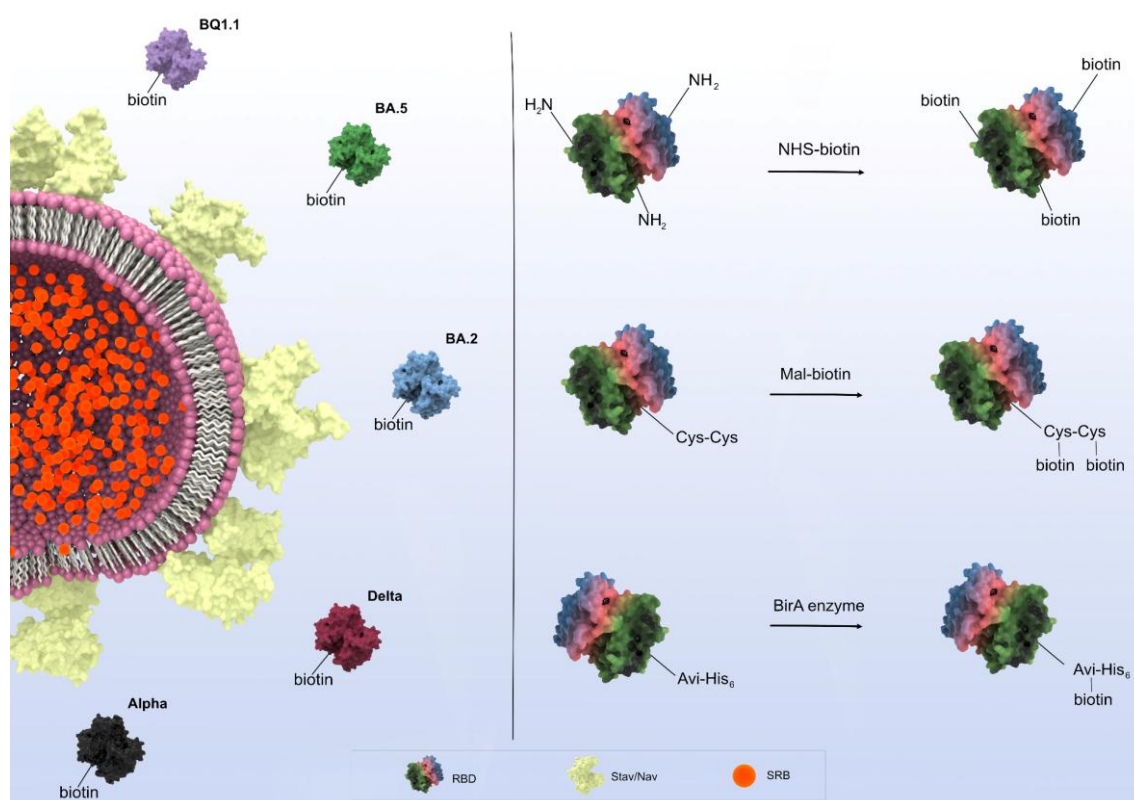


This chapter has been submitted for publication in the ACS journal *Analytical Chemistry* (28th April 2025).

## Authors' contributions

**Antje J. Baeumner** Conceptualization; writing – review and editing

**Miriam Breunig** Conceptualization; writing – review and editing

**Sebastian Einhauser** Pseudovirus neutralization assays**;** writing – review and editing

**Kilian Hoecherl** Writing — review and editing

**Johannes Konrad** Biotinylation of RBD via the Cys-tag

**Patrick Neckermann** Cloning of recombinant protein expression plasmids; expression, purification, and quality control of recombinant ACE2 and RBD; writing – review and editing

**Christina Reiner** Writing — review and editing

**Simon Streif** Conceptualization; HTS experiments; POC experiments; liposome synthesis and optimization; writing – original draft

**Ralf Wagner** Conceptualization; writing — review and editing

***Development of a serological liposome-based assay for SARS-CoV-2 variants with special emphasis on coupling chemistries required to maintain protein antigenicity***

## Abstract

The conjugation of proteins to the outer membrane of liposomes is a standard procedure used in bioanalytical and drug delivery approaches. Herein, we describe the development of a liposome-based surrogate assay for the quantification of SARS-CoV-2 neutralizing antibodies. Taking into consideration differences in amino acid sequences within the receptor binding domain (RBD) of SARS-CoV-2 Spike proteins derived from five selected variants of concern (VoC), the impact of coupling chemistries on physicochemical properties and antigenicity was studied. Naturally occurring lysine residues were used for standard EDC/NHS chemistry, while N-terminal Cys-tag and C-terminal Avi-tag were genetically added to the proteins for site-directed immobilization. Despite only minor differences regarding number, positioning and sequence context of lysine residues within the different RBD variants, those differences led to dramatic change in their functionality after EDC/NHS coupling. In contrast, site-specific biotinylation of the proteins alongside targeted immobilization on streptavidin- or neutravidin-modified liposomes resulted in a regain of functionality and enhanced storage stability across all variants. The developed adaptable liposome-based test showed excellent correlation to an established pseudovirus neutralization test and could identify variation of neutralization patterns of Alpha/Delta and Omicron variants in patient sera. The study highlights the benefits of using neutravidin-liposomes for site-directed protein immobilization with independence from proteins' amino acid sequence, enhanced storage stability and applicability to various biotinylation strategies, serving as a versatile platform technology that can be applied also for coupling of other proteins or peptides used for diagnostic purposes.

### 3.1.1 Introduction

Liposomes, self-assembled spherical vesicles consisting of a lipid bilayer and an aqueous cavity, have been widely applied for both drug delivery and bioanalytical tests. The large inner cavities allow for encapsulation of different drugs or markers, e.g. *m*-carboxyluminol[1], redox markers such as ferri/ferro hexacyanide[2] and $Ru(bpy)_3^{2+}$ [3], fluorophores[4] or even enzymes[5,6] and hence easily support chemiluminescent, electrochemical or optical multianalyte approaches. Liposomes are typically composed of phospholipids, with the hydrophobic tail lengths influencing the curvature and thus size[7], and sterols, such as cholesterol, reducing permeability of solutes and increasing rigidity and dispersion stability[8,9]. The use of phospholipids with functionalized headgroups, e.g. amine-, carboxy- and thiol-groups, enables fine-tuning of the surface charge as well as modification of liposomes with other molecules. Besides small molecules (e.g. biotin and fluorescein) and polymers, such as poly(ethylene glycol), they are often modified with proteins to facilitate specific interaction with analytes[4,10–13]. Addition of EDC and sulfo-NHS to COOH-liposomes is commonly used to generate an

amine-reactive sulfo-NHS-ester that subsequently reacts with $NH_2$-groups of the protein. This can be either the α-amino group of the N-terminal amino acid or the ε-amino group of lysines[14]. This approach therefore results in random orientation of lysine-containing proteins on the liposomal surface, further influenced by the pH value, the α-amino group being favored at pH 7 and the reactivity of the ε-amino group being enhanced at pH 8[15]. Alternative modification strategies include maleimide-coupling to thiols or coupling of azide- to alkyne-groups using click chemistry. These require the incorporation of tags if site-directed coupling is desired, e.g. cystein-tags for the former, while non-canonical amino acids, e.g. azido-homoalanine[16], are required for the latter. Otherwise, thiol-, azide- or -alkyne-NHS-esters can be used to randomly modify the protein via its amine groups[4,11]. Typically, the modification strategy is chosen case-by-case based on chemistry necessary for coupling the functional group of a liposome to a (tagged-)protein. However, in an ideal scenario one would have a ready-to-use liposome that carries always the same functional group, but can be used in a multitude of different assays simply by changing the (tagged-)protein, without the need for further optimizing additional coupling steps.

The global spread of SARS-CoV-2 in combination with the fast development and authorization of protective vaccines based on the viral Spike proteins, the major surface protein of SARS-CoV-2, resulted in a strong selection pressure against the Spike protein[17,18]. Neutralizing antibodies against the receptor binding domain (RBD), a 27 kDa domain of the trimeric Spike protein, responsible for the binding of the cellular angiotensin-converting enzyme 2 (ACE2) receptor, were quickly found to be a potential correlate of protection (CoP)[19–21]. With time, RBD underwent excessive mutations to escape control by neutralizing antibodies, resulting in the occurrence of different variants of concern (VOC) with continuously changing pre-dominance[18,22]. The first worldwide prevalent VOC was Alpha, occurring in the end of 2020, followed by the lineage Delta since mid of 2021. Delta was replaced by different sublineages of Omicron since beginning of 2022, ranging from BA.1, BA.2, BA.5, BQ1.1 towards the most recent strains of KP.3 sublineage[23]. All strains of the Omicron sublineage exhibited an enormous number of mutations within the RBD that altered antibody binding. Furthermore, these amino acid variations changed the physicochemical characteristics, particularly by rising the pI, and therefore made the RBDs more electropositive[24]. Serological tests for SARS-CoV-2 immunity should therefore ideally be adaptable to emerging VOCs, although commercial binding antibody tests, like the Elecsys® anti-SARS-CoV-2 S (Roche) and cPass™ SARS-CoV-2 Neutralization Antibody Detection Kit (GenScript®), still rely on the prototypic RBD.

In this manuscript, different conjugation strategies for the modification of liposomes with proteins were investigated to provide a versatile platform technology that can easily be adapted to other analytes. The receptor binding domain of SARS-CoV-2 (RBD) was chosen as model

protein due to its global importance and five different variants were investigated (Alpha, Delta, BA.2, BA.5 and BQ1.1). Non-directed modification using standard coupling chemistries was compared to a site-directed approach using streptavidin-liposomes and RBD biotinylated via N-terminal Cys- or C-terminal Avi-tags. Finally, the optimum conjugation strategy was used to facilitate the quantification of neutralizing antibodies in patient serum samples for each variant.

## 3.1.2 Experimental section

### 3.1.2.1 Chemicals and consumables

All chemicals were of analytical reagent grade. Bovine serum albumin fraction V (BSA), cholesterol from sheep wool (C8667, ≥ 99%), human serum albumin (HSA), *N*-Hydroxysulfosuccinimide sodium salt (sulfo-NHS, purity ≥ 98%), NHS-biotin (≥ 90%), Sephadex-G50 and G-100, skim milk powder (SMP), streptavidin from *Streptomyces avidinii*, Whatman Nucleopore™ Track-Etched membranes (1.0 μm, 0.4 μm and 0.2 μm diameter), ethanol, acetic acid, Amicon centrifugal filters with a 10kDa cutoff and Tween® 20 were purchased from Sigma Aldrich/Merck (Darmstadt, Germany); 1,2-dipalmitoyl-sn-glycero-3-phosphoethanolamine-*N*-(glutaryl) (sodium salt) (*N*-glutaryl-DPPE) from NOF America Corporation (NY, USA); the remaining phospholipids 1,2-dipalmitoyl-sn-glycero-3-phosphocholine (DPPC), 1,2-dipalmitoyl-sn-glycero-3-phospho-(1'-rac-glycerol) (sodium salt) (DPPG) and the extruder set from Avanti Polar Lipids (Alabaster, AL, USA). Sulforhodamine B (SRB) (S1307), (1-Ethyl-3-(3-dimethylaminopropyl) carbodiimide-hydrochloride) (EDC) (PG82079), neutralizing SARS CoV 2 Spike Protein (RBD) Polyclonal Antibodies (PA5-114451), neutravidin and black high binding 96-well microplates (Nunc MaxiSorp) were purchased from Thermo Fisher Scientific (Waltham, MA, USA); *n*-Octyl-β-D-glucopyranoside (OG) (≥ 98%, CN23), 2-(*N*-Morpholino)-ethane sulphonic acid (MES) (≥ 99%, 4259), *N*-2-Hydroxyethylpiperazine-*N'*-2-ethane sulphonic acid (HEPES) (≥ 99.5%, HN78), sucrose, sodium azide, Tris-(2-carboxyethyl)phosphine (TCEP), imidazole (Cat.# 2C4N.3), sodium chloride and dialysis membrane Spectra/Por© 4 (MWCO: 12-14 kDa) (2718.1) from Carl Roth (Karlsruhe, Germany). Clear streptavidin coated 96-well microplates (KaiSA96) were purchased from Uniogen (Turku, Finland). Phosphorous standard was obtained from Bernd Kraft GmbH (Den Haag, Netherlands). Chloroform, methanol and Spectra-Por® Float-A-Lyzer® G2 (1 mL, MWCO: 1000 kDa) were purchased from Fisher Scientific (Hampton, NH, USA). *N*-Succinimidyl 3-Maleimidopropionate (Mal-NHS), Biotin-PEG$_2$-Amine were purchased from TCI (Eschborn, Germany), bifunctional 3kDa Maleimide-Biotin-PEG was purchased from Rapp Polymere (Tuebingen, Germany). Coomassie R-250 was purchased from AppliChem (Darmstadt, Germany).

### 3.1.2.2 Buffer compositions

Hepes sucrose saline (HSS) buffer contained 200 mM sucrose, 200 mM NaCl, 10 mM HEPES and 0.01 w% $NaN_3$, pH 7.5. PBS buffer contained 137 mM NaCl, 2.7 mM KCl, 10 mM $Na_2HPO_4$ and 1.8 mM $KH_2PO_4$, pH 7.4. PBS-T contained 0.1 w% Tween® 20 in PBS. MES buffer contained 50 mM MES, 200 mM sucrose and 200 mM NaCl, pH 5.5.

### 3.1.2.3 Cell lines and culture conditions

Expi293 suspension cells (Thermo Fisher Scientific, Waltham, MA, USA) were cultivated in commercial Expi293 expression medium (Thermo Fisher Scientific, Waltham, MA, USA) at 37 °C, 8 % $CO_2$ and 90 rpm agitation. HEK-293T-ACE2 cells (kind gift from Prof. Stephan Pöhlmann, Göttingen, Germany) were cultivated in DMEM (Gibco/Thermo Fisher Scientific, Waltham, MA, USA) supplemented with 10 % fetal bovine serum and 1 % Penicilin/Streptomycin (both Pan Biotech, Aidenbach, Germany). Every fourth passage, medium was supplemented with 1 µg/mL Puromycin (InvivoGen, San Diego, CA, USA). HEK-293T-ACE2 cells were cultivated at 37 °C and 5 % $CO_2$.

### 3.1.2.4 Recombinant Proteins

The receptor-binding domain (RBD, residue 319-532) of SARS-CoV-2 Spike proteins were expressed and purified as previously described[25]. Briefly, the coding sequences, together with an N-terminal minimal tPA signal peptide and a C-terminal avi-hexahistidine tag, were cloned into a pcDNA5/FRT/TO-derived expression plasmid. Additionally, a RBD Alpha containing an N-terminal CAAC tag and a flexible $(G_4S)_3$ linker (NtCC)[26] between the signal peptide and the RBD sequence was generated, similar to NtCC-RBD[27]. Expression of recombinant proteins was done using the commercial ExpiFectamine 293 transfection kit (Thermo Fisher Scientific, Waltham, MA, USA). Soluble RBDs were purified 5 days post transfection via immobilized-metal affinity chromatography using HisTrap Excel columns (Cytiva, Marlborough, MA, USA) on a FPLC device (Äkta, Cytiva, Marlborough, MA, USA) with a linear gradient of 10-500 mM imidazole in phosphate-buffered saline (PBS; Cat#: 14190-094, Thermo Fisher Scientific, Waltham, MA, USA) gradient. RBD of Omicron variants BA.2, BA.5 and BQ1.1 were additionally polished with a size exclusion chromatography step. Four mg of Omicron RBD at 4 mg/mL were loaded on a Superdex 75 Increase 10/300 GL column (Cytiva, Marlborough, MA, USA), operated on a FPLC device (Äkta, Cytiva, Marlborough, MA, USA) in PBS at a flow rate of 0.8 mL/min. RBD-containing fractions were detected with reducing SDS-PAGE.

Human ACE2 was expressed and purified as described previously[28].

## 3.1.2.5  SDS-PAGE

For SDS-PAGE analysis the indicated amount of protein was heated at 95 °C for 10 min in 1x reducing SDS-PAGE buffer and loaded onto a self-casted 12.5% polyacrylamide gel (https://pubmed.ncbi.nlm.nih.gov/5432063/). The gel was run for 80 min at 140 V. Staining was done with Coomassie Staining solution (50% (v/v) ethanol, 10% (v/v) acetic acid, 0.25% (w/v) Coomassie Brilliant Blue G250 in $H_2O$) for 20 min and destained in 7% (v/v) acetic acid solution

## 3.1.2.6  Biotinylation of RBD

Proteins were biotinylated with different approaches, either enzymatically using BirA, or undirected chemically targeting amines or site-directed chemically targeting the N-terminal Cys-tag (NtCC).

RBD proteins were side-specifically biotinylated at the C-terminal avi-hexahistidine tag using the BirA biotin-protein ligase kit (Avidity) similar as described previously[29]. 30 nmol protein, at a final concentration of 100 µM in PBS, supplemented with 10 mM ATP, 10 mM Mg(OAc)$_2$ and 150 µM d-biotin, were biotinylated for 2 hours at 30 °C with 7.5 µg BirA. Biotinylated proteins were buffer exchanged into PBS via centrifugation in Amicon ultrafiltration devices three times to ensure separation of free biotin and ATP. Efficiency of biotinylation was monitored using a neutravidin shift assay. Briefly, 50 pmol of enzymatically biotinylated protein was denatured at 95 °C for 10 min in reducing SDS-PAGE buffer. After cooling down to RT, either 150 pmol neutravidin or same volume of PBS were added and subjected to SDS-PAGE analysis.

NHS-biotin was dissolved in DMSO (5 mg/mL) and diluted 1:10 in PBS (0.5 mg/mL). RBD was mixed with different equivalents of NHS-biotin and incubated for 2 h at 22 °C and 300 rpm in a Protein LoBind cup (Eppendorf, Hamburg, Germany). Samples were diluted with PBS (total volume ~400 µL) and purified via centrifugal filtration in 10 kDa Pierce concentrators (Thermo Fisher Scientific, Waltham, MA, USA) at 12000 RCF for 5 minutes with 4 washing steps (400 µL PBS). Finally, the biotinylated proteins were recovered and stored in Protein LoBind tubes. Concentrations were determined at a NanoDrop One (Thermo Fisher Scientific, Waltham, MA, USA) ($M_w$(RBD) = 26.97 kDa, $\varepsilon$(RBD) = 40.34).

Site-specific biotinylation was undertaken at the Cys-residues at the protein N-terminus. A short (PEG-2) and long (3kDa/PEG-68) PEG linker was chosen. The short linker was prepared by dissolving 5.3 mg (0.014 mmol) biotin-PEG$_2$-amine in 1 mL of dry and degassed DMF, then 3.25 mg Mal-NHS (0.012 mmol) were added, vortexed and reacted for 1 h at room temperature in the dark. The product (Mal-PEG$_2$-Biotin) was used without further purification as a frozen stock in DMF solution.

Long and short linker were both coupled under identical conditions. To 350 µL RBD in PBS solution 125 µg TCEP was added to a final concentration of 2.5 mM and reacted for 30 min. Afterwards, a 50-fold excess of Maleimide-Biotin-PEG and Mal-PEG$_2$-Biotin, respectively, was added and incubated for 16 h at room temperature. Biotinylated protein was purified and concentrated by buffer exchange via Amicon 10 kDa centrifugal filters. Characterization was carried out via HABA-Avidin Assay for biotin content using a colorimetric biotin assay kit (MAK171, Sigma Aldrich/Merck, Darmstadt, Germany). Protein concentration was determined via UV-absorbance.

### 3.1.2.7 Antisera

SARS-CoV-2 positive sera were obtained using samples from the prospective longitudinal multicenter cohort study (CoVaKo) in which acute SARS-CoV-2 BTIs and non-BTIs were analyzed. Study centers were the University Hospitals in Erlangen, Regensburg, Augsburg, Würzburg, and Munich (TUM and LMU), all located in Bavaria, Germany. The study design and cohort composition have been thoroughly described in Prelog et al.[30] and Einhauser et al.[31]. Additionally, seropositive samples were obtained from the TiCoKo19 cohort, previously described in Wagner et al.[32] and Einhauser et al.[33].

In particular, sera were selected to provide a variety of immune profiles and immunization backgrounds to resemble a real-world testing scenario. Thus, sera were selected for (wildtype) vaccination, sometimes combined with delta breakthrough infection, or vaccination (wildtype and Omicron adjusted) and Omicron breakthrough infection.

The TiKoCo study was approved by the Ethics Committee of the University of Regensburg, Germany (vote 20-1867-101) and adopted by the Ethics Committee of the University of Erlangen (vote 248_20 Bc). The CoVaKo study was approved by the Ethics Committee of the Friedrich-Alexander-University Erlangen-Nürnberg, Germany (vote 46_21 B) and adopted by the local ethics committees of all other study centers. The CoVaKo Clinical Trials registration was DRKS00024739. All study participants provided written informed consent. Both studies, TiCoKo19 and CoVaKo19 comply with the 1964 Declaration of Helsinki and its later amendments.

Seronegative pre-pandemic anonymized plasma samples from healthy adult blood donors ('BRK…') were purchased from the Bavarian Red Cross. Pooled Human Complement Serum (IR45270 and IR46827) was obtained from Innovative Research (Novi, MI, USA).

### 3.1.2.8 Liposome synthesis

Reverse-phase evaporation was chosen as synthesis method for liposomes as described previously[34]. 150 mM SRB and 140 mM NaCl were dissolved in 20 mM HEPES, pH 7.5

(4.5 mL) by sonication at 60 °C to prepare the encapsulant. Lipid mixtures (41.4 mol% cholesterol, 32.2 mol% DPPC, 18.4 mol% DPPG, 8.0 mol% N-glutaryl-DPPE) were prepared by addition of 3 mL chloroform and 0.5 mL methanol and sonication for 1 min, followed by addition of encapsulant (2 mL) and sonication for 4 min at 60 °C. A rotary evaporator (LABOROTA 4001, Heidolph, Germany) was used to evaporate the organic solvents at 60 °C by stepwise reduction of pressure (900 mbar for 10 min, 850 mbar for 5 min, 800 mbar for 5 min, 780 mbar for 20 min). The solution was vortexed another two times for 1 min with intermittent encapsulant addition (2 mL). The residual organic solvents were evaporated at 60 °C (750 mbar for 20 min, 600 mbar for 5 min, 500 mbar for 5 min, 400 mbar for 20 min). The size was controlled by extrusion at 65°C using polycarbonate membranes with pore sizes of 1 µm, 0.4 µm and 0.2 µm. Solutions were repeatedly pushed through the membranes with decreasing pore sizes, amounting to 21 repetitions for the 1 µm pore size and 11 repetitions for each of the smaller pore sizes. Size exclusion chromatography using a Sephadex G-50 column, followed by dialysis overnight against HSS buffer with 2 buffer exchanges in a dialysis membrane Spectra/Por© 4 (MWCO: 12-14 kDa) were used to remove excess encapsulant.

### 3.1.2.9  Characterization of liposomes

An inductively coupled plasma optical emission spectrometer (ICP-OES) (SpectroBlue TI/EOP) from SPECTRO Analytical Instruments GmbH (Kleve, Germany) was used to determine phospholipid concentrations, which in turn were used to calculate total lipid concentrations based on the mixture of lipids used for the synthesis. Phosphorous standard dilutions between 0 µM and 100 µM in 0.5 M $HNO_3$ were used for calibration of the device. Phosphorous was detected at 177.495 nm. Re-calibration was performed before each measurement using the 0 µM and 100 µM phosphorus dilutions. Liposome stock solutions were diluted 1:100 or 1:60 in 0.5 M $HNO_3$ and their phosphorous content determined.

Size and ζ-potential were measured via dynamic light scattering (DLS) using a Malvern Zetasizer Nano-ZS. Liposome stock solutions were diluted to 25 µM total lipids in HSS buffer in a polymethyl methacrylate (PMMA) semi-micro cuvette (Brand, Germany) for size and a disposable folded capillary cell (Malvern Panalytical, Germany) for ζ-potential measurements. The measurement temperature was set to 25 °C, the refractive index was 1.34, the material absorbance was zero and the dispersant viscosity 1.1185 mPa s. For ζ-potential measurements a dielectric constant of 78.5 was used and an equilibration time of 60 s applied before each measurement.

### 3.1.2.10     Modification of liposomes

Proteins were conjugated to carboxylated liposomes via EDC/sulfo-NHS chemistry. Liposomes were incubated with EDC and sulfo-NHS (1:100:180 ratio of carboxy-groups:EDC:sulfo-NHS)

for 1 h at room temperature (RT) and 300 rpm followed by addition of protein and another 1.5 h incubation at RT and 300 rpm. Excess reagents were removed via dialysis against HSS buffer overnight with one buffer exchange in a Spectra-Por® Float-A-Lyzer® G2 (1 mL, MWCO: 1000 kDa) for large volumes or via size exclusion chromatography with Sephadex G-50 or G-100 for small volumes (<50 µL). Total lipid concentrations were determined using ICP-OES and the conjugated liposomes were stored at 4 °C in Protein LoBind tubes (Eppendorf, Germany).

### 3.1.2.11 Heterogeneous binding assays

Proteins (1 µg/mL ACE2 or 2 µg/mL antibodies in PBS, 100 µL per well) were incubated in a high binding microplate overnight at 4°C. The plate was emptied and blocked for 1 h at 300 rpm with 1 w/v% BSA in PBS-T (150 µL per well). It was washed two times with PBS-T (150 µL per well) and three times with HSS (150 µL per well) before being used. Liposomes (1 µM total lipids if not stated otherwise) (mixed with RBD-biotin in case of streptavidin/neutravidin-liposomes) were added to the MTP (100 µL per well, n = 3) and incubated for 2 h at RT and 300 rpm. The plate was washed three times with HSS buffer (150 µL per well) before 30 mM OG in bidest. water (100 µL per well) was added. After 10 min incubation the fluorescence was measured three consecutive times with a BioTek SYNERGY neo2 fluorescence reader (Agilent Technologies, Santa Clara, CA, USA) ($\lambda_{Ex}$ = 560 $nm$ and $\lambda_{Em}$ = 585 $nm$, bandwidth 10, gain 150).

### 3.1.2.12 Surrogate virus neutralization test

ACE2-biotin (1 µg/mL in PBS, 100 µL per well) was incubated in a streptavidin microplate for 1 h at RT and 300 rpm. The plate was emptied and blocked for 1 h at 300 rpm with 10 µM biotin in PBS-T (150 µL per well). It was washed two times with PBS-T (150 µL per well) and three times with HSS (150 µL per well) before being used. Streptavidin/neutravidin-liposomes (1 µM total lipids if not stated otherwise) were mixed with RBD-biotin (25 ng/mL if not stated otherwise) and serum (0 to 4 v%) and incubated for 1 h at 30°C and 300 rpm. Samples were added to the MTP (100 µL per well, n = 3) and incubated for 2 h at RT and 300 rpm. The plate was washed three times with HSS buffer (150 µL per well) before 30 mM OG in bidest. water (100 µL per well) was added. After 10 min incubation the fluorescence was measured three consecutive times with a BioTek SYNERGY neo2 fluorescence reader ($\lambda_{Ex}$ = 560 $nm$ and $\lambda_{Em}$ = 585 $nm$, bandwidth 10, gain 150). Binding inhibition, given as percentage, was calculated as (1 – fluor. int./fluor. int. lowest serum dilution)*100. IC50 values were obtained via logistic fit with 0% as lower and 100% as upper limit with no weighting performed using the Origin 2020 software.

### 3.1.2.13    Pseudovirus neutralization test

Pseudovirus neutralization for SARS-CoV-2 was performed as described previously[35,36]. In brief, an inoculum containing $2.5 \times 10^5$ RLU/384-well of lentiviral SARS-CoV-2-Spike pseudotypes expressing luciferase, was neutralized using a 2-fold serum dilution series starting at 1:20 for one hour. After 48 h of infection of HEK293T-ACE2 positive cells, luciferase activity was determined using the BrightGlo reagent (Promega Corp, Madison, WI, USA). The 50% inhibitory dilution (ID50) of the sera was calculated in GraphPad Prism 8 (San Diego, CA, USA) by normalizing the data to both infected and noninfected cells, followed by curve fitting with the "log (inhibitor) vs. normalized response" algorithm. Neutralizing antibody titers were assessed against various SARS-CoV-2 variants, namely Alpha (B.1.1.7), Delta (B.1.617.2), and Omicron BA.2, BA.5 and BQ.1.1.

### 3.1.2.14    Antigenic Landscaping

Due to the limited number of sera measured in this manuscript, the antigenic map footprint was taken from visit four of Einhauser et al.[31]. As described there, the antigenic maps were computed using the Racmacs package with 1000 optimizations. Antigens not measured within this manuscript were removed from the maps. Antibody landscapes were generated by adding a third dimension to the antigenic map represented by the geometric mean titres to each variant and subsequently fitting a generalized additive model (GAM)[37] to the variant specific titer values and the according antigenic coordinates. This was used as a more flexible alternative to the traditional ablandscapes package's cone-shaped object calculation as no WT titers were available for the cone peak. GAMs were computed using the mgcv package. Landscapes were visualized in 3D using the r3js package[38].

### 3.1.2.15    Data evaluation and statistical analysis

Data were analyzed statistically using OriginPro 2024 Software. To compare three or more different samples, a one-way analysis of variance (ANOVA) with a post-hoc Tukey test was performed. p-values $\leq 0.05$ were considered statistically significant. * $p \leq 0.05$, ** $p \leq 0.01$, *** $p \leq 0.001$ and ns = not significant.

## 3.1.3  Results and discussion

### 3.1.3.1 Conventional EDC/sulfo-NHS coupling of RBD to COOH-liposomes

Modification of COOH-liposomes with RBD using EDC and sulfo-NHS chemistry worked well for Alpha, as shown previously[28], and Delta but not for Omicron variants. Among the Omicron variants, RBD-BA.2- and -BQ1.1-liposomes showed lower and RBD-BA.5-liposomes no binding to the recombinant ACE2 receptor (**Figure 1 A**). Additionally, the successful coupling

of all variants except for RBD-BA.5 was proven by both, increased hydrodynamic diameter and surface charge of liposomes, as demonstrated by DLS and ζ-potential measurements (**Figure S1**). Interestingly, although RBD-BA.5 showed neither differences in size or ζ-potential following EDC/sulfo-NHS coupling to liposomes nor in binding to ACE2, RBD-BA.5-liposomes still bound to immobilized polyclonal anti-RBD antibodies targeting multiple epitopes on the RBD[39] (**Figure 1 B**). This suggests an unfavorable orientation of RBD-BA.5 on the liposomal surface, preventing proper interaction with ACE2. In conclusion, it could be assumed that the coupling reaction is less efficient due to the absent proof of coupling via DLS measurements, and the low signals obtained upon binding by the immobilized antibodies.

To substantiate the hypothesis of a less efficient coupling reaction of RBD-BA.5 to liposomes, we compared the signals of RBD-BA.5- and RBD-BQ1.1-liposomes that were fabricated with varying amount of the respective RBD (**Figure 1 B**). Here, 1.0 mol% RBD-BA.5 generated even lower signals than 0.2 mol% RBD-BQ1.1 (one-way ANOVA, $p < 0.001$). The altered physicochemical properties towards higher electropositive surface of omicron RBD variants[24] may result in changed interaction with other surfaces, like liposomes, particularly by non-uniform distribution of the lysine residues on the RBD surface, aggravated by the use of a non-directed coupling strategy.
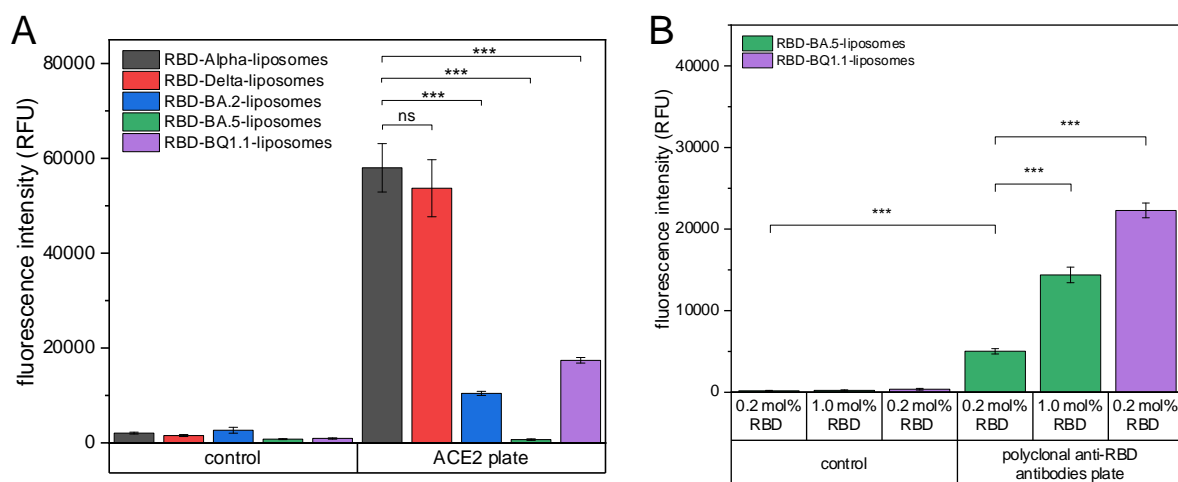


***Figure 1: A***) *ACE2 binding of liposomes modified with 0.2 mol% of different RBD variants. n = 3. (\*\*\* p < 0.001, ns = not significant).* ***B***) *Polyclonal anti-RBD antibodies binding of liposomes modified with 0.2 or 1.0 mol% of RBD-BQ1.1 and -BA.5 variants. n = 3. (\*\*\* p < 0.001).*

Therefore, we hypothesize that the location of the respective amino acids accessible for the coupling reaction strongly influence the coupling efficiency. Specifically, EDC and sulfo-NHS react with COOH-groups on the liposomes, producing an amine-reactive sulfo-NHS-ester that subsequently reacts with $NH_2$-groups of the protein, typically targeting the N-terminal α-amino group and the ε-amino group of lysines[14]. Alpha-RBD has 10 lysine residues (**see Figure S2**), of which three are located in (marked grey) or next to (marked with red arrows) the ACE2

binding motif. Since coupling via EDC/sulfo-NHS chemistry works well, it can be safely assumed that these lysine residues are unlikely to react with the sulfo-NHS-ester. Instead, the other lysines are favored, resulting in the proper orientation of the protein and enabling binding to ACE2. Aligning the sequences of the five RBD variants reveals an abundance of mutations, especially between Alpha/Delta and the Omicron variants (**Table S1**). Delta differs from BA.2 in 16 positions, including the substitution of a lysine residue (K417N) and the introduction of a new lysine residue (N440K). A possible explanation for the decreased ACE2 binding by RBD-BA.2-liposomes might be the unfavorable orientation of RBD-BA.2 during coupling, compared to Alpha and Delta.

Only 3 mutations differentiate RBD-BA.2 and -BA.5, none of which replace or introduce a lysine, but introducing an arginine (L452R), which might change the shielding of an already present lysine, causing it to be the favorite lysine for EDC/sulfo-NHS coupling, resulting in unfavorable orientation of RBD-BA.5 and hence completely preventing interaction with ACE2. For RBD-BQ1.1 a lysine residue which is adjacent to the ACE2 binding motif is replaced (K444T), while a new one is introduced outside of it (N460K). If the latter is favored for the reaction with the sulfo-NHS-ester, it would explain why RBD-BQ1.1-liposomes are able to bind to ACE2 again, while RBD-BA.5-liposomes aren't. Even if the difference in lysine residues between all RBD variants is only minute, the nucleophilic properties of lysine are strongly influenced by the surrounding microenvironment[40]. Therefore, changes in close proximity of lysines can alter their reactivity with sulfo-NHS-esters. A similar effect is seen of α-amino group in direct proximity to multiple histidines, where the high density of imidazole side-chains foster the reaction with 4-methoxyphenyl-esters under physiological conditions[41]. Another possible mechanism, which could have contributed to the different coupling orientation, might be the location of arginines (Q493R), which might be complexing the sulfo-NHS-ester and fostering reactions preferably with adjacent lysines compared to the reaction with the α-amino group of the N-terminus. Furthermore, arginine might influence the orientation of RBD by electrostatic interaction with the negatively charged lipid-bilayer, increasing the likelihood for reaction of surrounding lysines with the sulfo-NHS-ester.

The reaction of sulfo-NHS-esters with α-amino groups is favored around pH 7, while pH 8 enhances reactivity towards ε-amino groups of lysines[15]. When pH 8 was used during the coupling reaction, surprisingly though, decreased ACE2 binding ability for all variants was observed (data not shown). This suggests that the higher pH made some of the lysine residues located within or adjacent to the receptor binding motif more reactive, rather than those outside of it, bolstering our hypothesis.

There are conflicting data in literature regarding the affinity of ACE2 with the different VOCs, mainly influenced by different methods, either equilibrium-based or kinetic-based

measurements, or variations in the assay set-up and the use of either monomeric RBD or trimeric pre-fusion stabilized Spike protein[17,42–46]. All-in all, the binding of ACE2 to the different VOCs seems to be in a similar range. However, this was not reflected by the RBD-liposomes decorated with RBD using EDC/sulfo-NHS chemistry, where RBD-Alpha- and RBD-Delta-liposomes performed significantly better compared to RBD-BA.2- and RBD-BQ1.1-liposomes (one-way ANOVA, $p < 0.001$). This discrepancy is assumed to be due to different orientations on the liposomes, which resulted from the coupling chemistry and mutations within the variants. We conclude that sequence variations strongly impact the coupling efficiency and orientation of proteins using EDC/sulfo-NHS chemistry and predictions based on the type and location of the mutations are very difficult. It is therefore advisable to focus on directional coupling strategies that do not rely on the use of amino acids present throughout the protein peptide chain.

Protein production through recombinant and cell culture technologies relies on the cells' ability to produce a stable protein, and on purification and storage processes to maintain the stability of the protein solutions. Aggregation is an often seen phenomenon because of intrinsic factors, e.g. the protein structure, as well as extrinsic factors, e.g. the environment during expression, purification and storage[47]. Here, investigation of thermal stability of RBD variants by NanoDSF revealed that each RBD variant is present in a different state of multimerization (**Figure S3 A**) and that RBD-BA.2 and -BA.5 have lower melting temperatures compared to -Alpha, -Delta and -BQ1.1 (**Figure S3 B**). It remains unclear, whether this has an influence on coupling, or if the multimers disband into monomers during coupling due to the lower concentration, different environment (e.g. buffer), and shaking. The phenomenon will be further investigated in the future. However, stability during storage was exemplarily investigated for RBD-Alpha modified liposomes (**Figure S4**). Storage stability for up to 24 weeks was achieved when stored in PBS with additional 200 mM sucrose to ensure liposome and 0.04 w/v% HSA for RBD stability. Furthermore, it was found that storage at higher concentrations (100 µM) vs. lower concentrations (25 µM) enhanced RBD stability, as the latter showed a significant loss of binding ability to ACE2 already after 12 weeks, the former only after 36 weeks (one-way ANOVA, $p < 0.001$).

### 3.1.3.2 Alternative biotinylation strategies for random or site-directed coupling of RBD to streptavidin-liposomes

In prior research, liposomes modified with streptavidin (stav-liposomes) had been optimized and demonstrated to be stable for years at 4 °C[10]. Furthermore, random and site-directed biotinylation of proteins is well established[48,49]. These strategies and their effect on RBD variants were investigated here to find a more general alternative to replace EDC/sulfo-NHS-assisted protein coupling. More precisely, biotinylation of $NH_2$-residues using NHS-biotin,

directed biotinylation of an N-terminal Cys-tag, and enzymatic biotinylation of the C-terminal Avi-tag were compared to EDC/sulfo-NHS strategy optimized for the Alpha variant, which initially worked sufficient[28]. A critical issue to overcome in such an approach is the additional binding event between streptavidin and biotin, affected by the location and accessibility of the biotin tag, which can easily lead to lower surface coverage than the direct immobilization approach.

In line with previous observations, reaction of $NH_2$-groups with NHS-esters, in this case NHS-biotin, is generally feasible, as shown using RBD-Alpha, -BA.5 and -BQ1.1 (**Figure S5**). Interestingly, this enabled even the binding of RBD-BA.5-biotin modified stav-liposomes to ACE2, which was not feasible with standard EDC coupling as shown above, which even bolstered the suggested unfavorable *ab initio* interaction with the liposome surface, leading to a wrong orientation of RBD-BA.5 on liposomes. Random biotinylation of amino groups instead of direct coupling to the liposome hence slightly improves the orientation of RBD-BA.5, enabling interaction with ACE2. However, the use of 100 equivalents NHS-biotin resulted in excessive biotinylation of all three variants, preventing interaction with ACE2 for all of them. Therefore, the ratio between RBD and NHS-biotin was further optimized for the Alpha variant, where ratios of 1:2 and 1:5 of RBD to NHS-biotin appeared to work better than a 1:1 and 1:10 ratio (**Figure S6**). Highest signals were obtained with 75 ng/mL RBD-biotin (5 equiv.), followed by a hook effect for higher concentrations, and 100 ng/mL RBD-biotin (2 equiv.), reaching a plateau. While a 1:1 ratio is insufficient to biotinylate each RBD molecule, higher ratios appear to result in multiple, and likely inhomogeneous, biotinylation of each RBD, and increasing the likelihood to block lysine, which contribute to the ACE2 binding interface. When compared to the site-directed biotinylation strategies, the NHS-biotin approach produced by far the lowest signal intensities (**Figure 2 A**).

The modifications via Avi- or Cys-tag enable single, homogeneous and site-directed biotinylation of RBD molecules. While this limits each RBD to just one biotin moiety, and hence in theory lower efficiency in binding to streptavidin, they both have the clear advantages of not involving any critical lysine residues within the RBD molecule, yet display the RBD molecule with perfect orientation on the liposome surface as well as generate a higher reproducibility for future application in diagnostic assays. For coupling via the Cys-tag, various commercially available biotin-maleimide conjugates can be used, including those with spacers. Hence spacer-free and those including a 3 kDa polyethylene glycol (PEG) spacer conjugates were tested. The latter contains 68 monomers and a theoretical length in water of 19 nm[50]. Interestingly, liposomes tagged with RBD that was biotinylated spacer-free at the Cys-tag showed more than double the binding efficiency to ACE2 than those using the PEG spacer. This can in part be explained by the lower degree of biotinylation achieved with the PEG spacer

(0.6 ± 0.2 biotin per RBD) compared to no spacer (1.5 ± 0.5 biotin per RBD), as confirmed with a HABA assay. Degrees above one biotin per RBD are possible due to the two individual cysteines constituting the Cys-tag but are not thought to be beneficial. Besides the lower degree of biotinylation, the long spacer might sterically interfere with the ACE2 interaction. For other proteins introduction of a spacer might be favorable though and would need to be specifically tested.
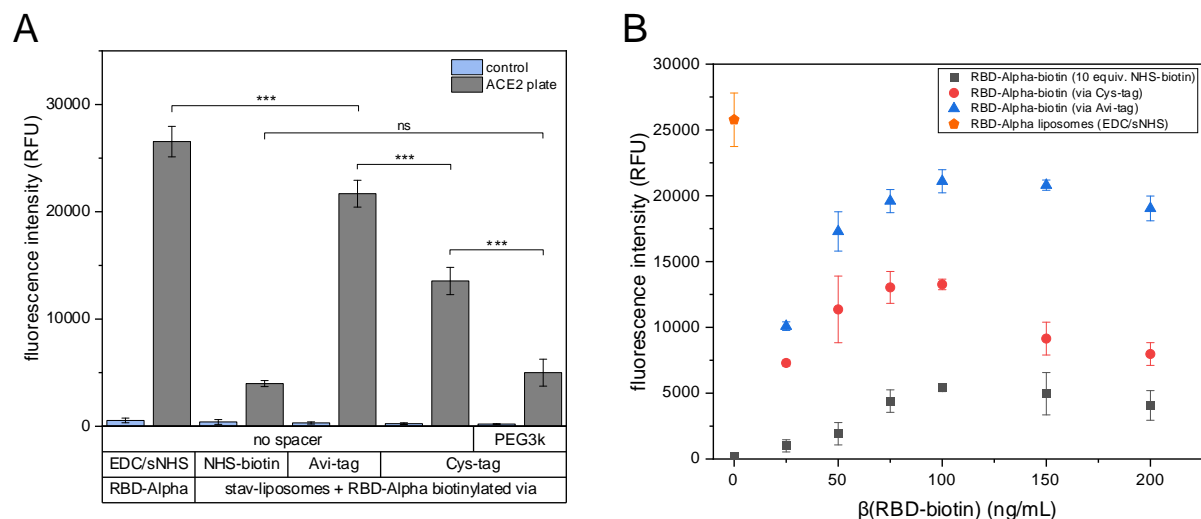


***Figure 2: A**) ACE2 binding of RBD-Alpha-liposomes (EDC/sNHS) and streptavidin-liposomes with various RBD-Alpha-biotin conjugates. n = 3. (*** p < 0.001, ns = not significant). **B**) ACE2 binding of streptavidin-liposomes plus RBD-Alpha-biotin modified using 10 equiv. NHS-biotin (10x), or biotinylated via the Cys-tag or the Avi-tag. n = 3.*

The Avi-tag consists of 15 amino acids that are recognized by *E. coli* biotin ligase (BirA), which biotinylates a specific lysine residue within the recognition-site[51]. The advantages of this approach are the natural spacer afforded by the remaining amino acids and the high consistency of the enzymatic reaction. An additional benefit is the potential combination with a His-tag, typically used for protein purification using Ni-NTA affinity chromatography[52], necessitating only a single engineering step of the corresponding DNA sequence. Successful enzymatic biotinylation was verified with a SDS-PAGE-based neutravidin shift assay, indicating quantitative biotinylation for Delta, BA.2 and BA.5 and almost quantitative biotinylation of Alpha and BQ1.1 RBD variants (**Figure S7**). Finally, by varying the concentration of the amount of biotinylated RBD used for binding to the liposomes, it could be shown that in all scenarios, an optimal RBD concentration can be found at 100 ng/mL, but that only the modification with the Avi-tag allows signals of the same strength as the direct EDC/NHS coupling of the Alpha RBD variant (**Figure 2 B**). It must be assumed that only the C-terminal afforded orientation on the liposomes leads to favorable interactions with ACE2, re-enacting the orientation of RBD within the context of Spike on the virus membrane of SARS-CoV-2. Therefore, this strategy was applied to all RBD variants and successful binding to ACE2 immobilized on a microtiter plate could be demonstrated, even for RBD-BA.5 (**Figure S8**).

Finally, again rather surprisingly, not all variants behaved the same with the blocking reagents used, where BA.2 demonstrated strong non-specific binding to BSA. In the end, skim milk powder was identified as a blocking agent that can be used equally well for all variants, avoiding non-specific binding (**Figure S9**).

### 3.1.3.3 Establishing the surrogate virus neutralization test

For the development of a surrogate virus neutralization test a competitive assay format was developed, in which antibodies inhibit RBD-liposomes from binding to ACE2, immobilized in a microtiter plate. Neutralizing antibodies present in a sample would interfere with this binding and lead to a lower signal. The assay principle has proven as a valid surrogate in an ELISA format[53] and had already been successfully established for the Alpha variant[28]. Initial studies demonstrated the importance of ACE2 orientation for immobilization, suggesting that only in the oriented format using biotinylated ACE2 sufficient binding sites are available to promote efficient binding between RBD-liposomes and ACE2 in this heterogeneous format. This effect was identified as the presence of pre-pandemic serum would disturb binding of all types of RBD-liposomes to randomly immobilized ACE2, but not to ACE2-biotin immobilized site-directed (**Figure S10** shows exemplary data for RBD-Alpha-liposomes). Blocking of streptavidin plates with biotin after immobilization of ACE2-biotin enabled their use for the new RBD-biotin approach, improving stav-liposome capture.

Secondly, liposomes were further optimized to serve as a truly general reagent for the immobilization of biotinylated proteins. Since streptavidin contains the amino acid sequence RYD (Arg-Tyr-Asp), which is known to interact with the sequence RGD (Arg-Gly-Asp) present in proteins[54], neutravidin-liposomes (nav-liposomes) were investigated as alternative. Neutravidin is a deglycosylated version of avidin and does not contain the RYD sequence. Interestingly, even though both ACE2 and RBD contain the RGD sequence, neither stav- nor nav-liposomes were captured in an ACE2-biotin coated plate in the presence of free RBD (50 to 200 ng/mL) (**Figure S11**). This suggests that the sequences are hidden within the protein structures (D in RGD motif in ACE2 is faced to the inner core of protein), or the binding kinetics are simply unfavorable, which is probably the case for RGD in RBD Alpha and Delta, were the RGD motif is exposed to the surface, according to the crystal structure 6vw1 in the pdb repository. Both stav- and nav-coated liposomes reacted similar with seronegative and seropositive samples (**Figure 3 A** and **B**), demonstrating the applicability of both liposome types. To obtain a universally applicable platform technology, and to prevent serum reactivity against streptavidin[55], nav-liposomes, which also showed a slightly higher IC50 (84 vs 69) compared to the stav-liposomes (**Figure 3 B**), were used for all subsequent studies.
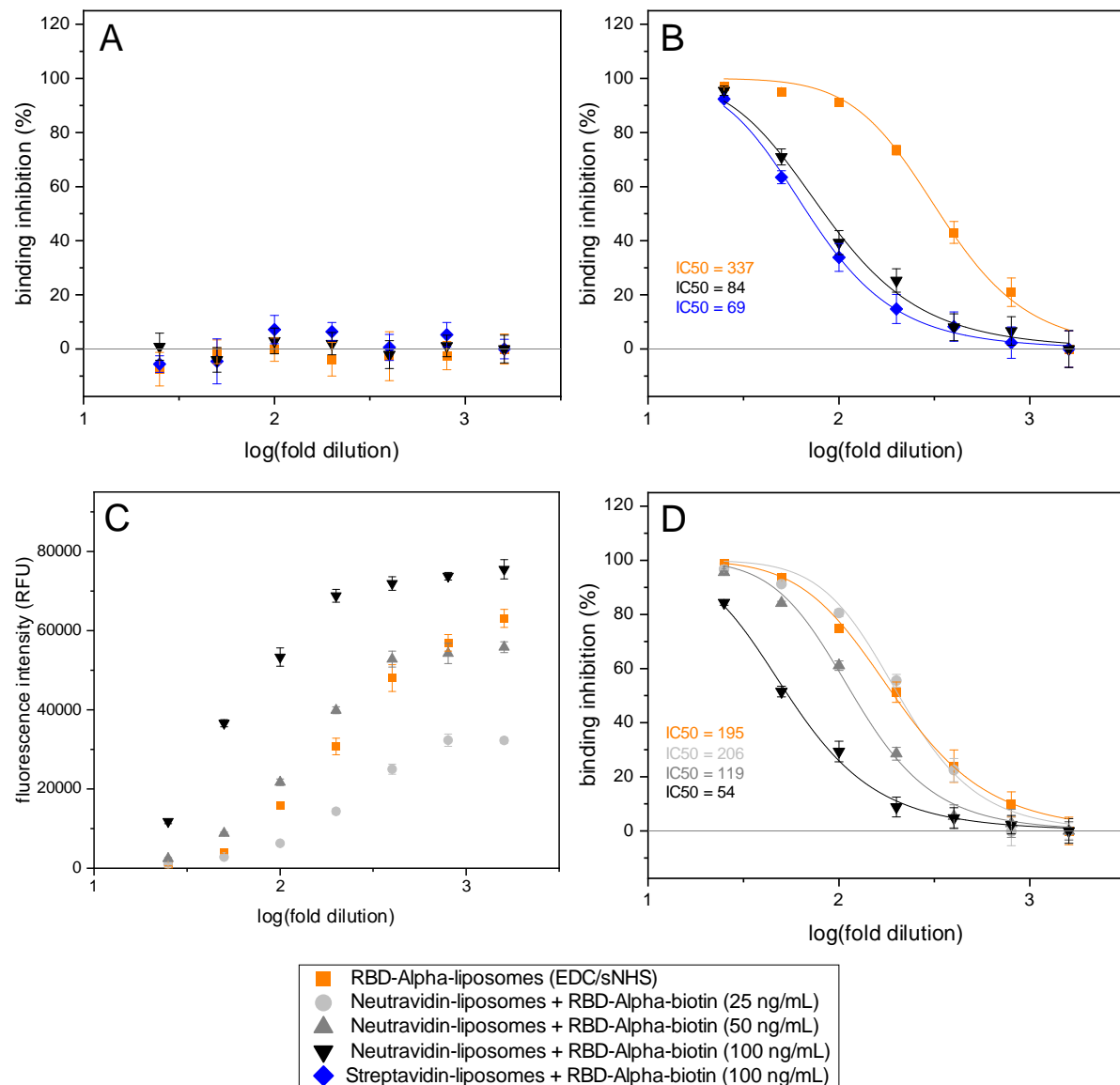
*Figure 8: Neutralization tests of RBD-Alpha-liposomes, and streptavidin- or neutravidin-liposomes plus RBD-Alpha biotinylated via the Avi-tag, with a pre-pandemic serum (BRK4500) (**A**), seropositive sample IR46827 (**B**), or seropositive sample IR45270 (**C** and **D**). RBD-Alpha-liposomes were used at a concentration of 1 µM for (**B**) and 0.5 µM for (**C** and **D**). n = 3.*

RBD-Alpha and pooled seropositive samples were used for a fine-tuning of assay conditions. In a competitive assay format, the concentrations of the binding partners play a crucial role for the obtainable limits of detection and need to be balanced with the signals obtained via the liposome concentration itself. The comparison of RBD-liposomes, RBD-nav-liposomes and RBD-stav-liposomes with the seropositive sample (IR46827) had revealed lower IC50 values for the format with stav/nav-liposome plus RBD-Alpha-biotin (69 and 84, respectively) compared to just RBD-Alpha-liposomes (337) (**Figure 3 B**). This can be explained with the approximately two times higher RBD loading for the stav/nav-liposome format, while the input liposome concentration was kept constant for the assay. Both formats produced identical IC50 values (206 and 195) for a different, less potent, seropositive sample (IR45270) when the same

RBD-Alpha content (25 ng/mL RBD-biotin or 0.5 µM RBD-Alpha liposomes) was used (**Figure 3 D**). However, the latter produced higher fluorescence intensities, which could only be matched with nav-liposomes when increasing the RBD-Alpha-biotin concentration by a factor of 2 again to 50 ng/mL (**Figure 3 C**), which resulted in a lower IC50 value (119) (**Figure 3 D**). As expected, the concentration of RBD-biotin was a key factor in achieving good detection ranges, but it is inversely associated to the capture efficiency in the ACE2 plate. In the end, since also the lower signal intensities enabled reliable detection, 25 ng/mL RBD-biotin was added to all nav-liposome assays to obtain good limits of detection. Furthermore, fluorescence enhancing effects of serum constituents had to be taken into account for data processing, as signals of a negative control in buffer were lower than those obtained for confirmed seronegative sera. This is exemplified by data normalization to the buffer control vs. the lowest serum concentration for RBD-BQ1.1-biotin (**Figure S12**). Addition of HSA instead of serum had the same effect (**Figure S13**) and could be developed into a generic negative control, but natural variation of human serum will need to be assessed in the future for a fine tuning of this negative control.

Finally, liposome concentrations of 1 µM total lipids and RBD-biotin concentrations of 25 ng/mL were chosen for the final assay as they produced the highest signal intensities with the lowest amount of RBD, which corresponds to optimum sensitivity. The current assay format allows the separate storage of stav/nav-liposomes and RBD-biotin variants. In addition to the previously mentioned high storage stability of stav-liposomes at 4 °C, also RBD-biotin was shown to have excellent stability under the same storage conditions for several weeks. Alternatively, the conjugate can be stored, but additional stability studies are recommended. However, since naturally occurring biotin in patient samples may interfere with the assay format, a pre-incubation of liposomes and RBD-biotin is recommended. Here, it was shown that when pre-incubating nav-liposomes and RBD-biotin, no interferences, i.e. false-positive signals, were observed with 575 nM free biotin (**Figure S14**), which resembles the threshold of the CLSI EP37 guideline[56] for a 1:25 dilution of serum. This high biotin concentration was chosen as it resembles three times the highest concentration measured in a patient with high biotin dose uptake.

### 3.1.3.4 Serum panel screening

Screening of five separate seronegative, pre-pandemic sera (four of them 1:1 pooled samples) showed some variation of non-specific binding inhibition (**Figure S15**). The results were used to determine the cut-off values, which were calculated for each variant separately as the average binding inhibition values of all serum samples plus 3-times the standard deviation and ranged from 29% to 38% (**Table S2**).

Finally, 10 seropositive samples with different immunization and infection backgrounds (pre-Omicron exposure vs. Omicron exposure, both groups including vaccine breakthrough infections) were tested for all five variants (**Figure S16**, **Table S3**). All samples were correctly identified as seropositive. Furthermore, IC50 values could be obtained when the serum dilution was within the dynamic range of the assay. Specifically, reliable IC50 values could be obtained for 5 sera (S1, S2, S3, S6, S7) using a serum dilution range of 1:25 to 1:3200. For three sera (S4, S5, S10) with higher antibody titers, the serum dilution range was increased to 1:51200. In the case of sera S8 and S9, the antibody titers were outside of the tested range (IC50 >3200). Based on this limited study, it is suggested to analyze patient sera starting with a 1:20 dilution followed by 2.5-fold series dilution, instead of the used 1:25 dilution followed by 2-fold series dilution.

Furthermore, the liposome assay could indeed provide relevant information with respect to the neutralization potential toward the various virus variants. Grouping of the sera based on the vaccination and infection history of the donors showed that sera from donors without Omicron booster or infection are overall less potent compared to the Omicron specific sera (**Figure 4**). Sera S1, S2, S3 and S7 show only very limited capability to neutralize Omicron variants but are able to neutralize Alpha and Delta with respectable titers. Serum S6 illustrates the immune escape of Omicron, starting with a drop of IC50 values for BA.2/BA.5 compared to Alpha/Delta and another one for BQ1.1. The same trend is visible for sera S4, S5 and S10, whose donors were exposed to Omicron, but had overall higher titers for all variants. S10 showed higher IC50 values for BA.2/BA.5 compared to Alpha/Delta, unlike the others. Overall, these data suggest that an Omicron vaccine breakthrough infection coincides with an increased neutralizing antibody breadth with a bias towards higher titers against variants which are antigenically close to the initial immunization antigen, in line with previously published data[31]. Furthermore, S8 and S9 illustrate, that this imprinted bias might be, at least for a short timeframe, overcome by repeated exposure to Omicron antigens, resulting in a maximum neutralization breadth over all tested variants. These findings are also reflected in the antibody landscapes for the pVNT as well as the liposome surrogate neutralization assay, which both reveal distinct patterns for Omicron vs. no Omicron antigen exposure (**Figure S17**).
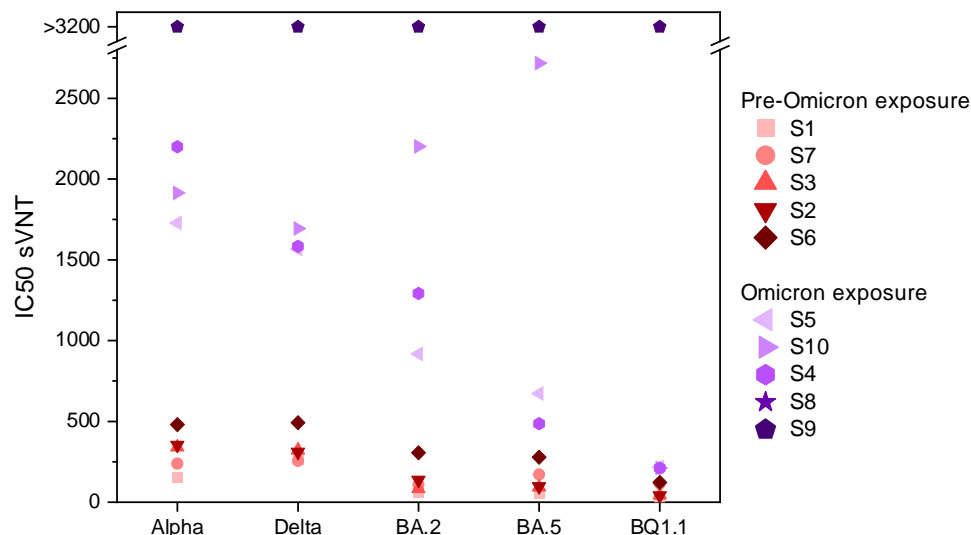
*Figure 4: Comparison of IC50 values obtained with the 10 seropositive samples for each RBD-variant in the liposome-based sVNT. Sorted by IC50 values for Alpha and grouped into samples excluding and including Omicron vaccine or infection. n = 3.*

The liposome-based neutralization test results correlated excellently and highly significant with those of the pVNT (**Table S4**), for both, overall comparison (Spearman r = 0.86, p < 0.0001) as well as variant specific comparison (all r > 0.9, all p < 0.00024) (**Figure 5**). These results show even higher correlations than traditional ELISA based ACE2 binding inhibition[53], highlighting the potential benefit of a more virus-resembling liposome format. Overall, these findings demonstrate that liposome-based ACE2 inhibition assays represent a safer, scalable, and effective alternative to traditional virus-based neutralization tests.
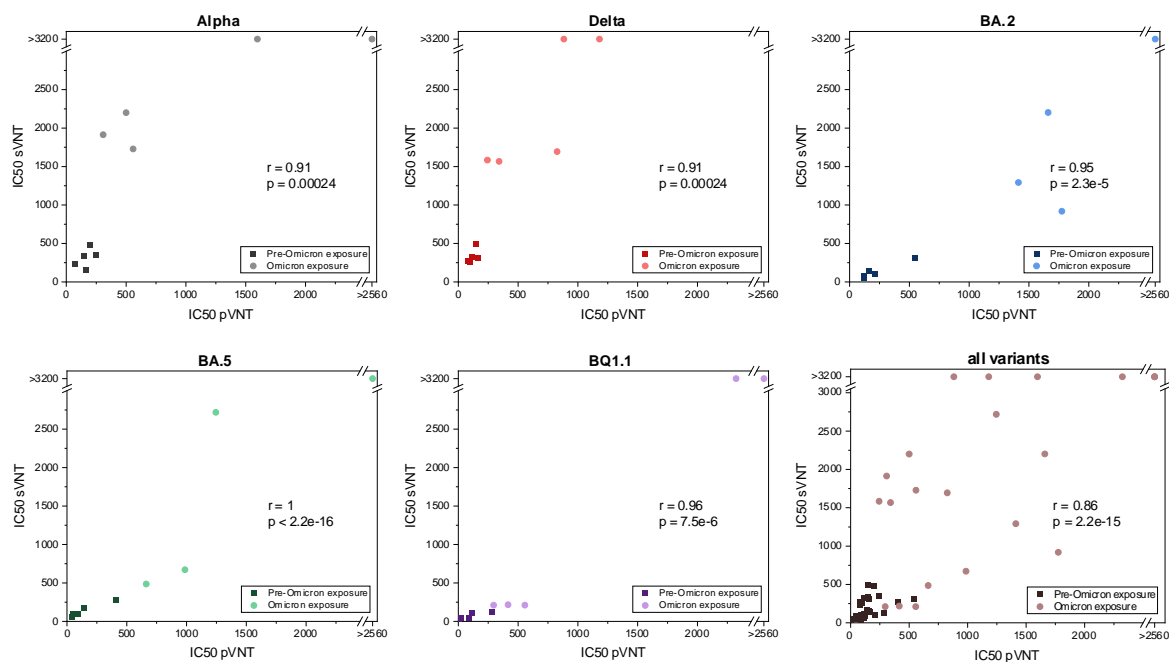


*Figure 5: Spearman correlation of IC50 values obtained in the sVNT and pVNT.*

## 3.1.4 Conclusion

Coupling of proteins to signaling labels is well established and ubiquitously used. By using five variants of the SARS-CoV-2 RBD protein, it could be shown how subtle sequence variations can lead to dramatically different coupling outcomes that are not easily predictable. Since the ultimate goal was the development of a standardized liposome-based assay platform technology, not only the protein coupling yield but also their functionality in binding to antibodies and the ACE2 receptor could easily be taken into consideration. Accordingly, altered physicochemical properties mediated by minor amino acid sequence variations can lead to unfavorable orientation of proteins on the liposomal surface after direct EDC/sulfo-NHS coupling. This obstacle could be overcome only to a minor extent by random NHS-biotin-mediated coupling, suggesting that proper orientation of RBD on the liposome surface rather than the distance to the liposome surface is crucial for favorable receptor interaction.

Site-specific biotinylation can mediate the proper orientation of the protein upon immobilization on streptavidin-liposomes. Strategies require genetic engineering of recombinant proteins and include the introduction of N- or C-terminal Avi- or Cys-tags for enzymatic or maleimide-mediated site-specific biotinylation and, at the same time, the avoidance of chemical alteration of lysine residues. Using RBD variants derived from 5 different VOCs we highlight the advantages of proper orientation and topologically correct display of antigens on the liposome surface, thus supporting standardized and optimal interaction with the ACE2 receptor. Altogether, our results show excellent correlations to conventional virus neutralization, highlighting the potential benefit of a virus-resembling liposome format.

Looking into the future, click chemistry might be a promising approach to facilitate site-directed protein modification of liposomes without relying on the biotin-streptavidin interaction. Display of alkyne- or azide-residues on liposomes can be easily achieved by the addition of functionalized lipids during synthesis or even via post-insertion. For the proteins, however, click chemistry requires the introduction of alkyne- or azide-residue containing non-canonical amino acids[16], making it less straight-forward than biotinylation of Avi- or Cys-tags.

## 3.1.5 References

(1) Mayer, M.; Takegami, S.; Neumeier, M.; Rink, S.; Jacobi von Wangelin, A.; Schulte, S.; Vollmer, M.; Griesbeck, A. G.; Duerkop, A.; Baeumner, A. J. *Angew Chem Int Ed Engl* **2018**, *57* (2), 408–411.

(2) Wongkaew, N.; He, P.; Kurth, V.; Surareungchai, W.; Baeumner, A. J. *Anal. Bioanal. Chem.* **2013**, *405* (18), 5965–5974.

(3) Zhan, W.; Bard, A. J. *Anal. Chem.* **2007**, *79* (2), 459–463.

(4) Annie Ho, J.; Wu, L.-C.; Chang, L.-H.; Hwang, K.-C.; Reuben Hwu, J.-R. *J Chromatogr B Analyt Technol Biomed Life Sci* **2010**, *878* (2), 172–176.

(5) ZHENG, Y.; CHEN, H.; LIU, X.; JIANG, J.; LUO, Y.; SHEN, G.; YU, R. *Talanta* **2008**, *77* (2), 809–814.

(6) Vamvakaki, V.; Chaniotakis, N. A. *Biosens. Bioelectron.* **2007**, *22* (12), 2848–2853.

(7) Bulbake, U.; Doppalapudi, S.; Kommineni, N.; Khan, W. *Pharmaceutics* **2017**, *9* (2).

(8) Briuglia, M.-L.; Rotella, C.; McFarlane, A.; Lamprou, D. A. *Drug Deliv Transl Res* **2015**, *5* (3), 231–242.

(9) Virden, J. W.; Berg, J. C. *Langmuir* **1992**, *8* (6), 1532–1537.

(10) Rink, S.; Kaiser, B.; Steiner, M.-S.; Duerkop, A.; Baeumner, A. J. *Anal. Bioanal. Chem.* **2022**, *414* (10), 3231–3241.

(11) Wen, H.-W.; Decory, T. R.; Borejsza-Wysocki, W.; Durst, R. A. *Talanta* **2006**, *68* (4), 1264–1272.

(12) Mao, L.; Yuan, R.; Chai, Y.; Zhuo, Y.; Xiang, Y. *Biosens. Bioelectron.* **2011**, *26* (10), 4204–4208.

(13) Viswanathan, S.; Rani, C.; Vijay Anand, A.; Ho, J.-A. A. *Biosens. Bioelectron.* **2009**, *24* (7), 1984–1989.

(14) Nanda, J. S.; Lorsch, J. R. Chapter Eight - Labeling a Protein with Fluorophores Using NHS Ester Derivitization. In *Methods in Enzymology : Laboratory Methods in Enzymology: Protein Part A*; Lorsch, J., Ed.; Academic Press, 2014; pp 87–94. DOI: 10.1016/B978-0-12-420070-8.00008-8.

(15) Brinkley, M. *Bioconjug Chem* **1992**, *3* (1), 2–13.

(16) Oude Blenke, E.; Klaasse, G.; Merten, H.; Plückthun, A.; Mastrobattista, E.; Martin, N. I. *J Control Release* **2015**, *202*, 14–20.

(17) Xue, S.; Han, Y.; Wu, F.; Wang, Q. *Protein Cell* **2024**, *15* (6), 403–418.

(18) Carabelli, A. M.; Peacock, T. P.; Thorne, L. G.; Harvey, W. T.; Hughes, J.; Peacock, S. J.; Barclay, W. S.; Silva, T. I. de; Towers, G. J.; Robertson, D. L. *Nat Rev Microbiol* **2023**, *21* (3), 162–177.

(19) Perry, J.; Osman, S.; Wright, J.; Richard-Greenblatt, M.; Buchan, S. A.; Sadarangani, M.; Bolotin, S. *PLOS ONE* **2022**, *17* (4), e0266852.

(20) Khoury, D. S.; Cromer, D.; Reynaldi, A.; Schlub, T. E.; Wheatley, A. K.; Juno, J. A.; Subbarao, K.; Kent, S. J.; Triccas, J. A.; Davenport, M. P. *Nat. Med.* **2021**, *27* (7), 1205–1211.

(21) Earle, K. A.; Ambrosino, D. M.; Fiore-Gartland, A.; Goldblatt, D.; Gilbert, P. B.; Siber, G. R.; Dull, P.; Plotkin, S. A. *Vaccine* **2021**, *39* (32), 4423–4428.

(22) Markov, P. V.; Ghafari, M.; Beer, M.; Lythgoe, K.; Simmonds, P.; Stilianakis, N. I.; Katzourakis, A. *Nat Rev Microbiol* **2023**, *21* (6), 361–379.

(23) *GISAID - Fiocruz.* https://gisaid.org/phylodynamics/global/fiocruz/ (accessed 2025-04-16).

(24) Barre, A.; Klonjkowski, B.; Benoist, H.; Rougé, P. *Viruses* **2022**, *14* (4).

(25) Peterhoff, D.; Glück, V.; Vogel, M.; Schuster, P.; Schütz, A.; Neubert, P.; Albert, V.; Frisch, S.; Kiessling, M.; Pervan, P.; Werner, M.; Ritter, N.; Babl, L.; Deichner, M.; Hanses, F.; Lubnow, M.; Müller, T.; Lunz, D.; Hitzenbichler, F.; Audebert, F.; Hähnel, V.; Offner, R.; Müller, M.; Schmid, S.; Burkhardt, R.; Glück, T.; Koller, M.; Niller, H. H.; Graf, B.; Salzberger, B.; Wenzel, J. J.; Jantsch, J.; Gessner, A.; Schmidt, B.; Wagner, R. *Infection* **2021**, *49* (1), 75–82.

(26) Peterhoff, D.; Thalhauser, S.; Sobczak, J. M.; Mohsen, M. O.; Voigt, C.; Seifert, N.; Neckermann, P.; Hauser, A.; Ding, S.; Sattentau, Q.; Bachmann, M. F.; Breunig, M.; Wagner, R. *Vaccines (Basel)* **2021**, *9* (6).

(27) Barbey, C.; Su, J.; Billmeier, M.; Stefan, N.; Bester, R.; Carnell, G.; Temperton, N.; Heeney, J.; Protzer, U.; Breunig, M.; Wagner, R.; Peterhoff, D. *Eur J Pharm Biopharm* **2023**, *192*, 41–55.

(28) Streif, S.; Neckermann, P.; Spitzenberg, C.; Weiss, K.; Hoecherl, K.; Kulikowski, K.; Hahner, S.; Noelting, C.; Einhauser, S.; Peterhoff, D.; Asam, C.; Wagner, R.; Baeumner, A. J. *Anal. Bioanal. Chem.* **2023**, *415* (8), 1421–1435.

(29) Fairhead, M.; Howarth, M. *Methods in molecular biology (Clifton, N.J.)* **2015**, *1266*, 171–184.

(30) Prelog, M.; Jeske, S. D.; Asam, C.; Fuchs, A.; Wieser, A.; Gall, C.; Wytopil, M.; Mueller-Schmucker, S. M.; Beileke, S.; Goekkaya, M.; Kling, E.; Geldmacher, C.; Rubio-Acero, R.; Plank, M.; Christa, C.; Willmann, A.; Vu, M.; Einhauser, S.; Weps, M.; Lampl, B. M. J.; Almanzar, G.; Kousha, K.; Schwägerl, V.; Liebl, B.; Weber, B.; Drescher, J.; Scheidt, J.; Gefeller, O.; Messmann, H.; Protzer, U.; Liese, J.; Hoelscher, M.; Wagner, R.; Überla, K.; Steininger, P. *J. Clin. Virol.* **2024**, *170*, 105622.

(31) Einhauser, S.; Asam, C.; Weps, M.; Senninger, A.; Peterhoff, D.; Bauernfeind, S.; Asbach, B.; Carnell, G. W.; Heeney, J. L.; Wytopil, M.; Fuchs, A.; Messmann, H.; Prelog, M.; Liese, J.; Jeske, S. D.; Protzer, U.; Hoelscher, M.; Geldmacher, C.; Überla, K.; Steininger, P.; Wagner, R. *eBioMedicine* **2024**, *110*, 105438.

(32) Wagner, R.; Peterhoff, D.; Beileke, S.; Günther, F.; Berr, M.; Einhauser, S.; Schütz, A.; Niller, H. H.; Steininger, P.; Knöll, A.; Tenbusch, M.; Maier, C.; Korn, K.; Stark, K. J.; Gessner, A.; Burkhardt, R.; Kabesch, M.; Schedl, H.; Küchenhoff, H.; Pfahlberg, A. B.; Heid, I. M.; Gefeller, O.; Überla, K. *Viruses* **2021**, *13* (6).

(33) Einhauser, S.; Peterhoff, D.; Beileke, S.; Günther, F.; Niller, H.-H.; Steininger, P.; Knöll, A.; Korn, K.; Berr, M.; Schütz, A.; Wiegrebe, S.; Stark, K. J.; Gessner, A.; Burkhardt, R.; Kabesch, M.; Schedl, H.; Küchenhoff, H.; Pfahlberg, A. B.; Heid, I. M.; Gefeller, O.; Überla, K.; Wagner, R. *Viruses* **2022**, *14* (6).

(34) Edwards, K. A.; Curtis, K. L.; Sailor, J. L.; Baeumner, A. J. *Anal. Bioanal. Chem.* **2008**, *391* (5), 1689–1702.

(35) Einhauser, S.; Peterhoff, D.; Niller, H. H.; Beileke, S.; Günther, F.; Steininger, P.; Burkhardt, R.; Heid, I. M.; Pfahlberg, A. B.; Überla, K.; Gefeller, O.; Wagner, R. *Diagnostics* **2021**, *11* (10), 1843.

(36) Sampson, A. T.; Heeney, J.; Cantoni, D.; Ferrari, M.; Sans, M. S.; George, C.; Di Genova, C.; Mayora Neto, M.; Einhauser, S.; Asbach, B.; Wagner, R.; Baxendale, H.; Temperton, N.; Carnell, G. *Viruses* **2021**, *13* (8).

(37) Wood, S. N. *J. R. Stat. Soc. Ser. B. Stat. Methodol.* **2003**, *65* (1), 95–114.

(38) GitHub. *GitHub - shwilks/r3js: R package of functions linking R to the threejs 3D plotting engine.* https://github.com/shwilks/r3js (accessed 2025-04-22).

(39) Chen, Y.; Zhao, X.; Zhou, H.; Zhu, H.; Jiang, S.; Wang, P. *Nat Rev Immunol* **2023**, *23* (3), 189–199.

(40) Abbasov, M. E.; Kavanagh, M. E.; Ichu, T.-A.; Lazear, M. R.; Tao, Y.; Crowley, V. M.; Ende, C. W. am; Hacker, S. M.; Ho, J.; Dix, M. M.; Suciu, R.; Hayward, M. M.; Kiessling, L. L.; Cravatt, B. F. *Nat. Chem.* **2021**, *13* (11), 1081–1092.

(41) Martos-Maldonado, M. C.; Hjuler, C. T.; Sørensen, K. K.; Thygesen, M. B.; Rasmussen, J. E.; Villadsen, K.; Midtgaard, S. R.; Kol, S.; Schoffelen, S.; Jensen, K. J. *Nat Commun* **2018**, *9* (1), 3307.

(42) Addetia, A.; Piccoli, L.; Case, J. B.; Park, Y.-J.; Beltramello, M.; Guarino, B.; Dang, H.; Melo, G. D. de; Pinto, D.; Sprouse, K.; Scheaffer, S. M.; Bassi, J.; Silacci-Fregni, C.; Muoio, F.; Dini, M.; Vincenzetti, L.; Acosta, R.; Johnson, D.; Subramanian, S.; Saliba, C.; Giurdanella, M.; Lombardo, G.; Leoni, G.; Culap, K.; McAlister, C.; Rajesh, A.; Dellota, E.; Zhou, J.; Farhat, N.; Bohan, D.; Noack, J.; Chen, A.; Lempp, F. A.; Quispe, J.; Kergoat, L.; Larrous, F.; Cameroni, E.; Whitener, B.; Giannini, O.; Cippà, P.; Ceschi, A.; Ferrari, P.; Franzetti-Pellanda, A.; Biggiogero, M.; Garzoni, C.; Zappi, S.; Bernasconi, L.; Kim, M. J.; Rosen, L. E.; Schnell, G.; Czudnochowski, N.; Benigni, F.; Franko, N.; Logue, J. K.; Yoshiyama, C.; Stewart, C.; Chu, H.; Bourhy, H.; Schmid, M. A.; Purcell, L. A.; Snell, G.; Lanzavecchia, A.; Diamond, M. S.; Corti, D.; Veesler, D. *Nature* **2023**, *621* (7979), 592–601.

(43) Wang, Q.; Iketani, S.; Li, Z.; Liu, L.; Guo, Y.; Huang, Y.; Bowen, A. D.; Liu, M.; Wang, M.; Yu, J.; Valdez, R.; Lauring, A. S.; Sheng, Z.; Wang, H. H.; Gordon, A.; Liu, L.; Ho, D. D. *Cell* **2023**, *186* (2), 279-286.e8.

(44) Han, P.; Li, L.; Liu, S.; Wang, Q.; Di Zhang; Xu, Z.; Han, P.; Li, X.; Peng, Q.; Su, C.; Huang, B.; Li, D.; Zhang, R.; Tian, M.; Fu, L.; Gao, Y.; Zhao, X.; Liu, K.; Qi, J.; Gao, G. F.; Wang, P. *Cell* **2022**, *185* (4), 630-640.e10.

(45) Li, L.; Liao, H.; Meng, Y.; Li, W.; Han, P.; Liu, K.; Wang, Q.; Li, D.; Zhang, Y.; Wang, L.; Fan, Z.; Zhang, Y.; Wang, Q.; Zhao, X.; Sun, Y.; Huang, N.; Qi, J.; Gao, G. F. *Cell* **2022**, *185* (16), 2952-2960.e10.

(46) Mader, A.-L.; Tydykov, L.; Glück, V.; Bertok, M.; Weidlich, T.; Gottwald, C.; Stefl, A.; Vogel, M.; Plentz, A.; Köstler, J.; Salzberger, B.; Wenzel, J. J.; Niller, H. H.; Jantsch, J.; Wagner, R.; Schmidt, B.; Glück, T.; Gessner, A.; Peterhoff, D. *iScience* **2022**, *25* (4), 104076.

(47) Wang, W.; Nema, S.; Teagarden, D. *International Journal of Pharmaceutics* **2010**, *390* (2), 89–99.

(48) Dundas, C. M.; Demonte, D.; Park, S. *Appl Microbiol Biotechnol* **2013**, *97* (21), 9343–9353.

(49) Choi-Rhee, E.; Schulman, H.; Cronan, J. E. *Protein Sci* **2004**, *13* (11), 3043–3050.

(50) Ma, Z.; LeBard, D. N.; Loverde, S. M.; Sharp, K. A.; Klein, M. L.; Discher, D. E.; Finkel, T. H. *PLOS ONE* **2014**, *9* (11), e112292.

(51) Li, Y.; Sousa, R. *Protein Expression and Purification* **2012**, *82* (1), 162–167.

(52) Spriestersbach, A.; Kubicek, J.; Schäfer, F.; Block, H.; Maertens, B. Chapter One - Purification of His-Tagged Proteins. In *Methods in Enzymology : Laboratory Methods in Enzymology: Protein Part A*; Lorsch, J., Ed.; Academic Press, 2014; pp 1–15. DOI: 10.1016/bs.mie.2014.11.003.

(53) Grunau, B.; Prusinkiewicz, M.; Asamoah-Boaheng, M.; Golding, L.; Lavoie, P. M.; Petric, M.; Levett, P. N.; Haig, S.; Barakauskas, V.; Karim, M. E.; Jassem, A. N.; Drews, S. J.; Sediqi, S.; Goldfarb, D. M. *Microbiol. Spectr.* **2022**, *10* (5), e0131522.

(54) a.marmieri. Biotin Binding Surfaces. *Biomat Srl,* Jul 21, 2020. https://www.biomat.it/applications-techniques/biotin-binding-surfaces/ (accessed 2025-02-27).

(55) Dahll, L. K.; Haave, E. M.; Dahl, S. R.; Aas, F. E.; Thorsby, P. M. *Scand J Clin Lab Invest* **2021**, *81* (2), 92–103.

(56) Luong, J. H. T.; Vashist, S. K. *ACS Omega* **2020**, *5* (1), 10–18.

### 3.1.6  Supplementary information

**EDC/sulfo-NHS coupling**

Modification of COOH-liposomes with RBD variants using EDC/sulfo-NHS chemistry led to a significant increase of the Z-average (**Figure S1 A**) for Alpha, Delta and BA.2 and of the ζ-potential (**Figure S1 B**) for Alpha, Delta, BA.2 and BQ1.1 (one-way ANOVA, $p < 0.001$). In the case of BA.5 the Z-average remained at 152 nm, and the ζ-potential at -28 ± 2 mV compared to -32 ± 2 mV for unmodified liposomes, suggesting unsuccessful modification.
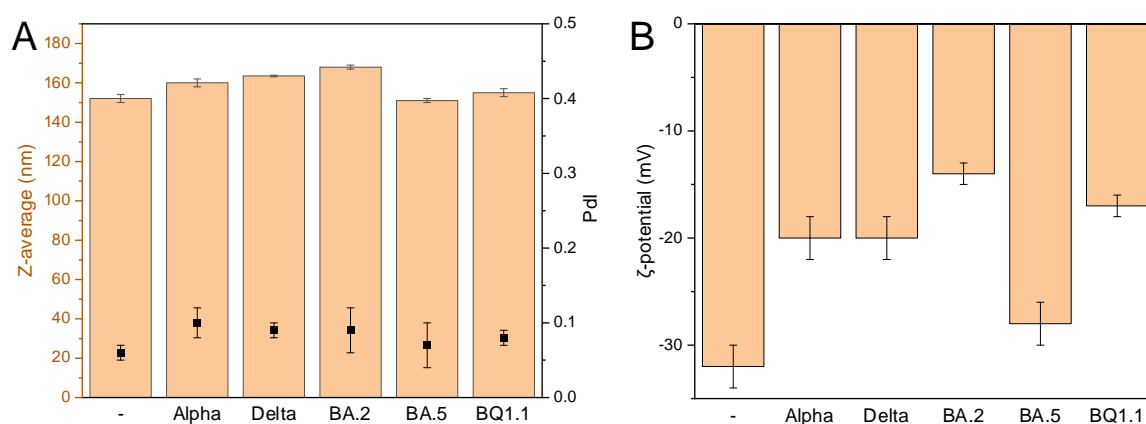


***Figure S1:*** *Z-average (**A**) and ζ-potential (**B**) of liposomes modified with 0.2 mol% of different RBD variants using EDC/sulfo-NHS chemistry. n = 3 (**A**) or 4 (**B**).*

The sequence alignment of the RBD variants (**Figure S2**) revealed four mutations between Alpha and Delta, 16 between Delta and BA.2, three between BA.2 and BA.5 and three between BA.5 and BQ1.1 (**Table S1**). Several of these amino acids are responsible for the interaction with ACE2 (marked with grey arrows in **Figure S2**) or are neighboring ones that are (marked with red arrows). Besides affecting affinity to ACE2, the mutations have an influence on the orientation of RBD on the liposomal surface after EDC/sulfo-NHS modification, the sulfo-NHS-ester reacting with ε-amino groups of lysines.
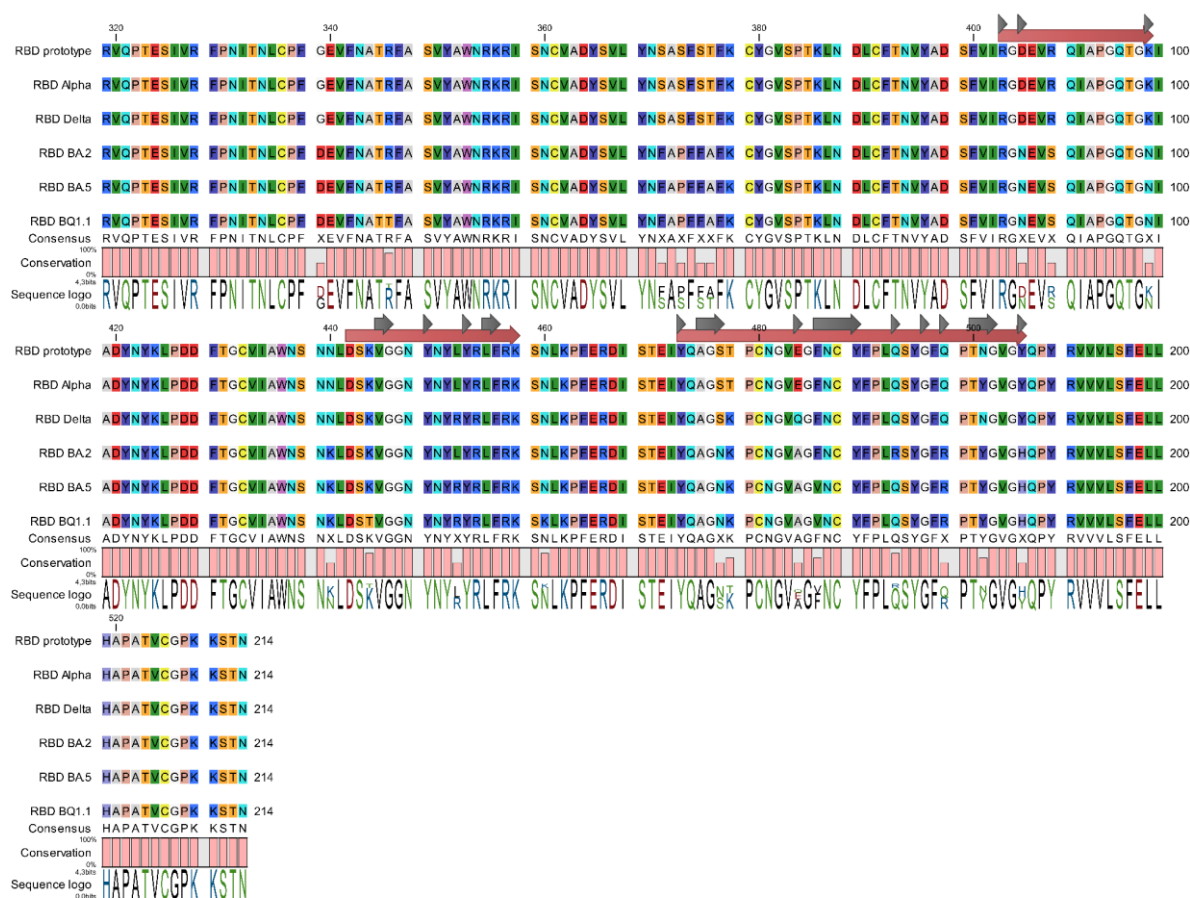


**Figure S2:** *The sequence alignment of various RBD variants. Mutations of amino acids responsible for interaction with ACE2 are marked in grey. The red arrows mark the neighboring amino acids that could interact with said amino acids, influencing their interaction with ACE2.*

***Table S1:*** *List of all mutations of RBD Alpha, RBD Delta, RBD BA.2, RBD BA.5 and RBD BQ1.1 in reference to the prototypic Spike nomenclature. Mutations of* amino acids within the domains responsible for the interaction with ACE2 are marked with grey background, neighboring ones that could influence the interaction with light orange background *and ones (theoretically) not affecting the interaction with white background. Nomenclature explained with the example G21D: amino acid G (glycine) in position 339 was exchanged with amino acid D (aspartic acid).*

| Alpha | Delta | BA.2 | BA.5 | BQ1.1 |
|-------|-------|------|------|-------|
|  |  | G339D | G339D | G339D |
|  |  |  |  | R346T |
|  |  | S371F | S371F | S371F |
|  |  | S373P | S373P | S373P |
|  |  | S375F | S375F | S375F |
|  |  | T376A | T376A | T376A |
|  |  | D405N | D405N | D405N |
|  |  | R408S | R408S | R408S |
|  |  | K417N | K417N | K417N |
|  |  | N440K | N440K | N440K |
|  |  |  |  | K444T |
|  | L452R |  | L452R | L452R |
|  |  |  |  | N460K |
|  |  | S477N | S477N | S477N |
|  | T478K | T478K | T478K | T478K |
|  | E484Q | E484A | E484A | E484A |
|  |  |  | F486V | F486V |
|  |  | Q493R |  |  |
|  |  | Q498R | Q498R | Q498R |
| Y501N |  | N501Y | N501Y | N501Y |
|  |  | Y505H | Y505H | Y505H |

NanoDSF measurements with a Prometheus Panta (NanoTemper Technologies GmbH) (0.36 mg/mL RBD in PBS, Prometheus standard capillaries PR-C002, initial measurement of the hydrodynamic diameter followed by thermal unfolding measurement from 20 °C to 90 °C with 0.05 °C intervals) revealed different melting points for RBD-BA.2 and -BA.5 compared to -Alpha, -Delta and -BQ1.1 (**Figure S3 A**). DLS measurements with the same device revealed that each variant is present in a different state of multimerization, hydrodynamic diameters ranging from ~4 nm for RBD-BQ1.1 to ~20 nm for -Delta. Denaturation during the thermal scan resulted in an increase of the hydrodynamic diameter for RBD-Alpha, -BA.5 and -BQ1.1 but not -Delta and -BA.2, which are present as larger multimers with ~12 nm and ~20 nm hydrodynamic diameters, respectively. It remains unclear whether this has an influence on coupling efficiency, because the coupling conditions, i.e., lower concentration, different buffer, and shaking could affect interactions between RBD molecules and thus multimerization.

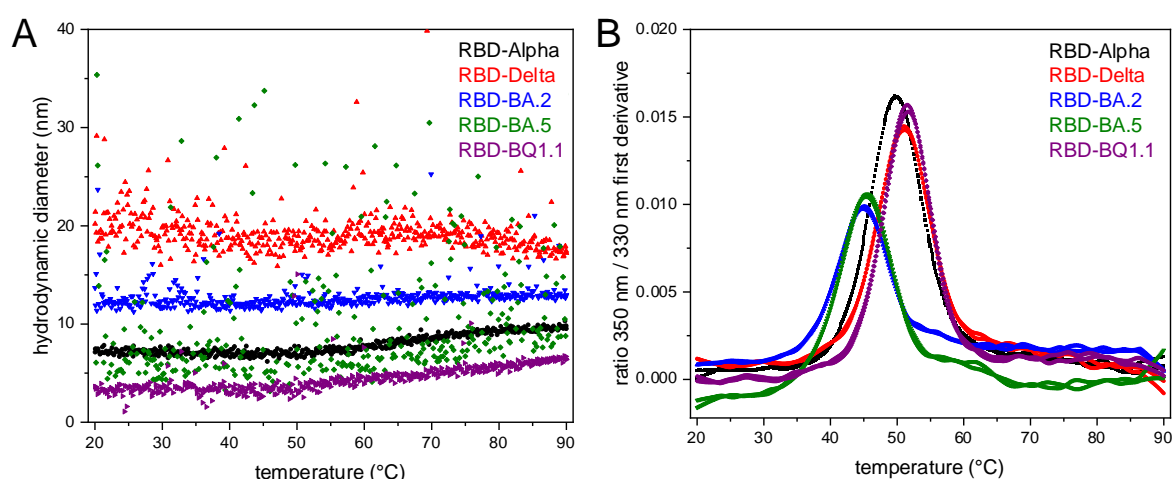

***Figure S3:*** *DLS measurement (**A**) and first derivative of the ratio of 350 nm to 330 nm fluorescence (**B**) during the thermal unfolding of RBD variants between 20 and 90 °C (0.05 °C intervals), measured in the Prometheus Panta. n = 2.*

Binding of liposomes modified with 0.2 mol% RBD-Alpha using EDC/sulfo-NHS chemistry to ACE2-biotin immobilized in a streptavidin plate was analyzed over the course of 36 weeks. Modified liposomes (25 µM or 100 µM) were stored in PBS with additional 200 mM sucrose with and without HSA. HSA improved stability slightly for storage at 25 µM total lipids, though only decreasing the signal loss rather than preventing it. In the case of storage at 100 µM total lipids with HSA, liposomes maintained their ACE2 binding capacity for 24 rather than 8 weeks. However, after 36 weeks of storage they also produced >50% lower signal intensities.
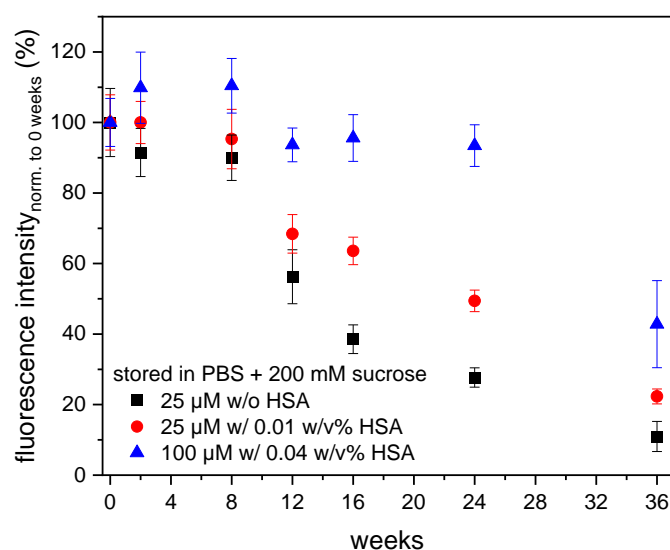


***Figure S4:*** *ACE2 binding of 0.2 mol% RBD-Alpha liposomes (stored at 25 or 100 µM in PBSS w/ and w/o HSA) after up to 36 weeks of storage, normalized to the initial intensities. Fluorescence intensities deviated significantly from the 0 weeks data-point for the 25 µM samples after 12 weeks, for the 100 µM sample after 36 weeks (one-way ANOVA, p < 0.001). n = 3.*

## Biotinylation strategies for RBD

Biotinylation of RBD-Alpha, -BA.5 and -BQ1.1 using 10 equivalents of NHS-biotin facilitated the capture of streptavidin-liposomes in an ACE2-coated high binding plate (**Figure S5**). Interestingly, even RBD-BA.5 facilitated capture, suggesting that the orientation upon biotinylation of $NH_2$-groups is preferrential to direct coupling to sulfo-NHS-activated COOH-liposomes via the $NH_2$-groups, possibly due to electrostatic repulsion. The use of 100 equivalents NHS-biotin per RBD resulted in excessive biotinylation, preventing interaction with ACE2 for all three variants. The use of lower equivalents of NHS-biotin was exemplarily investigated using RBD-Alpha (**Figure S6**). Highest signal intensities were obtained with 75 ng/mL RBD-Alpha-biotin modified using 5 equivalents NHS-biotin, and 100 ng/mL RBD-Alpha-biotin modified using 2 equivalents. Lower intensities were obtained for the conjugates biotinylated with 1 or 10 equivalents NHS-biotin, likely due to incomplete or excessive biotinylation.
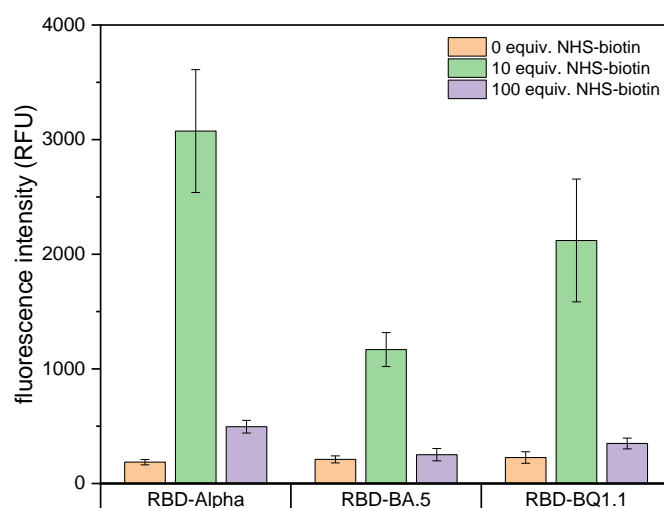


***Figure S5:*** *ACE2 binding of streptavidin-liposomes plus RBD-Alpha-, -BA.2- and -BQ1.1-biotin modified using 1, 10 or 100 equiv. NHS-biotin (150 ng/mL). n = 3.*
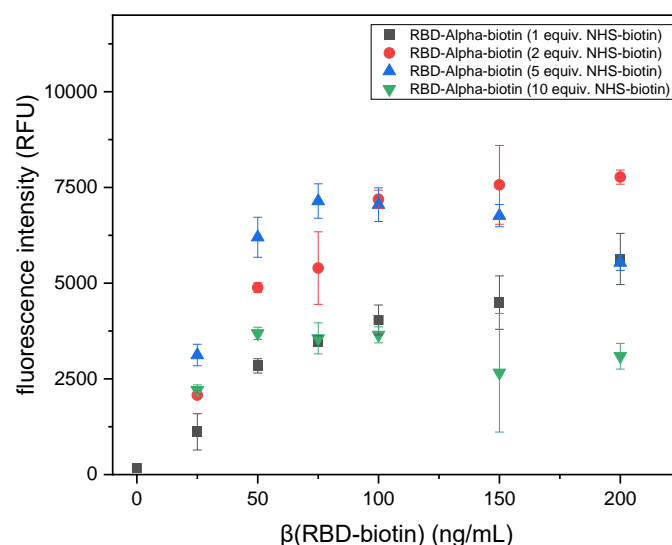
***Figure S6:*** *ACE2 binding of streptavidin-liposomes plus RBD-Alpha-biotin modified using 1, 2, 5 or 10 equiv. NHS-biotin (25 to 200 ng/mL). n = 3.*

In order to control successful enzymatic biotinylation of the RBD proteins, a SDS-PAGE-based neutravidin shift assay was conducted (**Figure S7**). 50 pmol biotinylated RBD were incubated at 95 °C for 10 min in reducing SDS-PAGE buffer. After cooldown to RT, either 150 pmol neutravidin or PBS were added and incubated for 5 min. Biotinylated RBD/neutravidin complexes run at higher molecular weight in the SDS-PAGE compared to biotinylated RBD alone.
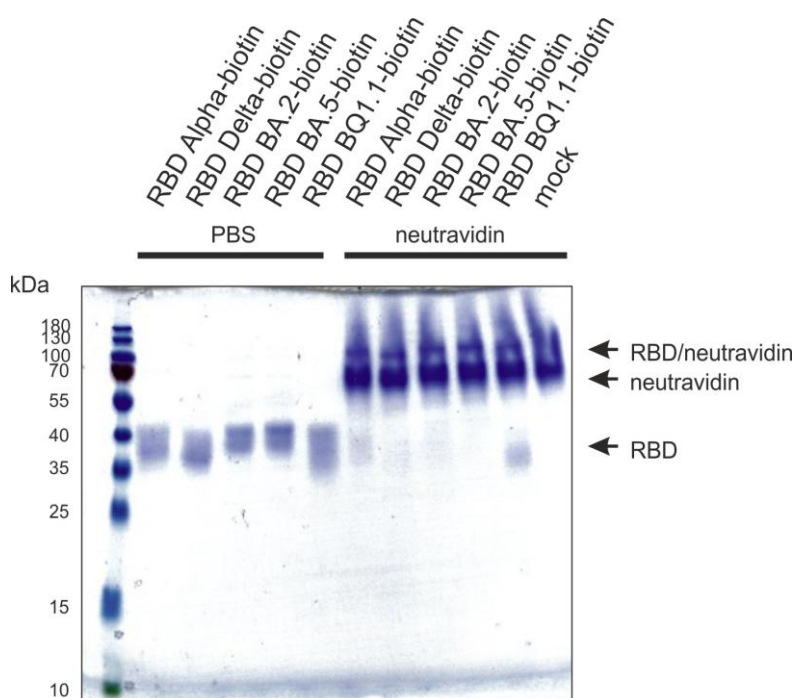


***Figure S7:*** *Neutravidin shift assay of enzymatically biotinalyted RBD proteins. Mock = PBS without RBD loaded.*

Biotinylation via the Avi-tag using *E. coli* biotin ligase (BirA) facilitated the immobilization of streptavidin liposomes in an ACE2-coated high binding plate for all five RBD variants (**Figure S8**). Maximum signal intensities were obtained with 100 ng/mL RBD-biotin in all cases, though intensities varied between variants. Highest signals were obtained for Delta, which produced intensities comparable to those of RBD-Alpha-liposomes modified using EDC/sulfo-NHS chemistry. Alpha and BA.2 produced similar signal intensities, BA.5 and BQ1.1 produced the lowest intensities.



***Figure S8:*** *ACE2 binding of streptavidin-liposomes plus biotinylated RBD-Alpha, -Delta, -BA.2, -BA.5 and -BQ1.1 (modified via the Avi-tag) (25 to 200 ng/mL). n = 3.*

RBD-BA.2-biotin resulted in extremely high non-specific binding of streptavidin-liposomes in a high binding plate blocked with BSA, coating of the plate with ACE2 did not result in a further signal increase (**Figure S9**). Blocking with skim milk powder (SMP) instead of BSA prevented non-specific binding and could be used for all variants.



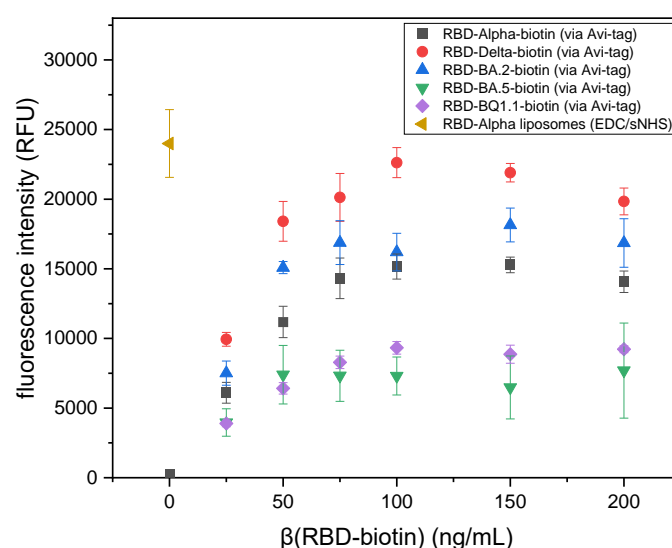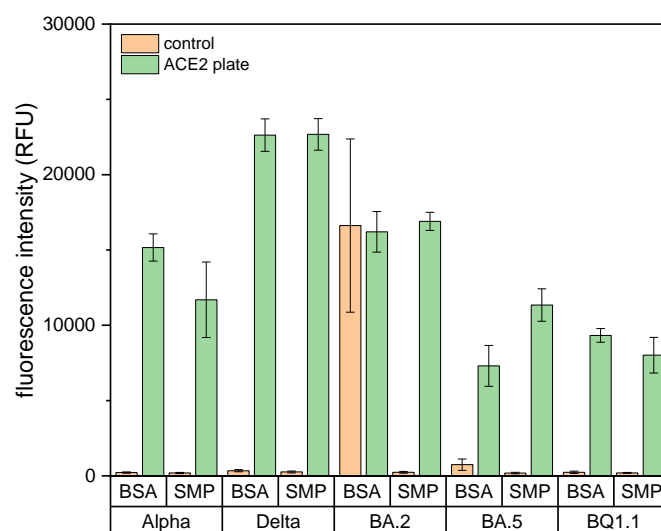***Figure S9:*** *Fluorescence intensities of streptavidin-liposomes plus biotinylated RBD-Alpha, -Delta, -BA.2, -BA.5 and -BQ1.1 (modified via the Avi-tag) (100 ng/mL), immobilized in an ACE2-coated high binding plate blocked with skim milk powder (SMP) or BSA. n = 3.*

**Establishing the surrogate virus neutralization test**

Pre-pandemic serum reduced signal intensities of RBD-Alpha-liposomes in an ACE2-coated high binding plate, correlating to increasing binding inhibition with increasing serum concentration (**Figure S10**). The avidity of the RBD-Alpha-liposomes to the randomly immobilized ACE2 appeared to be too low, serum constituents preventing their interaction. Site-directed immobilization of ACE2-biotin in a streptavidin plate improved avidity enough so that the seronegative sample did not show any influence on fluorescence intensities, corresponding to the expected binding inhibition values around 0%. The same was observed for streptavidin-liposomes with biotinylated RBD variants (data not shown). Therefore, ACE2-biotin coated and biotin blocked streptavidin-plates were used for the surrogate neutralization test using streptavidin-liposomes and biotinylated RBD.
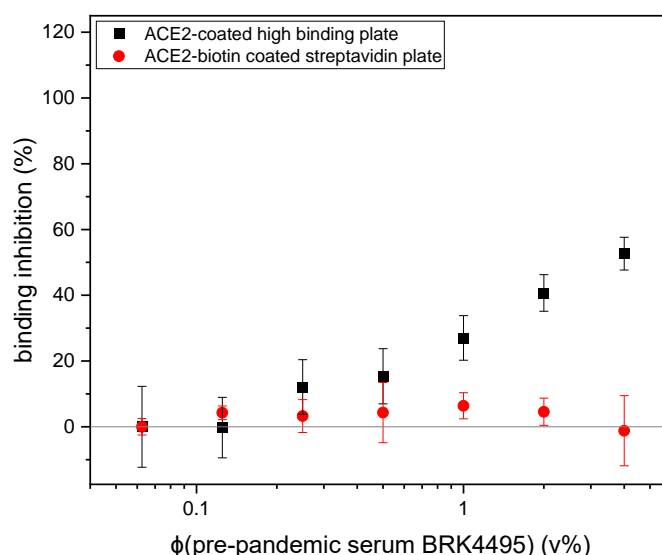


*Figure S10: Binding inhibition values of RBD-Alpha-liposomes and pre-pandemic serum BRK4495, immobilized in an ACE2-biotin coated streptavidin plate or an ACE2-coated high binding plate. n = 3.*

No non-specific binding of streptavidin- and neutravidin-liposomes was observed to an ACE2-biotin coated streptavidin-plate (**Figure S11**). The RGD sequence of ACE2 is inaccessible for binding of the RYD sequence of streptavidin. The same goes for the RGD sequence of RBD, probably due to binding beyond detection limit, as non-specific binding of streptavidin-liposomes to RBD would have led to the capture by immobilized ACE2. Thus, both streptavidin- and neutravidin-liposomes could be used for the SARS-CoV-2 surrogate virus neutralization test. Neutravidin-liposomes were chosen to make the assay more universally transferable to other analytes and matrices, which might contain proteins with accessible RGD sequence.



**Figure S11:** *Fluorescence intensities of streptavidin- and neutravidin-liposomes incubated in an ACE2-biotin coated streptavidin plate (blocked with biotin) with RBD (0, 50, 100 or 200 ng/mL). n = 3.*

### Development of a serological liposome-based assay for SARS-CoV-2 variants with special emphasis on coupling chemistries required to maintain protein antigenicity
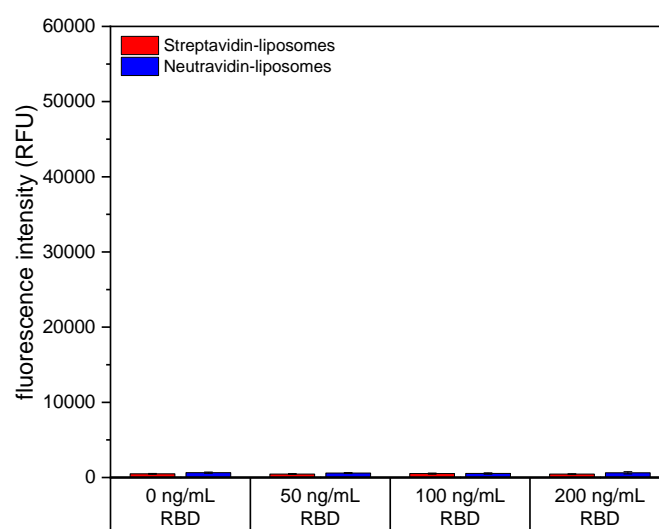
Seronegative samples were found to increase the fluorescence intensity obtained with neutravidin-liposomes plus RBD-biotin in an ACE2-biotin coated streptavidin plate. The effect was most pronounced for RBD-BQ1.1-biotin, as it produced the overall lowest signal intensities. Investigation of varying neutravidin-liposome to RBD-BQ1.1-biotin ratios with pooled pre-pandemic serum showed the same effect for all conditions (**Figure S12 A**). Normalization to the serum-free controls thus led to negative binding inhibition values (**Figure S12 B**). Normalization to the highest serum dilution, on the other hand, resulted in the expected binding inhibition values around 0% (**Figure S12 C**). For the final studies a neutravidin-liposome concentration of 1 µM and an RBD-biotin concentration of 25 ng/mL was chosen. The lower signal intensities obtained with lower RBD-biotin concentration were deemed worth the trade-off as they improve sensitivity.



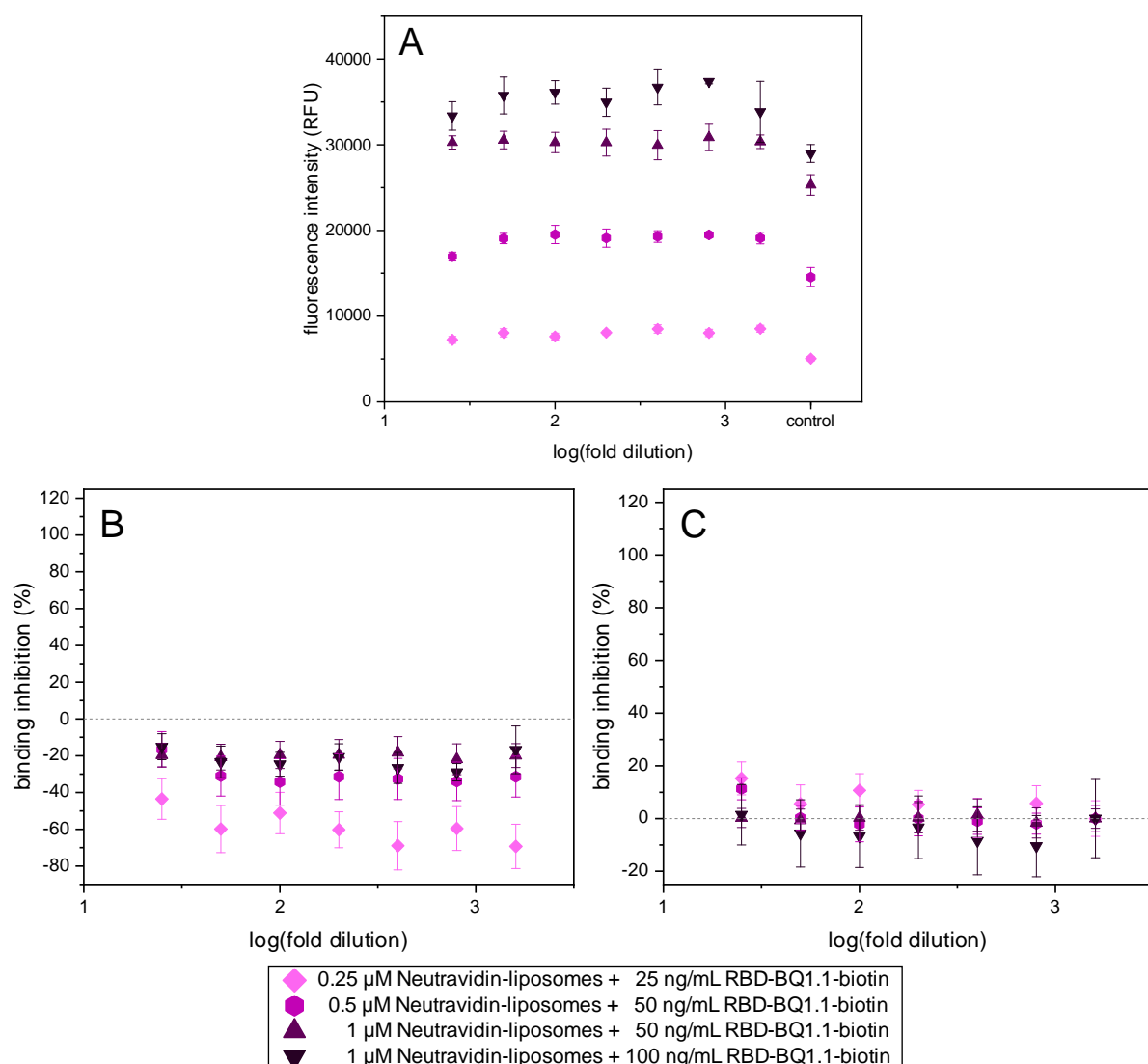*Figure S12: Fluorescence intensities (A) and binding inhibition values (B and C) of neutravidin-liposomes (0.25, 0.5 or 1 µM total lipids) plus RBD-BQ1.1 biotinylated via the Avi-tag (25, 50 or 100 ng/mL) and pooled pre-pandemic serum (BRK-4507-8-pool). n = 3. Binding inhibition, given as percentage, was calculated by normalization to the serum free samples (B) or the highest serum dilution (C).*

Addition of HSA instead of serum also resulted in increased fluorescence intensities for neutravidin-liposomes plus RBD-BQ1.1-biotin in an ACE2-biotin coated streptavidin plate (**Figure S13**). Either interaction with HSA promotes capture of the liposomes in the plate, or it might reduce non-specific binding to the reaction vial during pre-incubation, despite the use of Protein LoBind Eppendorf Tubes. No improvement was observed with protein low binding tubes from a different supplier (Sarstedt SafeSeal Protein Low Binding reaction vial). While addition of HSA to the control might be feasible it would require detailed analysis of the average HSA concentration of sera. For the investigated serum normalization to the HSA containing control would result in positive binding inhibition values, which would bias the fit for IC50 calculation. Instead, normalization to the highest serum dilution was performed for the serum panel screening.
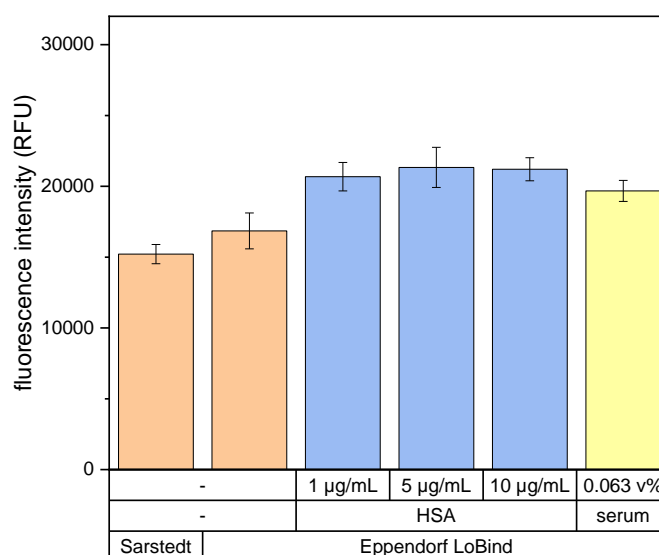


**Figure S13:** *ACE2 binding of neutravidin-liposomes plus biotinylated RBD-BQ1.1 (modified via the Avi-tag) (50 ng/mL) in presence of HSA (0, 10, 50 or 100 µg/mL) or serum. Samples were pre-incubated for 1 h at 30 °C and 300 rpm in Sarstedt or Eppendorf low binding reaction tubes. n = 3.*

Biotin interference was investigated by addition of 575 nM biotin instead of serum. This led to binding inhibition values below the determined cut-off values (**Table S2**) for all five variants when neutravidin-liposomes and RBD-biotin variants are pre-incubated overnight before incubation with biotin (**Figure S14**). The biotin concentration corresponds to the biotin threshold according to the CLSI EP37 guideline, factoring in the 1:25 dilution of the highest serum concentration tested. Thus, no false-positives would be observed even for such excessively high biotin concentrations, corresponding to three times the highest measured value for a person with high biotin dose uptake. For a commercial product the instructions would state that no biotin uptake should have taken place within the last 24 h to ensure proper function of the assay.
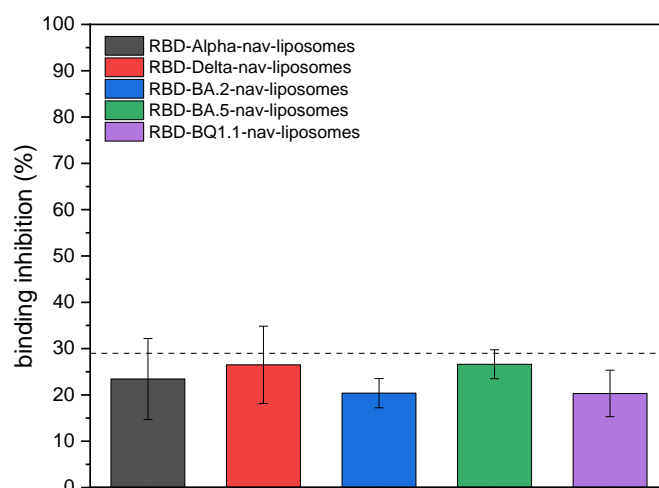


***Figure S14:*** *Effect of biotin (575 nM) on the ACE2 binding of neutravidin-liposomes plus biotinylated RBD variants (modified via the Avi-tag) (25 ng/mL). Samples were pre-incubated overnight at 4 °C before incubation with biotin (0 or 575 nM) for 1 h at 30 °C and 300 rpm. n = 3. Binding inhibition, given as percentage, was calculated as (1 – fluor. int./fluor. int. 0 nM biotin)\*100. The dotted line represents the lowest of the cut-off values determined using 5 seronegative samples (listed in* **Table S2***).*

**Serum panel screening**

A total of five (pooled) pre-pandemic sera were tested for all five RBD-biotin variants. Obtained binding inhibition values showed variation (**Figure S15**). Cut-off values were calculated for each variant as the average of binding inhibition values obtained for all tested serum dilutions plus three times the standard deviation. Cut-off values ranged from 29% for Alpha to 38% for BQ1.1 (**Table S2**).

*Table S2: Average binding inhibition values and standard deviations thereof for all five RBD variants. Cut-offs were calculated as the average plus three times the standard deviation.*

| Variant | Average binding inhibition | Cut-off (Average + 3 SD) |
|---------|----------------------------|--------------------------|
| Alpha | 0% ± 10% | 29% |
| Delta | 4% ± 10% | 34% |
| BA.2 | -1% ± 12% | 34% |
| BA.5 | -3% ± 13% | 35% |
| BQ1.1 | -5% ± 14% | 38% |

**Figure S15:** *Screening of five seronegative samples with the neutravidin-liposome-based neutralization test for the different RBD variants biotinylated via the Avi-tag. n = 3.The cut-off value (dashed grey line) was calculated as the average plus 3x SD of all binding inhibition values obtained with the respective variant.*

A total of 10 seropositive samples were screened for all five variants (**Figure S16**). Binding inhibition values above the cut-off values were obtained for all, enabling calculation of IC50 values (**Table S3**). One of these was below the investigated range, the highest concentration of serum S1 caused only 41% binding inhibition, the calculated IC50 value of 20 was hence classified as <25. In case of sera S8 and S9 all serum dilutions caused more than 50% binding inhibition for each variant, IC50 values were classified as >3200. Calculation of IC50 values for S4, S5 and S10 of Alpha, Delta, BA.2 and BA.5 required the testing of an additional four serum dilutions.
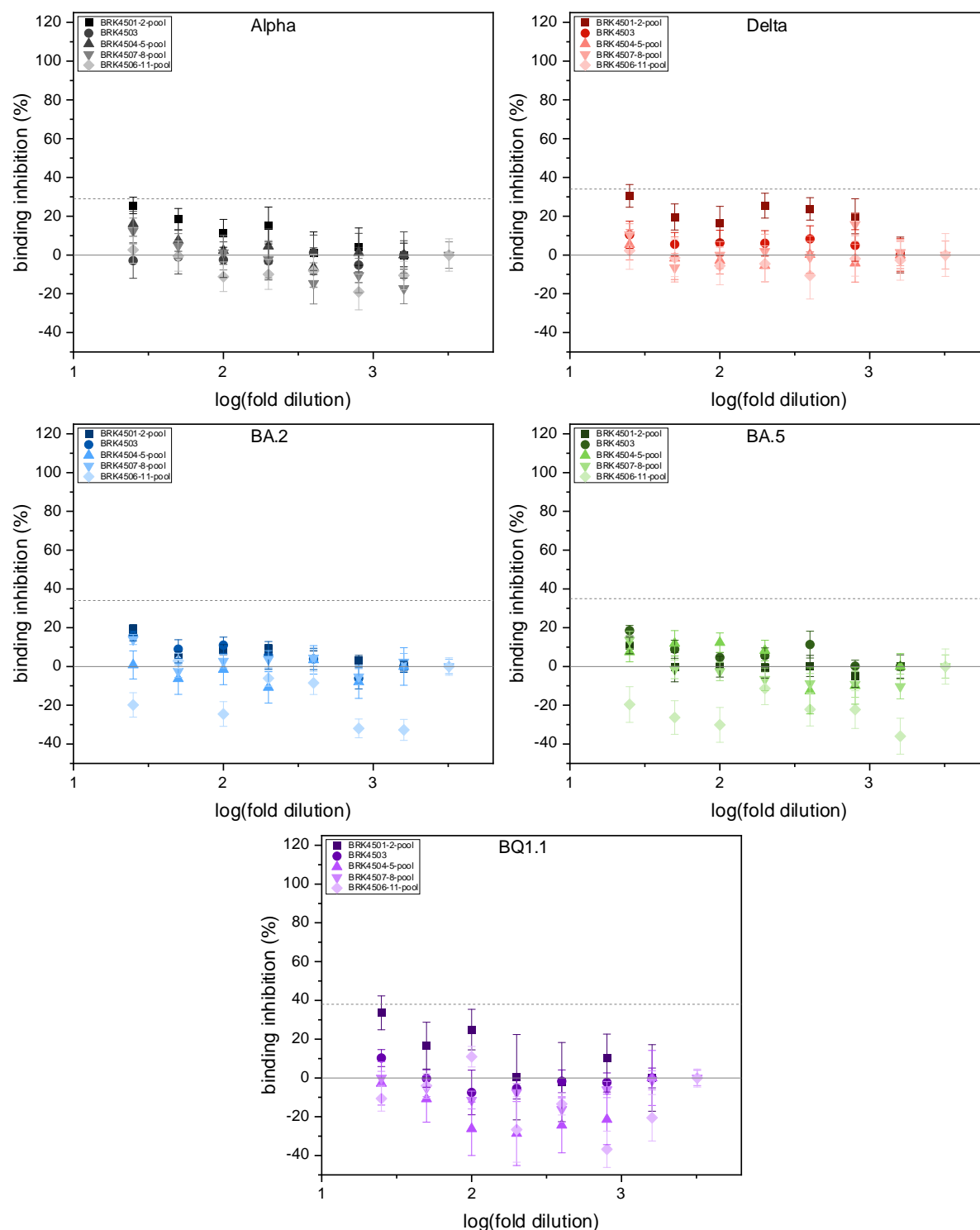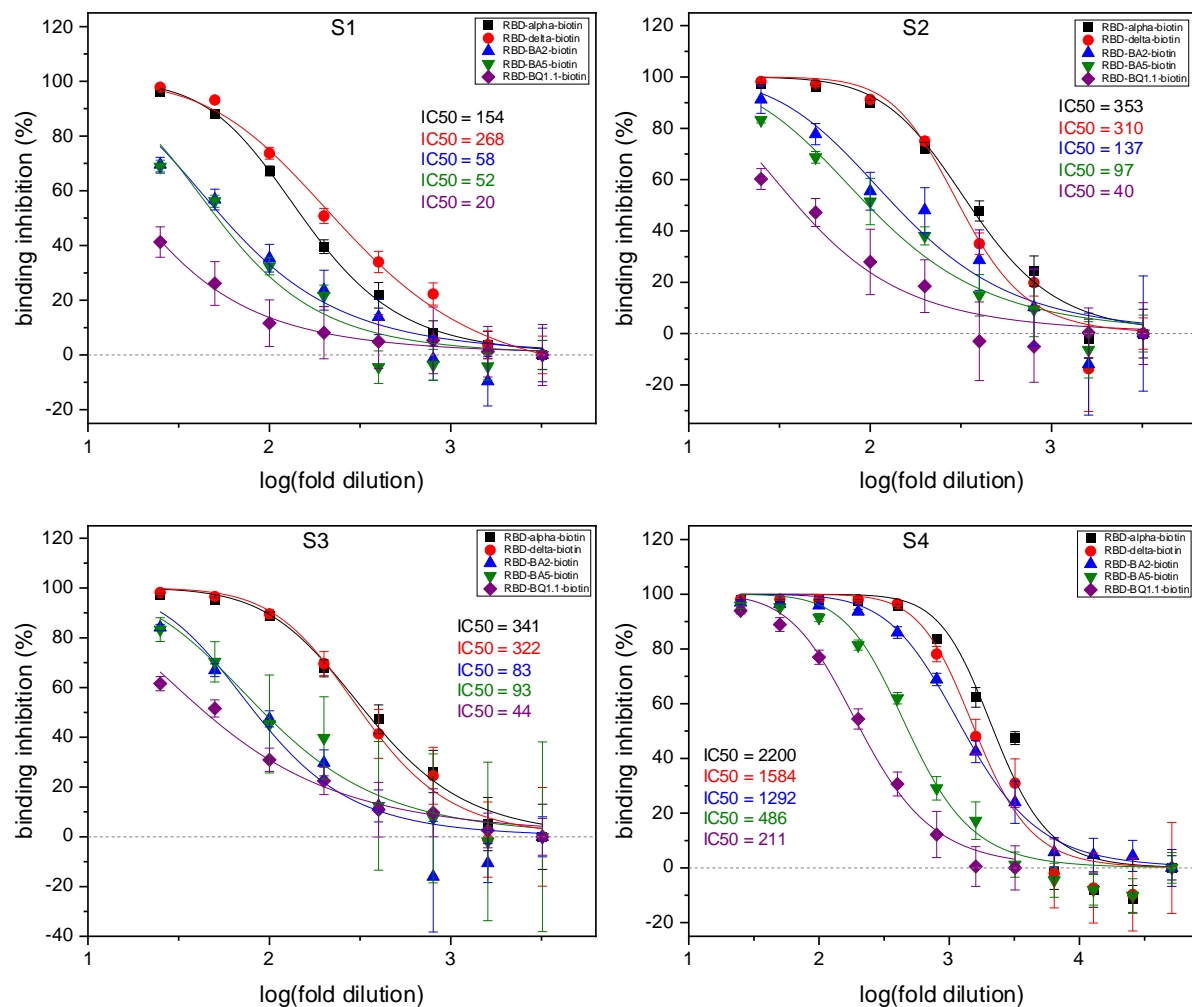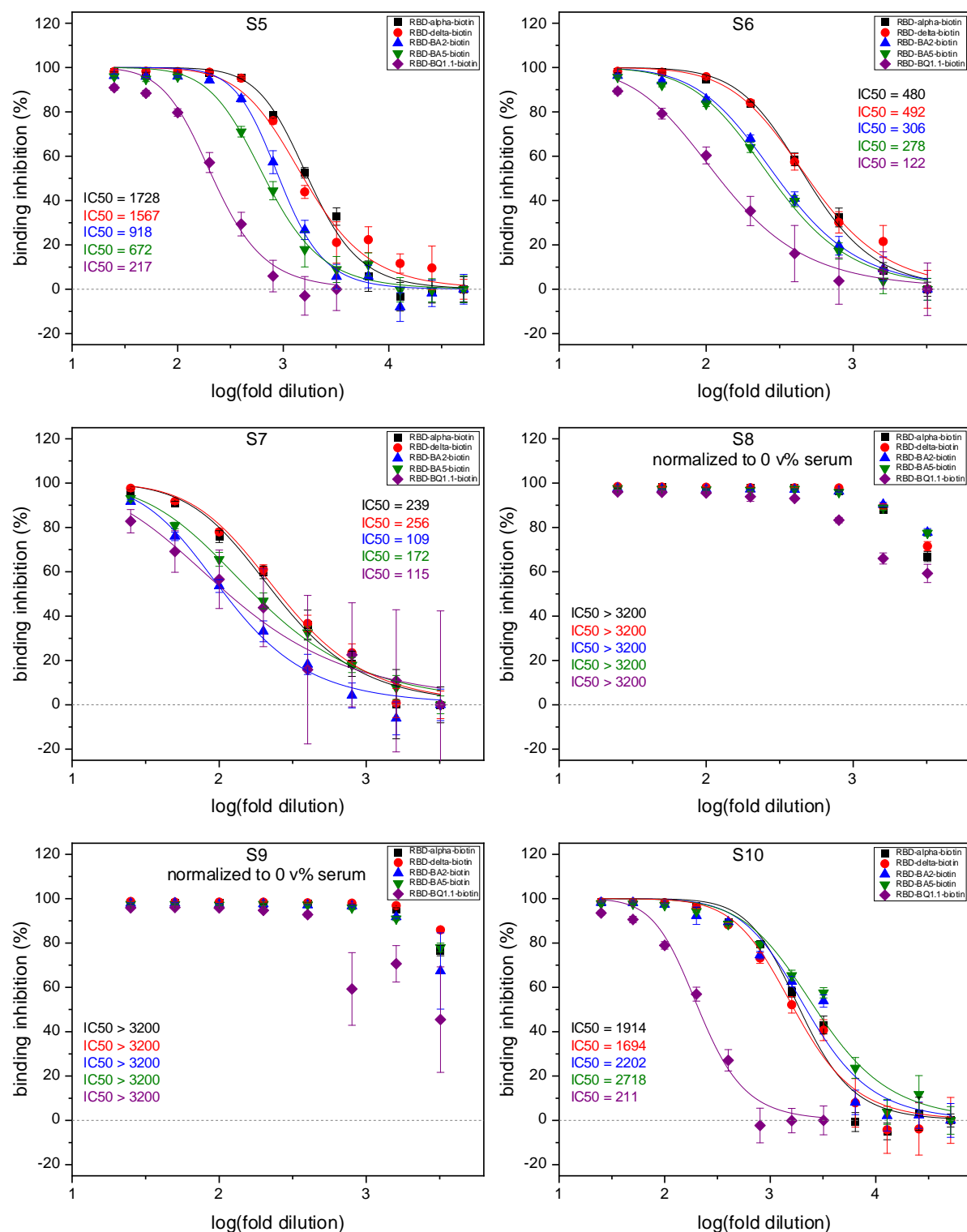
***Figure S16:*** *Screening of ten seropositive samples with the neutravidin-liposome-based neutralization test for the different RBD variants biotinylated via the Avi-tag. Binding inhibition was calculated by normalization to the highest serum dilution, unless stated otherwise. n = 3.*

***Table S3:*** *sVNT IC50 values for Alpha, Delta, BA.2, BA.5 and BQ1.1 RBD obtained in the neutravidin-liposome-based neutralization test for the 10 seropositive samples. Sera from individuals without omicron antigen exposure are marked in light grey, sera with omicron exposure history are marked in light blue.*

| Serum | Antigen exposure | alpha | delta | BA.2 | BA.5 | BQ1.1 |
|---|---|---|---|---|---|---|
| S1 | WT vaccine | 154 | 268 | 58 | 52 | <25 |
| S2 | WT vaccine | 353 | 310 | 137 | 97 | 40 |
| S3 | WT vaccine | 341 | 322 | 83 | 93 | 44 |
| S4 | WT vaccine + Omicron exposure | 2200 | 1584 | 1292 | 486 | 211 |
| S5 | WT vaccine + Omicron exposure | 1728 | 1567 | 918 | 672 | 217 |
| S6 | WT vaccine + Delta exposure | 480 | 492 | 306 | 278 | 122 |
| S7 | WT vaccine | 239 | 256 | 109 | 172 | 115 |
| S8 | WT vaccine + Omicron exposure | >3200 | >3200 | >3200 | >3200 | >3200 |
| S9 | WT vaccine + Omicron exposure | >3200 | >3200 | >3200 | >3200 | >3200 |
| S10 | WT vaccine + Omicron exposure | 1914 | 1694 | 2202 | 2718 | 211 |

*Table S4:* pVNT IC50 values for Alpha, Delta, BA.2, BA.5 and BQ1.1 RBD obtained in the pseudovirus neutralization test for the 10 seropositive samples. Sera from individuals without omicron antigen exposure are marked in light grey, sera with omicron exposure history are marked in light blue.

| Serum | Antigen exposure | alpha | delta | BA.2 | BA.5 | BQ1.1 |
|-------|------------------|-------|-------|------|------|-------|
| S1 | WT vaccine | 160.3 | 78.24 | 117.3 | 44.75 | 5.083 |
| S2 | WT vaccine | 245.7 | 161 | 163.7 | 88.89 | 88.27 |
| S3 | WT vaccine | 147.9 | 114.6 | 121.6 | 48.24 | 25.07 |
| S4 | WT vaccine + Omicron exposure | 500.5 | 243.4 | 1412 | 662.7 | 556.8 |
| S5 | WT vaccine + Omicron exposure | 558.6 | 341.5 | 1775 | 986.6 | 416.2 |
| S6 | WT vaccine + Delta exposure | 195.9 | 146.1 | 543.2 | 407.2 | 284.1 |
| S7 | WT vaccine | 76.22 | 96.29 | 209.2 | 141.5 | 110.3 |
| S8 | WT vaccine + Omicron exposure | >2560 | 1181 | >2560 | >2560 | >2560 |
| S9 | WT vaccine + Omicron exposure | 1598 | 882.9 | >2560 | >2560 | 2323 |
| S10 | WT vaccine + Omicron exposure | 826.4 | 308.2 | 1660 | 1245 | 295.9 |
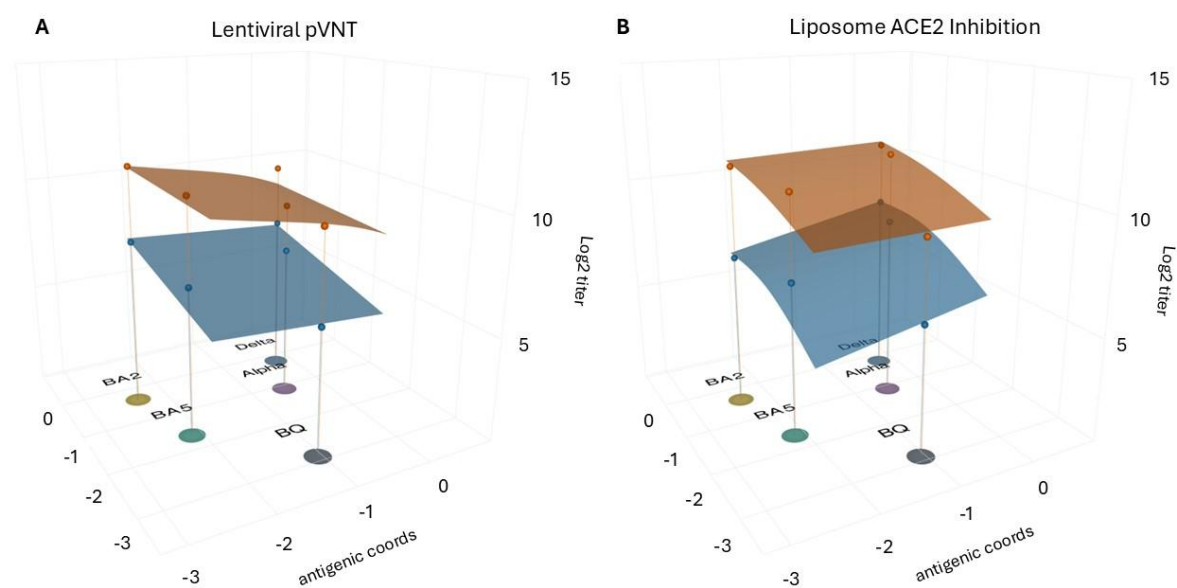
**Figure S17:** *Antigenic Landscapes achieved for the lentiviral pseudotype neutralization assay (A) and the liposome surrogate neutralization test (B). Sera with no omicron antigen exposure are described in blue, with omicron antigen exposure after initial wildtype vaccination in orange.*

## 3.2 Investigating spike protein conjugation as alternative to RBD modified liposomes

**Abstract**

The main target of neutralizing antibodies against SARS-CoV-2 is the receptor binding domain (RBD), a small subunit of the spike (S) protein. While RBD is easier to express, the S protein has the benefits of improved avidity to ACE2 due to its tetrameric structure, and detection of the more abundant neutralizing anti-Spike instead of only neutralizing anti-RBD antibodies. Here, we investigated the conjugation of three Omicron variants of the stabilized trimeric S protein (StabS) to liposomes using EDC/sulfo-NHS chemistry as alternative to RBD. StabS-BA.2 led to aggregation of modified liposomes, preventing their purification via size exclusion chromatography. StabS-BA.5 was successfully coupled to the liposomes, as shown via DLS measurements, but, like RBD-BA.5 modified liposomes, they were unable to bind to ACE2, likely due to unfavorable orientation. The modification with StabS-BQ1.1 facilitated ACE2 binding, 0.01 mol% StabS-BQ1.1-liposomes generating identical signal intensities as 0.2 mol% RBD-BQ1.1-liposomes, showcasing the higher avidity and proving the general feasibility of StabS modification as alternative to RBD. However, significant leakage of SRB was caused by modification of liposomes with StabS. The faced challenges could potentially be solved by the investigation of site-directed conjugation strategies in the future, making StabS the superior antigen for liposome-based neutralization tests.

**This chapter has not been published.**

### 3.2.1 Introduction

The SARS-CoV-2 virus, which caused the COVID-19 pandemic, consists of four structural and 16 non-structural proteins. The three structural proteins, the membrane protein (M), envelope protein (E) and spike protein (S), envelop the nucleocapsid protein (N), which forms a viral ribonucleoprotein with the viral RNA[1]. Infection or vaccination results in the formation of neutralizing antibodies (nAb) as part of the humoral immune response, helping to both contain an active infection and reduce the risk for reinfection[2,3]. Most nAbs were found to be directed against the S protein, more specifically the receptor binding domain (RBD)[4,5], located in the S1 subunit and responsible for interaction with the human angiotensin-converting enzyme 2 (ACE2) receptor[6]. Fusion of viral and host membranes is subsequently initiated by the S2 subunit, after cleavage of S1 by cellular transmembrane protease serine 2 (TMPRSS2) and lysosomal cathepsin proteases[7]. The native S protein forms a trimeric structure, mediating strong avidity to ACE2 due to the close proximity of three RBDs, but making the expression of recombinant S challenging and time-consuming. Besides the higher avidity, another argument for the use of trimeric S is its representation of the natural conformation, and hence of the antibody-mediated neutralization, compared to RBD. In the closed state of the S protein the CR3022 epitope of RBD is inaccessible due to masking by the neighboring protomer, only upon binding to ACE2 the open state is formed, uncovering the epitope[8,9]. When using RBD instead, the epitope is accessible at any time, which can result in the classification of anti-CR3022 antibodies as neutralizing rather than binding antibodies. Furthermore, the majority of anti-S antibodies target sites other than the RBD[10]. Both anti-S and anti-RBD antibody titers were found to serve as potential correlates of protection (CoP)[11–13]. Due to the easier expression, most of the surrogate virus neutralization tests for SARS-CoV-2 rely on the use of recombinant RBD[14], including the market dominant cPass SARS-CoV-2 Neutralization Antibody Detection Kit[15], but also many novel ELISA-type[16–19] and lateral flow assays[20–24]. For fluorescence-based sVNTs, such as microarrays and Luminex systems, on the other hand, the S protein was used more often than RBD[25–29].

Here, we investigated the modification of liposomes with stabilized trimeric S (StabS) protein using EDC/sulfo-NHS chemistry. This modification strategy had previously been successfully used to establish a quantitative high-throughput screening and a qualitative lateral flow assay for the detection of neutralizing anti-RBD antibodies for the Alpha variant[30]. Rapid antigenic drift of SARS-CoV-2 has led to the emergence of variants of concern, which quickly displace the dominant variant at the time due to superior characteristics, including higher transmissibility, immune escape and lower susceptibility to antiviral drugs or nAbs[31]. Omicron variants started to emerge in the end of 2021 and are now the predominant variants causing infection. Hence, three StabS Omicron variants were investigated instead of the Alpha variant.

### 3.2.2  Experimental section

3.2.2.1  Chemicals and consumables

All chemicals were of analytical reagent grade. Cholesterol from sheep wool (C8667, ≥ 99%), medium binding BRAND 96-well black flat bottom microplates, *N*-Hydroxysulfosuccinimide sodium salt (sulfo-NHS, purity ≥ 98%), Sephacryl S-500 HR, Sephadex-G50, Whatman Nucleopore™ Track-Etched membranes (1.0 µm, 0.4 µm and 0.2 µm diameter) and Tween 20 were purchased from Sigma Aldrich/Merck (Darmstadt, Germany); 1,2-dipalmitoyl-sn-glycero-3-phosphoethanolamine-*N*-(glutaryl) (sodium salt) (*N*-glutaryl-DPPE) from NOF America Corporation (NY, USA); the remaining phospholipids 1,2-dipalmitoyl-sn-glycero-3-phosphocholine (DPPC), 1,2-dipalmitoyl-sn-glycero-3-phospho-(1'-rac-glycerol) (sodium salt) (DPPG) and the extruder set from Avanti Polar Lipids (Alabaster, AL, USA). Dextran (amino, 10000 MW and 70000 MW), sulforhodamine B (SRB) (S1307) and (1-Ethyl-3-(3-dimethylaminopropyl) carbodiimide-hydrochloride) (EDC) (PG82079), were purchased from Thermo Fisher Scientific (Waltham, MA, USA); *n*-Octyl-β-D-glucopyranoside (OG) (≥ 98%, CN23), 2-(*N*-Morpholino)-ethane sulphonic acid (MES) (≥ 99%, 4259), *N*-2-Hydroxyethylpiperazine-*N'*-2-ethane sulphonic acid (HEPES) (≥ 99.5%, HN78), sucrose, sodium azide, sodium chloride and dialysis membrane Spectra/Por© 4 (MWCO: 12-14 kDa) (2718.1) from Carl Roth (Karlsruhe, Germany). Clear streptavidin coated 96-well microplates (KaiSA96) were purchased from Uniogen (Turku, Finland). Phosphorous standard was obtained from Bernd Kraft GmbH (Den Haag, Netherlands). Chloroform and methanol were purchased from Fisher Scientific (Hampton, NH, USA). RBD, StabS and ACE2-biotin were provided by our collaborators from the University Hospital Regensburg and Microcoat Biotechnologie GmbH (Bernried, Germany).

3.2.2.2  Buffer compositions

Hepes sucrose saline (HSS) buffer contained 200 mM sucrose, 200 mM NaCl, 10 mM HEPES and 0.01 w/v% $NaN_3$, pH 7.5. PBS buffer contained 137 mM NaCl, 2.7 mM KCl, 10 mM $Na_2HPO_4$ and 1.8 mM $KH_2PO_4$, pH 7.4. PBS-T contained 0.1 w/v% Tween 20 in PBS. MES buffer contained 50 mM MES, 200 mM sucrose and 200 mM NaCl, pH 5.5.

3.2.2.3  Liposome synthesis

Reverse-phase evaporation was chosen as synthesis method for liposomes as described previously[32]. SRB and NaCl (150 mM SRB and 140 mM NaCl) were dissolved in 20 mM HEPES, pH 7.5 (4.5 mL) by sonication at 60 °C to prepare the encapsulant. Lipid mixtures (41.4 mol% cholesterol, 32.2 mol% DPPC, 18.4 mol% DPPG, 8.0 mol% *N*-glutaryl-DPPE) were prepared by addition of 3 mL chloroform and 0.5 mL methanol and sonication for 1 min, followed by addition of encapsulant (2 mL) and sonication for 4 min at 60 °C. A rotary

evaporator (LABOROTA 4001, Heidolph, Germany) was used to evaporate the organic solvents at 60 °C by stepwise reduction of pressure (900 mbar for 10 min, 850 mbar for 5 min, 800 mbar for 5 min, 780 mbar for 20 min). The solution was vortexed another two times for 1 min with intermittent encapsulant addition (2 mL). The residual organic solvents were evaporated at 60 °C (750 mbar for 20 min, 600 mbar for 5 min, 500 mbar for 5 min, 400 mbar for 20 min). The size was controlled by extrusion at 65 °C using polycarbonate membranes with pore sizes of 1 µm, 0.4 µm and 0.2 µm. Solutions were repeatedly pushed through the membranes with decreasing pore sizes, amounting to 21 repetitions for the 1 µm pore size and 11 repetitions for each of the smaller pore sizes. Size exclusion chromatography using a Sephadex G-50 column, followed by dialysis overnight against HSS buffer with 2 buffer exchanges in a dialysis membrane Spectra/Por© 4 (MWCO: 12-14 kDa) were used to remove excess encapsulant.

### 3.2.2.4  Liposome characterization

An inductively coupled plasma optical emission spectrometer (ICP-OES) (SpectroBlue TI/EOP) from SPECTRO Analytical Instruments GmbH (Kleve, Germany) was used to determine phospholipid concentrations, which in turn were used to calculate total lipid concentrations based on the mixture of lipids used for the synthesis. Phosphorous standard dilutions between 0 µM and 100 µM in 0.5 M $HNO_3$ were used for calibration of the device. Phosphorous was detected at 177.495 nm. Re-calibration was performed before each measurement using the 0 µM and 100 µM phosphorus dilutions. Liposome stock solutions were diluted 1:100 or 1:60 in 0.5 M $HNO_3$ and their phosphorous content determined.

Size and ζ-potential were measured via dynamic light scattering (DLS) using a Malvern Zetasizer Nano-ZS. Liposome stock solutions were diluted to 25 µM total lipids in HSS buffer in a polymethyl methacrylate (PMMA) semi-micro cuvette (Brand, Germany) for size and a disposable folded capillary cell (Malvern Panalytical, Germany) for ζ-potential measurements. The measurement temperature was set to 25 °C, the refractive index was 1.34, the material absorbance was zero and the dispersant viscosity 1.1185 mPa s. For ζ-potential measurements a dielectric constant of 78.5 was used and an equilibration time of 60 s applied before each measurement.

### 3.2.2.5  Liposome modification

Proteins were conjugated to carboxylated liposomes via EDC/sulfo-NHS chemistry. Liposomes were incubated with EDC and sulfo-NHS (1:100:180 ratio of carboxy-groups:EDC:sulfo-NHS) for 1 h at room temperature (RT) and 300 rpm followed by addition of protein and another 1.5 h incubation at RT and 300 rpm. Excess reagents were removed via size exclusion chromatography with Sephadex G-50 (for RBD-modified liposomes) or Sephacryl S-500 HR

(for StabS-modified liposomes). Total lipid concentrations were determined using ICP-OES and the conjugated liposomes were stored at 4 °C in Protein LoBind tubes.

### 3.2.2.6 Determination of maximum and unlysed fluorescence

Liposomes were diluted in HSS (5 µM total lipids) and added to a black 96-well microplate (100 µL per well, n = 4). The fluorescence was measured three consecutive times with a BioTek SYNERGY neo2 fluorescence reader ($\lambda_{Ex}$ = 560 $nm$ and $\lambda_{Em}$ = 585 $nm$, bandwidth 10, gain 100). Liposomes were lysed by addition of 300 mM OG (10 µL per well) and incubation for 10 min at RT and 300 rpm before the fluorescence was measured again. Fluorescence intensities of the lysed liposomes are referred to as maximum fluorescence intensities. Unlysed fluorescence was calculated by normalization of the fluorescence intensity of the liposomes before addition of OG (unlysed) to that after incubation with OG (lysed). Errors were calculated using Gaussian error propagation.

### 3.2.2.7 Heterogeneous ACE2 binding assay

ACE2-biotin (1 µg/mL in PBS, 100 µL per well) was incubated in a streptavidin plate for 1 h at RT and 300 rpm. The plate was washed two times with PBS-T (150 µL per well) and three times with HSS (150 µL per well) before being used. Liposomes (1 µM total lipids) were added to the MTP (100 µL per well, n = 3) and incubated for 2 h at RT and 300 rpm. The plate was washed three times with HSS buffer (150 µL per well) before 30 mM OG in bidest. water (100 µL per well) was added. After 10 min incubation the fluorescence was measured three consecutive times with a BioTek SYNERGY neo2 fluorescence reader ($\lambda_{Ex}$ = 560 $nm$ and $\lambda_{Em}$ = 585 $nm$, bandwidth 10, gain 150). In case of normalization to initial fluorescence intensities errors were calculated using Gaussian error propagation.

## 3.2.3 Results and discussion

### 3.2.3.1 Modification with StabS-BA.5

Carboxylated liposomes were modified with the BA.5 variant of the stabilized trimeric spike protein (StabS) as alternative to RBD-BA.5, which was shown in the previous chapter to be oriented unfavorably for ACE2 binding after EDC/sulfo-NHS coupling to liposomes. DLS measurements revealed a slight increase of the Z-average and the ζ-potential for both StabS concentrations (**Figure 1 A** and **B**). The increase was lower for 0.01 mol% StabS-BA.5, while 0.05 mol% StabS-BA.5 resulted in similar liposome characteristics compared to liposomes modified with 0.2 mol% RBD-Alpha. While RBD and the top of the S1 protein are predominantly positively charged, the S2 subunit and underlying core of S1 are negatively charged[33]. This nonuniform charge distribution enhances attachment to the negatively charged receptor and

membrane, and promotes spike corona stability[34]. Hence, both proteins expectedly have a different effect on the surface charge and hydrodynamic diameter. Additionally, coupling efficiencies likely vary for the two proteins. A 4-fold higher concentration of the ~15 times smaller RBD has the identical impact on the hydrodynamic diameter and surface charge as StabS, suggesting that only a fraction of StabS has been coupled to the liposomes. As before, no significant increase of either characteristic was observed for the modification with RBD-BA.5.
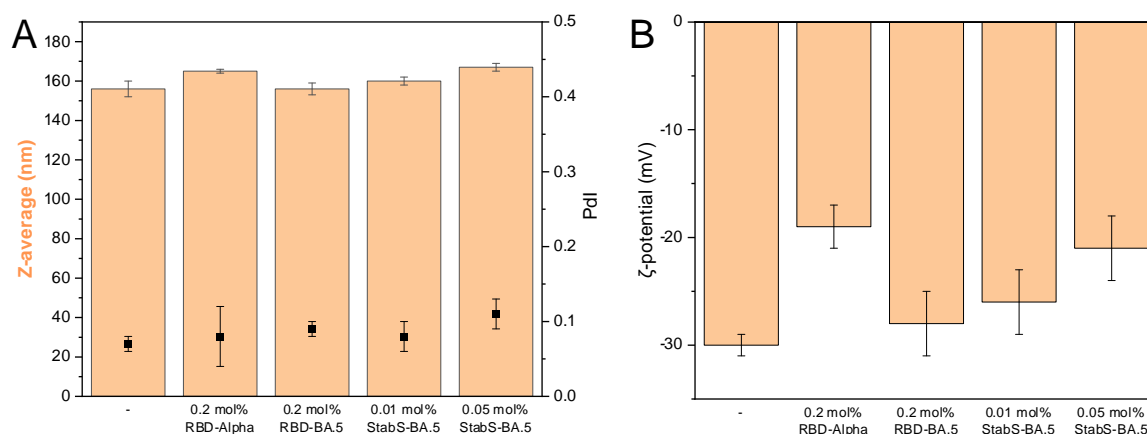


*Figure 1: Z-average and PdI (A, n = 3) and ζ-potential (B, n = 4) of liposomes modified with 0.2 mol% RBD-Alpha or -BA.5, or 0.01 or 0.05 mol% StabS-BA.5.*

Lysed fluorescence intensities decreased by 50% or 66% for modification with 0.01 mol% and 0.05 mol% StabS-BA.5, respectively, compared to unmodified liposomes (**Figure 2**), which was attributed to leakage of SRB. However, no second band of free SRB was observed during purification of StabS-BA.5 modified liposomes via size exclusion chromatography. The StabS protein appears to interact with the lipid bilayer, facilitating diffusion of SRB, despite lacking the hydrophobic stalk domain responsible for membrane anchorage. This is also an issue for the modification with RBD-Alpha, where modification consistently resulted in ~30% lower lysed fluorescence intensities compared to unconjugated liposomes, and unlysed fluorescence increased from ~2% to ~15%. Even during storage, the interaction of RBD with the lipid bilayer causes continuous leakage of SRB, as discussed in chapter 2.2. Both RBD and StabS have to be in close proximity, i.e. conjugated, to the liposomal surface to induce leakage. Addition of each protein without coupling reagents did not show any significant effect on lysed or unlysed fluorescence intensities. The increased unlysed fluorescence values upon RBD and StabS conjugation can be attributed in part to the lower SRB concentration due to leakage, resulting in lower self-quenching. Additionally, leaked SRB might intercalate into the proteins, resulting in increased fluorescence intensities due to reduced hydration-mediated quenching[35].

No binding to ACE2 was observed for 0.2 mol% RBD-BA.5 and 0.01 mol% StabS-BA.5 modified liposomes in the heterogeneous assay (**Figure S1**). Interestingly, 0.05 mol% StabS-

BA.5-liposomes showed a 2-fold higher signal in the ACE2 coated wells compared to the control. This does either suggest that a very small fraction of StabS-BA.5 was coupled in an orientation facilitating binding to ACE2, or that other StabS domains bind non-specifically to ACE2. In case of the former, the use of higher StabS-BA.5 concentrations might enable stronger ACE2 binding. However, it would further increase leakage of SRB, reducing fluorescence intensities and thus sensitivity of the liposomes. Modification of liposomes with StabS-BA.5 was therefore assessed not to be a promising alternative to RBD-BA.5 modification, neither promoting ACE2 binding.
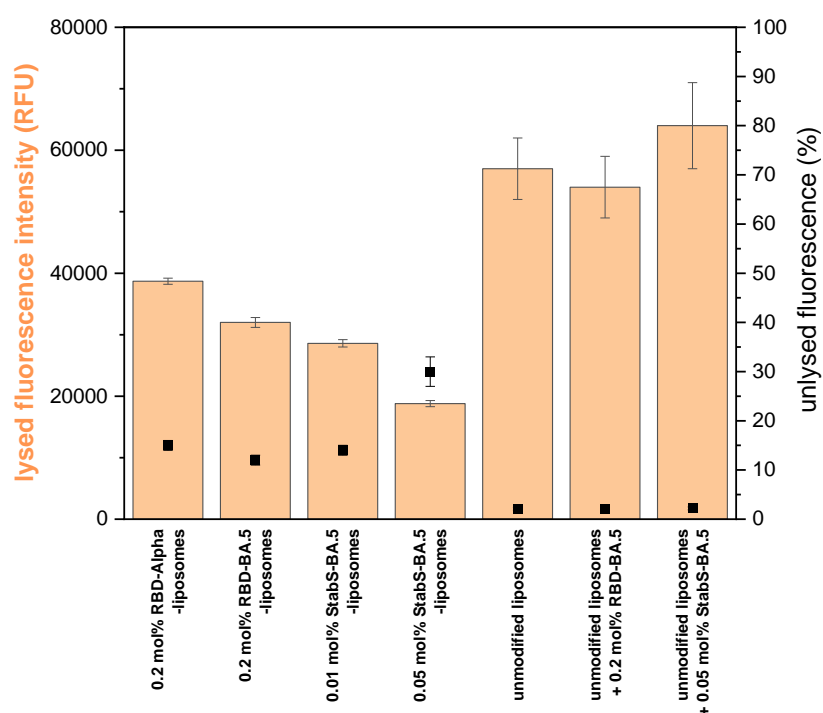


*Figure 2: Lysed and unlysed fluorescence of liposomes modified or incubated with 0.2 mol% RBD-Alpha or -BA.5, or 0.01 or 0.05 mol% StabS-BA.5. n = 4.*

### 3.2.3.2 Modification with other StabS Omicron variants

The conjugation of StabS-BA.2 to liposomes resulted in the formation of aggregates, which were too large to be purified via SEC, and instead got stuck in or on top of the resin (**Figure S2**). Mutations of the BA.2 variant compared to BA.5 might have resulted in favored cross-linking of StabS-BA.2, in turn resulting in aggregation of the modified liposomes. Alternatively, StabS-BA.2 might have been present as multimer, similar to the observations for the RBD variants discussed in chapter 2.2, which could have been coupled to multiple liposomes. NanoDSF measurements or EDC/sulfo-NHS coupling to liposomes including a desalting step before addition of the protein could provide further insights in the future.

Instead, the focus was put on the third investigated StabS variant, BQ1.1, which did not cause aggregation of modified liposomes. However, a second, drawn-out, band was visible during

purification via SEC, attributed to leaked SRB (**Figure S3**). The fluorescence measurement revealed a 40% lower lysed fluorescence for 0.01 mol% StabS-BQ1.1-liposomes compared to the unmodified liposomes, while 0.05 mol% StabS-BQ1.1 led to an 85% decrease of lysed fluorescence, correlating to an almost complete loss of encapsulant (**Table 1**). DLS measurements confirmed successful modification of liposomes with both 0.01 and 0.05 mol% StabS-BQ1.1, the Z-average increasing by up to 30 nm and the ζ-potential by up to 25 mV.

*Table 1: Characteristics (Z-average, PdI, ζ-potential, lysed and unlysed fluorescence) of unmodified liposomes and ones conjugated to 0.01 or 0.05 mol% StabS-BQ1.1.*

| Liposome modified with | Z-average / nm | PdI | ζ-potential / mV | lysed fluor. / RFU | unlysed fluor. / % |
|---|---|---|---|---|---|
| - | 152 ± 2 | 0.06 ± 0.01 | -32 ± 2 | 57000 ± 5000 | 2.1 ± 0.3 |
| **0.01 mol% StabS-BQ1.1** | 163 ± 2 | 0.10 ± 0.01 | -22 ± 2 | 33900 ± 1000 | 20 ± 3 |
| **0.05 mol% StabS-BQ1.1** | 185 ± 3 | 0.18 ± 0.02 | -7 ± 1 | 5800 ± 200 | 31 ± 6 |

Furthermore, a heterogeneous assay revealed strong binding of both StabS-BQ1.1 modified liposomes to ACE2 (**Figure 3**). Identical signal intensities were observed for liposomes modified with 0.2 mol% RBD-BQ1.1 or 0.01 mol% StabS-BQ1.1. Factoring in the six times lower lysed fluorescence, the liposomes modified with the higher StabS-BQ1.1 concentration (0.05 mol%) likely bound better to ACE2, producing only three times lower signals compared to the lower StabS-BQ1.1 concentration (0.01 mol%). This suggests that further optimization of the concentration might improve the signal intensity in the ACE2 binding assay. However, it is a trade-off between signal improvement due to higher StabS coverage, and therefore improved binding to ACE2, and signal loss due to leakage induced by higher StabS concentration. In any case, the fact that liposome modification with 0.01 mol% StabS resulted in similar ACE2 binding compared to modification with 20 times higher RBD concentration highlights the benefit of using the Spike protein, the trimeric structure significantly improving avidity due to the three adjacent RBDs. The 0.01 mol% StabS-BQ1.1 liposomes were retested after 3 months of storage in HSS and were shown to maintain their ACE2 binding ability, unlike RBD modified liposomes (data not shown). However, unlysed fluorescence increased from 20 ± 3% to 33 ± 2%, suggesting that the direct conjugation to the liposomal surface facilitated slow diffusion of SRB through the lipid bilayer, as observed for RBD-Alpha-liposomes (see chapter 2.2).

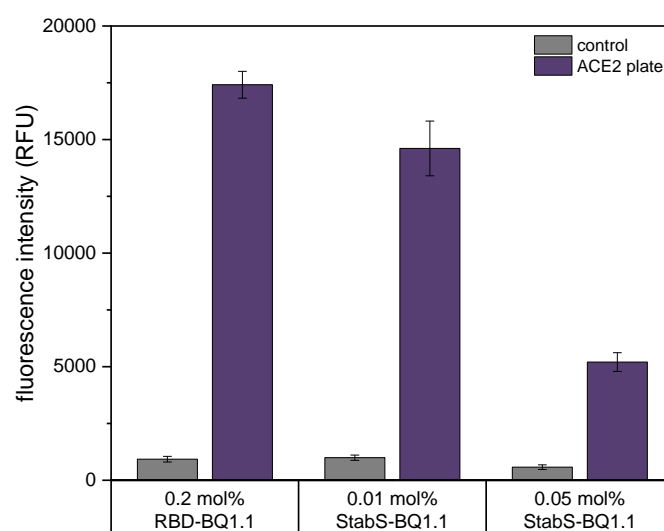*Figure 3: ACE2 binding of liposomes modified with 0.2 mol% RBD-BQ1.1 or 0.01 or 0.05 mol% StabS-BQ1.1. n = 3.*

Lastly, a neutralization test with polyclonal anti-RBD antibodies (PA5-114451) was conducted for 0.01 mol% StabS-BQ1.1-liposomes. Surprisingly, no neutralization was observed for any of the tested antibody concentrations, while 0.01 µg/mL started to show a neutralizing effect for 0.2 mol% RBD-Alpha-liposomes and 0.5 µg/mL were sufficient to cause almost complete neutralization (**Figure 4**). The lack of neutralization observed for StabS-BQ1.1 modified liposomes might be due to the immune escape of Omicron variants. The commercial antibodies were generated in rabbits using RBD as antigen, likely the wild type or Alpha variant. Liposomes modified with RBD-BQ1.1 had also been tested using the same antibodies, but did show almost no binding to ACE2 even in the absence of antibodies. Comparison of ACE2 binding of various modified liposomes right after coupling revealed that conjugation is highly consistent for RBD-Alpha and StabS-BQ1.1, but not RBD-BQ1.1 (**Figure S4**). The reduced signals in the ACE2 binding assay were attributed to degradation or aggregation of the RBD-BQ1.1 stock solution, affecting orientation on the liposomes after conjugation, a problem that was faced on multiple occasions for EDC/sulfo-NHS coupling of different RBDs.
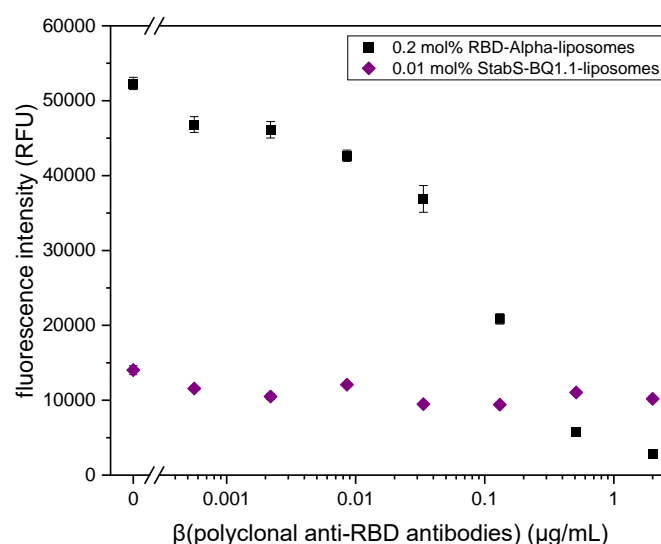
*Figure 4: Neutralization test with neutralizing polyclonal anti-RBD antibodies (PA5-114451) of liposomes modified with 0.2 mol% RBD-Alpha or 0.01 mol% StabS-BQ1.1. n = 3.*

### 3.2.4  Conclusion

The modification of liposomes with StabS Omicron variants using EDC/sulfo-NHS chemistry proved challenging, inducing liposome aggregation for the BA.2 variant and leakage of SRB for the BA.5 and BQ1.1 variants. Nonetheless, the successful modification of liposomes with 0.01 mol% StabS-BQ1.1 facilitated strong binding to ACE2 and showcased the superior avidity of StabS to ACE2 compared to RBD, mediated by its tetrameric structure. Reduction of the antigen coverage without loss of signal intensity is highly beneficial, making the test more sensitive, because lower amounts of antibodies can already achieve complete neutralization. Furthermore, it might be more cost-effective, depending on the cost of large-scale expression of StabS and RBD. Since modification using EDC/sulfo-NHS would require further optimization for each variant, and it remains unclear whether orientation of StabS-BA.5 enabling ACE2 binding could be achieved at all, site-directed conjugation strategies of StabS variants would be favorable. The prime candidate being the adaptation of the strategy using neutravidin-liposomes plus biotinylated protein, discussed in the previous chapter for RBD. The approach would enable separate storage of liposomes and StabS, each under optimum conditions, and circumvent the issue of leakage during StabS modification. However, it requires protein engineering for the addition of an Avi- or Cys-tag to the StabS protein, which can cause problems with protein expression or folding, making it a time-consuming endeavor. With both neutralizing anti-S and anti-RBD antibodies determined as potential CoP[11,12,36], the investigation of the biotinylation of RBD, which had been successfully expressed with a Cys-tag for the Alpha and Avi-tags for all variants already, was prioritized over the investigation of StabS biotinylation.

### 3.2.5  References

(1) Wang, M.-Y.; Zhao, R.; Gao, L.-J.; Gao, X.-F.; Wang, D.-P.; Cao, J.-M. *Front. Cell. Infect. Microbiol.* **2020**, *10*, 587269.

(2) Long, Q.-X.; Tang, X.-J.; Shi, Q.-L.; Li, Q.; Deng, H.-J.; Yuan, J.; Hu, J.-L.; Xu, W.; Zhang, Y.; Lv, F.-J.; Su, K.; Zhang, F.; Gong, J.; Wu, B.; Liu, X.-M.; Li, J.-J.; Qiu, J.-F.; Chen, J.; Huang, A.-L. *Nat. Med.* **2020**, *26* (8), 1200–1204.

(3) Garcia-Beltran, W. F.; Lam, E. C.; Astudillo, M. G.; Yang, D.; Miller, T. E.; Feldman, J.; Hauser, B. M.; Caradonna, T. M.; Clayton, K. L.; Nitido, A. D.; Murali, M. R.; Alter, G.; Charles, R. C.; Dighe, A.; Branda, J. A.; Lennerz, J. K.; Lingwood, D.; Schmidt, A. G.; Iafrate, A. J.; Balazs, A. B. *Cell* **2021**, *184* (2), 476-488.e11.

(4) Shi, R.; Shan, C.; Duan, X.; Chen, Z.; Liu, P.; Song, J.; Song, T.; Bi, X.; Han, C.; Wu, L.; Gao, G.; Hu, X.; Zhang, Y.; Tong, Z.; Huang, W.; Liu, W. J.; Wu, G.; Zhang, B.; Wang, L.; Qi, J.; Feng, H.; Wang, F.-S.; Wang, Q.; Gao, G. F.; Yuan, Z.; Yan, J. *Nature* **2020**, *584* (7819), 120–124.

(5) Lau, E. H. Y.; Tsang, O. T. Y.; Hui, D. S. C.; Kwan, M. Y. W.; Chan, W.; Chiu, S. S.; Ko, R. L. W.; Chan, K. H.; Cheng, S. M. S.; Perera, Ranawaka A. P. M.; Cowling, B. J.; Poon, L. L. M.; Peiris, M. *Nat. Commun.* **2021**, *12* (1), 63.

(6) Klein, S.; Cortese, M.; Winter, S. L.; Wachsmuth-Melm, M.; Neufeldt, C. J.; Cerikan, B.; Stanifer, M. L.; Boulant, S.; Bartenschlager, R.; Chlanda, P. *Nat. Commun.* **2020**, *11* (1), 5885.

(7) Walls, A. C.; Park, Y.-J.; Tortorici, M. A.; Wall, A.; McGuire, A. T.; Veesler, D. *Cell* **2020**, *183* (6), 1735.

(8) Yuan, M.; Wu, N. C.; Zhu, X.; Lee, C.-C. D.; So, R. T. Y.; Lv, H.; Mok, C. K. P.; Wilson, I. A. *Science (New York, N.y.)* **2020**, *368* (6491), 630–633.

(9) Wu, N. C.; Yuan, M.; Bangaru, S.; Huang, D.; Zhu, X.; Lee, C.-C. D.; Turner, H. L.; Peng, L.; Yang, L.; Burton, D. R.; Nemazee, D.; Ward, A. B.; Wilson, I. A. *PLoS Pathog* **2020**, *16* (12), e1009089.

(10) Voss, W. N.; Hou, Y. J.; Johnson, N. V.; Delidakis, G.; Kim, J. E.; Javanmardi, K.; Horton, A. P.; Bartzoka, F.; Paresi, C. J.; Tanno, Y.; Chou, C.; Abbasi, S. A.; Pickens, W.; George, K.; Boutz, D. R.; Towers, D. M.; Mcdaniel, J. R.; Billick, D.; Goike, J.; Rowe, L.; Batra, D.; Pohl, J.; Lee, J.; Gangappa, S.; Sambhara, S.; Gadush, M.; Wang, N.; Person, M. D.; Iverson, B. L.; Gollihar, J. D.; Dye, J. M.; Herbert, A. S.; Finkelstein, I. J.; Baric, R. S.; Mclellan, J. S.; Georgiou, G.; Lavinder, J. J.; Ippolito, G. C. Prevalent, protective, and convergent IgG recognition of SARS-CoV-2 non-RBD spike epitopes. *American Association for the Advancement of Science,* Apr 5, 2021. https://www.science.org/doi/10.1126/science.abg5268 (accessed 2025-03-24).

(11) Perry, J.; Osman, S.; Wright, J.; Richard-Greenblatt, M.; Buchan, S. A.; Sadarangani, M.; Bolotin, S. *PLOS ONE* **2022**, *17* (4), e0266852.

(12) Khoury, D. S.; Cromer, D.; Reynaldi, A.; Schlub, T. E.; Wheatley, A. K.; Juno, J. A.; Subbarao, K.; Kent, S. J.; Triccas, J. A.; Davenport, M. P. *Nat. Med.* **2021**, *27* (7), 1205–1211.

(13) Earle, K. A.; Ambrosino, D. M.; Fiore-Gartland, A.; Goldblatt, D.; Gilbert, P. B.; Siber, G. R.; Dull, P.; Plotkin, S. A. *Vaccine* **2021**, *39* (32), 4423–4428.

(14) Streif, S.; Baeumner, A. J. *Anal. Chem.* **2025**.

(15) Ahn, M.-J.; Kang, J.-A.; Hong, S. M.; Lee, K.-S.; Kim, D. H.; Song, D.; Jeong, D. G. *Biochem. Biophys. Res. Commun.* **2023**, *646*, 8–18.

(16) Bian, S.; Shang, M.; Tao, Y.; Wang, P.; Xu, Y.; Wang, Y.; Shen, Z.; Sawan, M. *Vaccines (Basel)* **2024**, *12* (4), 352.

(17) Liu, H.; Liu, T.; Wang, A.; Liang, C.; Zhu, X.; Zhou, J.; Chen, Y.; Liu, Y.; Qi, Y.; Chen, W.; Zhang, G. *Anal. Chem.* **2024**, *96* (46), 18437–18444.

(18) Klüpfel, J.; Paßreiter, S.; Rumpf, M.; Christa, C.; Holthoff, H.-P.; Ungerer, M.; Lohse, M.; Knolle, P.; Protzer, U.; Elsner, M.; Seidel, M. *Anal. Bioanal. Chem.* **2022**, 1–14.

(19) Wang, X.; Shao, S.; Ye, H.; Li, S.; Gu, B.; Tang, B. *Sci. Rep.* **2023**, *13* (1), 22253.

(20) Deenin, W.; Khongchareonporn, N.; Ruxrungtham, K.; Ketloy, C.; Hirankarn, N.; Wangkanont, K.; Rengpipat, S.; Yakoh, A.; Chaiyo, S. *Anal. Chem.* **2024**, *96* (14), 5407–5415.

(21) Mahmud, M. A.; Xu, L. H.; Usatinsky, A.; dos Santos, C. C.; Little, D. J.; Tsai, S. S. H.; Rackus, D. G. *Anal. Chem.* **2024**.

(22) Fulford, T. S.; Van, H.; Gherardin, N. A.; Zheng, S.; Ciula, M.; Drummer, H. E.; Redmond, S.; Tan, H.-X.; Boo, I.; Center, R. J.; Li, F.; Grimley, S. L.; Wines, B. D.; Nguyen, T. H. O.; Mordant, F. L.; Ellenberg, P.; Rowntree, L. C.; Kedzierski, L.; Cheng, A. C.; Doolan, D. L.; Matthews, G.; Bond, K.; Hogarth, P. M.; McQuilten, Z.; Subbarao, K.; Kedzierska, K.; Juno, J. A.; Wheatley, A. K.; Kent, S. J.; Williamson, D. A.; Purcell, D. F. J.; Anderson, D. A.; Godfrey, D. I. *eBioMedicine* **2021**, *74*, 103729.

(23) Lim, S. M.; Cheng, H. L.; Jia, H.; Kongsuphol, P.; D/O Shunmuganathan, B.; Chen, M. W.; Ng, S. Y.; Gao, X.; Turaga, S. P.; Heussler, S. P.; Somani, J.; Sengupta, S.; Tay, D. M. Y.; McBee, M. E.; Young, B. E.; MacAry, P. A.; Sikes, H. D.; Preiser, P. R. *Bioeng. Trans. Med.* **2022**, *7* (2), e10293.

(24) Bian, L.; Li, Z.; an He; Wu, B.; Yang, H.; Wu, Y.; Hu, F.; Lin, G.; Zhang, D. *Biomaterials* **2022**, *288*, 121694.

(25) Fenwick, C.; Turelli, P.; Pellaton, C.; Farina, A.; Campos, J.; Raclot, C.; Pojer, F.; Cagno, V.; Nusslé, S. G.; D'Acremont, V.; Fehr, J.; Puhan, M.; Pantaleo, G.; Trono, D. *Sci. Transl. Med.* **2021**, *13* (605).

(26) Lynch, K. L.; Zhou, S.; Kaul, R.; Walker, R.; Wu, A. H. *Clin. Chem.* **2022**, *68* (5), 702–712.

(27) Mravinacova, S.; Jönsson, M.; Christ, W.; Klingström, J.; Yousef, J.; Hellström, C.; Hedhammar, M.; Havervall, S.; Thålin, C.; Pin, E.; Tegel, H.; Nilsson, P.; Månberg, A.; Hober, S. *New Biotechnol.* **2022**, *66*, 46–52.

(28) Ho, T.-S.; Du, P.-X.; Su, W.-Y.; Santos, H. M.; Lin, Y.-L.; Chou, Y.-Y.; Keskin, B. B.; Pau, C. H.; Syu, G.-D. *Biosens. Bioelectron.* **2022**, *204*, 114067.

(29) Su, W.-Y.; Du, P.-X.; Santos, H. M.; Ho, T.-S.; Keskin, B. B.; Pau, C. H.; Yang, A.-M.; Chou, Y.-Y.; Shih, H.-C.; Syu, G.-D. *Anal. Chem.* **2022**, *94* (17), 6529–6539.

(30) Streif, S.; Neckermann, P.; Spitzenberg, C.; Weiss, K.; Hoecherl, K.; Kulikowski, K.; Hahner, S.; Noelting, C.; Einhauser, S.; Peterhoff, D.; Asam, C.; Wagner, R.; Baeumner, A. J. *Anal. Bioanal. Chem.* **2023**, *415* (8), 1421–1435.

(31) Markov, P. V.; Ghafari, M.; Beer, M.; Lythgoe, K.; Simmonds, P.; Stilianakis, N. I.; Katzourakis, A. *Nat Rev Microbiol* **2023**, *21* (6), 361–379.

(32) Edwards, K. A.; Curtis, K. L.; Sailor, J. L.; Baeumner, A. J. *Anal. Bioanal. Chem.* **2008**, *391* (5), 1689–1702.

(33) Božič, A.; Podgornik, R. *Bioinformatics Advances* **2024**, *4* (1), vbae053.

(34) Adamczyk, Z.; Batys, P.; Barbasz, J. *Current Opinion in Colloid & Interface Science* **2021**, *55*, 101466.

(35) Kitamura, M.; Murakami, K.; Yamada, K.; Kawai, K.; Kunishima, M. *Dyes and Pigments* **2013**, *99* (3), 588–593.

(36) Sobhani, K.; Cheng, S.; Binder, R. A.; Mantis, N. J.; Crawford, J. M.; Okoye, N.; Braun, J. G.; Joung, S.; Wang, M.; Lozanski, G.; King, C. L.; Roback, J. D.; Granger, D. A.; Boppana, S. B.; Karger, A. B. *Vaccines (Basel)* **2023**, *11* (11), 1644.

### 3.2.6 Supplementary information
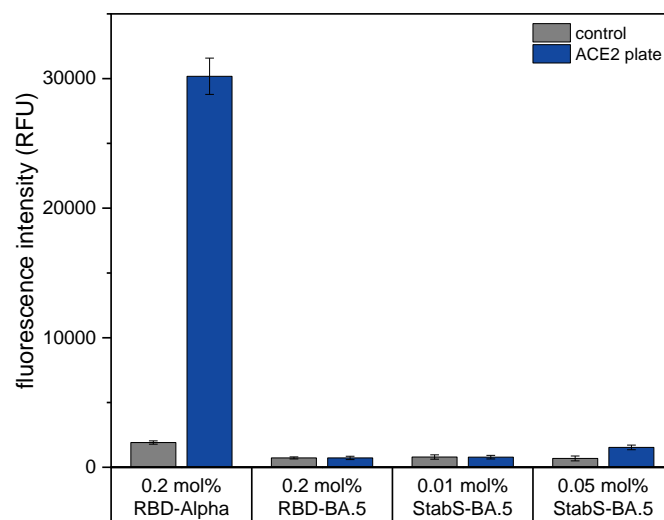


**Figure S1:** *ACE2 binding of liposomes modified with 0.2 mol% RBD-Alpha or -BA.5, or 0.01 or 0.05 mol% StabS-BA.5. n = 3.*



**Figure S2:** *SEC of liposomes modified with 0.01 mol% (A) or 0.05 mol% StabS-BA.2 (B).*
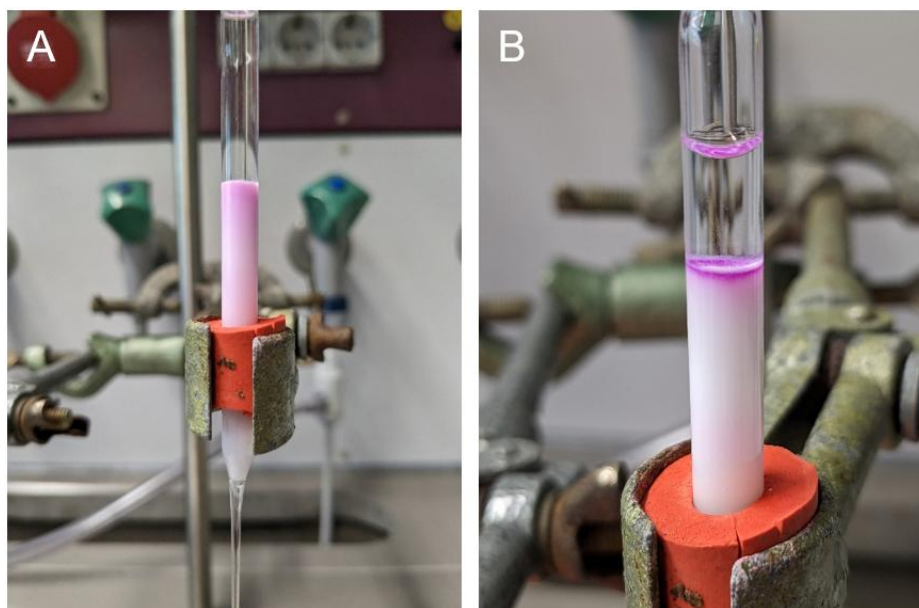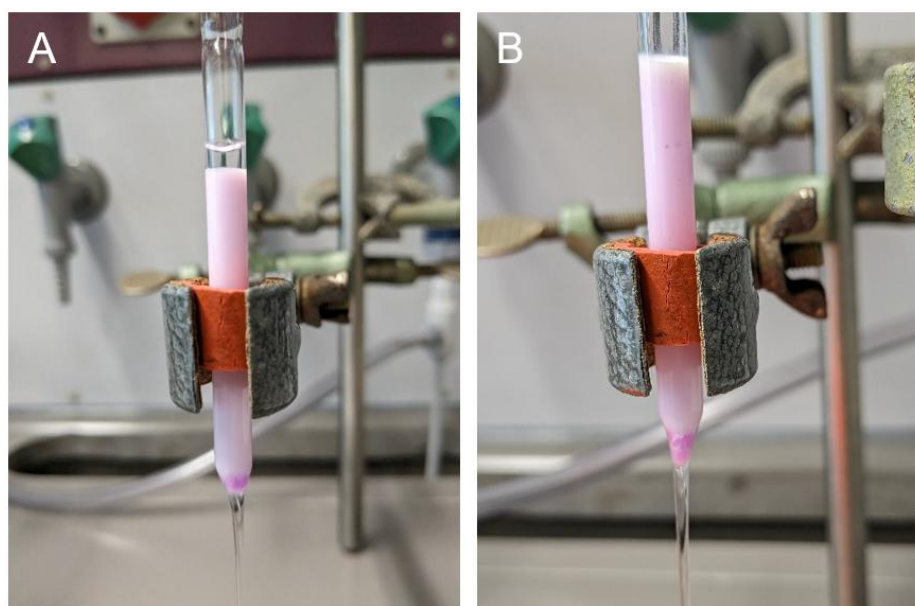
*Figure S3: SEC of liposomes modified with 0.01 mol% (A) or 0.05 mol% StabS-BQ1.1 (B).*
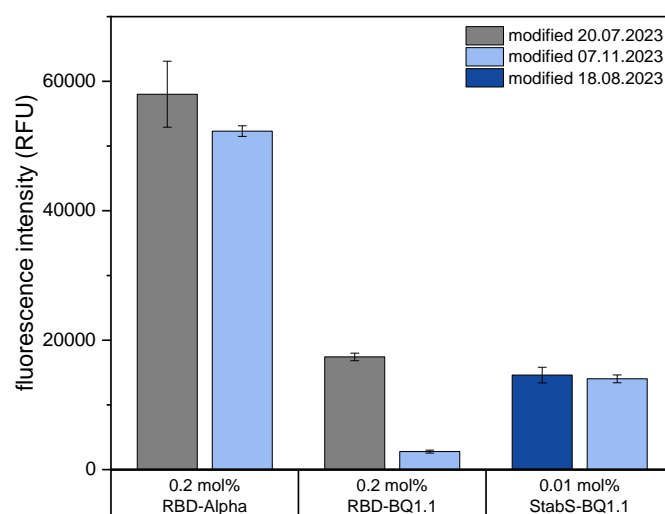


*Figure S4: ACE2 binding of liposomes modified with 0.2 mol% RBD-Alpha or -BQ1.1, or 0.01 mol% StabS-BQ1.1. ACE2 binding assays were conducted right after coupling. n = 3.*

# 4 Optimization of the POC neutralization test toward quantitative detection and improved user-friendliness

## Abstract

Different approaches to improve the sensitivity and the user-friendliness of the established qualitative neutralization test discussed in chapter 2.1 were investigated. The RBD coverage could be decreased 2-fold to 0.1 mol% without affecting liposome capture, requiring lower quantities of neutralizing antibodies to achieve complete neutralization. Reduction of the LFA strip width from 5 mm to 3 mm resulted in increased signal intensities for identical sample volumes. Increasing the serum concentration could further improve the sensitivity in the future. To reduce handling steps, and thus improve user-friendliness, addition of a polyvinyl alcohol (PVA) barrier was investigated. However, the Sci FlexArrayer S3 was unable to dispense highly concentrated viscous PVA solutions, and produced inhomogeneous results for lower concentrations, most barriers either achieved break-through times of 2 to 4 minutes or completely blocked the membrane. Printing of a wax barrier with a gap to reduce the flow rate and thus increase interaction times was investigated as alternative. The strategy is a promising solution to omit the pre-incubation step, but requires a different means of quantification than normalization of the test line signal to the signal of the anti-FITC control line. Normalization to a second test line which captures neutralized RBD-liposomes was envisioned. However, both anti-human Ig and protein A test lines were unable to capture the anti-RBD antibodies bound to RBD-liposomes in the desired range of serum. This was attributed to large quantities of other antibodies in serum that are not directed against RBD, and non-specific interaction of HSA with antibodies. Lastly, the replacement of the polystreptavidin test line with an ACE2 test line was investigated. This led to significantly lower signals due to the weaker interaction between ACE2 and RBD compared to biotin and (poly)streptavidin. Further optimization is required to achieve a semi-quantitative or quantitative read-out for the POC neutralization test in the future.

**This chapter has not been published.**

## 4.1 Introduction

Point-of-care testing (POCT) has evolved to be an important diagnostic tool accepted by the population at large, prime examples being pregnancy tests and the continuous monitoring of glucose levels for diabetes patients. These diagnostic tests enable the on-site detection of biomarkers, drugs, metabolites and pathogens by a lay person, making them a vital part for future healthcare considering developments toward digital and telemedicine-based systems[1]. To be true POCT, and not laboratory or near-patient tests, they should fulfill the ASSURED criteria (affordable, sensitive, specific, user-friendly, rapid and robust, equipment-free, and deliverable), or even better the REASSURED criteria, additionally including real-time connectivity and ease of specimen collection and environmental friendliness[2]. During the COVID-19 pandemic, rapid lateral flow antigen tests were in great demand and contributed to a high extent to the pandemic control[3,4]. While easy to perform, they lacked in sensitivity and were strongly impacted by the specimen collection, i.e. the depth and duration of the nasal swab[5].

A common strategy to improve the sensitivity of lateral flow assays (LFAs) is the use of more sensitive detection methods, including fluorescence, chemiluminescence and surface enhanced Raman scattering (SERS), instead of a colorimetric read-out[6]. However, these alternatives are typically not equipment-free and rely on the use of specific detection devices. Colorimetric signals, most commonly generated using gold nanoparticles (AuNP), can be analyzed with the naked eye or using a smartphone camera. Alternatively, the use of sulforhodamine B (SRB) encapsulating liposomes was shown to improve the sensitivity of a POCT for interleukin 6 compared to conventional AuNPs[7]. Other strategies to consider for improved sensitivity are site-directed immobilization of the capture probe, slowed flow, signal amplification, or pre-incubation. Biotinylation of the capture probe facilitates site-directed immobilization on a polystreptavidin test line[8], while conjugation with the cellulose binding domain does the same for paper-based POCT[9,10]. Reduction of the flow rate can be achieved by the introduction of wax pillars[11], compression of the membrane[12], or the use of membranes with smaller pore size. The resulting longer interaction time between analyte, signaling probe and capture probe can lead to higher capture efficiency, similar to a pre-incubation step. Here, it is important to consider the aspect of user-friendliness, incubation in a separate vial requiring involvement of the user. Instead, timed-release of reagents by introduction of a dissolvable barrier without further activity of the user is to be favored, options including salt[13], sugar[14], wax[15] and polymer barriers[16,17]. A polyvinyl alcohol barrier was used by Han et al. for the timed-release of a Au-ion amplification solution[18]. Similar approaches would be required for tests based on enzymatic reactions, such as horseradish-peroxidase, to remain one-step assays[19]. The read-out should also be of consideration for a high user-friendliness, i.e., most intuitive

signaling strategy, as the generation of a signal is typically associated with the presence of the analyte, stronger signals correlating to higher analyte concentration. However, this is not necessarily the case for competitive POC tests, such as the detection of neutralizing antibodies. Here, high neutralizing antibody titers prevent the capture of the signaling probe by the capture probe, corresponding to a decreasing signal[20–22]. This 'signal-off' approach might be confusing for the user and shifts the detection range to high antibody titers. Addition of a second test line consisting of anti-human Ig antibodies or protein A can enable a 'signal-on' approach instead, capturing neutralized rather than non-neutralized particles, shifting the detection range toward low antibody titers[23–25]. Furthermore, it provides a means for quantification of neutralizing antibody titers by normalization of the signals obtained for neutralized and non-neutralized particles to one another. These tests often use patient serum, requiring special sample preparation including centrifugation. For true POCT the use of finger-prick blood would be necessary, combined with commercially available blood separation pads to separate red blood cells and plasma on the LFA strip directly without the need for additional equipment.

Here, we investigated different strategies to improve both the sensitivity and user-friendliness of an established liposome-based POC neutralization test for SARS-CoV-2[8]. The approaches included the reduction of the antigen coverage of liposomes, investigation of different on-strip incubation techniques and the use of a second test line to capture neutralized particles.

## 4.2  Experimental section

### 4.2.1  Chemicals and consumables

All chemicals were of analytical reagent grade. Bovine serum albumin fraction V (BSA), cholesterol from sheep wool (C8667, ≥ 99%), human serum albumin (HSA), *N*-Hydroxysulfosuccinimide sodium salt (sulfo-NHS, purity ≥ 98%), polyvinyl alcohol (Mw 9000-10000, 80% hydrolyzed), Sephadex-G50, streptavidin from *Streptomyces avidinii*, Whatman Nucleopore™ Track-Etched membranes (1.0 µm, 0.4 µm and 0.2 µm diameter) and Tween 20 were purchased from Sigma Aldrich/Merck (Darmstadt, Germany); 1,2-dipalmitoyl-sn-glycero-3-phosphoethanolamine-*N*-(glutaryl) (sodium salt) (*N*-glutaryl-DPPE) from NOF America Corporation (NY, USA); the remaining phospholipids 1,2-dipalmitoyl-sn-glycero-3-phosphocholine (DPPC), 1,2-dipalmitoyl-sn-glycero-3-phospho-(1'-rac-glycerol) (sodium salt) (DPPG) and the extruder set from Avanti Polar Lipids (Alabaster, AL, USA). Sulforhodamine B (SRB) (S1307), black high binding 96-well microplates (Nunc MaxiSorp) and (1-Ethyl-3-(3-dimethylaminopropyl) carbodiimide-hydrochloride) (EDC) (PG82079) were purchased from Thermo Fisher Scientific (Waltham, MA, USA); *n*-Octyl-β-D-glucopyranoside (OG) (≥ 98%,

CN23), 2-(*N*-Morpholino)-ethane sulphonic acid (MES) (≥ 99%, 4259), *N*-2-Hydroxyethylpiperazine-*N'*-2-ethane sulphonic acid (HEPES) (≥ 99.5%, HN78), sucrose, sodium azide, sodium chloride and dialysis membrane Spectra/Por© 4 (MWCO: 12-14 kDa) (2718.1) from Carl Roth (Karlsruhe, Germany). Phosphorous standard was obtained from Bernd Kraft GmbH (Den Haag, Netherlands). Chloroform, methanol and Spectra-Por® Float-A-Lyzer® G2 (1 mL, MWCO: 1000 kDa) were purchased from Fisher Scientific (Hampton, NH, USA). Polystreptavidin R was obtained from BioTeZ Berlin-Buch GmbH (Berlin, Germany), Protein A from Sino Biological (Peking, China), polyclonal goat anti-human IgA + IgG + IgM (H+L) and monoclonal mouse anti-FITC antibody from Jackson ImmunoResearch (West Grove, PA, USA) and monoclonal S309 anti-RBD human IgG1 antibody from Biorbyt (Cambridge, United Kingdom). Monoclonal human anti-RBD antibody CR3022, RBD, ACE2 and ACE2-biotin were provided by our collaborators from the University Hospital Regensburg. UniSart CN95 and CN150 membranes were purchased from Sartorius (Göttingen, Germany). Glass conjugate pad 8980 was bought from Ahlstrom Munksjö (Helsinki, Finland). The waste pad 270 was obtained from Kenosha BV (Amstelveen, Netherlands).

### 4.2.2 Buffer compositions

HEPES sucrose saline (HSS) buffer contained 200 mM sucrose, 200 mM NaCl, 10 mM HEPES and 0.01 w/v% $NaN_3$, pH 7.5. PBS buffer contained 137 mM NaCl, 2.7 mM KCl, 10 mM $Na_2HPO_4$ and 1.8 mM $KH_2PO_4$, pH 7.4. PBS-T contained 0.1 w/v% Tween 20 in PBS. MES buffer contained 50 mM MES, 200 mM sucrose and 200 mM NaCl, pH 5.5. Carbonate buffer contained 100 mM $NaHCO_3$, pH 9.

### 4.2.3 Liposome synthesis

Reverse-phase evaporation was chosen as synthesis method for liposomes as described previously[26]. 150 mM SRB and 140 mM NaCl were dissolved in 20 mM HEPES, pH 7.5 (4.5 mL) by sonication at 60 °C to prepare the encapsulant. Lipid mixtures (41.4 mol% cholesterol, 32.2 mol% DPPC, 18.4 mol% DPPG, 8.0 mol% *N*-glutaryl-DPPE) were prepared by addition of 3 mL chloroform and 0.5 mL methanol and sonication for 1 min, followed by addition of encapsulant (2 mL) and sonication for 4 min at 60 °C. A rotary evaporator (LABOROTA 4001, Heidolph, Germany) was used to evaporate the organic solvents at 60 °C by stepwise reduction of pressure (900 mbar for 10 min, 850 mbar for 5 min, 800 mbar for 5 min, 780 mbar for 20 min). The solution was vortexed another two times for 1 min with intermittent encapsulant addition (2 mL). The residual organic solvents were evaporated at 60 °C (750 mbar for 20 min, 600 mbar for 5 min, 500 mbar for 5 min, 400 mbar for 20 min). The size was controlled by extrusion at 65 °C using polycarbonate membranes with pore sizes of 1 µm, 0.4 µm and 0.2 µm. Solutions were repeatedly pushed through the membranes with decreasing pore sizes, amounting to 21 repetitions for the 1 µm pore size and 11 repetitions

for each of the smaller pore sizes. Size exclusion chromatography using a Sephadex G-50 column, followed by dialysis overnight against HSS buffer with two buffer exchanges in a dialysis membrane Spectra/Por© 4 (MWCO: 12-14 kDa) were used to remove excess encapsulant.

### 4.2.4 Liposome characterization

An inductively coupled plasma optical emission spectrometer (ICP-OES) (SpectroBlue TI/EOP) from SPECTRO Analytical Instruments GmbH (Kleve, Germany) was used to determine phospholipid concentrations, which in turn were used to calculate total lipid concentrations based on the mixture of lipids used for the synthesis. Phosphorous standard dilutions between 0 µM and 100 µM in 0.5 M $HNO_3$ were used for calibration of the device. Phosphorous was detected at 177.495 nm. Re-calibration was performed before each measurement using the 0 µM and 100 µM phosphorus dilutions. Liposome stock solutions were diluted 1:100 or 1:60 in 0.5 M $HNO_3$ and their phosphorous content determined.

Size and ζ-potential were measured via dynamic light scattering (DLS) using a Malvern Zetasizer Nano-ZS. Liposome stock solutions were diluted to 25 µM total lipids in HSS buffer in a polymethyl methacrylate (PMMA) semi-micro cuvette (Brand, Germany) for size and a disposable folded capillary cell (Malvern Panalytical, Germany) for ζ-potential measurements. The measurement temperature was set to 25 °C, the refractive index was 1.34, the material absorbance was zero and the dispersant viscosity 1.1185 mPa s. For ζ-potential measurements a dielectric constant of 78.5 was used and an equilibration time of 60 s applied before each measurement.

### 4.2.5 Liposome modification

Proteins were conjugated to carboxylated liposomes via EDC/sulfo-NHS chemistry. Liposomes were incubated with EDC and sulfo-NHS (1:100:180 ratio of carboxy-groups:EDC:sulfo-NHS) for 1 h at room temperature (RT) and 300 rpm followed by addition of protein and another 1.5 h incubation at RT and 300 rpm. Excess reagents were removed via dialysis against HSS buffer overnight with one buffer exchange in a Spectra-Por® Float-A-Lyzer® G2 (1 mL, MWCO: 1000 kDa). Total lipid concentrations were determined using ICP-OES and the conjugated liposomes were stored at 4 °C in Protein LoBind tubes (Eppendorf, Germany).

### 4.2.6 Heterogeneous binding assays

ACE2 (1 µg/mL), protein A and anti-human Ig (5 µg/mL in PBS, 100 µL per well) were incubated in a Nunc MaxiSorp high binding plate overnight at 4 °C. The plate was washed two times with PBS-T (150 µL per well) and three times with HSS (150 µL per well) before being used. Liposomes (1 µM total lipids) mixed with serum (0 to 2 v%) or antibodies (0.2 µg/mL) and HSA

(0 or 2 w/v%) in HSS were added to the MTP (100 µL per well, n = 3) and incubated for 2 h at RT and 300 rpm. The plate was washed three times with HSS buffer (150 µL per well) before 30 mM OG in bidest. water (100 µL per well) was added. After 10 min incubation the fluorescence was measured three consecutive times with a BioTek SYNERGY neo2 fluorescence reader ($\lambda_{Ex} = 560\ nm$ and $\lambda_{Em} = 585\ nm$, bandwidth 10, gain 150). In case of normalization to initial fluorescence intensities, errors were calculated using Gaussian error propagation.

### 4.2.7 Dispensing of test and control lines and PVA barriers

Polystreptavidin, ACE2 and anti-FITC antibodies in PBS (0.5 mg/mL) were dispensed on membrane strips (2.5 x 6 cm) with the Sci FlexArrayer S3 (Scienion, Germany). Solutions were first aspirated from a clear 96-well U-bottom microtiter plate (Greiner, Austria) applying 5% pressure for 10000 µs and subsequently dispensed with 20% pressure, 700 µs pulse and 500 µm spot pitch. A total of 110 spots were dispensed on each membrane strip and dried for 1 h at 37 °C in an incubator. PVA was dispensed from the bulk solution, parameters were varied in an attempt to achieve reliable jet formation and avoid dripping or clogging of the nozzle.

### 4.2.8 Wax printing

Barriers of 0.1 mm thickness with 0.2 to 0.9 mm wide gaps every 3 mm in A5 format were designed in InkScape 1.1.1 and saved as PDF (600 DPI). Black barriers were printed on the CN95 membrane (A5 sheet) using a Xerox ColorCube 8570 wax printer. The membrane was placed in the oven at 95 °C for 5 minutes to melt the wax. The membrane sheet was cut into 2.5 cm wide segments with one barrier each and used for LFA strip preparation.

### 4.2.9 LFA strip preparation

Sample pad grade 8980 (1.9 cm) and waste pad (1.6 cm) were added with an overlap of 2 mm above and below the CN95 or CN150 membrane (2.5 cm) on a white PVC backing (7.2 cm height, 0.3 mm thickness). Materials were assembled in 5 cm pieces that were cut to 3 mm or 5 mm wide strips with a paper cutter (Dahle 562).

### 4.2.10 Lateral flow assay

If not stated otherwise, FITC- and RBD-liposomes (16.7 µM, 0.1 mol% RBD) were mixed with ACE2-biotin (6 equiv. per RBD) in HSS buffer, containing 2 w/v% HSA unless serum was added, and pipetted into the wells of a clear microtiter plate (30 µL or 50 µL). LFA test strips with polystreptavidin test line and anti-FITC control line were placed into the wells and washed with HSS (25 µL) after 5 minutes. Signals were analyzed after another 20 minutes using either a self-build photo box with a Canon EFS 18-55mm lens (**Figure S1**), or an ESEQuant LFR

device, provided by Microcoat Biotechnology GmbH (Bernried, Germany). Settings for the former were ISO 100, aperture 3.5, exposure time 1/30 s, focal length 18 mm, white balance daylight (5200K), manual focus, and the raw files were analyzed using ImageJ (split color channels, subtract background (50 pixels), invert, measure test line and background with 115x35 pixel rectangle). Signal intensities were calculated by subtracting the background intensity from the test line intensity. The measurement parameters of the ESEQuant LFR device were set to Type: Reflective (520 nm), Signal Noise 10 mV, Channel E1/D2, Start 34 mm, End 48 mm, Control line Position 45 mm, Test line Position 39 mm, Tolerance 1.5 mm, Left 1.2 mm, Right 1.2 mm. The reflectance of the test and control line at 520 nm was quantified as peak height.

## 4.3  Results and discussion

### 4.3.1  Influence of RBD coverage and test strip width

The optimization of the RBD coverage was discussed for 10 mM SRB encapsulating liposomes in chapter 2.1. The optimum of 0.2 mol% was subsequently used for 150 mM SRB encapsulating liposomes in both the HTS and LFA format. The RBD coverage was later re-investigated with additional amounts of RBD. Here, it was found that 0.2 mol% RBD remained the optimum for the HTS format, resembling the lowest amount of RBD required to obtain maximum signal intensities. In the LFA format, on the other hand, 0.1 mol% RBD were found to be sufficient, leading to maximum signals already (**Figure 1**). This analysis underlined the excellent control over the coupling reaction. The large standard deviation obtained with 0.12 to 0.16 mol% RBD could either be due to inconsistency in the imaging setup, which at the time was a self-build photo box (**Figure S1**), or variations between the individual runs. Reduction of the RBD coverage is expected to coincide with improved sensitivity of the neutralization test, less antibodies being required to achieve full neutralization.
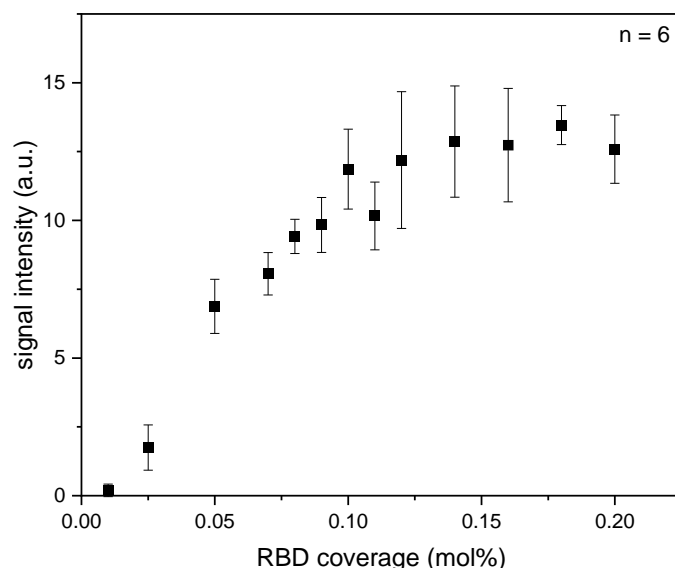
***Figure 1:*** *Influence of the RBD coverage of liposomes on the signal intensity in the LFA. Samples were run with 10 v% seronegative pooled serum. n = 6.*

Another simple means to improve sensitivity is the reduction of the test strip width. Identical amounts of liposomes should then result in stronger test line intensities, given that sufficient polystreptavidin is used to capture more particles. This could be shown with 3 mm wide LFA strips, which produced 30% higher signals compared to 5 mm wide ones with the same sample volume, i.e., with the same amount of liposomes (**Figure 2**). In theory the signal should have increased by 60%, if all liposomes were captured. The reduced test strip width might have altered the flow, affecting liposome capture. The use of identical liposome to serum to volume ratios resulted in similar signal intensities, as shown for 50 µL sample volume on 5 mm and 30 µL sample volume on 3 mm wide LFA strips, using 10 v% serum each. Increasing serum concentration led to a slight reduction of signal intensity for both sample volumes on the 3 mm wide LFA strips. This can either be due to changed flow properties, e.g. slower flow induced by increased viscosity, or non-specific interaction of serum constituents with the liposomes or polystreptavidin. For a final assay, the use of higher serum concentrations would however be beneficial, improving sensitivity, and is worthwhile further optimization. Ideally, one could use finger-prick blood for a commercial product, combined with a blood separation pad. While lancets for diabetes patients draw on average only ~3 µL of whole blood[27], mean volumes between 42 µL and 118 µL can be drawn with different lancets[28], thus higher plasma concentrations could be investigated in the future.
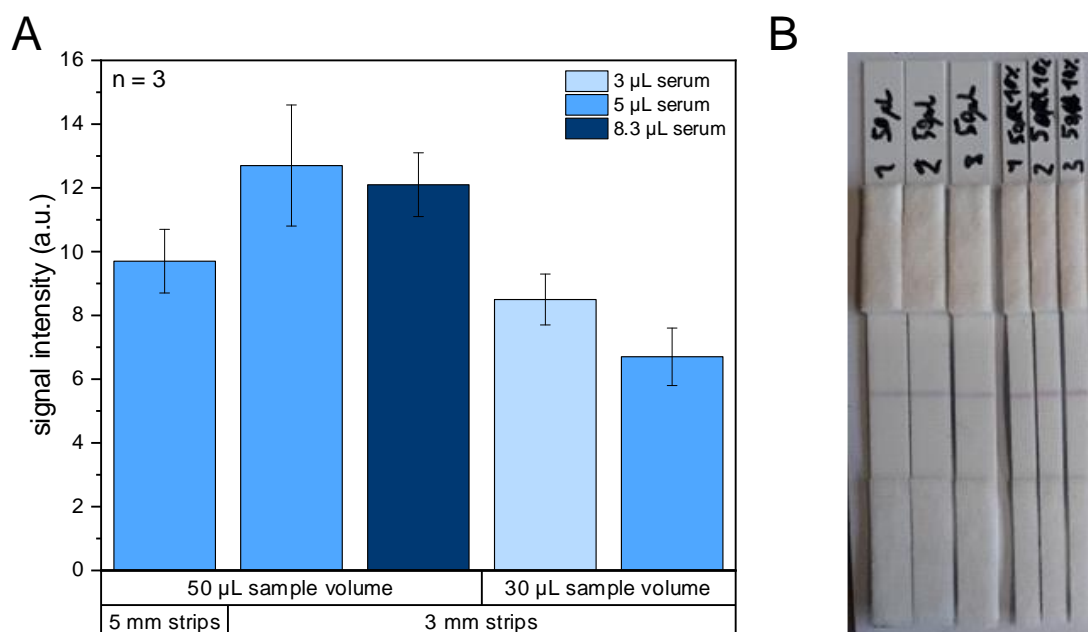
*Figure 2: **A**) Influence of test strip width (3 mm or 5 mm), and pre-pandemic serum (3 to 8.3 µL) and sample volumes (30 or 50 µL) on the signal intensity of RBD-liposomes (10 µM tL, 0.1 mol% RBD). n = 3. **B**) Comparison of 5 mm and 3 mm wide LFA strips tested with identical serum (5 µL) and sample volume (50 µL). n = 3.*

### 4.3.2  Investigation of on-strip incubation strategies

The POC neutralization test discussed in chapter 2.1 relied on a 15-minute pre-incubation step of RBD-liposomes with serum. Omitting this step would improve user-friendliness, but result in a lower sensitivity of the assay, because patient antibodies have less time to interact with RBD. Several alternative strategies were investigated to facilitate incubation on the LFA strip instead.

#### 4.3.2.1  Dispensing of a polyvinyl alcohol barrier

The introduction of a polyvinyl alcohol (PVA) barrier was shown to facilitate the timed release of a signal amplification solution for the POC test for human cardiac troponin I by Han et al.[18]. We investigated the use of a PVA barrier to allow for a 15-minute incubation of the liposome-serum-ACE2-biotin mixture on the LFA strip prior to dissolution of the barrier and subsequent capture of liposomes by the streptavidin test line. PVA solutions were dispensed on nitrocellulose membranes using the SciFlex Arrayer S3 (Scienion, Germany), a device used for precision spotting in the nL range. Individual drops were dispensed close enough to one another to achieve a homogeneous line after their spread. Important parameters as the PVA concentration, the pressure and pulse applied for drop dispensing, as well as the spot pitch were investigated to achieve consistent dispensing of a homogeneous PVA barrier and to avoid dripping. It was determined that the viscosity of the solution was too high for reliable dispensing for PVA concentrations above 15 w/v%, the nozzle clogging after 1 to 2 min. Lower PVA concentrations were however unable to fully block the pores of the nitrocellulose membrane, thus only briefly slowing the flow of the solution, rather than actively blocking it.

Many variations of the dispensing parameters for 15 w/v% PVA were investigated, including the application of up to three separate lines or overlaying of multiple lines. While the membranes could effectively be blocked, the barriers either dissolved quickly or not at all. Sorting of the samples by break-through times with 1-minute intervals shows that most barriers caused too short break-through times of 2 to 4 minutes or complete blocking of the membrane (**Figure S2**). Furthermore, results were very inconsistent, even within lots, some samples not showing any break-through while others did. Exemplary data for an individual line (**A**) and for three separate lines with 1 mm offset (**B**) can be found in **Figure 3**, which shows the influence of the spot pitch on break-through times. Changing back to the membrane with lower pore-size, CN150, also showed inconsistent results (data not shown). For comparison, Han et al. used nitrocellulose membranes from Whatman (FF80HP, FF120HP and FF170HP) and dispensed their PVA barriers (up to 30 w/v%) using a precision line dispenser. They achieved reagent release times of up to 25 minutes with very low standard deviations for each barrier height. It is likely that the SciFlex Arrayer S3 is not capable to produce homogeneous PVA barriers, in part due to incompatibility with viscous solutions. Additionally, dispensing of a line comprised of individual dots, rather than by continuous contact-dispensing as common for a line dispenser, is prone to inhomogeneous spread of the solution, producing weaknesses in the overlapping area. On-strip incubation facilitated by a PVA barrier was therefore not further investigated.
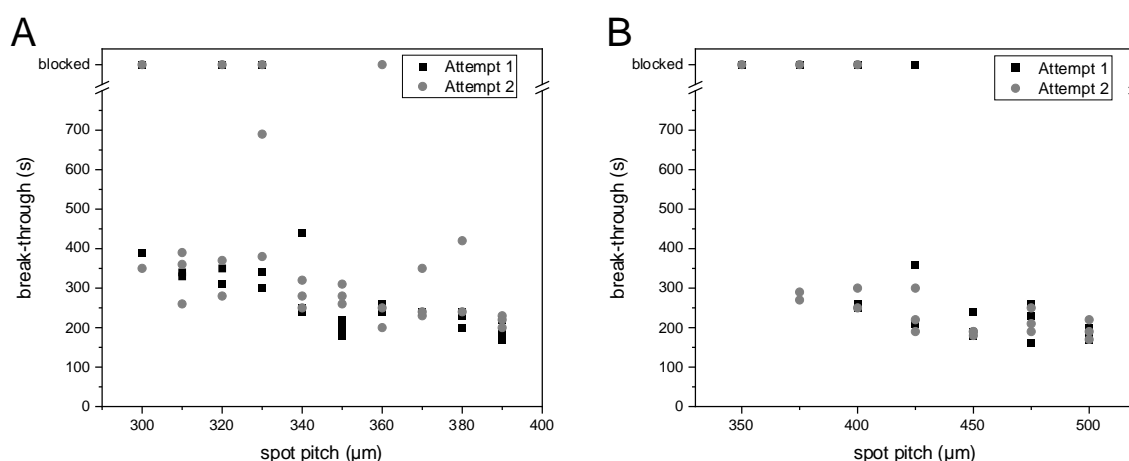


***Figure 3:*** *Exemplary break-through times for test strips (CN95 membrane) with PVA barriers (15 w/v%) dispensed with **A**) 40% pressure, 3500 µs pulse, and varying spot pitch, or **B**) 40% pressure, 500 µs pulse, and varying spot pitch as 3 separate lines with 1 mm offset. 'Blocked' refers to strips where the barrier was not dissolved, preventing the solution from reaching the waste pad.*

### 4.3.2.2 Printing of a wax barrier with gaps

Sena-Torralba et al. printed wax barriers on both CN95 and CN150 membranes and dissolved them using Tween20, achieving retention times of up to 12 minutes[15]. However, the addition of a surfactant would induce liposome lysis in the case of the liposome-based neutralization

test. Instead, the application of a wax barrier with a defined gap was investigated. This artificial narrowing of the test strip results in a reduced flow rate, providing longer interaction time for the assay components prior to capture by the test line. While reduced flow rates are usually achieved by using membranes with smaller pore sizes, this was not an option, because roughly 20% of patient sera induced liposome aggregation, preventing their migration on the CN150 but not the CN95 membrane (see chapter 2.1). Wax barriers of 0.1 mm height with gaps of 0.2 to 0.9 mm width were printed on CN95 membranes and melted at 95 °C for 5 minutes. This led to the spread of the wax between the nitrocellulose fibers, the 0.2 mm and 0.3 mm gaps becoming invisible to the naked eye (**Figure S3**). Nonetheless, solution was able to penetrate the wax barrier with ≥0.3 mm gap, but not the one with 0.2 mm gap (**Figure 4**). However, the flow was slowed to such an extent by the 0.3 mm gap that the solution was unable to reach the waste pad, drying out beforehand. For gaps with 0.4 to 0.9 mm width, solutions managed to reach the waste pad. Analysis of the test and control lines with an ESEQuant LFR device (Qiagen, Netherlands) 20 minutes after washing buffer addition revealed a trend of decreasing peak heights with decreasing gap width (**Figure 5**). This was due to incomplete migration of the liposomes for 0.4 mm and 0.5 mm gaps at the time of analysis. Subsequent analysis 30 minutes after washing buffer addition revealed increased signals (data not shown). Signals for 0.8 mm and 0.9 mm gaps had decreased by this time due to the onset of drying, complicating the comparison of signals for each gap width. The data underline however the general feasibility to use a wax barrier with gap to reduce the flow rate and thus increase interaction times. Previously, the concentration of FITC-liposomes was adapted to achieve matching test and control line intensities for seronegative samples. Normalization of the test line signal to that of the control line provided a means to measure the binding inhibition of seropositive samples. However, it remains unclear if the reduced flow rate influences the capture of both RBD- and FITC-liposomes to the same extent. To facilitate better comparison of the effect of the gap on the interaction between neutralizing antibodies and RBD-liposomes, a means for quantification other than the normalization to the anti-FITC control line is required. The best candidate was discerned to be the addition of a second test line to capture neutralized particles directly, which will be discussed in the next chapter.
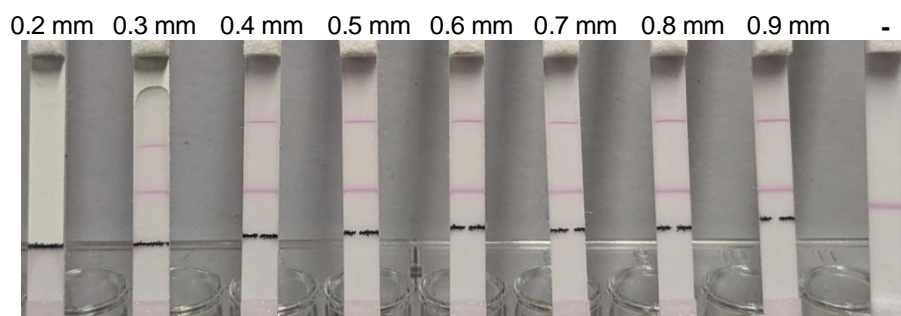
0.2 mm  0.3 mm  0.4 mm  0.5 mm  0.6 mm  0.7 mm  0.8 mm  0.9 mm  **-**



***Figure 4:*** *LFA strips without (-) or with wax barrier (0.1 mm height) with gaps with varying size (0.2 to 0.9 mm) 20 minutes after addition of the washing buffer. The samples (30 µL) contained RBD- and FITC-liposomes, ACE2-biotin and HSA (2 w/v%). The LFA strip on the right contained an anti-IgG instead of an anti-FITC control line.*
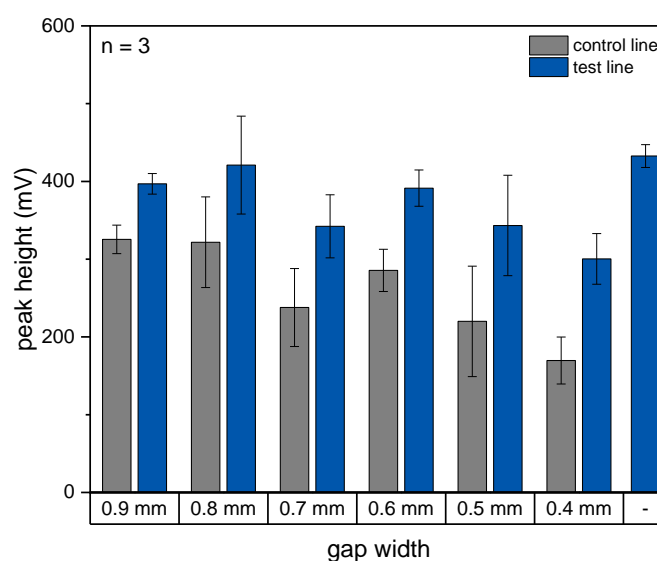


***Figure 5:*** *Peak heights of LFA strips without (-) or with wax barrier (0.1 mm height) with gaps with varying size (0.4 to 0.9 mm) 20 minutes after addition of the washing buffer. The samples (30 µL) contained RBD- and FITC-liposomes, ACE2-biotin and HSA (2 w/v%). n = 3.*

## 4.3.3 Attempting a 'signal-on' strategy to improve sensitivity and user-friendliness

The capture of neutralized RBD particles can in theory be facilitated by either anti-human Ig antibodies or protein A, both of which have been used as secondary test lines for POC neutralization tests[23–25]. The latter binds strongly to human IgG1, IgG2 and IgG4 and moderately to IgM, IgA and IgE antibodies[29]. Polyclonal goat anti-human IgA + IgG + IgM antibodies were chosen as preferred candidate for the liposome-based neutralization test, as the use of antibodies in the LFA, i.e. the anti-FITC control line, was established already. First tests with the established conditions and various seropositive samples showed neutralization, i.e. an inhibited signal for the streptavidin test line, but no neutralized RBD-liposomes were captured by the anti-human Ig test line. A titration curve using 16.7 v% of seropositive serum IR38811 revealed complete neutralization of liposome concentrations up to 40 µM total lipids and very faint test lines for 50 and 60 µM total lipids (**Figure 6 A**). Titration of the serum for a

fixed RBD-liposome concentration (16.7 µM) showed full neutralization only for 10 and 20 v% serum (**Figure 6 B**). Lower serum concentrations led to partial neutralization and overall lower test and control line intensities, because they coincided with lower amounts of HSA and therefore more non-specific interaction with the membrane. Nonetheless, neutralized RBD-liposomes should have been captured by the anti-human Ig test line in all cases. It is possible that the serum contains too many antibodies besides those directed against RBD, which are captured instead of the anti-RBD antibodies bound to RBD-liposomes.
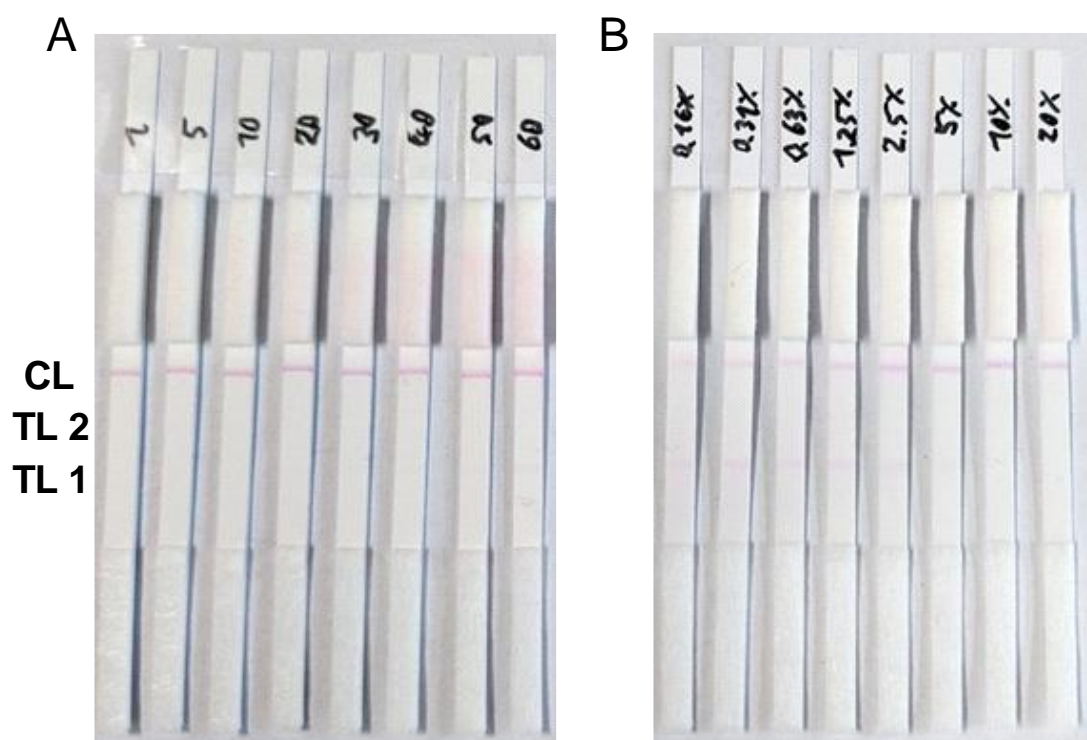


**Figure 6:** *Titration of **A**) RBD-liposomes (1 to 60 µM total lipids) or **B**) seropositive serum IR38811 (0.16 to 20 v%) on LFA strips with polystreptavidin (TL 1) and anti-human Ig (TL 2) test lines and anti-FITC control line (CL).*

Titration of the seropositive serum in a heterogeneous binding assay confirmed its neutralizing ability, fluorescence intensities of RBD-liposomes in ACE2 coated wells starting to decrease for concentrations of 0.1 v% serum and higher (**Figure 7**). As in the LFA, no binding of neutralized RBD-liposomes to immobilized anti-human Ig antibodies was observed. Protein A, on the other hand, was able to capture neutralized particles at the lower serum concentrations, while higher concentrations led to decreased capture efficiency. This suggests again that there are too many other antibodies, which are captured instead of the anti-RBD antibodies bound to the bulky RBD-liposomes. Another issue could be non-specific interaction with HSA, which was shown to be a problem for the capture of aptamer-modified liposomes by Pia Schraml. Actually, this could be shown to be the case using monoclonal anti-RBD antibodies instead of serum. Both the CR3022 and the S309 antibody facilitated the capture of RBD-liposomes in both anti-human Ig and protein A coated wells (**Figure 8**). The presence of 2 w/v% HSA

reduced the fluorescence intensities by at least 80% and in some cases fully prevented the capture of RBD-liposomes. This effect must be due to the interaction of HSA with either the Fc region of the anti-RBD antibodies or with the immobilized anti-human Ig antibodies and protein A. Yanaka et al. showed that the interaction of HSA with the Fc region of antibodies can have an inhibiting effect on various Fc receptor-mediated functions and pharmacokinetics[30]. The interaction of RBD-liposomes with ACE2 is not affected by HSA, even when monoclonal antibodies are bound to the RBD. The potential interaction of HSA with the Fc region of anti-RBD antibodies does not appear to sterically hinder binding of the receptor binding site to ACE2, but hinders capture by anti-human Ig or protein A. Since HSA makes up around 50% of serum proteins, there is no way to avoid the interaction. Instead, fine-tuning of the RBD-liposome to serum ratio might provide a suitable range of serum concentrations for which the protein A test line can be used for normalization.
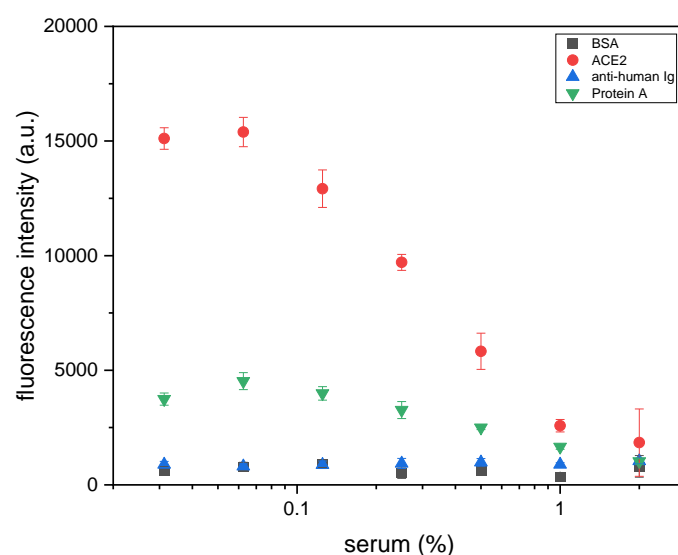


***Figure 7:*** *Binding assay of RBD-liposomes with seropositive serum IR38811 (0.032 to 2 v%) in a high binding microtiter plate coated with ACE2, anti-human Ig antibodies or protein A and blocked with BSA. n = 3.*
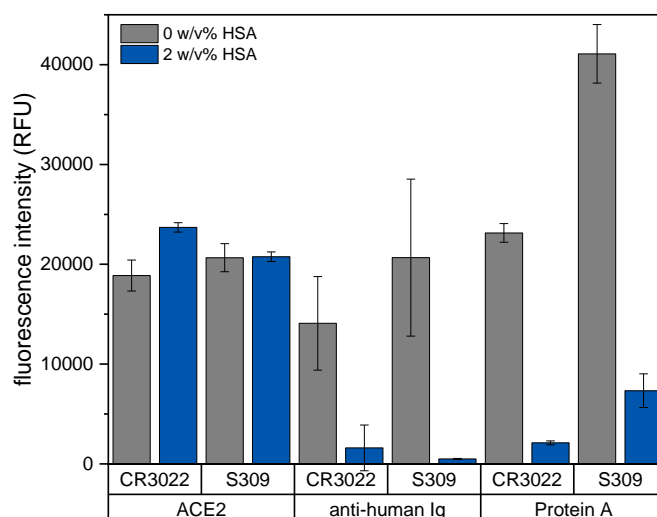
***Figure 8:*** *Binding assay of RBD-liposomes with CR3022 or S309 anti-RBD antibody (0.2 µg/mL) and HSA (0 or 2 w/v%) in a high binding microtiter plate coated with ACE2, anti-human Ig antibodies or protein A. n = 3.*

LFA strips with a polystreptavidin (1 µg/cm) and a concentrated protein A test line (5 µg/cm) were prepared. Titration of seropositive serum IR45270 (0.04 to 5 v%) finally showed successful capture of neutralized RBD-liposomes with 0.3125 v% serum (**Figure 9**). As expected, higher serum concentration again led to decreasing signal intensities for both test lines, HSA or large quantities of other antibodies preventing capture of the neutralized RBD-liposomes. The ratio of the signals of the protein A test line normalized to the polystreptavidin test line increased up to 0.625 v% serum but decreased again for 1.25 v% before slightly increasing again. Without interference of HSA, the ratio should keep increasing with increasing serum concentration, until all RBD-liposomes are neutralized and a signal is only observed for the protein A test line. The inhibitory effect of HSA on the capture of neutralized RBD-liposomes was confirmed for the LFA by a titration curve of HSA with a fixed concentration of seropositive serum IR45270 (0.625 v%). The ratio of the test line signals remained constant at first but started to drop for HSA concentrations of 0.25 w/v% and higher (**Figure 10**). Assuming a maximum HSA concentration of 50 mg/mL in serum[31], the 0.125 w/v% HSA would correspond to ~2.5 v% serum. Combined with the 0.625 v% neutralizing serum this would suggest that up to ~3 v% serum should be usable in the neutralization LFA without having an inhibiting effect on the protein A line signal. However, the previous experiment showed a decrease of the protein A line signal with 1.25 v% serum already. Overall, the effects of HSA and antibody interference drastically limit the potential of the test line for the capture of neutralized RBD-liposomes.
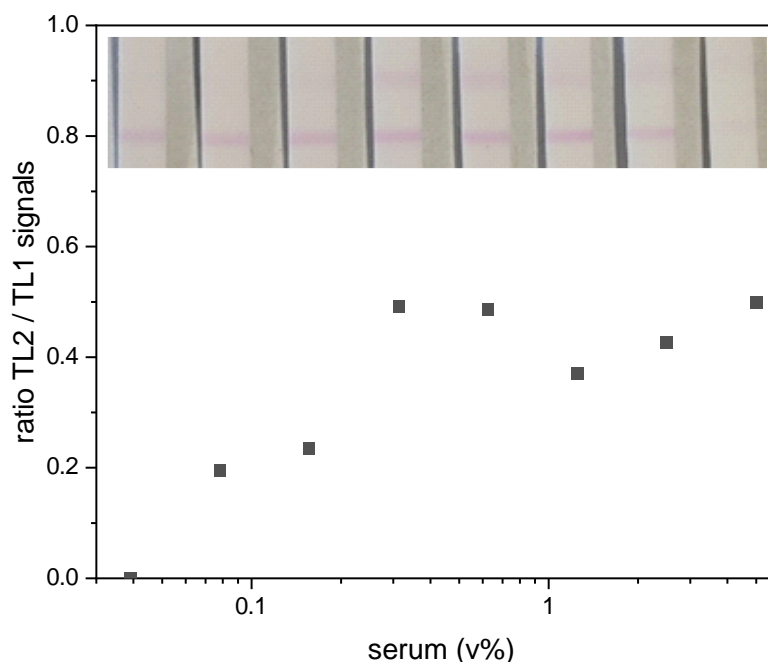
*Figure 9: Titration of seropositive serum IR45270 (0.04-5 v%) with RBD-liposomes and ACE2-biotin on LFA strips with polystreptavidin (TL 1) and protein A (TL 2) test lines (from bottom to top). Ratios of protein A test line to polystreptavidin test line signals were determined using an ESEQuant LFR device. n = 1.*



*Figure 10: Titration of HSA (0 to 1 w/v%) with RBD-liposomes, seropositive serum IR45270 (0.0625 v%) and ACE2-biotin on LFA strips with polystreptavidin (TL 1) and protein A (TL 2) test lines (from bottom to top). Ratios of protein A test line to polystreptavidin test line signals were determined using an ESEQuant LFR device. n = 1.*

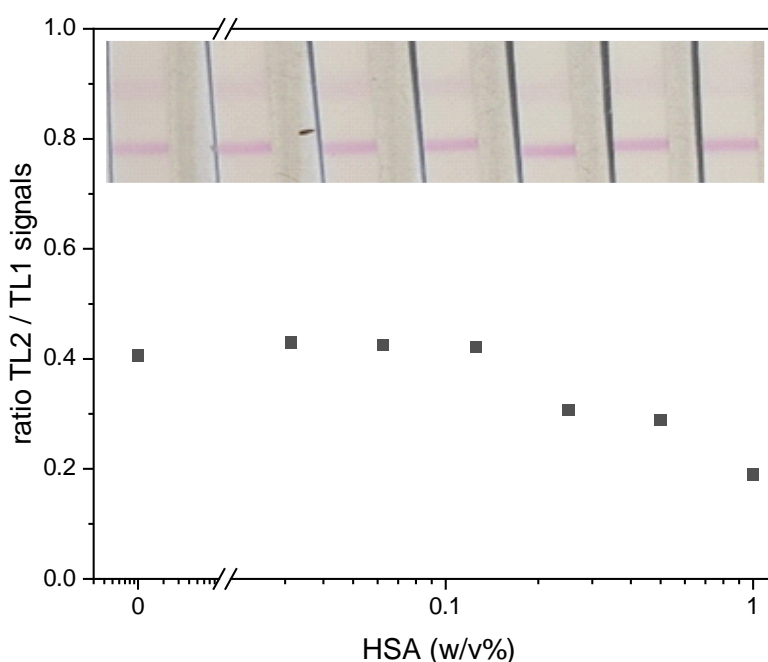Similar issues were likely faced by Connelly et al., who used a protein A test line to capture neutralized RBD-AuNPs and diluted their samples 1:800, ending up with only 0.14 nL serum per test[23]. Duan et al., on the other hand, successfully applied 10 µL serum and captured their

neutralized RBD-EuNPs on an anti-human IgG + IgM + IgA test line[24]. While they didn't manage to capture all neutralized conjugates, as seen by the lower increase of the signal of the anti-human Ig test line compared to that of the ACE2 test line, they did not appear to face the issue of HSA interference. The lower signal increase is likely due to the capture of other antibodies not directed against RBD. Addition of Tween20 and a commercial blocking solution to their Tris-HCl buffer might have prevented non-specific interaction of HSA with the antibodies. Investigation of different buffers and blocking agents, excluding Tween20, which would induce liposome lysis, might enable the use of the anti-human Ig or protein A test line for the liposome-based neutralization test in the future.

### 4.3.4  Investigation of ACE2 test line

To facilitate the use of neutravidin-liposomes incubated with biotinylated RBD in the POC format, instead of liposomes covalently modified with RBD, the application of an ACE2 instead of a polystreptavidin test line was investigated. In the established POC format (see chapter 2.1), ACE2-biotin is mixed with RBD-liposomes prior to addition to the LFA strip and leads to binding of non-neutralized liposomes to the streptavidin test line. With neutravidin-liposomes, this procedure would lead to cross-binding of ACE2-biotin to the neutravidin-liposomes instead of the streptavidin test line. Blocking with biotin after incubation of neutravidin-liposomes with RBD-biotin would be another option of overcoming this issue but complicates the assay protocol and reduces user-friendliness. All experiments discussed in this chapter were conducted using streptavidin-liposomes, because the neutravidin-liposomes had not been established at the time.

First experiments with an ACE2 test line using the standard concentration of 0.5 mg/mL showed no binding of RBD-liposomes or streptavidin-liposomes plus RBD-biotin. This suggests that the protein is orientated with the binding site facing the nitrocellulose fibers, or that the liposomes flow too fast for the ACE2-RBD interaction to occur. Drop casting of the ACE2 stock solution (1.09 mg/mL) on the membrane enabled the capture of RBD-liposomes, if used at high concentration (50 µM or 100 µM tL) (**Figure S4**). To enable the use of even higher concentrations, ACE2 was pre-concentrated in centrifugal filters (10 kDa Pierce concentrator, 12000 RCF, 5 min), resulting in a concentration of 4.3 mg/mL. Dispensing of 2 mg/mL ACE2 as test line showed a weak signal for 16.7 µM RBD-liposomes already (data not shown). Interestingly, dispensing of 4.3 mg/mL ACE2 led to lower signals compared to 2 mg/mL. This could be either due to an overload of ACE2, which might be washed away later together with captured liposomes. Or the ACE2 molecules adsorb so closely they block each other's binding sites. Besides dispensing of ACE2 in PBS, the addition of 1 w/v% BSA or the use of a carbonate buffer (pH 9) have been featured in literature[24,32–34]. However, dispensing of 0.5, 1 or 2 mg/mL ACE2 in either of the two led to weaker signals compared to PBS (data

not shown). Similarly, dispensing of a mixture of polystreptavidin and ACE2-biotin did not improve binding, leaving dispensing of 2 mg/mL ACE2 in PBS as the optimum. Finally, both formats, i.e. RBD- and streptavidin-liposomes, were compared using either polystreptavidin or ACE2 test lines (**Figure 11**). While RBD-liposomes bound strongly to the polystreptavidin test line with ACE2-biotin, almost no binding was observed to the ACE2 test line. Changing from the CN95 membrane to one with smaller pore-size (CN150) led to improved binding to the ACE2 test line due to longer interaction times enabled by the slower flow. The streptavidin-liposomes plus RBD-biotin showed essentially no binding to either test line. Further investigation is required to transfer this format to the LFA, focusing on biotin blocking for streptavidin/neutravidin-liposomes, different ACE2 immobilization strategies and running buffers.
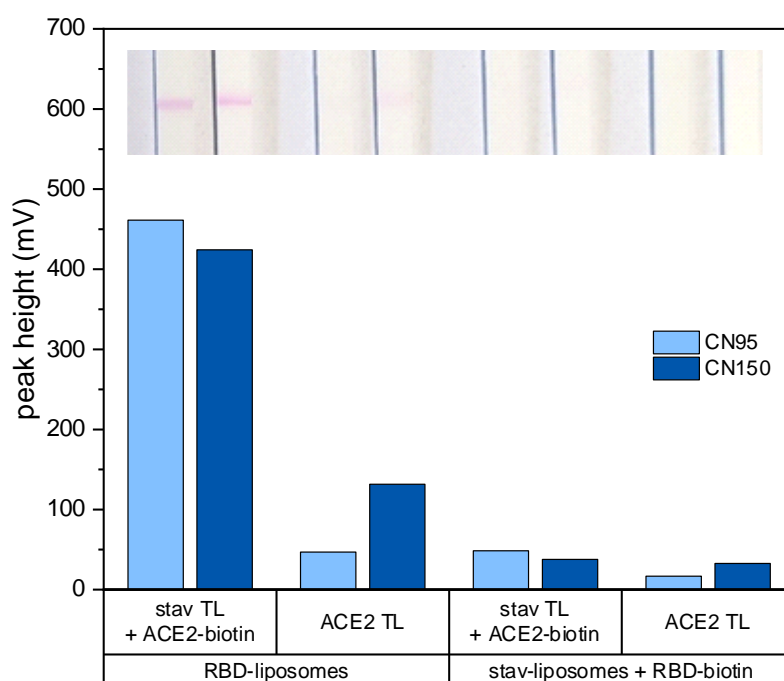


**Figure 11:** *Comparison of binding of RBD-liposomes (16.7 µM tL, 0.1 mol% RBD) or streptavidin-liposomes (16.7 µM tL) plus RBD-biotin (1 mol%) to a an ACE2 (2 mg/mL) or a polystreptavidin test line plus ACE2-biotin. n = 1.*

## 4.4 Conclusion

Reduction of the RBD coverage and LFA strip width as well as the increase of serum concentration were determined as promising and simple approaches to improve the sensitivity of the liposome-based POC neutralization test. Additionally, the capture of neutralized RBD-liposomes by an anti-human Ig or protein A test line was expected to further improve the sensitivity as well as the user-friendliness, higher neutralizing antibody titers correlating to an increase of the signal. However, interference of HSA and high concentrations of other

antibodies complicated the capture of the neutralized particles. Further investigation of buffer composition and blocking agents are warranted in light of the stated benefits of the 'signal-on' strategy. User-friendliness being an important criterion for the development of POC tests, replacement of the pre-incubation step in a reaction vial by on-strip incubation is highly desirable. Multiple strategies for this purpose are available and the most suitable one must be chosen considering the availablity of equipment. While the printing of a wax barrier is an interesting approach in academia, the discontinuation of commercial wax printers would require innovation for implementation in an industrial setting. Instead, the application of a PVA barrier might be favored, if compatible with the dispensing machinery, high viscosity preventing the technology transfer from line dispensers to high-precision non-contact dispensing platforms. Alternative strategies could be the use of a laser scriber to remove layers of the membrane, the restricted flow path resulting in a slowed flow and a smaller test line area, and hence more particles per area[35–37]. However, incorporation of such a step into existing assembly lines is difficult. An easier solution could be provided by simple compression of the membrane, resulting in a slower flow[38]. This could be achieved either by an additional machine prior to LFA strip assembly, or by a casing with a precisely manufactured protrusion and subsequent closing with defined pressure. Implementation of a piece of plastic between sample pad and membrane is another simple option to facilitate on-strip incubation, but would require removal by the user after a defined time. Lastly, the immobilization of the capture protein needs to be considered. For weak interaction between target and capture protein, biotinylation provides a means to increase interaction time between the proteins, especially when combined with an on-strip incubation step, and facilitates site-directed capture by a polystreptavidin test line. This additionally enables fine-tuning and minimization of the amount of capture protein needed, an important factor considering the cost of protein production. However, if the biotin-streptavidin interaction is used to facilitate site-directed conjugation of the target protein to the signaling agent, direct immobilization of the capture protein as test line is preferable, unless a biotin blocking step is added.

## 4.5 References

(1) Rink, S.; Baeumner, A. J. *Anal. Chem.* **2023**.

(2) Land, K. J.; Boeras, D. I.; Chen, X.-S.; Ramsay, A. R.; Peeling, R. W. *Nat Microbiol* **2019**, *4* (1), 46–54.

(3) Cavazza, M.; Sartirana, M.; Wang, Y.; Falk, M. *Eur J Public Health* **2023**, *33* (5), 937–943.

(4) Paltiel, A. D.; Zheng, A.; Sax, P. E. *Annals of internal medicine* **2021**, *174* (6), 803–810.

(5) Høeg, T. B.; Prasad, V. *Public Health Pract (Oxf)* **2023**, *6*, 100451.

(6) Bishop, J. D.; Hsieh, H. V.; Gasperino, D. J.; Weigl, B. H. *Lab Chip* **2019**, *19* (15), 2486–2499.

(7) Rink, S.; Kaiser, B.; Steiner, M.-S.; Duerkop, A.; Baeumner, A. J. *Anal. Bioanal. Chem.* **2022**, *414* (10), 3231–3241.

(8) Streif, S.; Neckermann, P.; Spitzenberg, C.; Weiss, K.; Hoecherl, K.; Kulikowski, K.; Hahner, S.; Noelting, C.; Einhauser, S.; Peterhoff, D.; Asam, C.; Wagner, R.; Baeumner, A. J. *Anal. Bioanal. Chem.* **2023**, *415* (8), 1421–1435.

(9) Elter, A.; Bock, T.; Spiehl, D.; Russo, G.; Hinz, S. C.; Bitsch, S.; Baum, E.; Langhans, M.; Meckel, T.; Dörsam, E.; Kolmar, H.; Schwall, G. *Sci Rep* **2021**, *11* (1), 7880.

(10) Kongsuphol, P.; Jia, H.; Cheng, H. L.; Gu, Y.; Shunmuganathan, B. D.; Chen, M. W.; Lim, S. M.; Ng, S. Y.; Tambyah, P. A.; Nasir, H.; Gao, X.; Tay, D.; Kim, S.; Gupta, R.; Qian, X.; Kozma, M. M.; Purushotorman, K.; McBee, M. E.; MacAry, P. A.; Sikes, H. D.; Preiser, P. R. *Commun. Med.* **2021**, *1* (1), 46.

(11) Rivas, L.; Medina-Sánchez, M.; La Escosura-Muñiz, A. de; Merkoçi, A. *Lab Chip* **2014**, *14* (22), 4406–4414.

(12) Alam, N.; Tong, L.; He, Z.; Tang, R.; Ahsan, L.; Ni, Y. *Ind. Eng. Chem. Res.* **2023**, *62* (44), 18800–18809.

(13) He, X.; Liu, Z.; Yang, Y.; Li, L.; Wang, L.; Li, A.; Qu, Z.; Xu, F. *ACS Sens* **2019**, *4* (6), 1691–1700.

(14) Tang, R.; Alam, N.; Li, M.; Xie, M.; Ni, Y. *Carbohydrate Polymers* **2021**, *268*, 118259.

(15) Sena-Torralba, A.; Ngo, D. B.; Parolo, C.; Hu, L.; Álvarez-Diduk, R.; Bergua, J. F.; Rosati, G.; Surareungchai, W.; Merkoçi, A. *Biosens. Bioelectron.* **2020**, *168*, 112559.

(16) Jahanshahi-Anbuhi, S.; Henry, A.; Leung, V.; Sicard, C.; Pennings, K.; Pelton, R.; Brennan, J. D.; Filipe, C. D. M. *Lab Chip* **2014**, *14* (1), 229–236.

(17) Alam, N.; Tong, L.; He, Z.; Tang, R.; Ahsan, L.; Ni, Y. *Cellulose (Lond)* **2021**, *28* (13), 8641–8651.

(18) Han, G.-R.; Koo, H. J.; Ki, H.; Kim, M.-G. *ACS Appl. Mater. Interfaces* **2020**, *12* (31), 34564–34575.

(19) Ishii, M.; Preechakasedkit, P.; Yamada, K.; Chailapakul, O.; Suzuki, K.; Citterio, D. *ANAL. SCI.* **2018**, *34* (1), 51–56.

(20) Mahmud, M. A.; Xu, L. H.; Usatinsky, A.; dos Santos, C. C.; Little, D. J.; Tsai, S. S. H.; Rackus, D. G. *Anal. Chem.* **2024**.

(21) Deenin, W.; Khongchareonporn, N.; Ruxrungtham, K.; Ketloy, C.; Hirankarn, N.; Wangkanont, K.; Rengpipat, S.; Yakoh, A.; Chaiyo, S. *Anal. Chem.* **2024**, *96* (14), 5407–5415.

(22) Yu, H.; Liu, H.; Yang, Y.; Guan, X. *ACS Omega* **2022**, *7* (41), 36254–36262.

(23) Connelly, G. G.; Kirkland, O. O.; Bohannon, S.; Lim, D. C.; Wilson, R. M.; Richards, E. J.; Tay, D. M.; Jee, H.; Hellinger, R. D.; Hoang, N. K.; Hao, L.; Chhabra, A.; Martin-Alonso, C.;

Tan, E. K. W.; Koehler, A. N.; Yaffe, M. B.; London, W. B.; Lee, P. Y.; Krammer, F.; Bohannon, R. C.; Bhatia, S. N.; Sikes, H. D.; Li, H. *Cell Rep. Methods* **2022**, 100273.

(24) Duan, X.; Shi, Y.; Zhang, X.; Ge, X.; Fan, R.; Guo, J.; Li, Y.; Li, G.; Ding, Y.; Osman, R. A.; Jiang, W.; Sun, J.; Luan, X.; Zhang, G. *Biosens. Bioelectron.* **2022**, *199*, 113883.

(25) Li, J.; Liu, B.; Tang, X.; Wu, Z.; Lu, J.; Liang, C.; Hou, S.; Zhang, L.; Li, T.; Zhao, W.; Fu, Y.; Ke, Y.; Li, C. *Int. J. Infect. Dis.* **2022**, *121*, 58–65.

(26) Edwards, K. A.; Curtis, K. L.; Sailor, J. L.; Baeumner, A. J. *Anal. Bioanal. Chem.* **2008**, *391* (5), 1689–1702.

(27) Grady, M.; Pineau, M.; Pynes, M. K.; Katz, L. B.; Ginsberg, B. *J Diabetes Sci Technol* **2014**, *8* (4), 691–698.

(28) Serafin, A.; Malinowski, M.; Prażmowska-Wilanowska, A. *Postgraduate Medicine* **2020**, *132* (3), 288–295.

(29) *Handbook of affinity chromatography*, 2nd ed.; Chromatographic science series, v. 92; Taylor & Francis, 2006.

(30) Yanaka, S.; Yogo, R.; Yagi, H.; Onitsuka, M.; Wakaizumi, N.; Yamaguchi, Y.; Uchiyama, S.; Kato, K. *Front. Immunol.* **2023**, *14*, 1090898.

(31) Peters, T., Ed. *All about albumin*:*Biochemistry, genetics and medical applications*; Academic Press, 1995.

(32) Huang, R.-L.; Fu, Y.-C.; Wang, Y.-C.; Hong, C.; Yang, W.-C.; Wang, I.-J.; Sun, J.-R.; Chen, Y.; Shen, C.-F.; Cheng, C.-M. *Vaccines (Basel)* **2022**, *10* (2).

(33) Lee, J.-H.; Choi, M.; Jung, Y.; Lee, S. K.; Lee, C.-S.; Kim, J.; Kim, J.; Kim, N. H.; Kim, B.-T.; Kim, H. G. *Biosens. Bioelectron.* **2021**, *171*, 112715.

(34) Schobesberger, S.; Thumfart, H.; Selinger, F.; Spitz, S.; Gonzalez, C.; Pei, L.; Poglitsch, M.; Ertl, P. *Anal. Chem.* **2024**, *96* (7), 2900–2907.

(35) Bikkarolla, S. K.; McNamee, S. E.; McGregor, S.; Vance, P.; McGhee, H.; Marlow, E. L.; McLaughlin, J. *AIP Advances* **2020**, *10* (12).

(36) Iles, A. H.; He, P. J. W.; Katis, I. N.; Horak, P.; Eason, R. W.; Sones, C. L. *Talanta* **2022**, *248*, 123579.

(37) Katis, I. N.; He, P. J. W.; Eason, R. W.; Sones, C. L. *Biosens. Bioelectron.* **2018**, *113*, 95–100.

(38) Park, S. B.; Shin, J. H. *BioChip J* **2022**, *16* (4), 480–489.

## 4.6 Supplementary information



***Figure S1:*** *Pictures of the photo box in the opened state. A front cover is added to ensure that no light can penetrate from the outside during imaging.*
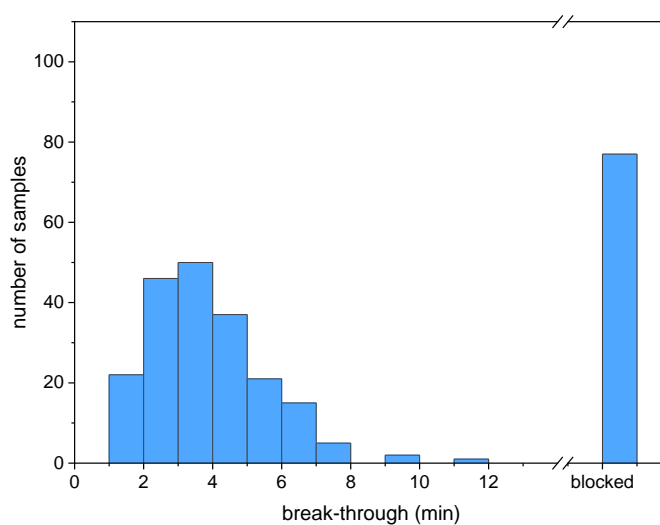


***Figure S2:*** *Number of samples that showed break-through times in the respective 1-minute intervals.*
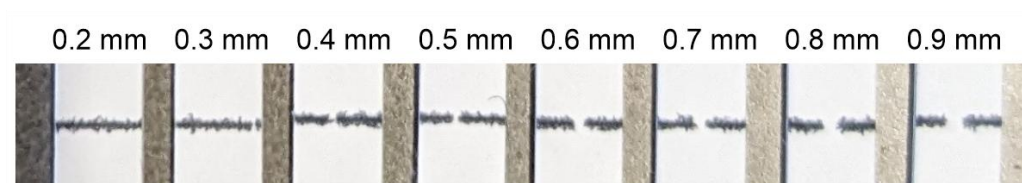
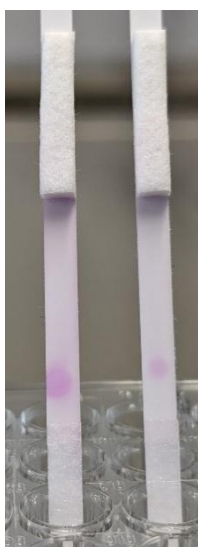*Figure S3:* LFA strips with wax barrier (0.1 mm width) with gaps of varying size (0.2 to 0.9 mm).



*Figure S4:* Binding of RBD-liposomes (100 µM or 50 µM tL from left to right) to ACE2 (1.09 mg/mL in PBS) drop-cast on an LFA strip.

# 5 Conclusion and Perspective

The potential of sulforhodamine B encapsulating liposomes was harnessed to develop a SARS-CoV-2 neutralization test in two different formats using either fluorescence or colorimetric detection. This strategy stands out as it requires the optimization of only one and not two separate signaling conjugates, which can lead to a significant reduction of the development time and production costs. Furthermore, it has the benefit of higher sensitivity in the lateral flow assay compared to commercial gold nanoparticles, as shown by the 10-fold lower limit of detection for interleukin-6 reported by Rink et al.[1]. The highly sensitive fluorescence read-out enabled quantitative detection of neutralizing antibodies in the HTS format, which correlated well to an established pseudovirus neutralization test. No statement can be made regarding the correlation to other sVNTs, such as ELISAs using RBD conjugated to horeseradish-peroxidase. This would be an interesting aspect to determine which assay is best suited for commercialization, but requires screening of identical serum panels. Commercialization of the developed tests would require the large-scale production of liposomes. The applied reverse-phase evaporation method is adequate for smaller quantities, a single lot would be sufficient for over ten thousand tests, assuming no waste. For larger quantities, microfluidic systems might be better suited, known for their high reproducibility and easy fine-tuning of liposome size and encapsulation yields by variation of the ratio of lipid mixture to encapsulant and the flow rates[2]. Upscaling of these systems is typically done by parallelization of separate microfluidic chips and holds the potential for automation when combined with tangential flow filtration to remove excess encapsulant.

Consideration of commercialization also needs to account for drawbacks determined during the development phase. In the case of the liposome-based neutralization test these are the shelf-life of RBD-liposomes, currently limited to 24 weeks rather than years, and more importantly the incompatibility to RBD of different variants of concern. Mutations of Omicron variants influence the orientation on the liposome and thus availability of the receptor binding site. Protein conjugation using EDC/sulfo-NHS chemistry, despite its simple and widespread use, is therefore not applicable to structurally similar proteins, if comparability is desired. The approach is however well suited to proteins that will be coupled with favorable orientation, for example those with multiple binding centers, such as the tetrameric streptavidin. Combined with site-directed biotinylation the latter mediates not only favorable orientation of the protein on the surface of liposomes, but provides a platform that can be easily adapted to different analytes and allows for separate storage, and thus long shelf-lifes, of assay components. Cys- or Avi-tags can be genetically engineered for recombinant proteins, while mere biotinylation using NHS-biotin might be sufficient for those proteins that can not be expressed

recombinantly. The platform is not limited to the detection of neutralizing antibodies, and can quickly be adapted to other protein-protein interactions, relevant not only for biomarkers in the field of diagnostic testing, but also drug development, lifestyle, nutrition, and food safety applications.

Liposomes further have the capability to encapsulate other molecules, such as enzymes[3], luminophores[4] or redoxmarkers[5], and can thus facilitate the use of other detection methods. However, the change of encapsulant might affect liposome formation, as observed for high SRB concentrations, which lead to low encapsulation yields for liposomes with low cholesterol content[6]. Adaptation might therefore not be straight-forward and require additional optimization of the lipid composition. This, in turn, offers the possibility to incorporate different functionalized lipids, and choose from the multitude of coupling chemistries available for protein conjugation to liposomes. Besides the EDC/sulfo-NHS coupling to carboxylated liposomes used in this work, coupling to amino, thiol, and alkyne groups are common examples that can even facilitate site-directed protein conjugation. A promising conjugation strategy is provided by click chemistry, especially strain-promoted alkyne-azide cycloaddition, even though it requires the introduction of alkyne- or azide-residue containing non-canonical amino acids via genetic engineering to be site-directed. Alternatively, maleimide-NHS-ester conjugates should facilitate orientated conjugation of Cys-tagged proteins to $NH_2$-liposomes. The liposome surface charge and the buffer conditions need to be considered for all conjugation strategies, as they can influence the coupling efficiency.

Looking forward, liposomes could further enhance the field of diagnostics by enabling multi-analyte detection strategies. For the POC test developed in this work, it could be envisioned to prepare liposome conjugates for different analytes, distinguishable due to the encapsulation of different dyes with distinct absorbance bands. This could be various respiratory diseases, for example SARS-CoV-2, Influenza, and RSV, that would be detected on a single LFA strip. The strategy cannot be applied to different variants of the same virus, which would all be neutralized by the same antibodies and bind to the same receptor, causing a mixed color of the test line, significantly complicating quantification. Similarly, preparation of spectrally distinct fluorescent liposomes would not be an improvement for the HTS format, unless testing for different analytes in the same well is desired. This might be of interest for a homogeneous assay format, in which liposome lysis is induced or prevented upon binding to the analyte, as recently shown using SRB liposomes, where lysis was mediated by the complement system[6]. Sensitivity of this assay is highly influenced by the self-quenching properties of the encapsulated fluorophore. Ideally, it leads to at least a 100-fold increase of fluorescence upon release of the fluorophore, as is the case for liposomes encapsulating 150 mM SRB. However, these are not stable in serum due to the high cholesterol content, and only 10 mM SRB

encapsulating liposomes can be used so far, which show lower self-quenching and only a 10-fold increase of fluorescence upon release. The investigation of different fluorescent dyes with strong self-quenching properties, such as cyanine green derivatives, could be highly beneficial.

Finally, the implementation of an on-strip incubation step is thought to significantly improve both the sensitivity and the user-friendliness of POC tests. Depending on available equipment this can be realized by complete blocking of the membrane with a dissolvable barrier[7,8], or reduction of the flow rate by mechanical compression of the membrane[9] or narrowing of the test strip. Printing of a wax barrier with a gap provides a simple means to implement the latter. Alternatively, the removal of layers of the membrane using a laser allows for precise tuning of the flow properties and reduction of the test line width, improving sensitivity[10,11]. For non-competitive assays the improvement can be quantified with a simple titration curve of the analyte. In the case of competitive assays, such as the neutralization test, where increased analyte concentrations correspond to a decrease of the signal, this is less straight-forward. Incorporation of a 'signal-on' strategy can in theory resolve this problem and should be investigated in more detail.

In conclusion, the advancements made in this thesis highlight the transformative potential of liposome-based sensing strategies in diagnostics. Continued research and development in this area will undoubtedly lead to further innovations, including the broadening of read-out capabilities, implementation of multiplexing and improved handling, solidifying the role of liposomes as a cornerstone in the future of diagnostic testing and other fields deploying tests based on protein-protein interaction.

## References

(1) Rink, S.; Kaiser, B.; Steiner, M.-S.; Duerkop, A.; Baeumner, A. J. *Anal. Bioanal. Chem.* **2022**, *414* (10), 3231–3241.

(2) Kotouček, J.; Hubatka, F.; Mašek, J.; Kulich, P.; Velínská, K.; Bezděková, J.; Fojtíková, M.; Bartheldyová, E.; Tomečková, A.; Stráská, J.; Hrebík, D.; Macaulay, S.; Kratochvílová, I.; Raška, M.; Turánek, J. *Sci Rep* **2020**, *10* (1), 5595.

(3) Lin, C.; Guo, Y.; Zhao, M.; Sun, M.; Luo, F.; Guo, L.; Qiu, B.; Lin, Z.; Chen, G. *Anal. Chim. Acta* **2017**, *963*, 112–118.

(4) Mayer, M.; Takegami, S.; Neumeier, M.; Rink, S.; Jacobi von Wangelin, A.; Schulte, S.; Vollmer, M.; Griesbeck, A. G.; Duerkop, A.; Baeumner, A. J. *Angew Chem Int Ed Engl* **2018**, *57* (2), 408–411.

(5) Wongkaew, N.; He, P.; Kurth, V.; Surareungchai, W.; Baeumner, A. J. *Anal. Bioanal. Chem.* **2013**, *405* (18), 5965–5974.

(6) Hoecherl, K.; Streif, S.; Rink, S.; Behrent, A.; Holzhausen, F.; Griesche, C.; Rogoll, C.; Foedlmeier, M.; Gebhard, A.; Kulikowski, K.; Schaefer, N.; Pauly, D.; Baeumner, A. J. *Anal. Bioanal. Chem.* **2025**.

(7) Han, G.-R.; Koo, H. J.; Ki, H.; Kim, M.-G. *ACS Appl. Mater. Interfaces* **2020**, *12* (31), 34564–34575.

(8) Tang, R.; Alam, N.; Li, M.; Xie, M.; Ni, Y. *Carbohydrate Polymers* **2021**, *268*, 118259.

(9) Park, S. B.; Shin, J. H. *BioChip J* **2022**, *16* (4), 480–489.

(10) Iles, A. H.; He, P. J. W.; Katis, I. N.; Horak, P.; Eason, R. W.; Sones, C. L. *Talanta* **2022**, *248*, 123579.

(11) Katis, I. N.; He, P. J. W.; Eason, R. W.; Sones, C. L. *Biosens. Bioelectron.* **2018**, *113*, 95–100.

# Curriculum Vitae

Simon Streif
simon.streif@ur.de

**Hochschulausbildung:**

| | |
|---|---|
| 06/2021 – 04/2025 | **Promotionsstudium Chemie**, Universität Regensburg <br> „*Development of liposome-based sensing strategies for clinical diagnostics*" <br> Institut für Analytische Chemie, Chemo- und Biosensorik <br> (Prof. Dr. Antje J. Bäumner) |
| 08/2018 – 03/2021 | **Masterstudiengang Chemie**, Universität Regensburg <br> „*Development toward POC testing for SARS-CoV-2 immunity status*" <br> Institut für Analytische Chemie, Chemo- und Biosensorik <br> (Prof. Dr. Antje J. Bäumner) |
| 08/2018 – 01/2019 | **Auslandssemester**, Universität Göteborg |
| 10/2015 – 07/2018 | **Bachelorstudiengang Chemie**, Universität Regensburg <br> „*Electrospinning of emeraldine base polyaniline nanofibers with reduced graphene oxide*" <br> Institut für Analytische Chemie, Chemo- und Biosensorik <br> (Prof. Dr. Antje J. Bäumner) |

# Publications

[1] **Streif, S.**, Neckermann, P., Spitzenberg, C., Weiß, K., Hoecherl, K., Kulikowski, K., Hahner, S., Noelting, C., Einhauser, S., Peterhoff, P., Asam, C., Wagner, R., Baeumner, A. J. Liposome-based high-throughput and point-of-care assays toward the quick, simple and sensitive detection of neutralizing antibodies against SARS-CoV-2 in patient sera. *Anal. Bioanal. Chem.* 415, 1421–1435 (2023).

[2] **Streif, S.**, Baeumner, A. J. Advances in Surrogate Neutralization Tests for High-Throughput Screening and the Point-of-Care. *Anal. Chem.* 97, 10, 5407–5423 (2025).

[3] Hoecherl, K., **Streif, S.**, Rink, S., Behrent, A., Holzhausen, F., Griesche, C., Rogoll, C., Foedlmeier, M., Gebhard, A., Kulikowski, K., Schaefer, N., Pauly, D., Baeumner, A. J. A homogeneous immunoassay technology based on liposomes and the complement system enables one-step, no-wash, rapid diagnostics directly in serum. *Anal. Bioanal. Chem.* 417, 3257–3273 (2025).

# Presentations

**Oral Presentations**

05/2024          **BBMEC 2024**: „Exploring the simplification of an adaptive liposome-based neutralization test"

09/2023          **EBS 2023**: „ Liposome-based high-throughput and point-of-care neutralization tests for SARS-CoV-2"

**Poster Presentations**

04/2024          **Analytica 2024**: „Liposome-based high-throughput and point-of-care neutralization tests for SARS-CoV-2"

06/2022          **Analytica 2022**: „Liposome-based high-throughput and point-of-care assay for the quick, simple and sensitive detection of neutralizing antibodies against SARS-CoV-2 in patient sera"

# Eidesstattliche Erklärung

Ich erkläre hiermit an Eides statt, dass ich die vorliegende Arbeit ohne unzulässige Hilfe Dritter und ohne Benutzung anderer als der angegebenen Hilfsmittel angefertigt habe; die aus anderen Quellen direkt oder indirekt übernommenen Daten und Konzepte sind unter Angabe des Literaturzitats gekennzeichnet.

Weitere Personen waren an der inhaltlich-materiellen Herstellung der vorliegenden Arbeit nicht beteiligt. Insbesondere habe ich hierfür nicht die entgeltliche Hilfe eines Promotionsberaters oder anderer Personen in Anspruch genommen. Niemand hat von mir weder unmittelbar noch mittelbar geldwerte Leistungen für Arbeiten erhalten, die im Zusammenhang mit dem Inhalt der vorgelegten Dissertation stehen.

Die Arbeit wurde bisher weder im In- noch im Ausland in gleicher oder ähnlicher Form einer anderen Prüfungsbehörde vorgelegt.

Regensburg, den 30.04.2025

Simon Streif (Author)